



Terms and Conditions of Use of Digitised Theses from Trinity College Library Dublin

Copyright statement

All material supplied by Trinity College Library is protected by copyright (under the Copyright and Related Rights Act, 2000 as amended) and other relevant Intellectual Property Rights. By accessing and using a Digitised Thesis from Trinity College Library you acknowledge that all Intellectual Property Rights in any Works supplied are the sole and exclusive property of the copyright and/or other IPR holder. Specific copyright holders may not be explicitly identified. Use of materials from other sources within a thesis should not be construed as a claim over them.

A non-exclusive, non-transferable licence is hereby granted to those using or reproducing, in whole or in part, the material for valid purposes, providing the copyright owners are acknowledged using the normal conventions. Where specific permission to use material is required, this is identified and such permission must be sought from the copyright holder or agency cited.

Liability statement

By using a Digitised Thesis, I accept that Trinity College Dublin bears no legal responsibility for the accuracy, legality or comprehensiveness of materials contained within the thesis, and that Trinity College Dublin accepts no liability for indirect, consequential, or incidental, damages or losses arising from use of the thesis for whatever reason. Information located in a thesis may be subject to specific use constraints, details of which may not be explicitly described. It is the responsibility of potential and actual users to be aware of such constraints and to abide by them. By making use of material from a digitised thesis, you accept these copyright and disclaimer provisions. Where it is brought to the attention of Trinity College Library that there may be a breach of copyright or other restraint, it is the policy to withdraw or take down access to a thesis while the issue is being resolved.

Access Agreement

By using a Digitised Thesis from Trinity College Library you are bound by the following Terms & Conditions. Please read them carefully.

I have read and I understand the following statement: All material supplied via a Digitised Thesis from Trinity College Library is protected by copyright and other intellectual property rights, and duplication or sale of all or part of any of a thesis is not permitted, except that material may be duplicated by you for your research use or for educational purposes in electronic or print form providing the copyright owners are acknowledged using the normal conventions. You must obtain permission for any other use. Electronic or print copies may not be offered, whether for sale or otherwise to anyone. This copy has been supplied on the understanding that it is copyright material and that no quotation from the thesis may be published without proper acknowledgement.

Investigation of the potential use of ruthenium-ODN conjugates as antisense agents in Chronic Myeloid Leukaemia

by

Yvonne Kavanagh



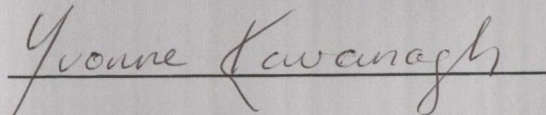
A thesis submitted to the University of Dublin for the degree of
Doctor of Philosophy

Department of Chemistry
University of Dublin
Trinity College

October 2001

DECLARATION

This thesis has not been submitted as an exercise for a degree at this or any other University. The work described herein has been carried out by the author alone, except where otherwise stated. The author agrees that the college library may lend or copy this thesis upon request.

A handwritten signature in cursive script that reads "Yvonne Kavanagh". The signature is written in dark ink and is positioned above a horizontal line.

Yvonne Kavanagh

October 2001

For my parents, Tom and Norrie

Acknowledgements

I would like to thank Prof. John Corish and Prof. John Kelly, in their respective roles as heads of department, for the use of the facilities in the Chemistry department. I would also like to thank Prof. Kevin Devine for the use of the facilities in the Genetics department. I wish to express my gratitude to my supervisors Dr. Peter Boyle and Prof. John Kelly for all their support, encouragement and enthusiasm during the course of my research. I would also like to thank Dr. Mark Lawler for all his help and advice with the work.

I wish to acknowledge Prof. R. Jeremy H. Davies and Clarke Stevenson of the School of Biology and Biochemistry, Queen's University Belfast for all their assistance and advice with the oligonucleotide work. Thanks also to Michelle Higgins and the Brussels group for their kind donations of $\text{Ru}(\text{phen})_2\text{Cl}_2$ and $\text{Ru}(\text{TAP})_2\text{Cl}_2$. I would like to express gratitude to Enterprise Ireland, the Trinity Trust, the Health and Research Board and BOC gases for financial support.

A special thank you to the technical staff of both the Chemistry and Genetics departments for their extraordinary ability to perform near-miracles at the shortest of notice. Thanks to Dr. Martin Feeney for all his advice on gels and lamps and Dr. John O'Brien for running the NMR spectra. I would also like to thank the postgraduate students in the Genetics department for all their help and advice.

I would like to thank all the past and present members of the Boyle and Kelly research groups for all their support and friendship. A special mention to Conor for teaching me all the gel techniques, and more importantly, all the associated survival techniques, to Fabien for his friendship and generosity and memorable "balcony" parties and to Tom for his great friendship and support - the countless hours of chat, gossip, debate, coffee-drinking and general abuse made the time go much quicker!

Thanks also to all my other postgraduate friends in the department, without whom things would have been much duller. A special mention to the gang from I.T. Tallaght, "Thorri's angels" and the (very talented) footballing lads. I'd also like

to thank "the girls" for their constant support and encouragement and lastly, Dave, for all his support, both practical and emotional, along with a constant supply of enthusiasm and humour.

Summary

The work presented in this thesis describes the synthesis of two ruthenium oligodeoxynucleotide (ODN) conjugates and their application as potential photoactive antisense agents in a model Chronic Myeloid Leukaemia (CML) system. The target 34mer ODN sequence chosen for the model system represents the messenger RNA sequence transcribed from the breakpoint region of the *bcr / abl* oncogene on the Philadelphia chromosome, an abnormal chromosome specific to CML cells. The overall aim of this work is augmentation of an antisense effect through site-specific photochemical targeting of the target 34mer ODN sequence thus, in theory, suppressing leukaemic mRNA expression and subsequent oncoprotein production.

Two ruthenium polypyridyl complexes, $[\text{Ru}(\text{phen})_2\text{phen}']^{2+}$ and $[\text{Ru}(\text{TAP})_2\text{phen}']^{2+}$, were synthesised. Activation of the carboxylic acid functionality on the phen' ligand to the corresponding N-hydroxysuccinimido ester allowed for direct coupling with a hexylamino-derivatised 17mer ODN yielding the corresponding ruthenium-ODN conjugate. Both conjugates were purified by gel electrophoresis and electroelution and characterised by spectroscopic and HPLC methods. After hybridisation of each conjugate with the target strand, the ruthenium complex was orientated in such a way as to achieve optimal interaction with the target guanine residue on the target strand (G21) situated 21 bases from its 5'-end.

After irradiation of the model system, the interaction between both ruthenium-ODN conjugates and the 5'-end radioactively labeled target 34mer ODN strand was analysed by polyacrylamide gel electrophoresis (PAGE), visualised by

autoradiography and quantified by phosphoimagery. The $[\text{Ru}(\text{phen})_2\text{phen}']\text{-ODN}$ conjugate induced base sensitive site-specific modifications at G21 in the target strand, which were revealed as strand breaks after piperidine treatment. The $[\text{Ru}(\text{TAP})_2\text{phen}']\text{-ODN}$ conjugate formed site-specific photoadducts with G21 in the target strand. Experiments with the free ruthenium complexes $[\text{Ru}(\text{phen})_2\text{phen}']^{2+}$ and $[\text{Ru}(\text{TAP})_2\text{phen}']^{2+}$ in the presence of the target 34mer ODN showed guanine specific cleavage and photoadduct formation respectively. Experiments were carried out with the inclusion of various additions in order to understand the mechanism of photooxidative damage in the model system.

Variant target strands were also studied in which the target G21 target was moved in increments towards the 3'-end of the target 34mer ODN in order to investigate the range of photooxidative damage. Nonsense strand experiments were carried out in order to ensure specificity of each ruthenium-ODN conjugate for the leukaemic mRNA sequence and results revealed no induction of damage in random ODN sequences.

Finally, in order to investigate any damage induced in each ruthenium-ODN conjugate during the course of the irradiations, each conjugate was radiolabeled at the 3'-end and the experiments were repeated in the presence of non-labeled target 34mer ODN. Results suggested that the conjugates were capable of self-interaction, thus decreasing the overall yield of photocleavage and photoadduct formation observed in the model system.

Table of Contents

Chapter 1 Introduction

1.1	Primary structure of nucleic acids	1
1.2	Secondary structure of nucleic acids	4
1.2.1	Hairpins	6
1.2.2	DNA melting temperature	7
1.2.3	Various DNA conformations	8
1.3	Tertiary structure of nucleic acids	10
1.4	Solid state synthesis of oligodeoxynucleotides	11
1.5	Gene expression	13
1.6	Targeting of nucleic acids	14
1.6.1	Antigene approach	15
1.6.2	Antisense therapy	18
1.7	Modified antisense oligonucleotides	20
1.8	Chronic myeloid leukaemia (CML)	23
1.9	Photocleavage of nucleic acids	26
1.9.1	Electron transfer (type I damage)	28
1.9.2	Energy transfer (type II damage)	29
1.9.3	Adduct formation	29
1.10	Guanine oxidation	30
1.11	Photochemical targeting by ruthenium complexes	35
1.11.1	General properties of ruthenium (II) complexes	35
1.11.2	Interaction of ruthenium (II) polypyridyl complexes with DNA	37

1.12	Ruthenium (II) complex – oligodeoxynucleotide conjugates	41
1.13	Synthesis of ruthenium (II) – oligodeoxynucleotide conjugates	42
1.13.1	Post-solid phase oligodeoxynucleotide modification	43
1.13.2	Solid phase coupling of ruthenium complex and oligodeoxynucleotide	52
1.14	Limitations of previous work	65
1.15	Aims of work	67
Chapter 2 Synthesis of ruthenium-oligodeoxynucleotide conjugates		
2.1	Introduction	69
2.2	Synthesis of 5-(4-carboxybutanamido)-1,10-phenanthroline	70
2.3	Synthesis of 1,4,5,8-tetraazaphenanthrene (TAP)	71
2.3.1	Synthesis of 6-nitroquinoxaline	71
2.3.2	Synthesis of 5-amino-6-nitroquinoxaline	72
2.3.3	Synthesis of 5,6-diaminoquinoxaline	73
2.3.4	Synthesis of 1,4,5,8-tetraazaphenanthrene	73
2.4	Synthesis of ruthenium bis(1,10)-5-(4-carboxybutanamido)-1,10-phenanthroline dihexafluorophosphate	74
2.5	Synthesis of ruthenium bis(1,4,5,8-tetraazaphenanthrene)-5-(4-carboxybutanamido)-1,10-phenanthroline	76
2.6	Activation of $[\text{Ru}(\text{phen})_2\text{phen}'](\text{PF}_6)_2$ and $[\text{Ru}(\text{TAP})_2\text{phen}'](\text{PF}_6)_2$ and subsequent coupling of both complexes to 17mer oligodeoxynucleotide	77
2.7	Ruthenium-oligonucleotide conjugate purification and isolation	81
2.8	Analysis of ruthenium-oligonucleotide conjugates	86

2.8.1	Conjugate 1: [Ru(phen) ₂ phen`]-ODN	86
2.8.2	Conjugate 2; [Ru(TAP) ₂ phen`]-ODN	87

Chapter 3 Interaction between [Ru(phen)₂phen`]-ODN and target 34mer

3.1	Introduction	88
3.2	Description of model system	89
3.2.1	Hybridisation of complementary strand regions	91
3.2.2	Ionic strength conditions	92
3.2.3	Irradiation conditions	92
3.2.4	Piperidine treatment	93
3.2.5	Analysis of cleavage products	94
3.3	Photocleavage studies using free ruthenium complexes	95
3.3.1	Photocleavage of target 34mer ODN by [Ru(phen) ₃] ²⁺	95
3.3.2	Photocleavage of target 34mer ODN by [Ru(phen) ₂ phen`] ²⁺	98
3.4	Effect of various additions on the photocleavage of target 34mer ODN by [Ru(phen) ₃] ²⁺ and [Ru(phen) ₂ phen`] ²⁺	99
3.4.1	Effect of sodium azide (NaN ₃) and argon	99
3.4.2	Effect of D ₂ O	101
3.4.3	Effect of ammonium persulfate	101
3.5	Mechanism of base damage with free ruthenium complexes	103
3.6	Photocleavage of 34mer ODN target by [Ru(phen) ₂ phen`]-ODN conjugate	103
3.7	Effect of presence of sodium nitrite filter	108
3.8	Non-denaturing gel work	110

3.9	Effect of various additions on the photocleavage of target 34mer ODN by [Ru(phen) ₂ phen']-ODN conjugate	113
3.9.1	Effect of sodium azide (NaN ₃) and argon	113
3.9.2	Effect of D ₂ O	115
3.9.3	The role of singlet oxygen in guanine oxidation	116
3.9.4	Effect of ammonium persulfate	117
3.9.5	Effect of desferrioxamine	119
3.10	Nonsense strand work	120
3.11	Variant strand work	122
3.12	3'-end labeling	131
3.13	Conclusions	135
Chapter 4 Interaction between [Ru(TAP)₂phen']-ODN and target 34mer		
4.1	Introduction	137
4.2	Description of model system	138
4.2.1	Hybridisation of complementary strand regions	140
4.2.2	Ionic strength conditions	140
4.2.3	Irradiation conditions	141
4.2.4	Analysis of photoadduct formation	141
4.3	Photoadduct formation using free ruthenium complexes	142
4.3.1	Photoadduct formation between target 34mer ODN and [Ru(TAP) ₂ phen'] ²⁺ and target 34mer ODN and [Ru(TAP) ₃] ²⁺	142
4.4	Photoadduct formation between 34mer ODN target and [Ru(TAP) ₂ phen']-ODN conjugate	152

4.5	Piperidine treatment	157
4.6	Effect of the presence of sodium nitrite filter	158
4.7	Non-denaturing gel work	159
4.8	Effect of various additions on photoadduct formation between target 34mer ODN and [Ru(TAP) ₂ phen']-ODN conjugate	162
4.8.1	Effect of sodium azide (NaN ₃) and argon	162
4.8.2	Effect of D ₂ O	164
4.8.3	Mechanism of photoadduct formation	165
4.8.4	Effect of ammonium persulfate	167
4.8.5	Effect of desferrioxamine	167
4.9	Nonsense strand work	169
4.10	Variant strand work	172
4.11	3'-end labeling	183
4.12	Conclusions	184
Chapter 5 Materials and methods		
5.1	Apparatus	187
5.1.1	Spectroscopic measurements	187
5.1.2	HPLC	187
5.1.3	Instruments	187
5.1.4	Autoradiography	188
5.1.5	Phosphoimagery	188
5.1.6	Light source	189
5.2	Reagents	189

5.3	Solutions and buffers	189
5.3.1	Solvents	189
5.3.2	Water	190
5.3.3	Buffers	190
5.4	Synthesis of ligands	191
5.4.1	5-Amino-1,10-phenanthroline	191
5.4.2	5-(4-Carboxybutanamido-1,10-phenanthroline)	192
5.4.3	6-Nitroquinoxaline	193
5.4.4	5-Amino-6-nitroquinoxaline	194
5.4.5	5,6-Diaminoquinoxaline	195
5.4.6	1,4,5,8-Tetraazaphenanthrene	195
5.5	Synthesis of ruthenium complexes	196
5.5.1	Ruthenium bis(1,10-phenanthroline)-5-(4-carboxybutanamido) -1,10-phenanthroline dihexafluorophosphate	196
5.5.2	Ruthenium bis(1,4,5,8-tetraazaphenanthrene) -5-(4-carboxybutanamido)-1,10-phenanthroline dihexafluorophosphate	197
5.6	Ruthenium complex activation	197
5.6.1	Activation of $[\text{Ru}(\text{phen})_2\text{phen}'](\text{PF}_6)_2$ to give the corresponding N-hydroxysuccinimido ester	197
5.6.2	Activation of $[\text{Ru}(\text{TAP})_2\text{phen}'](\text{PF}_6)_2$ to give the corresponding N-hydroxysuccinimido ester	198
5.7	Coupling reactions	198

5.8	Oligodeoxynucleotide synthesis	200
5.9	Radiolabeling experiments	200
5.9.1	5'-end labeling	200
5.9.2	3'-end labeling	201
5.10	Sample preparation	202
5.10.1	5'-end labeled work	202
5.10.2	3'-end labeled work	204
5.11	Experimental setup	204
5.12	Piperidine treatment	205
5.13	G + A experiment	205
5.14	Polyacrylamide gel electrophoresis (PAGE)	205
5.14.1	Denaturing gel	205
5.14.2	Non-denaturing gel	206
5.15	Autoradiography	207
5.16	Phosphoimagery	208
	Conclusions and future work	209
	References	211

Figures and tables

Figure 1.1	Purine and pyrimidine bases	1
Figure 1.2	Pentose sugars	2
Figure 1.3	<i>Anti</i> and <i>syn</i> orientations of adenosine	2
Figure 1.4	Common sugar puckers	3
Figure 1.5	Four bases linked by 3', 5'-phosphodiester bonds	4
Figure 1.6	H-bonding between complementary base pairs	5
Figure 1.7	Major and minor DNA grooves	6
Figure 1.8	Hairpin structure	7
Figure 1.9	Different DNA conformations	9
Figure 1.10	Tertiary DNA structure	10
Figure 1.11	Solid state ODN synthesis	12
Figure 1.12	Normal gene expression	13
Figure 1.13	Hoogsteen base pairing	16
Figure 1.14	Basis of antisense inhibition	19
Figure 1.15	Antisense ODN modifications	22
Figure 1.16	Creation of <i>bcr-abl</i> oncogene and p210 oncoprotein	25
Figure 1.17	Molecular orbital diagram of energy levels of the principle orbitals and transitions which occur for a Ru(II) octahedral complex	36
Figure 1.18	structures of some common polypyridyl ligands	38
Figure 1.19	Photoadduct formed between $[\text{Ru}(\text{TAP})_3]^{2+}$ and GMP	40
Figure 1.20	$[\text{Ru}(\text{DIP})_2\text{DIP}']\text{-ODN}$ conjugate	44

Figure 1.21	Modified cytidine and thymidine bases	45
Figure 1.22	$[\text{Ru}(\text{phen})_2\text{dppz}]^{2+}$ conjugated to 15mer	47
Figure 1.23	Two ruthenium complexes separated by duplex region	48
Figure 1.24	$[\text{Ru}(\text{TAP})_2(\text{dip})]^{2+}$ tethered to central uracil nucleotide in 17mer ODN	49
Figure 1.25	Phosphoramidite derivative of bipyridine-based linker	51
Figure 1.26	DNA duplex containing internal ruthenium complex	51
Figure 1.27	Ruthenium complex – oligonucleotide conjugate	54
Figure 1.28	$[\text{Ru}(\text{phen})(\text{phen})(\text{dppz})]$ -ODN conjugate	56
Figure 1.29	Ruthenium-derivatised nucleoside	57
Figure 1.30	$[\text{Ru}(\text{bipy})_2(\text{pmbc})](\text{PF}_6)_2$ -derivatised nucleoside	58
Figure 1.31	Ruthenium complex linked to the terminal phosphate via a short ethylene spacer	59
Figure 1.32	Ruthenium-thymidine derivative	60
Figure 1.33	Ruthenium-bridged DNA hairpin	62
Figure 1.34	$[\text{Ru}(\text{phen})_2\text{dppz}]$ -oligonucleotide	63
Figure 1.35	Diagrammatic representation of the model system with the 24mer target and complementary ruthenium-9mer	65
Figure 1.36	Diagrammatic representation of the model system with the 34mer target and complementary ruthenium-17mer	68
Figure 2.1	Diagrammatic representation of electroelution apparatus	82
Figure 2.2	Diagrammatic representation of PAGE apparatus	83
Figure 2.3	Diagrammatic representation of conjugation experiment after	

	UV shadowing	85
Figure 2.4	UV-vis spectrum of conjugate 1	86
Figure 2.5	Structure of [Ru(phen) ₂ phen']-oligonucleotide conjugate	86
Figure 2.6	UV-vis spectrum of conjugate 2	87
Figure 2.7	Structure of [Ru(TAP) ₂ phen']-oligonucleotide conjugate	87
Figure 3.1	Model system of target 34mer and [Ru(phen) ₂ phen']-ODN conjugate	90
Figure 3.2	Mechanism of piperidine treatment at modified nucleobase	93
Figure 3.3	Hydrolysis of RNA under alkaline conditions	94
Figure 3.4	34mer ODN cleavage by [Ru(phen) ₃] ²⁺	96
Figure 3.5	Phosphoimagery results for 34mer ODN with [Ru(phen) ₃] ²⁺ , 10 mM potassium phosphate buffer / 100 mM NaCl, 10 min irradiation	97
Figure 3.6	Phosphoimagery results for 34mer ODN with [Ru(phen) ₃] ²⁺ , 10 mM potassium phosphate buffer, 10 min irradiation	97
Figure 3.7	34mer ODN cleavage by [Ru(phen) ₂ phen'] ²⁺	98
Figure 3.8	Effect of azide and argon on 34mer ODN cleavage with [Ru(phen) ₃] ²⁺	100
Figure 3.9	Effect of azide and argon on 34mer ODN cleavage with [Ru(phen) ₂ phen'] ²⁺	100
Figure 3.10	Phosphoimagery results for 34mer ODN with [Ru(phen) ₂ phen'] ²⁺ , 10 mM potassium phosphate buffer / 100 mM NaCl, 10 min irradiation, S ₂ O ₈ ²⁻	102

Figure 3.11	Comparison of 34mer ODN cleavage by $[\text{Ru}(\text{phen})_2\text{phen}']^{2+}$ in presence and absence of persulfate	102
Figure 3.12	34mer ODN cleavage by $[\text{Ru}(\text{phen})_2\text{phen}']$ -ODN conjugate	105
Figure 3.13	Phosphoimagery results of 34mer ODN cleavage by $[\text{Ru}(\text{phen})_2\text{phen}']$ -ODN after irradiation times of a) 2.5min, b) 5min, c) 10min and d) 20min	106
Figure 3.14	Comparison of G21 cleavage in target 34mer ODN by $[\text{Ru}(\text{phen})_2\text{phen}']$ -ODN in presence and absence of sodium nitrite filter	109
Figure 3.15	Phosphoimagery results for G21 specific cleavage of target 34mer ODN by $[\text{Ru}(\text{phen})_2\text{phen}']$ -ODN after 20 mins irradiation in the absence of sodium nitrite filter	109
Figure 3.16	Phosphoimagery results for G21 specific cleavage of target 34mer ODN by $[\text{Ru}(\text{phen})_2\text{phen}']$ -ODN after 20 mins irradiation in the presence of sodium nitrite filter	110
Figure 3.17	Comparison of 34mer target / $[\text{Ru}(\text{phen})_2\text{phen}']$ -ODN duplex with free 34mer target on non-denaturing gel	112
Figure 3.18	Comparison of G21 cleavage in target 34mer ODN by $[\text{Ru}(\text{phen})_2\text{phen}']$ -ODN conjugate a) with no additions and b) under argon atmosphere	114
Figure 3.19	Comparison of G21 cleavage in target 34mer ODN by $[\text{Ru}(\text{phen})_2\text{phen}']$ -ODN conjugate a) with no additions and b) in D_2O	115

Figure 3.20	Comparison of % G21 cleavage in target 34mer ODN under normal conditions and with inclusion of additions	116
Figure 3.21	Comparison of 34mer target cleavage by [Ru(phen) ₂ phen`]-ODN conjugate in presence and absence of persulfate	117
Figure 3.22	Phosphoimagery results for cleavage of target 34mer ODN by [Ru(phen) ₂ phen`]-ODN after 10 mins irradiation in presence of persulfate	118
Figure 3.23	Comparison of % cleavage in target 34mer ODN by [Ru(phen) ₂ phen`]-ODN in presence and absence of persulfate	119
Figure 3.24	Sequences of original 34mer target and nonsense strands	120
Figure 3.25	Results of nonsense strand experiments in presence of ruthenium-ODN conjugate and free [Ru(phen) ₂ phen`] ²⁺	121
Figure 3.26	Sequences of variant strands 1-6 with region complementary to 17mer ODN of ruthenium-ODN conjugate shown in red	123
Figure 3.27	Results of experiments with variants 1-6 in presence of [Ru(phen) ₂ phen`]-ODN conjugate	124
Figure 3.28	Phosphoimaging results for variants 1-6. Arrows indicate the site and extent of base damage	125
Figure 3.29	Original 34mer hairpin structure	127
Figure 3.30	Sequences of variant strands 1-6 with complementary regions within each strand underlined and double-stranded regions shown in red	127
Figure 3.31	Variant 3 hairpin structure	128

Figure 3.32	Variant 2 hairpin structure	128
Figure 3.33	Variant 4 hairpin structure	129
Figure 3.34	Sequences of original variant 3 and non-hairpinning variant 3	130
Figure 3.35	Comparison of damage induced in $[\text{Ru}(\text{phen})_2\text{phen}']\text{-ODN}$ conjugate in absence and presence of target 34mer ODN	132
Figure 3.36	Structure of ruthenium-ODN conjugate with shorter linker chain	134
Figure 4.1	Model system of target 34mer and $[\text{Ru}(\text{TAP})_2\text{phen}']\text{-ODN}$ conjugate	139
Figure 4.2	Phosphoimaging results for diluted 34mer ODN with $[\text{Ru}(\text{TAP})_2\text{phen}']^{2+}$ (1×10^{-4} M stock solution), 10 mM potassium phosphate buffer after a) 0 min irradiation and b) 20mins irradiation	145
Figure 4.3	Phosphoimaging results for diluted 34mer ODN with $[\text{Ru}(\text{TAP})_2\text{phen}']^{2+}$ (1×10^{-5} M stock solution), 10 mM potassium phosphate buffer after a) 0 min irradiation and b) 20mins irradiation	146
Figure 4.4	34mer target ODN in presence of $[\text{Ru}(\text{TAP})_3]^{2+}$	148
Figure 4.5	Phosphoimaging results for 34mer ODN with $[\text{Ru}(\text{TAP})_3]^{2+}$ (1×10^{-4} M stock solution), 10 mM potassium phosphate buffer after a) 0 min irradiation, b) 5 min irradiation and c) 10 min irradiation	149
Figure 4.6	34mer target ODN in presence of $[\text{Ru}(\text{TAP})_2\text{phen}']^{2+}$	150
Figure 4.7	Phosphoimaging results for 34mer ODN with $[\text{Ru}(\text{TAP})_2\text{phen}']^{2+}$	

	(1 x 10 ⁻⁴ M stock solution), 10 mM potassium phosphate buffer after a) 0 min irradiation, b) 5 min irradiation and c) 10 min irradiation	151
Figure 4.8	Diagrammatic representation of cross-linked ruthenium-conjugate / target 34mer ODN species before and after denaturing gel analysis	154
Figure 4.9	Photoadduct formation between 34mer ODN and [Ru(TAP) ₂ phen ⁻]-ODN	155
Figure 4.10	Phosphoimagery results of 34mer ODN in presence of [Ru(TAP) ₂ phen ⁻]-ODN conjugate after a) 0 mins irradiation and b) 10 mins irradiation	156
Figure 4.11	Comparison of yields of photoadduct formation between target 34mer and [Ru(TAP) ₂ phen ⁻]-ODN conjugate in presence and absence of sodium nitrite filter	159
Figure 4.12	Comparison of 34mer target / [Ru(TAP) ₂ phen ⁻]-ODN duplex with free 34mer target on non-denaturing gel	160
Figure 4.13	Phosphoimagery results comparing non-denaturing results of a) 34mer target only and b) 34mer target ODN in presence of [Ru(TAP) ₂ phen ⁻]-ODN conjugate	161
Figure 4.14	Phosphoimagery results comparing photoadduct formation with target 34mer ODN and [Ru(TAP) ₂ phen ⁻]-ODN conjugate a) with no additions, b) with azide and c) under argon atmosphere	163
Figure 4.15	Phosphoimagery results comparing photoadduct formation with	

	target 34mer ODN and [Ru(TAP) ₂ phen']-ODN conjugate a) with no additions and b) in the presence of D ₂ O	165
Figure 4.16	Comparison of % photoadduct formation with target 34mer ODN and [Ru(TAP) ₂ phen']-ODN conjugate with no additions and in presence of azide, argon and D ₂ O	166
Figure 4.17	Comparison of % photoadduct formation with target 34mer ODN and [Ru(TAP) ₂ phen']-ODN conjugate with no additions and in presence of persulfate and desferrioxamine	168
Figure 4.18	Phosphoimagery results comparing photoadduct formation with target 34mer ODN and [Ru(TAP) ₂ phen']-ODN conjugate a) with no additions and b) in presence of desferrioxamine	168
Figure 4.19	Results of nonsense strand experiments in presence of [Ru(TAP) ₂ phen']-ODN conjugate	170
Figure 4.20	Phosphoimagery results of nonsense strand experiments in the presence of [Ru(TAP) ₂ phen']-ODN conjugate a) with no irradiation and b) after 10 mins irradiation	171
Figure 4.21	Results of experiments with variants 1-6 in presence of [Ru(TAP) ₂ phen']-ODN conjugate	173
Figure 4.22	Crosslinked species formed between original 34mer ODN and [Ru(TAP) ₂ phen']-ODN conjugate	175
Figure 4.23	Comparison of mobility of crosslinked fragments through denaturing gel matrix	176
Figure 4.24	Crosslinked species formed with variant 3	177

Figure 4.25	Faster crosslinked species formed with variant 2	178
Figure 4.26	Slower crosslinked species formed with variant 2	179
Figure 4.27	Faster crosslinked species formed with variant 4	180
Figure 4.28	Results of experiments with non-hairpinning variant 3 in the presence of [Ru(TAP) ₂ phen']-ODN conjugate	182
Scheme 1.6	Phosphoramidite formation from starting hydroxyl group	53
Scheme 1.7	Conversion of alcohol into corresponding phosphonate	55
Scheme 2.1	Synthesis of 5-(4-carboxybutanamido)-1,10-phenanthroline	70
Scheme 2.2	Synthesis of 6-nitroquinoxaline	71
Scheme 2.3	Synthesis of 5-amino-6-nitroquinoxaline	72
Scheme 2.4	Synthesis of 5,6-diaminoquinoxaline	73
Scheme 2.5	Synthesis of 1,4,5,8-tetraazaphenanthrene	74
Scheme 2.6	Synthesis of [Ru(phen) ₂ phen'](PF ₆) ₂	75
Scheme 2.7	Synthesis of [Ru(TAP) ₂ phen'](PF ₆) ₂	77
Scheme 2.8	Conversion of [Ru(phen) ₂ phen'](PF ₆) ₂ and [Ru(TAP) ₂ phen'](PF ₆) ₂ to the corresponding N-hydroxysuccinimido esters	79
Scheme 2.9	Synthesis of ruthenium-oligonucleotide conjugates	80
Table 3.1	Comparison of 34mer cleavage with [Ru(phen) ₃] ²⁺ under high and low salt conditions	97
Table 3.2	Percentage yield of G21 cleavage by [Ru(phen) ₂ phen']-ODN conjugate at different irradiation times	107
Table 3.3	Percentage cleavage by [Ru(phen) ₂ phen']-ODN conjugate at guanine sites in variant strands 1-6	126

Table 3.4 Comparison of cleavage yields seen in variant strands in presence and absence of sodium nitrite filter. Filtered results shown in red 131

Abbreviations

DNA	deoxyribonucleic acid
RNA	ribonucleic acid
ODN	oligodeoxynucleotide
G	guanine
C	cytosine
A	adenine
T	thymine
U	uracil
GMP	guanosine monophosphate
mRNA	messenger ribonucleic acid
rRNA	ribosomal ribonucleic acid
tRNA	transfer ribonucleic acid
PS-ODN	phosphorothioate oligodeoxynucleotide
MP-ODN	methylphosphonate oligodeoxynucleotide
TFO	triplex forming oligodeoxynucleotide
CML	Chronic Myeloid Leukaemia
<i>abl</i>	Abelson gene
<i>bcr</i>	breakpoint cluster region gene
CMV	cytomegalovirus
Ph'	Philadelphia chromosome
BMT	bone marrow transplantation
Ru-ODN	ruthenium-linked 17mer

phen	1,10-phenanthroline
phen'	5-(4-carboxybutanamido)-1,10-phenanthroline
TAP	1,4,5,8-tetraazaphenanthrene
TSU	N, N, N', N'-tetramethyl(succinimido)uronium tetrafluoroborate
HOBt	1-hydroxybenzotriazole
DCC	dicyclohexylcarbodiimide
EDC	N-dimethylaminopropyl-N-ethylcarbodiimide
NHS	N-hydroxysuccinimide
DIPEA	diisopropylethylamine
EDTA	ethylenediaminetetraacetic acid
TBE	tris / borate / EDTA
TEMED	N, N, N', N'-tetramethylethylenediamine
DMT	dimethoxytrityl
PAGE	polyacrylamide gel electrophoresis
PNK	polynucleotide kinase
TdT	terminal deoxynucleotidyl transferase
ATP	adenosine triphosphate
NMR	nuclear magnetic resonance
HPLC	high performance liquid chromatography
TLC	thin layer chromatography
UV/vis	ultra violet / visible
IR	infra red

CHAPTER 1

INTRODUCTION

1.1 Primary structure of nucleic acids

Deoxyribonucleic acid (DNA) and ribonucleic acid (RNA), the hereditary molecules of life, are composed of long linear chains called nucleic acids, the basic unit of which is the nucleotide. Each individual nucleotide consists of a heterocyclic base, a pentose sugar (together referred to as a nucleoside) and a phosphate group *i.e.* a nucleotide is a nucleoside phosphorylated at a free sugar hydroxyl. The heterocyclic bases are pyrimidines (cytosine (C), thymine (T) and uracil (U)) and purines (adenine (A) and guanine (G)) (figure 1.1). The nucleotide sequence is determined by the sequence of individual heterocyclic bases and is referred to as the primary structure of a particular nucleic acid.

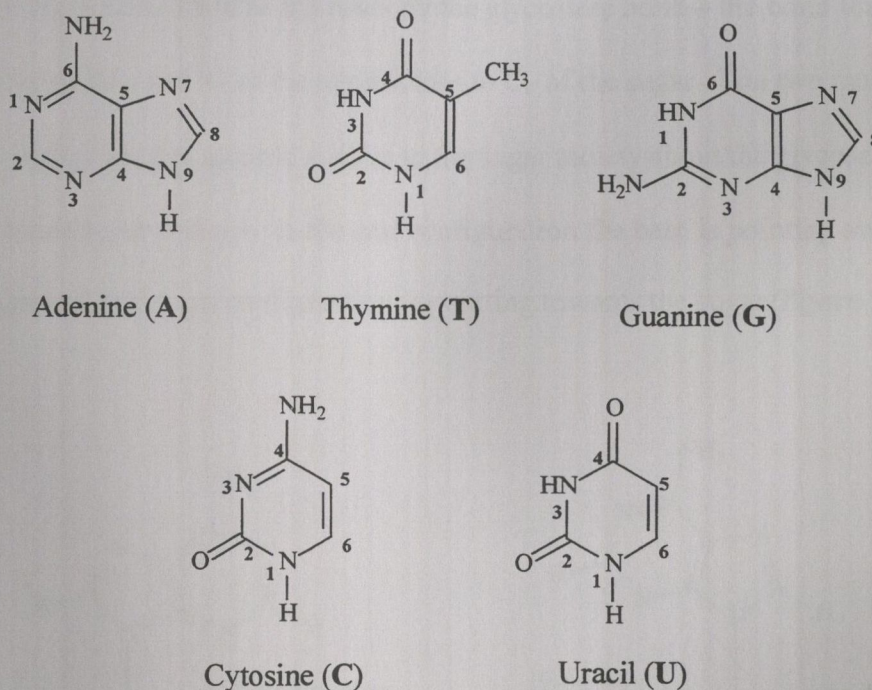


Figure 1.1 Purine and pyrimidine bases

In DNA the sugar component of the nucleotide is the pentose sugar 2'-deoxyribose whereas the sugar moiety in RNA is ribose (**figure 1.2**). Adenine, guanine and cytosine occur in both types of nucleic acid, but thymine (5-methyluracil) found in DNA, is replaced by uracil in RNA.

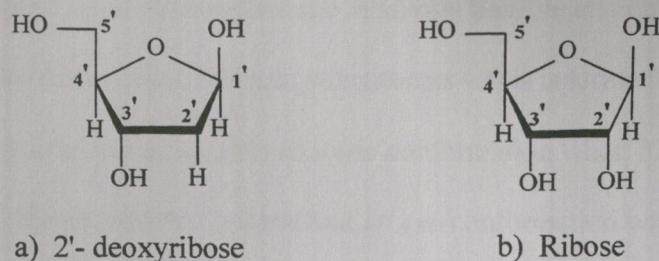


Figure 1.2 Pentose Sugars

The furanose sugars are joined to the bases by the glycosidic bond – the bond that joins N₉ of the purines and N₁ of the pyrimidines to C_{1'} of the sugar. The two main orientations that a base can assume relative to the sugar moiety about the glycosol C_{1'}-N link are termed *anti* and *syn*. In the *anti* configuration the base is pointing away from the sugar and in the *syn* configuration is pointing towards the sugar (**figure 1.3**).

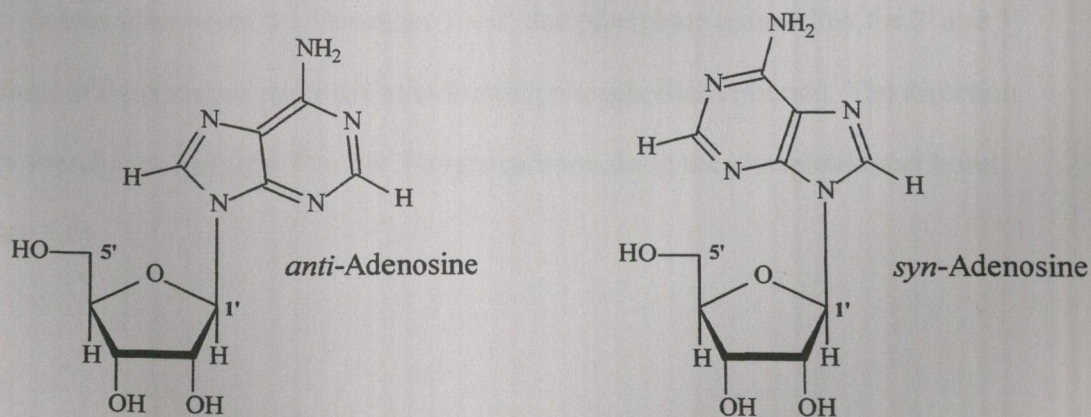


Figure 1.3 *Anti* and *syn* orientations of adenosine

Pyrimidines usually only adopt the *anti* conformation due to the steric interference between the sugar residue and the pyrimidine's C₂ substituent in the *syn* conformation. Purine residues can adopt both *syn* and *anti* conformations. In the majority of double-stranded nucleic acids, the bases adopt the *anti* conformation.

The furanose sugars themselves are relatively flexible and are twisted out-of-plane to minimize interactions between substituents – this is termed sugar puckering. The out-of-plane atom is said to have an *endo* conformation when it is displaced to the same side of the ring as the C_{5'} atom and an *exo* conformation when displaced to the opposite side of the ring from the C_{5'} atom. The two most commonly observed puckers are close to either C_{2'}-*endo* and C_{3'}-*endo* (figure 1.4).

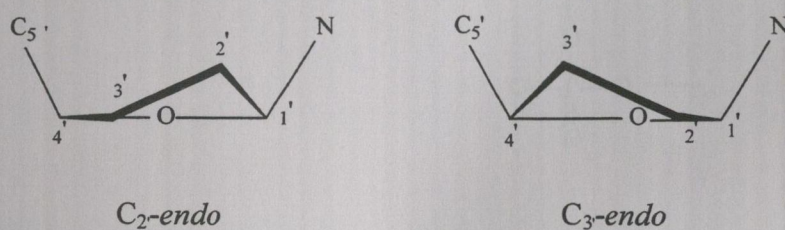


Figure 1.4 Common sugar puckers

It was discovered by Alexander Todd¹ that phosphate groups link the 3' and 5' positions of consecutive sugar moieties forming phosphodiester bonds. The direction of the strand runs from the 5' to the 3'-sugar carbons along the phosphodiester bond (figure 1.5).

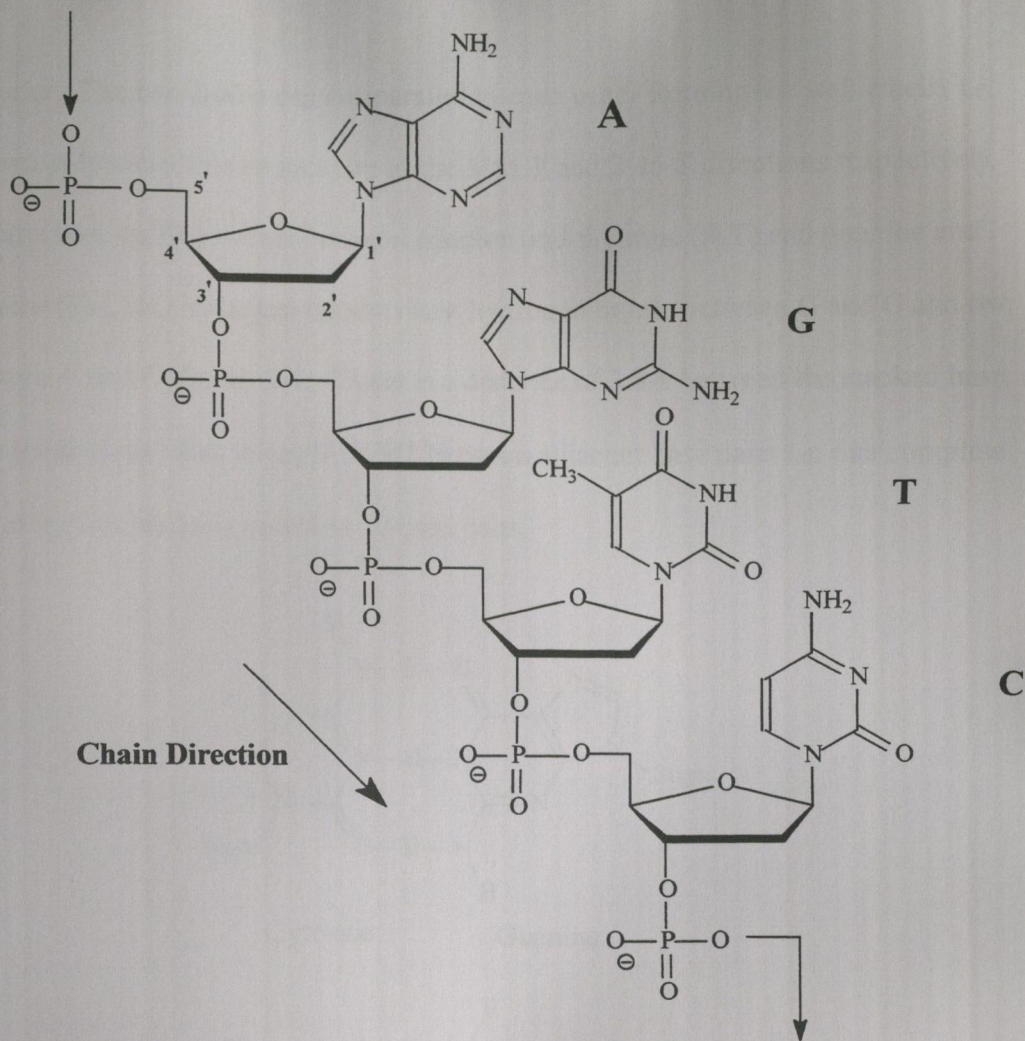


Figure 1.5 Four bases linked by 3',5'-phosphodiester bonds.

1.2 Secondary structure of nucleic acids

This primary structure information, along with Chargaff's² base composition theory which stated that DNA has an equal number of adenine and thymine residues and an equal number of guanine and cytosine residues, led to the eventual elucidation of the famous DNA double-helix structure by Watson and Crick in 1953.³ The secondary structure of DNA consists of two complementary polynucleotide strands coiled around a common axis resulting in a right-handed double helix 20Å in

diameter. The two chains run antiparallel to each other forming the stable helix *i.e.* the two polynucleotide strands run in the 5' to 3' and 3' to 5' directions respectively. Specific base pairing occurs between adenine and thymine (A.T) and guanine and cytosine (G.C) *via* hydrogen bonds; three hydrogen bonds between G and C and two between A and T (**figure 1.6**). There is a distance of 3.4Å between the stacked base pairs (helical rise) and an angle of 36° between adjacent base pairs *i.e.* one complete turn of the double helix contains 10 base pairs.

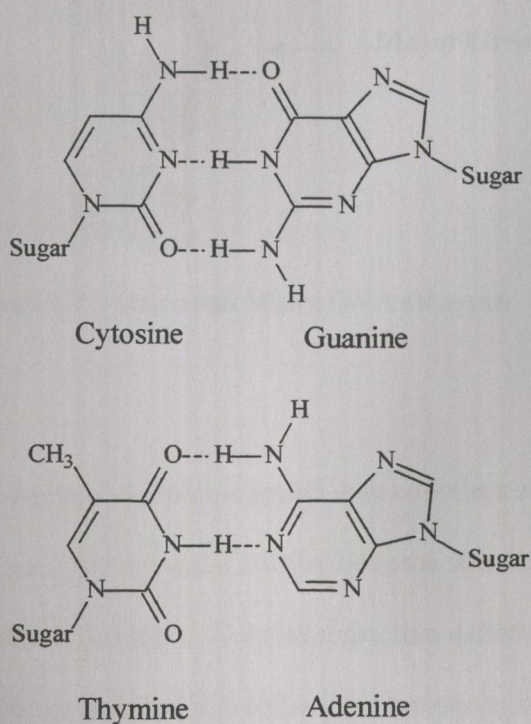


Figure 1.6 H-bonding between complementary base pairs

The hydrophilic sugar-phosphate “backbone” of the helix is to the outside of the molecule with the nitrogenous bases stacked inside the helix, their planes almost perpendicular to the helix axis. The double helices of DNA and RNA contain two

deep spiral grooves known as the major and minor grooves (**figure 1.7**), with the major groove giving more direct access to the bases. The major groove is found at the N7 (purine) or C5 (pyrimidine) side of a base pair with the minor groove located on the opposite side.

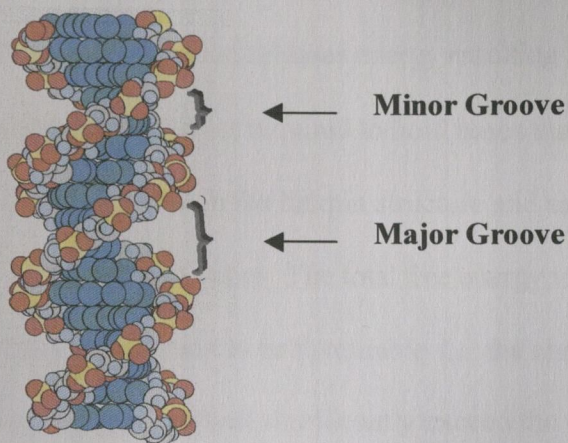


Figure 1.7 Major and Minor DNA Grooves

1.2.1 Hairpins

On occasion, a single nucleotide strand may contain a sequence of bases that is complementary to a nearby sequence within the same strand. The chain may then fold back on itself forming a duplex secondary structure called a hairpin. Hairpins consist of a base-paired double-helical region (also known as the stem) and a loop of unpaired bases at one end (**figure 1.8**). The likelihood of hairpin formation within any given single stranded DNA sequence can be predicted by calculations of the free energy for the formation the hairpin structure with reactions that require energy having a positive free energy value and reactions that release energy having a

negative free energy value. The overall free energy of a hairpin structure is given by the formula:

$$\Delta G_{\text{total}} = \Sigma \Delta G_X + \Sigma \Delta G_Y$$

$\Sigma \Delta G_X$ is the sum of the individual reactions involved in hairpin formation as each base pair is added. Base pair formation releases energy resulting in a negative $\Sigma \Delta G_X$ value. $\Sigma \Delta G_Y$ is the sum of the energies required to hold bases that are not complementary in an unpaired state in the hairpin structure and as energy is required for this process, $\Sigma \Delta G_Y$ is a positive value. The total free energy value must be negative overall for hairpin formation to be favourable *i.e.* the energy released by the individual base pairing in a hairpin must significantly exceed the energy required to maintain the loop (non-complementary regions of a hairpin).

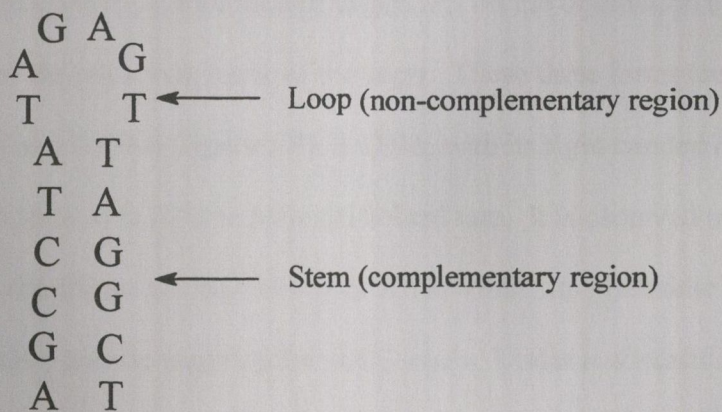


Figure 1.8 Hairpin Structure

1.2.2 DNA melting temperature (T_m)

The double strand helix of a duplex DNA structure can be disrupted when heated and this strand separation is referred to as denaturation or melting. DNA

denaturation can be monitored by UV absorption analysis due to the fact that the DNA absorption value is approximately 40% less than that which would be displayed by a mixture of free nucleotides of the same composition. This observation is known as the hypochromic effect. A decline in this effect is observed in DNA upon heating with the absorption values increasing towards that of the free bases. The melting temperature (T_m) refers to the midpoint of the temperature range over which the DNA is denatured. DNA base composition influences its T_m value. As G.C base pairs are harder to break than A.T base pairs, the more G.C base pairs in a duplex the greater the melting temperature value will be. The melting temperature increases approximately 0.4°C for every 1% increase in G.C content.

1.2.3 Various DNA conformations

DNA can adopt different conformations depending on the orientation of the nucleoside and the puckering mode of the sugar. These three forms are known as B-DNA, A-DNA and Z-DNA (**figure 1.9**). B-DNA, with its right-handed helix, is the most common form with 10 base pairs per helical turn. It is observed under normal physiological conditions *i.e.* high humidity and low salt. Its glycosidic bond has an *anti* conformation and the sugar pucker is C_2' -endo. Under low humidity and high salt conditions, B-DNA can undergo a reversible conformational change forming A-DNA. A-DNA has a flatter and wider right-handed helix than B-DNA with 11 base pairs per helical turn. Like B-DNA its glycosidic bond adopts the *anti* conformation but in this case the sugar pucker is C_3' -endo. A-DNA is found in RNA and RNA-DNA hybrids. Z-DNA, found under high salt conditions, has a left-handed double

helix with 12 base pairs per helical turn. It can be stabilised with a high concentration of NaCl and MgCl₂. Its name is derived from the zigzag line seen between successive phosphate groups around the helix on a strand of Z-DNA. In this form the pyrimidines adopt a C_{2'}-endo sugar pucker and an *anti* glycosidic bond conformation, with the purines adopting a C_{3'}-endo sugar pucker and a *syn* glycosidic bond conformation. To date the biological function and significance of Z-DNA remains unknown.

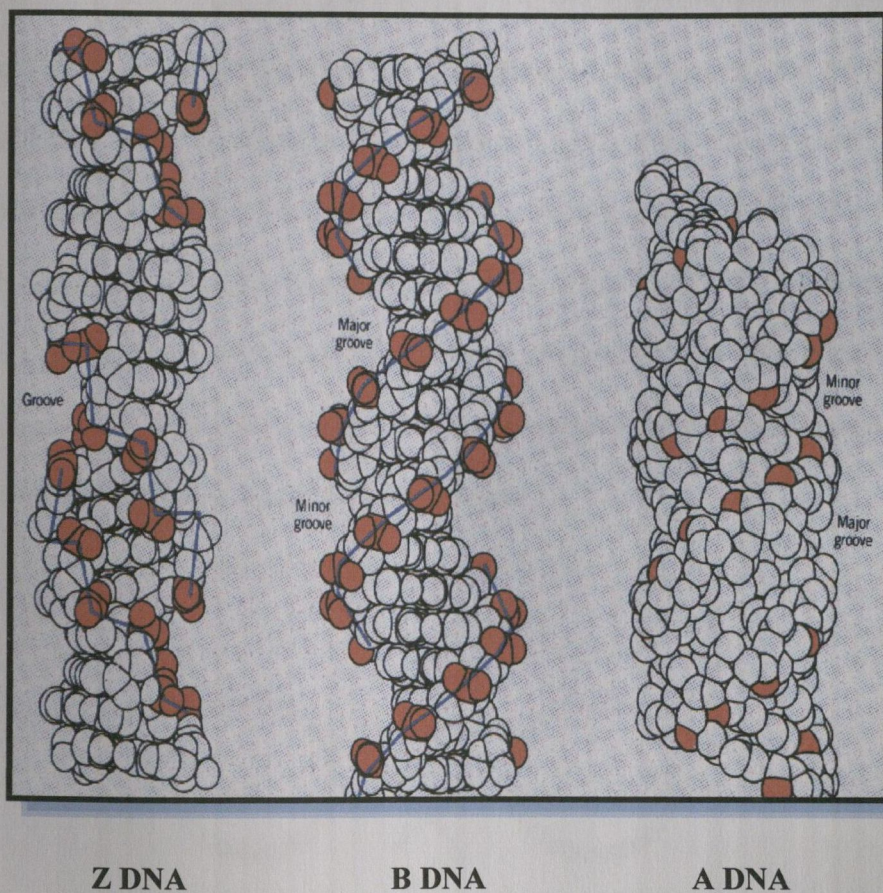


Figure 1.9 Different DNA conformations⁴

1.3 Tertiary structure of nucleic acids

In vivo, many DNA molecules are circular *i.e.* they do not have free 5' or 3' ends. Under normal physiological conditions most circular DNA molecules are supercoiled *i.e.* the DNA duplex is twisted in space around its own axis (the helix crosses over itself one or more times). Supercoiling is necessary to minimise the amount of space occupied by the long double helices. It can only occur in closed structures and any molecule lacking supercoiling, whether closed or open, is described as relaxed. Relaxed and supercoiled DNA, so-called topoisomers, can be interconverted by cutting and resealing the DNA (**figure 1.10**). *In vivo*, the DNA molecules of all organisms exhibit negative supercoiling *i.e.* the DNA is twisted about its own axis in the opposite direction from the right-handed double helix. This type of DNA is said to be underwound. Supercoiling in the same direction as the double helix produces an overwound DNA with positive supercoils. Enzymes called topoisomerases (*e.g.* DNA gyrase in *E.Coli*) are responsible for supercoiling and regulate the superhelicity of natural DNA molecules.

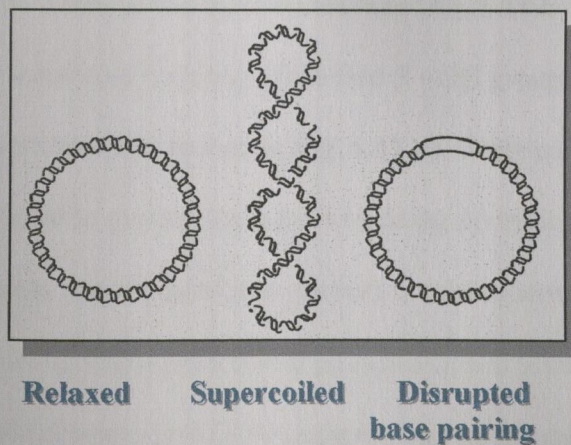


Figure 1.10 Tertiary DNA structure

1.4 Solid state synthesis of oligodeoxynucleotides

Oligodeoxynucleotides (ODNs) are short synthetic pieces of single-stranded DNA of a known sequence. Previous work by groups such as Caruthers *et al.*^{5,6,7} and Itakura *et al.*⁸ has led to the development of solid support based techniques by which ODNs of a defined sequence can be easily synthesised using automated DNA synthesisers. Oligoribonucleotide synthesis is hindered by the presence of the 2' OH group on the ribose sugar that requires selective protection leading to subsequent steric problems during internucleotide linkage formation. The development of silyl-based protecting groups for this 2' position⁹ led to automated RNA synthesis being reported in 1987 by Ogilvie *et al.*¹⁰.

In most cases, solid phase ODN synthesis is carried out by the phosphoramidite method in which the DNA phosphodiester bond is made using phosphoramidite chemistry (**figure 1.11**). Initially the nucleoside chosen to be at the 3' end of the ODN is attached to a solid silica support through its 3' hydroxyl group and the 5' hydroxyl group is protected with dimethoxytrityl (DMT) (**fig. 1.11.a**). The next step involves removal of the DMT group by acid cleavage (**fig. 1.11.b**) and this is followed by tetrazole-catalysed coupling of the free 5' -OH group with the next DMT-protected phosphoramidite monomer (**fig. 1.11.c**). After coupling, unreacted 5'-OH groups are acylated to prevent them from building up truncated oligomer sequences. The trivalent phosphite-triester product is subsequently oxidised using aqueous iodine to the more stable pentavalent phosphotriester state (**fig 1.11.d**). This process is repeated until the required ODN sequence has been synthesised. The last

stage involves removal of all protecting groups, cleavage of the oligomer from the solid support using aqueous ammonia and subsequent PAGE / HPLC purification.

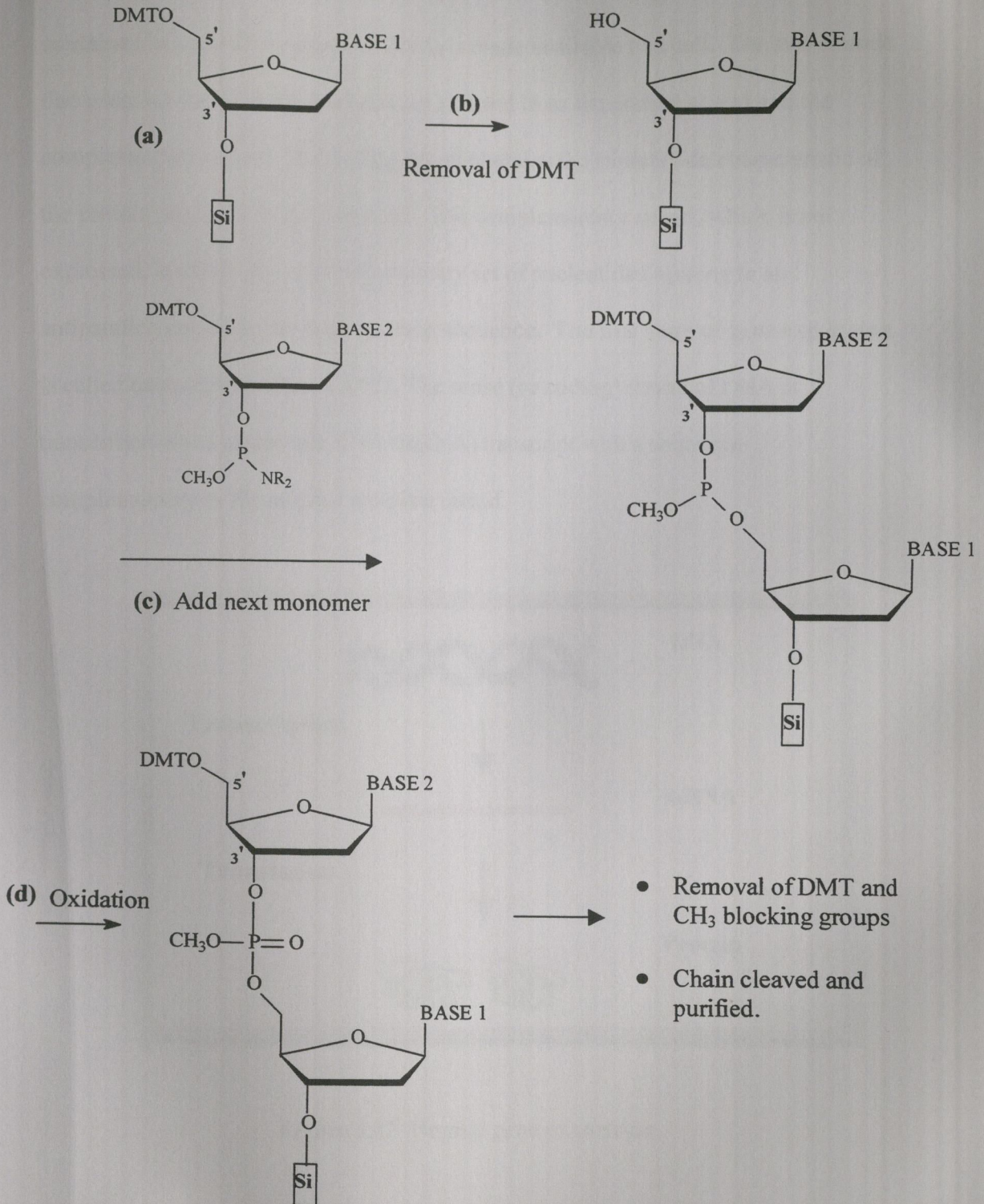


Figure 1.11 Solid State ODN synthesis

1.5 Gene expression

Following the determination of the DNA structure much work including that of Crick^{11,12}, Brenner¹¹ and Yanofsky¹³ showed how the biological information contained in a gene (a segment of DNA) is made available to a cell. The two strands that make up the DNA double helix are referred to as the coding strand and the complementary strand. The coding strand contains the triplet code characteristic of the protein sequence to be expressed. The complementary strand, which is not expressed, is made up of a complementary set of nucleotides running in an antiparallel fashion to the coding strand sequence. The first stage of gene expression is called transcription (**figure 1.12**). The sense (or coding) strand of DNA is transcribed into a messenger RNA (mRNA) transcript with a sequence complementary to the original template strand.

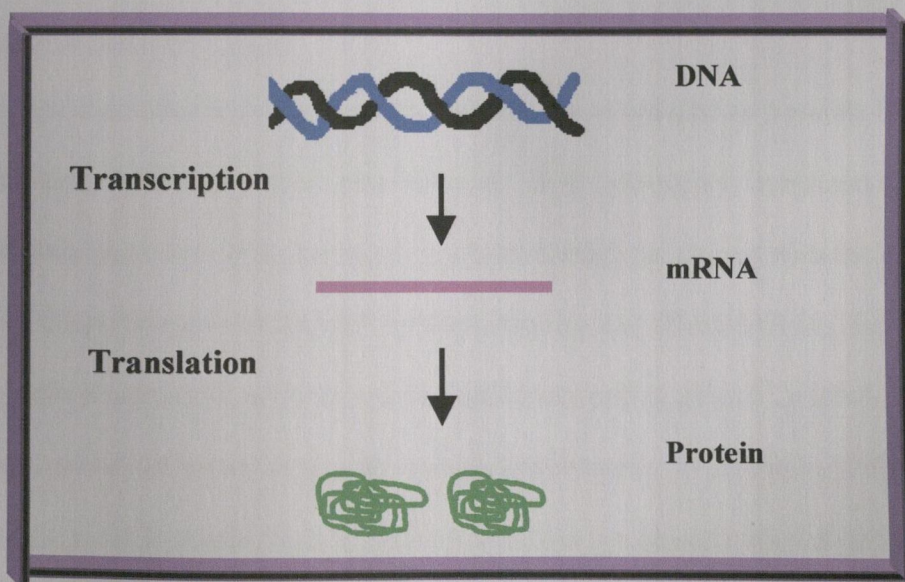


Figure 1.12 Normal gene expression

Three major types of RNA exist; ribosomal RNA (rRNA), transfer RNA (tRNA) and messenger RNA (mRNA). Ribosomal RNA and transfer RNA are the end products of gene expression and they themselves play functional roles in protein synthesis.

Messenger RNA is the only class of RNA that takes part in translation – the second stage of gene expression. In this step the mRNA sequence of bases that is translated into the protein is referred to as the “sense” strand. The nucleotide sequence of the mRNA molecule directs the synthesis of a polypeptide by a complex series of events mediated by both rRNA and tRNA. Polypeptides are composed of amino acids and each triplet of adjacent ribonucleotides on mRNA specifies one amino acid of the polypeptide. Therefore the information contained in a particular gene dictates the composition of the corresponding protein. Elucidation of this knowledge made therapeutic intervention at the level of the nucleic acid possible.

1.6 Targeting of nucleic acids

Ideally, drugs that target DNA or RNA should be as specific as possible for cells containing the disease-causing nucleic acid. Host cytotoxicity continues to be a major problem in modern drug therapy (*e.g.* chemotherapy in cancer) with the vast majority of drugs failing to distinguish between healthy and affected DNA. For example, with bleomycin¹⁴, a DNA-cleaving antibiotic, and cisplatin¹⁵, a DNA-crosslinker, undesired host cytotoxicity remains problematic. In principle, if disease-causing nucleic acids can be targeted exclusively, host cytotoxicity should be kept to a minimum or eliminated completely. Rapid advances in molecular biology over the past couple of decades have led to a greater understanding of genetic mechanisms and

currently several approaches for the therapeutic targeting of nucleic acids are being developed.¹⁶

“Gene therapy” is a broad term referring to the integration of new genetic material into the genome, which is then passed onto the progeny of the manipulated cells minus the defective genes.^{17,18} Inhibition of gene expression at the transcriptional level can be achieved in a number of ways¹⁹ and one such approach, the antigene approach, involves targeting DNA with triple helix forming ODNs thus blocking mRNA production. A third approach, antisense therapy, involves disruption of gene expression at the translational level.

1.6.1 Antigene approach

The antigene approach involves inhibition of gene expression at the transcriptional level *i.e.* the aim is to prevent double-stranded DNA from being transcribed into messenger RNA. This approach is affected using triplex forming oligonucleotides (TFOs) capable of binding to the double-stranded helix forming a triple helix and thus interfering with the transcription mechanism.²⁰

TFOs specifically bind to homopurine regions in the major groove of DNA forming hydrogen bonds with the purine bases. It is possible for thymine in a TFO to form a bond with an adenine already bound to another thymine in the conventional Watson-Crick manner in the double helix. This is also observed for protonated cytosine in a TFO and guanine of a guanine-cytosine Watson-Crick base pair in the double helix. This so-called Hoogsteen base pairing is the bonding pattern observed in triplex formation (**figure 1.13**). Homopyrimidine TFOs bind to the homopurine

region of the duplex in a parallel direction through Hoogsteen hydrogen bonds^{21,22} whereas homopurine TFOs bind antiparallel to the purine region of the duplex *via* reverse Hoogsteen hydrogen bonds.²³

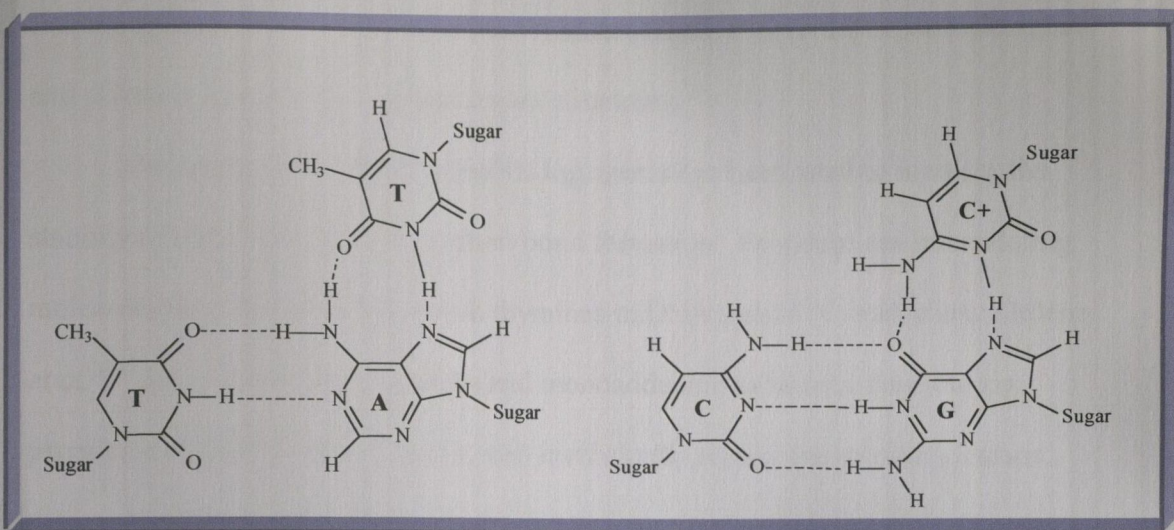


Figure 1.13 Hoogsteen base pairing

In order to form two hydrogen bonds with G in a G.C base pair, cytosine must be protonated. Homopyrimidine ODNs can form stable triple helices at acidic pH but this stability decreases as pH increases therefore a typical pyrimidine TFO will only form a triplex in conditions of pH less than 6 and due to this pH dependency, triplex formation is unstable under normal physiological conditions. Triplex formation with purine TFOs is independent of pH.²⁴

Extensive research has been carried out with a view to increasing the stability of triplex formation whilst retaining the desired target specificity and to overcome the pH dependency of pyrimidine TFO binding.²⁵ Compounds shown to promote triplex formation include anthraquinones²⁶, benzopyridoinole derivatives²⁷ and

benzopyridoquinoxalines. These are tetracyclic aromatic crescent-shaped molecules that interact with the Crick-Hoogsteen base pair of the T.A x T triplet and covalent attachment of these molecules to TFOs has been shown to increase triplex stability.²⁸ Following from this work 6-amino benzoindoloquinoline derivatives were designed and shown to specifically stabilise triplex structures.²⁹

Conjugation of TFOs to crosslinking agents has been used to increase the stability of triplex binding *via* covalent bond formation. Psoralens are intercalating molecules that form cross-links with thymines in DNA upon UV irradiation. Hélène *et al.*^{30,31} have shown that crosslinks and monoadducts can be introduced using psoralen-coupled TFOs and that the cell inefficiently repairs the resulting lesions.

Alkylating agents conjugated to TFOs have also been shown to form cross-links with specific DNA sequences resulting in site-specific cleavage under alkaline conditions. Young *et al.* formed covalent crosslinks between a TFO and the double helix using a TFO into which an alkylating base had been incorporated.³² Dervan *et al.* have reported sequence-specific double strand helix alkylation and cleavage of DNA induced by TFOs with a nondiffusible bromoacetyl electrophile attached at the 5' end.^{33,34,35} The TFO can also be attached to a DNA cleaving agent to achieve site specific cleavage of the target *e.g.* Cu²⁺-phenanthroline conjugates have been shown to achieve duplex strand cleavage.³⁶

Hélène *et al.* have shown that TFOs conjugated to small ligands (*e.g.* benzopyridoinole³⁷ and dibenzophenanthroline³⁸ derivatives) can stabilise triplexes through strong π - π electronic orbital overlap and went on to report a new group of sequence-specific DNA cleaving agents composed of small ligands covalently

attached to ethylenediaminetetraacetic acid (EDTA).^{39,40} Nordèn *et al.*⁴¹ have studied the effect of ligand size on triple strand stabilization using [ruthenium (phen)₂X] complexes, where phen = 1,10-phenanthroline and X = dipyridophenazine (DPPZ) or benzodipyridophenazine (BDPPZ). It was found that the third chelate ligand was responsible for third-strand stabilization in the following order of increasing ability; phen < BDPPZ < DPPZ, therefore not being directly related to ligand size.

1.6.2 Antisense therapy

Modification of gene expression at the translational level is the principle aim of antisense therapy. The target in this approach is a specific region of the mRNA (the sense strand) that has been transcribed from the disease-causing gene of interest and the vectors are referred to as antisense oligodeoxynucleotides (ODNs). An antisense ODN is a synthetic oligonucleotide with a sequence that is complementary to a portion of the targeted mRNA and which binds to the mRNA through Watson-Crick complementary base recognition. Antisense inhibition is effected in two ways. Firstly, mRNA binding by the antisense ODN physically blocks the cell's translation apparatus from synthesising disease-causing proteins in the normal way (**figure 1.14**) and secondly by activation of RNaseH. RNaseH is a ubiquitous cellular enzyme (a ribonuclease) first described by Stein *et al.* in 1970.⁴² It specifically recognises RNA / antisense DNA duplexes and cleaves only the RNA strand of this duplex.⁴³ The antisense ODN is then free to go on to attack further mRNA targets.⁴⁴

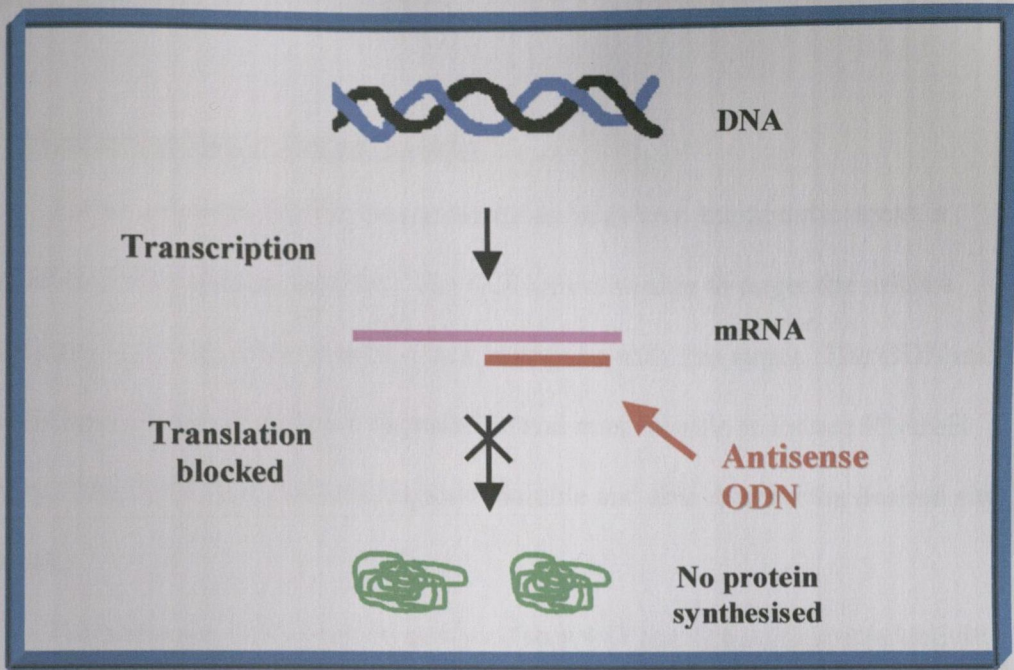


Figure 1.14 Basis of antisense inhibition

Antisense inhibition using an ODN was first seen in 1978 when Zamecnik and Stephenson inhibited Rous virus replication using a 13mer ODN complementary to a portion of the viral RNA.^{45,46} There have been varying degrees of success with antisense therapy despite widespread clinical trials.⁴⁷ The first, and to date the only commercially available antisense ODN for drug therapy was approved by the FDA in August 1998. This phosphorothioate ODN, known as Vitravene, is designed to treat human cytomegalovirus (CMV)-induced retinitis often found in HIV patients.^{48,49}

CMV is a typical human herpesvirus, the term cytomegalo meaning cell of great size, referring to the appearance of the infected cells.⁵⁰

1.7 Modified antisense oligonucleotides

For an antisense ODN to be successful as an *in vivo* therapeutic agent, a number of criteria must be fulfilled. The ODN must be able to target the mRNA specifically and form stable Watson-Crick base pairs with this target. The ODN must be sufficiently stable to nuclease degradation and must be able to induce RNaseH activity. The ODN should also be aqueous soluble and able to enter the desired site of attack.

The antisense ODN must be designed so it will provide sufficient selectivity for the mRNA target and no other random sequence within the human genome. It is generally accepted that an ODN 15-25 bases in length will provide this desired selectivity⁵¹.

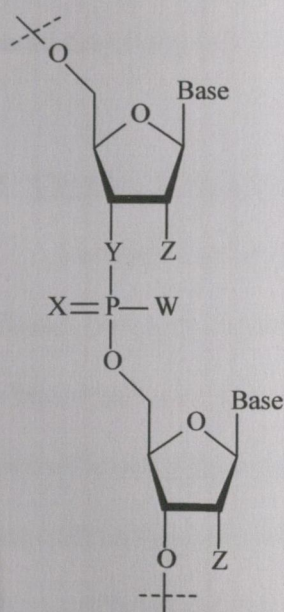
Unmodified natural ODNs containing a phosphodiester backbone (**figure 1.15.a**) form stable Watson-Crick base pairs with RNA targets inducing RNaseH activity, but are quickly degraded by cellular nucleases which target and hydrolyze the phosphodiester linkage. Recently Chattopadhyaya *et al.* have shown that antisense oligonucleotides modified at the 3'-end with phenazine (PZN) and dipyridophenazine (DPPZ) improve the extent of RNaseH promoted hydrolysis compared with the native DNA / RNA counterpart along with increased nuclease resistance.⁵² The large polyanionic nature of the backbone also causes problems with cellular uptake of the antisense ODN. The major obstacles limiting the success of

antisense therapy have been recently reviewed⁵³ and antisense therapeutics are now centered around the synthesis of ODNs with various modifications to improve their *in vivo* therapeutic potential.⁵⁴ A common approach is modification of the antisense ODN phosphodiester backbone to introduce a greater degree of nuclease resistance, while still retaining the ability to arrest mRNA translation.^{55, 56}

Phosphorothioate oligodeoxynucleotides (PS-ODNs) are ODNs in which one of the non-bridging oxygens on the phosphate of the phosphodiester backbone is replaced with a sulfur (**figure 1.15.b**). PS-ODNs are synthesised using standard phosphoramidite chemistry followed by sulfur oxidation of the internucleotide linkage.⁵⁷ They bind to target mRNA with the same affinity as PO-ODNs but are more resistant to nuclease degradation. They also mediate RNaseH degradation of RNA after hybridisation. There is, however, some concern that PS-ODNs can induce non-specific effects from their interaction with cellular proteins.⁵⁸

Like PO-ODNs, PS analogues are also polyanionic and unable to diffuse across the cell membrane. Antisense ODNs must be able to penetrate the membrane in order to down-regulate gene expression. PO- and PS-ODN cellular uptake is thought to take place by pinocytosis,⁵⁹ which results in the ODN compartmentalisation, and further membrane penetration is then needed for any antisense activity.⁶⁰ A solution to this problem has been the introduction of some degree of lipophilicity into the ODN backbone by attachment of various hydrophobic groups to the antisense ODNs to improve cellular uptake. 5' cholesterol-conjugated ODNs⁶¹ and cholesterol-conjugated antisense ODNs⁶² have displayed improved cellular uptake.

Another approach has been the development of neutral isosteres of the phosphodiester linkage – this group of molecules are called methylphosphonates (MP-ODNs). MP-ODNs are ODNs in which the acidic hydroxyl of the PO-linkage is replaced by a methyl group (**figure1.15.c**). These molecules are more lipophilic and are totally nuclease resistant. On the other hand, MP-ODNs do not bind as well to the target strand, they target RNaseH poorly and exhibit poor aqueous solubility.⁶³



Internucleotide Linkage/ Modification	W	X	Y	Z
a) Phosphodiester (PO)	O ⁻	O	O	H
b) Phosphorothioate (PS)	S ⁻	O	O	H
c) Methylphosphonate (MP)	CH ₃	O	O	H
d) PS -2'-O-methyl (alkyl) ribonucleotide	S ⁻	O	O	OCH ₃

Figure 1.15 Antisense ODN modifications

A new direction has been the development of mixed backbone oligonucleotides (MBOs) that contain all the required properties for antisense activity, while at the same time reducing polyanionic- related effects to a minimum.⁶⁴

These modifications are generally combined with a PS-ODN backbone with two

modifications in particular (PS-2'-O- methyl (alkyl) ribonucleotides (**figure 1.15.d**) and methylphosphonate ODNs) having been significant in reducing undesired side effects while still retaining therapeutic activity. The 2' position has been shown to be a useful site for oligonucleotide modifications, improving binding affinity to RNA target and increasing stability, nuclease resistance and lipophilicity. 2' modified ODNs are not capable of inducing RNaseH activity and this has been overcome using antisense ODNs with 2' modifications at the terminal ends only. The resulting unmodified "gap" is capable of inducing RNaseH recognition and cleavage whilst overall the antisense ODN retains the advantages gained from modification.⁶⁵

1.8 Chronic Myeloid Leukaemia (CML)

Leukaemia refers to a group of diseases of the haematopoietic system, the hallmark being an accumulation of abnormally large numbers of white blood cells in the blood and bone marrow. The white blood cells grow at the expense of the red blood cells and platelets leading to symptoms such as anaemia, bleeding and bruising. Stem cells mature into either lymphocytic blood cells (B- and T- lymphocytes) or myeloid cells (all other blood cells) and leukaemias are classified as either myeloid or lymphocytic depending on the type of blood cell involved. CML is one type of leukaemia that affects the myeloid cells. It presents in the chronic (first) stage that can last 3-6 years. This is followed by an accelerated phase where white blood cell production increases rapidly and symptoms worsen. This then proceeds to the final, or blast crisis phase, which is usually resistant to treatment and is almost always fatal.⁶⁶ Myeloablative therapy followed by allogeneic bone marrow transplantation

(BMT) is the standard treatment for leukaemia⁶⁷ and although successful, it is limited by the availability of suitable donors.

Almost all cells (95%) affected by CML possess a chromosome called the Philadelphia chromosome (Ph') thus making them genetically distinct from healthy cells.⁶⁸ The Ph' is a result of a reciprocal translocation (the exchange of pieces of genetic information) between chromosomes 9 and 22; t(9;22). During the t(9;22) translocation the Abelson (*abl*) gene located on chromosome 9 is translocated onto the breakpoint cluster region (*bcr*) gene on chromosome 22 resulting in the chimeric oncogene termed *bcr-abl* (**figure 1.16**). Expression of this *bcr-abl* oncogene gives rise to an abnormal 8.5kb mRNA transcript that encodes for a 210kD fusion protein.⁶⁹ This p210 protein has increased protein tyrosine kinase activity and it has been reported that activation of this kinase is the first step in CML oncogenesis⁷⁰ by possibly blocking affected cells from apoptosis (cell suicide) thus leading to the physical manifestations of CML *i.e.* *bcr-abl* may play a part in suppression of normal apoptotic pathways.⁷¹

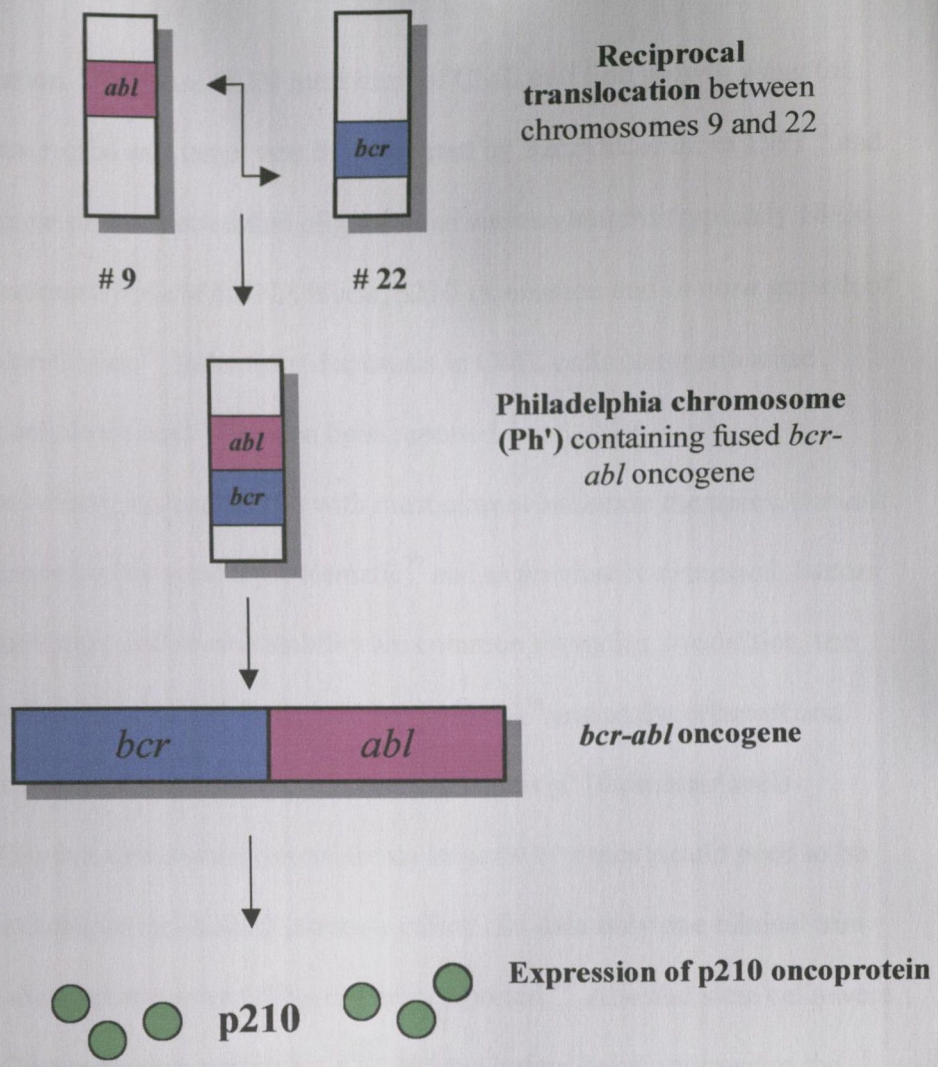


Figure 1.16 Creation of *bcr-abl* oncogene and p210 oncoprotein

The *bcr-abl* oncogene has become a popular antisense ODN target in CML research due to its ubiquitous nature in CML cells, but as the native *bcr* and *abl* genes play important roles in cells themselves it is important that the *bcr-abl* breakpoint region is targeted and not only the *bcr* or *abl* regions on the oncogene.⁷² The ultimate aim using antisense therapy in CML is the optimisation of the down-regulation of

bcr-abl expression. Antisense ODN inhibition of CML cell line growth using the *bcr-abl* junction region as a target was first reported by Szczylik *et al.* in 1991⁷³ and many groups have since reported that oligomers of various lengths (typically 18-26 bases) have decreased *bcr-abl* mRNA levels, p210 expression and *in vitro* growth of CML cells and cell lines.⁷⁴ Induction of apoptosis in CML cells using antisense ODNs⁷⁵ and arachidonic acid⁷⁶ has also been reported.

Despite limited success, and as with most current antisense therapies, *bcr-abl* antisense intervention has proved problematic⁷⁷ and as previously discussed, factors such as cellular uptake and *in vivo* stability are common obstacles. In addition, the p210^{*bcr-abl*} protein has a relatively long half-life (>40hrs)⁷⁸ and as the effect of one antisense treatment wears off after 8-24 hours, this leaves p210 protein levels unchanged. This is a disadvantage considering large ODN doses would need to be administered to achieve the desired antisense effect. To date only one clinical trial using *bcr-abl*-directed antisense ODNs has been reported.⁷⁹ Affected stem cells were treated with a 26mer phosphorothioate ODN *in vitro* before being returned to the patient as an autograft. Transient Ph' negativity was observed in some patients.

1.9 Photocleavage of nucleic acids

There has been much interest in the design and use of chemical agents that can damage and cleave nucleic acids after photochemical activation and their subsequent application to systems where down-regulation of gene expression by photooxidative damage of the target nucleic acid is required. If the chosen molecule

is sensitive to light at wavelengths greater than 300nm it can be selectively excited in the presence of nucleic acids to induce strand damage.⁸⁰

The molecules that absorb a specific wavelength of light are called photocleavage agents or photosensitisers and after absorption of a photon of light, an electron is transferred into a higher orbital thus generating an excited molecule. If the lifetime of the excited species is long enough, it can go on to react with a variety of substrates *e.g.* DNA. Irradiation at a specific wavelength followed by a reaction is referred to as photosensitisation

Photosensitisers can react either directly or indirectly with a nucleic acid target leading to modifications of the target itself and furthermore can react either with the sugars or the nucleobases. In the former case, the photosensitiser can initiate H-atom abstraction from the sugar rings leading to direct cleavage of the strand. More often the latter case is observed with attack occurring at the bases and the extent of cleavage is only observed after hot piperidine (DNA) or aniline (RNA) treatment. Generally if a photosensitiser shows no direct DNA cleavage but does show base-specific piperidine-labile (or aniline-labile) cleavage it can be assumed that nucleobase modification is the main event.

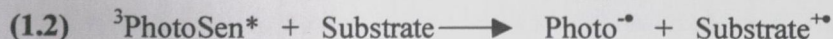
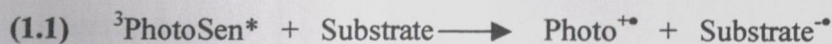
Excitation of a photosensitiser does not change the spin of the electron that is transferred to another orbital thus generating the excited molecule in the so-called singlet state (¹PhotoSen*). Generally the lifetime of excited singlet states are very short (in the range of picoseconds to nanoseconds) and therefore there is a low probability of the molecule reacting with other molecules. Fluorescence is the term that describes the return of an excited state electron to the ground state. Alternately,

the excited singlet state photosensitiser ($^1\text{PhotoSen}^*$) can undergo a spin conversion to a triplet state ($^3\text{PhotoSen}^*$) which has a much longer lifetime relative to the singlet state and is more likely to react with other molecules. Three main pathways exist by which nucleobase photocleavers function:

1. Electron transfer from the base to the excited-state photocleaver.
2. Energy transfer from the excited photocleaver to molecular oxygen ($^3\text{O}_2$) producing singlet oxygen ($^1\text{O}_2$) which then reacts with the base.
3. Adduct formation between the photoexcited compound and base.

1.9.1 Electron transfer (type I damage)

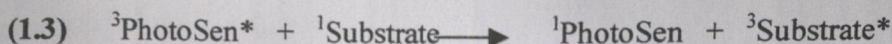
In an electron-transfer pathway, the substrate (nucleobase) is reduced or oxidised by the photosensitiser with the ground state radicals of the photosensitiser and substrate being formed (equations 1.1 & 1.2). The radical cation produced may remove a hydrogen atom from a nearby ribose sugar and induce a direct break in the nucleic acid backbone.



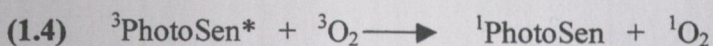
This is often referred to as a type I pathway and will be a localised reaction in the vicinity of photosensitiser excitation unless there can be rapid hole migration through the nucleic acid.

1.9.2 Energy transfer (type II damage)

In an energy-transfer pathway, the excited molecule returns to its ground state and the substrate becomes excited (**equation 1.3**).



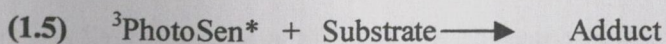
Triplet oxygen (${}^3\text{O}_2$, which is a triplet radical in its ground state) is a good substrate for triplet excited state molecules generating singlet oxygen (${}^1\text{O}_2$) (**equation 1.4**).



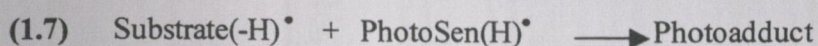
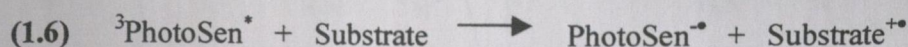
Singlet oxygen reactivity is high enough to directly modify DNA⁸¹ and ${}^1\text{O}_2$ also has a relatively long lifetime of 2-4 μs and can therefore travel several μm in solution before its decay to ${}^3\text{O}_2$. This type of damage is often referred to as type II damage and because of singlet oxygen's ability to travel, base damage is not always localised at the site of photosensitiser excitation.

1.9.3 Adduct formation

In an adduct forming pathway, the photoexcited molecule combines with a substrate and an adduct is formed (**equation 1.5**).



Adduct formation proceeds *via* a type I (electron transfer) pathway. The excited states of certain molecules have been shown to be sufficiently oxidising to undergo electron transfer with nucleobases (**equation 1.6**) and that the photoadduct is formed by combination of the deprotonated radical cation and the protonated reduced photosensitiser^{82,83} (**equation 1.7**):



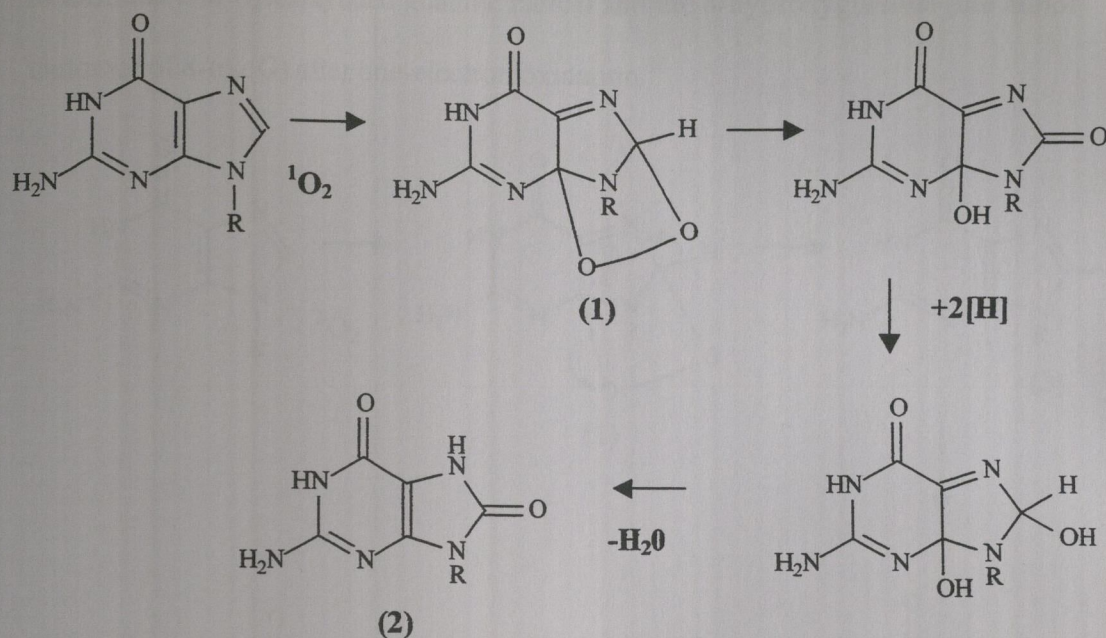
1.10 Guanine oxidation

Guanine has the lowest oxidation potential of all the bases^{84,85} and is generally the preferred site of photooxidative damage as well as being the most reactive towards singlet oxygen.^{81,86} It has been acknowledged that the oxidation potential of guanine in a helical DNA structure may have a slightly lower value than the isolated nucleoside.⁸⁷ In electron and energy transfer pathways, cleavage occurs almost exclusively at guanine sites.

It has been established that 7,8-dihydro-8-oxoguanine (8-oxoG) is a major product of guanine oxidative damage,^{88,89,90} but the mechanism by which it is formed still remains unclear. In the case of singlet oxygen (type II) damage, it has been suggested by Devasagayam *et al.*⁹¹ that ¹O₂ undergoes a [4 + 2] cycloaddition reaction across the imidazole ring of guanine resulting in an unstable endoperoxide

intermediate (1) which is subsequently reduced to yield the 8-oxo product (2)

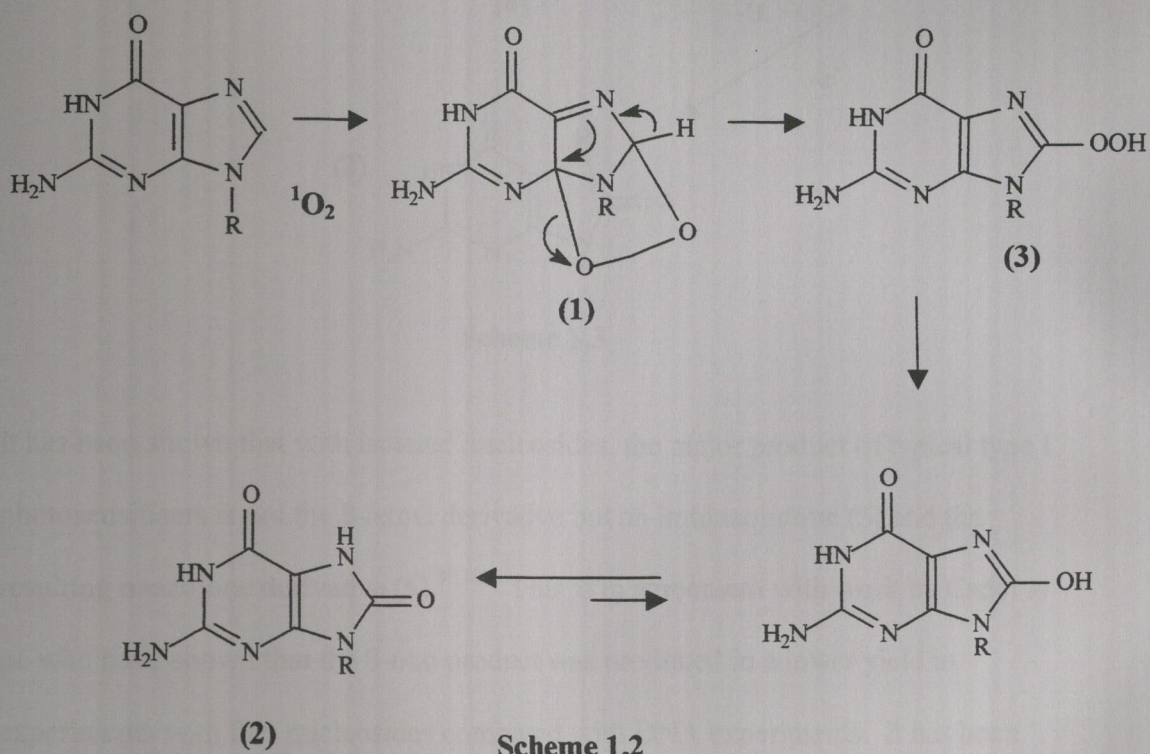
(scheme 1.1).



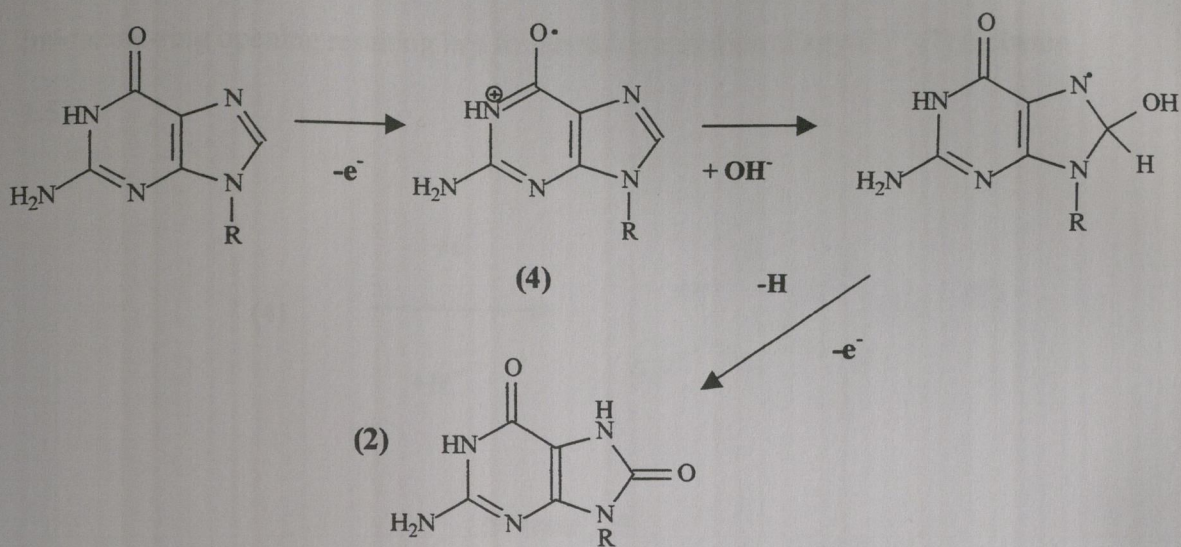
Scheme 1.1

Sheu *et al.*^{92,93} have suggested that the endoperoxide intermediate (1) in type II damage rearranges to form the reactive 8-hydroperoxy product (3). This molecule, being a strong oxidant, is thought to donate an oxygen atom to other oxidisable molecules in the system yielding the final 8-oxo product (2) (scheme 1.2). The same workers characterised the endoperoxide photooxidation product by low-temperature NMR studies using the analogous 8-methylguanosine derivative in which the methyl group at position 8 stabilised the resultant endoperoxide allowing for easier characterisation.⁹⁴

An alternative electron transfer pathway was suggested by Boiteux *et al.*⁹⁵ in which singlet oxygen reacts with guanine as a one electron oxidant forming a guanine radical cation and a superoxide radical anion. The guanine radical cation may go on to form the C-8-hydroxylated guanine radical and the 8-hydroxyguanine (the minor tautomer of 8-oxoG) after one-electron oxidation.⁹⁶

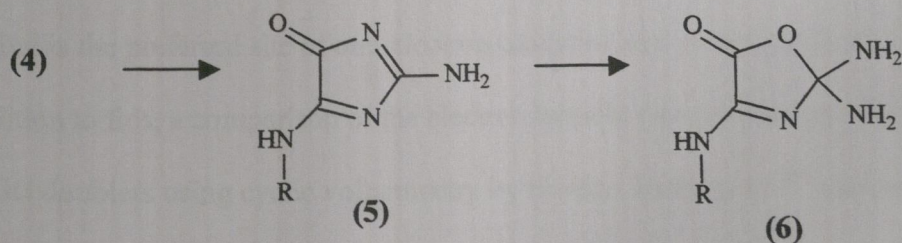


In electron transfer (type I) pathways, 8-oxoG formation is thought to proceed *via* the initial formation of a guanine radical cation (4) followed by its subsequent hydration⁹⁷ (**scheme 1.3**). This has been demonstrated by Cadet *et al.*⁹⁸ in a series of reactions involving photoinduced production of 8-oxoG by riboflavin (a predominantly type I pathway photosensitiser) in calf thymus DNA.



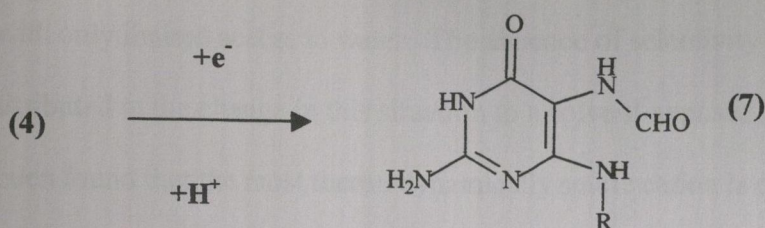
Scheme 1.3

It has been shown that with isolated nucleosides, the major product of typical type I photosensitisers is not the 8-oxoG derivative but an imidazolidone (5) and the resulting oxazolone derivative (6).^{99,100} This is in agreement with work by Cadet *et al.* who have shown that the 8-oxo product was produced in a lower yield in experiments with free nucleosides compared with DNA experiments. It has been postulated that DNA base stacking promotes hydroxylation at C8 of guanine's imidazole ring.¹⁰¹ These products seem to be the result of the deprotonation of the guanine radical cation followed by a rearrangement (**scheme 1.4**).



Scheme 1.4

The 8-hydroxy-7, 8-dihydroguanyl radical has also been shown to stabilise by imidazole-ring opening resulting in a formamidopyrimidine (Fapy-G)⁹⁵ (7) (scheme 1.5).



Scheme 1.5

In conclusion, 8-oxoG is the main photooxidation product of type II damage. Oxazolone and Fapy-G are the major products of type I damage along with some 8-oxoG production.

Reactivity of guanines towards oxidants is sequence sensitive and it has been found that Gs located 5' in a GG doublet are more reactive towards oxidants than those located 3' ¹⁰² (the so-called 5'-GG-3' effect) and has been observed in photochemical reactions in double-stranded DNA ¹⁰³ but is absent in single strands. ¹⁰⁴ Evidence to support this 5' selectivity includes molecular orbital calculations of stacked nucleobases which indicated that a G located 5' to another guanine has a lower ionization potential with the HOMO located mainly on the 5' guanine and therefore is the preferred site of one-electron oxidation and electrophilic attack. ^{103,105} In addition to this, a comparison of the electron transfer rate constants of 5'-G and 3'-G of GG doublets using cyclic voltammetry by Holden Thorp *et al.* ¹⁰⁶ has shown the

5'-G to be approximately 12 times more reactive than the 3'-G. The observation in double strands has been explained by the π -stacking effect of the bases in which an electron is expected to be removed from the 5' G of a purine sequence thus forming the guanine radical cation *i.e.* the radical cation is stabilised by the well-ordered duplex structure with only limited access to water. The absence of selectivity in single strands is attributed to the change in this situation to a solvent-exposed, single strand.¹⁰⁷ It has been found that the most thermodynamically stable cation is one formed in-between two other purines, favourably guanines, therefore the order of reactivity is GGGG > GGG > GG > GA > GT \approx GC. The main site of damage is underlined in each case.¹⁰³

1.11 Photochemical targeting by ruthenium complexes

The development of redox-active transition metal complex oligonucleotide conjugates as vectors in gene therapy and as probes for the study of electron and energy transfer in DNA is an area of intensive research,^{108,109} with the study of ruthenium polypyridyl complex – nucleic acid interactions, as described by the work in this thesis, forming a significant portion of this research.¹¹⁰

1.11.1 General properties of ruthenium (II) complexes

Ruthenium complexes possess a number of characteristics which make them suitable for use in DNA interaction studies; they are photoactive following illumination, absorb in the visible region (in contrast to the UV absorption seen for

nucleic acids), have long-lived luminescent lifetimes (making them useful as photophysical probes) and they are also thermally stable.

Ruthenium complexes also exhibit a certain degree of “tunability” in relation to their redox potentials depending on their attached ligands.¹¹¹ Ruthenium (II) is a d^6 system forming octahedral complexes with bidentate polypyridyl ligands. These ligands are generally colourless with σ - donor orbitals localised on the nitrogen atoms and π - donor and π^* - acceptor orbitals delocalised on the aromatic rings. Irradiation in the visible region results in the singlet MLCT (metal to ligand charge transfer) excited state *i.e.* the promotion of an electron from a π_M metal orbital to the π^* ligand orbital. A ligand centered (LC) excited state arises from promotion of an electron from π_L to π_L^* (figure 1.17).

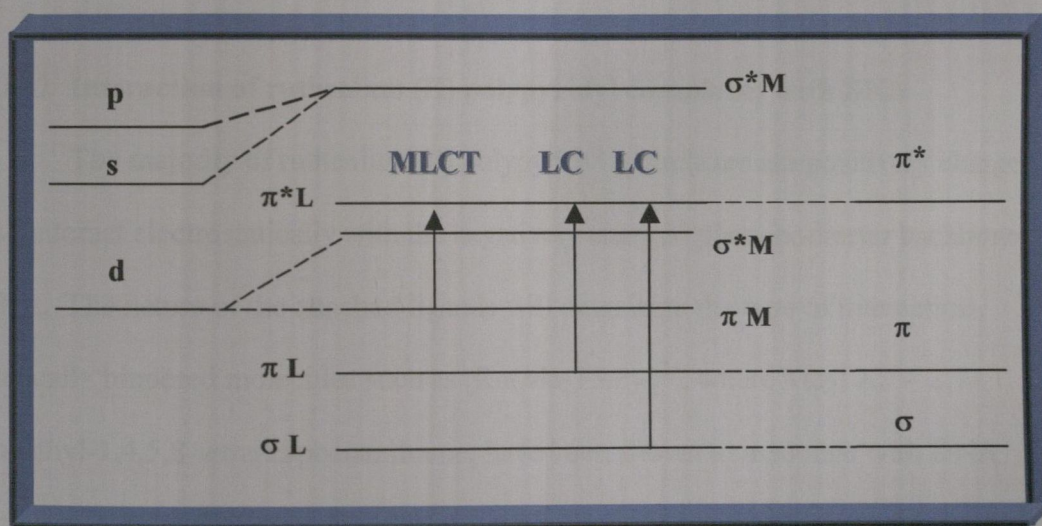


Figure 1.17 Molecular orbital diagram of energy levels of the principle orbitals and transitions which occur for a Ru(II) octahedral complex.

After the population of the $^1\text{MLCT}$ (singlet metal to ligand charge transfer) excited state, rapid deactivation to the $^3\text{MLCT}$ (triplet metal to ligand charge transfer state) occurs by intersystem crossing, and in this state, complex reactivity corresponds mainly to redox processes. Ru(II) complexes are strong oxidants and reductants in the $^3\text{MLCT}$ state.¹¹² The redox properties of Ru (II) complexes are influenced by the nature of the attached ligands. Complexes with strong π -acceptor ligands stabilise the filled metal orbitals resulting in high oxidation potentials *i.e.* complexes with two or three π -acceptor ligands are the most likely to abstract electrons (are the most oxidising) in the excited state.¹¹³

The absorption spectrum of Ru (II) polypyridyl complexes exhibit two main absorptions; an intra-ligand $\pi \rightarrow \pi^*$ transition (LC) in the UV region (<300nm) and a $d \rightarrow \pi^*$ MLCT transition in the 400 – 500nm region.¹¹⁴

1.11.2 Interaction of ruthenium (II) polypyridyl complexes with DNA

The majority of ruthenium (II) polypyridyl complexes are positively charged and interact electrostatically with the negatively charged phosphodiester backbone of DNA. The nature of the attached ligands will determine the type of interaction. Sterically hindered molecules such as $[\text{Ru}(\text{Me}_2\text{TAP})_3]^{2+}$, where $\text{Me}_2\text{TAP} = 2,7$ -dimethyl-1,4,5,8-tetraazaphenanthrene, have been shown to associate with DNA through electrostatic interactions and not through interaction with the nucleobases,¹¹⁵ whereas smaller and less sterically hindered molecules such as $[\text{Ru}(\text{TAP})_3]^{2+}$, where $\text{TAP} = 1,4, 5, 8$ -tetraazaphenanthrene, may enter the major or minor grooves of the DNA duplex.¹¹⁶ Another possibility for binding is intercalation of a planar part of the

molecule between the DNA base pairs. It has been shown for $[\text{Ru}(\text{phen})_3]^{2+}$, where phen = 1,10-phenanthroline, that one ligand may be partially intercalated between the nucleobases but for $[\text{Ru}(\text{bipy})_3]^{2+}$, where bipy = 2,2'-bipyridine, that there is insufficient π -electron overlap to effect this type of binding.¹¹¹ Many ruthenium complexes have been shown unambiguously to associate with DNA in an intercalative manner. Examples include $[\text{Ru}(\text{phen})_2\text{DPPZ}]^{2+}$, where DPPZ = dipyrido[3,2- α :2',3'- c]phenazine¹¹⁷ and $[\text{Ru}(\text{phen})_2\text{PHEHAT}]^{2+}$, where PHEHAT = 1,10-phenanthroline[5,6- b]-1,4,5,8,9,12-hexaazatriphenylene,¹¹⁸ with the planar DPPZ and PHEHAT ligands inserted between the base pairs.

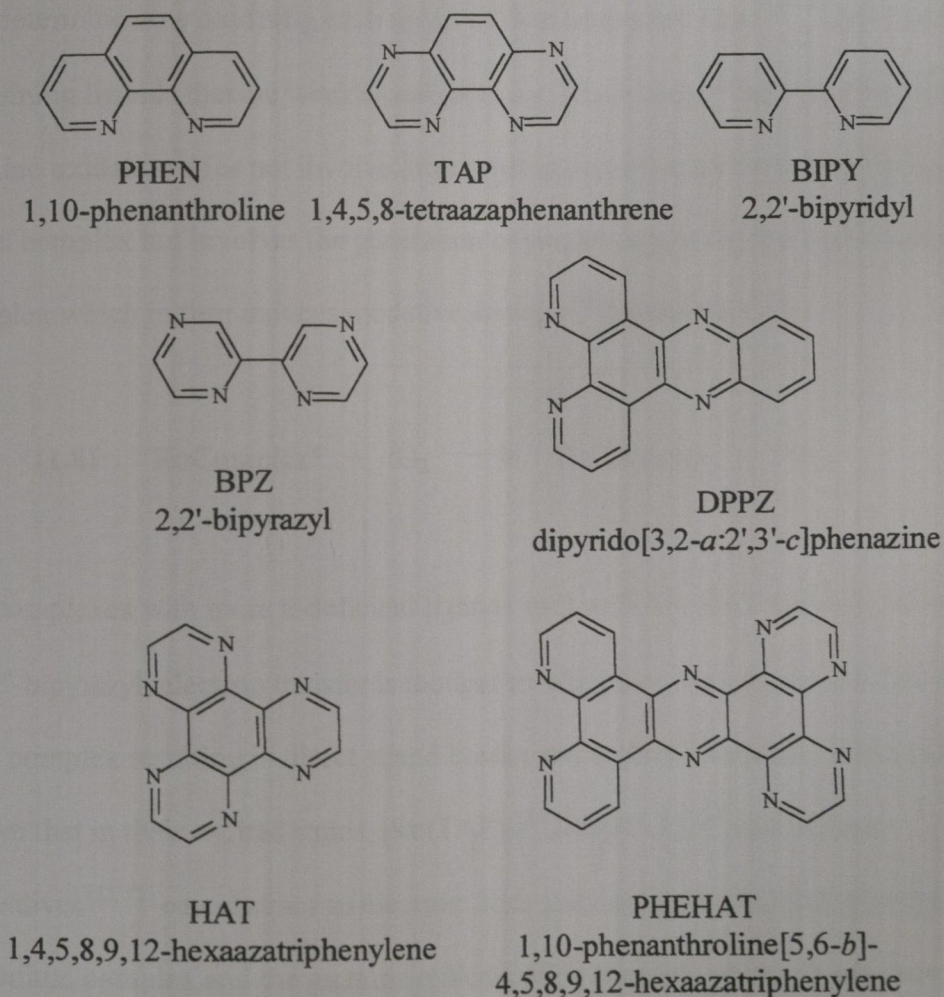
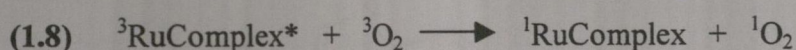


Figure 1.18 Structures of some common polypyridyl ligands

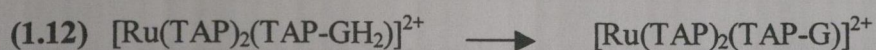
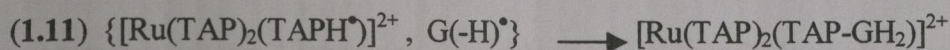
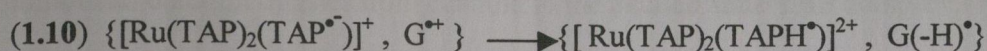
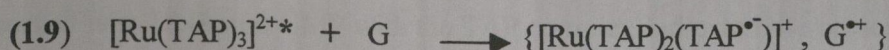
The binding affinity of the bifunctional ruthenium (II) complex $[\text{Ru}(\text{TAP})_2\text{POQ}]^{2+}$ was studied, where the POQ ligand refers to an aminochloroquinoline unit linked to an aminophenanthroline ligand through an amide bond. The binding affinity of the ruthenium complex linked to the aminochloroquinoline by the flexible chain was compared to the “mother” $[\text{Ru}(\text{TAP})_2\text{phen}]^{2+}$ complex and it was found that the addition of the aminochloroquinoline moiety increased the binding affinity of the bifunctional complex for DNA.¹¹⁹

The nature of the attached ligands in a ruthenium (II) polypyridyl complex will also affect the photoreactivity of the complex. The particular choice of ligands will determine how oxidising each complex is in its excited state.¹²⁰ For complexes containing ligands that are weak π -acceptors *e.g.* $[\text{Ru}(\text{phen})_3]^{2+}$ and $[\text{Ru}(\text{bipy})_3]^{2+}$, guanine oxidation does not involve direct abstraction of an electron from the guanine to the complex but involves the generation of singlet oxygen by the excited state complex which in turn induces oxidative damage¹²¹ (**equation 1.8**):



For complexes with more π -deficient ligands such as TAP, HAT and bpz, where bpz = 2,2'-bipyrazyl, electron transfer is thought to take place from guanine to the excited state complex resulting in direct strand breaks and adduct formation. It has been shown that in their excited states, $[\text{Ru}(\text{TAP})_3]^{2+}$, $[\text{Ru}(\text{HAT})_3]^{2+}$ and various derivatives^{122, 123} can abstract an electron from guanine producing the reduced ruthenium complex and the guanine radical cation (**equation 1.9**). It has been

proposed that the final photoadduct is formed by protonation of the reduced ruthenium complex (**equation 1.10**) and combination with the deprotonated guanine radical cation (**equation 1.11**) followed by rearomatisation by loss of two hydrogen atoms to give the final photoadduct product (**equation 1.12**):



It has been shown that photoaddition of $[\text{Ru}(\text{TAP})_3]^{2+}$ on guanosine monophosphate (GMP) takes place between the C-2 of one TAP ligand and the exocyclic amino group of the guanine nucleobase¹²⁴ (**figure 1.19**):

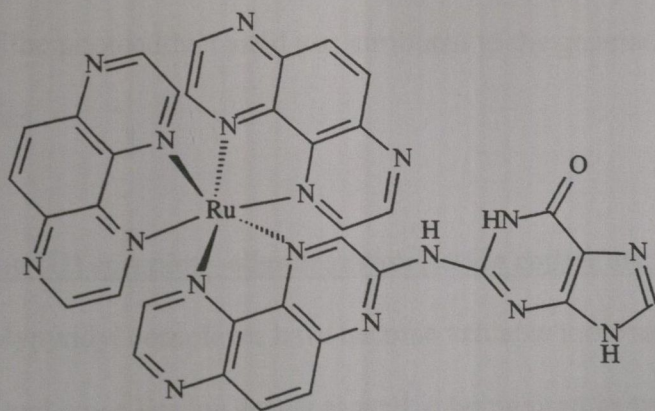


Figure 1.19 Photoadduct formed between $[\text{Ru}(\text{TAP})_3]^{2+}$ and GMP

Jacquet *et al.*⁸³ subsequently isolated and characterised the photoadduct formed between $[\text{Ru}(\text{TAP})_2\text{bpy}]^{2+}$ and calf-thymus DNA showing the adduct was formed between one TAP ligand and the NH_2 group on guanine.

Moucheron *et al.*¹²⁵ carried out photophysical studies on the two ruthenium complexes $[\text{Ru}(\text{phen})_2\text{PHEHAT}]^{2+}$ and $[\text{Ru}(\text{TAP})_2\text{PHEHAT}]^{2+}$. Emission quenching observed with DNA and GMP with the TAP complex indicated the presence of photoinduced electron transfer from guanine to the excited state TAP complex. No such photoinduced electron transfer behavior was observed with the analogous phenanthroline system. Vicendo *et al.*^{126,127} have shown that $[\text{Ru}(\text{bpz})_3]^{2+}$ is capable of photoadduct formation with both single and double stranded oligonucleotides, citing electron transfer from the guanine to the excited state complex as the principle DNA damaging process. The yield of photoadduct production was seen to increase significantly upon inclusion of Cu / Zn superoxide dismutase (SOD). The oxidation potential of SOD is lower than that of guanine, and this may contribute to electron transfer from SOD to excited $[\text{Ru}(\text{bpz})_3]^{2+}$ generating the $[\text{Ru}(\text{bpz})_3]^+$ species. The enhancement of the photoadduct yield was attributed to the generation of this +1 ruthenium species.

1.12 Ruthenium (II) complex –oligodeoxynucleotide conjugates

Ru (II) polypyridyl complexes have become valuable tools as DNA and RNA cleaving agents and cross-linking agents as well as being used in studies of energy- and electron- transfer in DNA¹²⁸ and these qualities have made them very applicable to the area of gene therapy. As discussed in section 1.6, gene therapy involves

targeting a specific sequence or site on the gene of interest resulting in inhibition of its regular function. Oligodeoxynucleotides (ODNs) with a sequence complementary to the region of interest are generally the vectors of choice in this type of work, but ODNs labeled with metallo-complexes such as Ru (II) polypyridyl complexes, are an area of growing interest. The photochemical properties of the ruthenium complex can be exploited once the sequence of interest has been targeted causing photooxidative damage or photoadduct formation at the chosen target site. In this way the labeled metallo-oligodeoxynucleotides enhance the inhibitory effect seen using the ODN on its own. These conjugates have shown potential in both therapeutic and diagnostic applications.

1.13 Synthesis of ruthenium (II)- oligodeoxynucleotide conjugates

Due to the importance of specificity and proximity with the target of choice, it is vital that the ruthenium complex is tethered to the oligonucleotide in such a way that interaction between the target sequence and the Ru-ODN conjugate is optimal. Varying the attachment site of the ruthenium complex on the oligonucleotide or the manner in which it is linked to the oligonucleotide can have a profound effect on the final system and as a result there has been growing interest in the synthesis of ruthenium-oligonucleotide conjugates. Presently there are two main routes by which ruthenium-oligonucleotide conjugates are synthesised. The first route involves attachment of the ruthenium complex to the functionalised oligodeoxynucleotide after the solid-phase synthesis on an automated DNA synthesiser. The second route involves the synthesis of the phosphoramidite derivative of the ruthenium complex

and its subsequent incorporation into the oligodeoxynucleotide chain during the course of the solid-phase synthesis.

1.13.1 Post-solid phase oligodeoxynucleotide modification

When a ruthenium complex is tethered to an oligodeoxynucleotide using this approach, the initial step involves the incorporation of a functional group onto a specific position on the oligonucleotide during the solid-phase synthesis. This is then followed by reaction of the ruthenium complex with the functionalised oligonucleotide in solution.

Bannwarth *et al.*¹²⁹ synthesised various complexes of the type $[\text{Ru}(\text{DIP})_2(\text{DIP}')]^{2+}$ (where DIP = 4,7 -dipenylphenanthroline and DIP' refers to a modified DIP ligand bearing a carboxylic acid functional group with an alkyl spacer chain of a specific length). The complexes were converted to the corresponding N-hydroxysuccinimido esters using N, N, N', N' - tetramethyl(succinimido)uronium tetrafluoroborate (TSU) with a view to direct reaction with 5'-amino functionalised oligonucleotides. The 5'-amino group was introduced in two ways. Firstly, the phosphoramidite of 5'-amino-5'-deoxythymidine was introduced as a building block at the end of the oligodeoxynucleotide solid-phase synthesis to produce the 5'-amino modified oligonucleotide where the 5'-terminal OH group has been replaced by an NH₂ group. Secondly the oligonucleotide was 5'-end modified with (2-cyanoethyl)[(diisopropyl)amino]{3-[(4-methoxytrityl)amino]propoxy} phosphine which resulted in replacement of the 5'-terminal OH group with H₂N(CH₂)₃OPO₃⁻ *i.e.* 5'-NH₂ modified with a spacer group between the amino group and the

oligonucleotide fragment. After synthesis, the 5'-NH₂ modified oligonucleotides were cleaved from the solid-phase column, deprotected and dialysed against KCl to replace and NH₄⁺ ions with K⁺ ions that might interfere with the final coupling reaction. The activated esters of the ruthenium complexes were coupled in solution with the 5'-modified oligonucleotides and the final ruthenium-oligonucleotide conjugates (**figure 1.20**) were isolated using reverse-phase HPLC. Initial studies with the conjugates showed that the presence of the ruthenium complex had no effect on the oligonucleotide's ability to hybridise specifically to single-stranded complementary sequences.

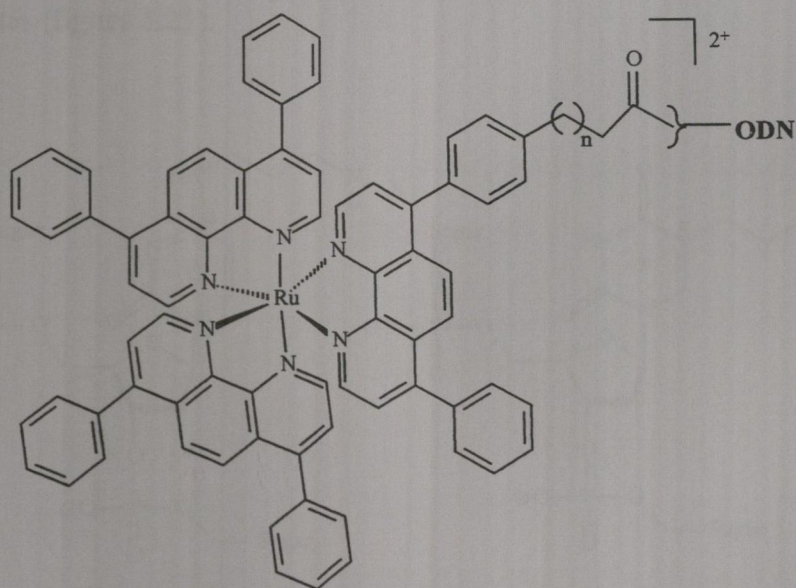


Figure 1.20 [Ru(DIP)₂(DIP')]-ODN conjugate

Telser *et al.*¹³⁰ also reported the synthesis of ruthenium-oligonucleotides involving post-solid-phase modification of the oligonucleotide. A linker arm terminating in a primary amine was attached to both cytidine and thymidine

nucleosides. They were both then subsequently converted to their phosphoramidites and included in the automated synthesis of the oligonucleotides resulting in two octamers containing a modified cytidine and a modified thymidine respectively, within the octamer sequence. Purification and isolation was achieved using reverse-phase HPLC. The ligand 4-carboxy-4'-methyl-2,2'-bipyridine was synthesised, converted to its succinimido ester and reacted in solution with the C- or T-modified octamer to give the corresponding bipyridine-labeled octamers. The bipyridine-labeled octamers were then reacted in solution with $[\text{Ru}(\text{bipy})_2(\text{H}_2\text{O})_2]^{2+}$ followed by desalting and reverse-phase HPLC purification to produce oligonucleotides containing a derivative of $[\text{Ru}(\text{bpy})_3]^{2+}$ attached at either the C⁵ thymidine or C⁴ cytidine sites (**figure 1.21**).

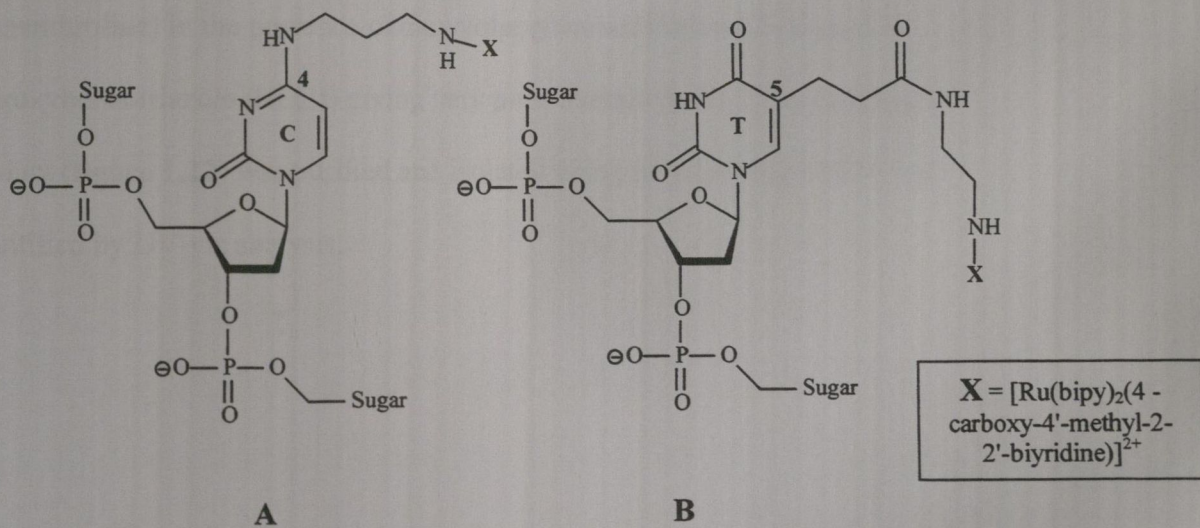


Figure 1.21 Modified cytidine (**A**) and thymidine (**B**) bases

Melting temperature studies on the effect of the ruthenium label on duplex formation of the octamer with its complementary strand found the thymidine-modified system formed a more stable duplex than the cytidine-modified system. A cytidine-modified system with no ruthenium label exhibited "normal" melting curve behaviour, indicating that the attachment of the linkage to the amino group involved in Watson-Crick base-pairing, may interfere with the normal duplex formation in the labeled system.

Barton *et al.*¹³¹ reported the coupling of a ruthenium (II) dipyrrophenazine complex to a 5'-end functionalised 15mer oligonucleotide. The oligonucleotide was synthesised on an automated synthesiser with a hexylamino group $-(\text{CH}_2)_6\text{-NH}_2-$ at the 5'-end. The oligonucleotide was cleaved from the solid support and coupled in solution with $[\text{Ru}(\text{phen}')_2\text{dppz}]^{2+}$ (where phen' = 5-(4-carboxybutanamido)-1,10-phenanthroline) in the presence of dicyclohexylcarbodiimide (DCC) and 1-hydroxybenzotriazole (HOBt) giving very poor overall yields. The conjugated product (**figure 1.22**) was purified and isolated using reverse-phase HPLC and quantified by UV-vis analysis.

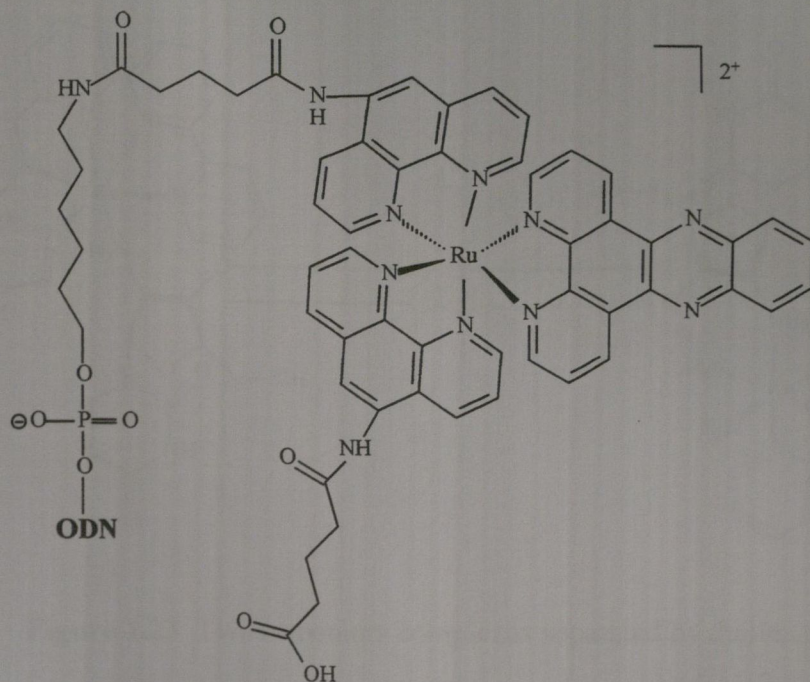


Figure 1.22 $[\text{Ru}(\text{phen}')_2\text{dppz}]^{2+}$ conjugated to 15mer

Addition of the complementary 15mer sequence to the ruthenium-labeled oligonucleotide showed intense luminescence in comparison to the single strand conjugate alone, indicating the use of the conjugate as a type of “molecular light switch” in the presence of the complementary sequence. The intense luminescence has been attributed to intercalation of the dppz ligand into the double helix formed between the conjugate single strand and its complementary strand.

Meade *et al.*¹³² have reported an approach for the preparation of ruthenium-labeled duplex DNA derivatives where the duplex consists of two individual ruthenium-oligonucleotide conjugates with each complex attached to a primary amino at the 2'-position of the 5'-terminal ribose on complementary strands, hybridised together resulting in two ruthenium complexes separated by eight base pairs (**figure 1.23**).

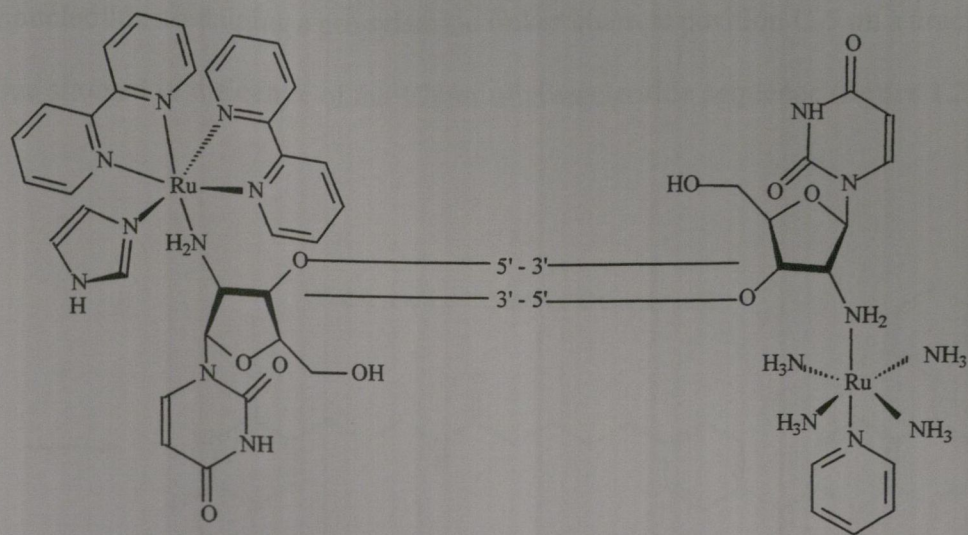


Figure 1.23 Two ruthenium complexes separated by duplex region

Using standard phosphoramidite chemistry, a phosphoramidite-derivatised uracil nucleoside bearing a 2'-amino group was introduced as the 5'-terminal base in an octamer and was then annealed to its complementary sequence before reaction with $[\text{Ru}(\text{bipy})_2\text{CO}_3]$ followed by imidazole. The complementary strand served as a large hydrogen-bonded blocking group to protect the other bases from attack by the ruthenium complex. The ruthenium-oligonucleotide conjugate was isolated by reverse-phase HPLC. The procedure was repeated tethering $[\text{Ru}(\text{NH}_3)_4(\text{py})]^{2+}$ to the complementary octamer. Annealing of the two conjugates gave the desired duplex bearing the two ruthenium complexes at alternate ends. The modified duplex had a melting temperature approximately 8°C lower than the unmodified duplex. The group went on to use the system for electron transfer studies through DNA.

Ortmans *et al.*¹³³ synthesised ruthenium-labeled oligonucleotide conjugates in which the ruthenium complex was tethered to an amino-modified 17mer

oligonucleotide containing a propylamine linker chain at position C-5 on a uracil residue situated in the centre of the 17mer oligonucleotide sequence (**figure 1.24**).

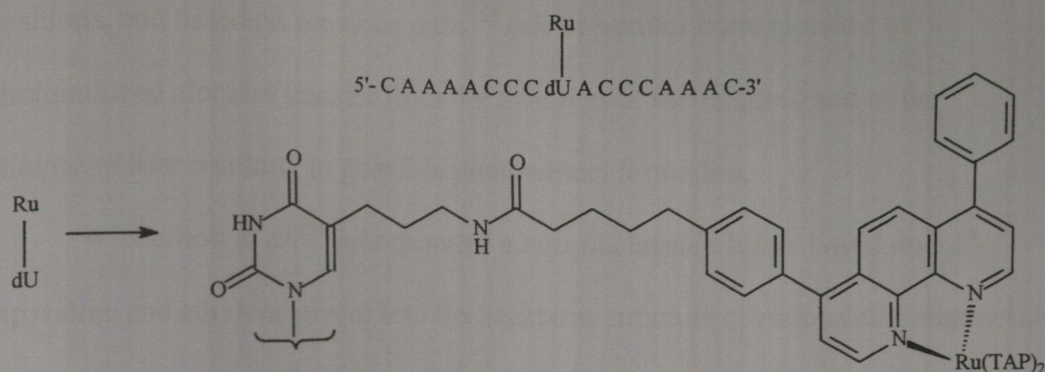


Figure 1.24 $[\text{Ru}(\text{TAP})_2(\text{dip}')]^{2+}$ tethered to central uracil nucleotide in 17mer ODN

Initially the modified uracil phosphoramidite precursor containing the propylamine chain was synthesised with the amino group protected by a Fmoc group. The phosphoramidite of 5'-aminopropyl-2'-deoxyuridine was introduced as one of the building blocks in the final automated synthesis of the 17mer oligonucleotide. The ODN was then cleaved from the solid support, deprotected and treated with KCl to replace NH_4^+ ions by K^+ ions. The ruthenium complex $[\text{Ru}(\text{TAP})_2(\text{dip}')]^{2+}$ (where dip' is a 4,7-diphenylphenanthroline ligand functionalised with a carboxylic acid) was activated to the corresponding succinimido ester using TSU and then reacted in solution with the modified oligonucleotide. The coupled product was purified by polyacrylamide gel electrophoresis (PAGE) and characterised by electrospray (ES) mass spectrometry having been obtained in yields of approximately 20%. Melting temperature studies of the conjugates showed the presence of the ruthenium complex

did not have any effect on binding and thermal stability of the duplex relative to the non-labeled counterpart. Luminescence quenching was observed when the conjugate formed a duplex with its complementary 17mer strand, which had guanines at certain positions, and based on previous data,¹²³ this behaviour corresponded to photoinduced electron transfer from the guanines of the target strand to the photosensitiser resulting in possible photoadduct formation.

Wiederholt *et al.*¹³⁴ incorporated a non-nucleoside linker based on 2,2'-bipyridine and ethylene glycol into the backbone structure of various oligonucleotides to provide a site for the formation of ruthenium complexes. The bipyridine linker was synthesised and converted to the corresponding dimethoxytrityl protected phosphoramidite suitable for use in oligonucleotide synthesis (**figure 1.25**). The linker was then incorporated into the solid-phase synthesis of the oligonucleotides using standard phosphoramidite chemistry. The modified oligonucleotides were deprotected, cleaved from the solid support and desalted on a Sephadex column. The modified oligonucleotide was then refluxed with cis-dichloro (2,2'-bipyridine) ruthenium(II) dihydrate with addition of pyridine halfway through the reaction to remove any non-specifically bound ruthenium (*e.g.* from the N-7 of guanine). The final conjugate was purified on a Sephadex G-25 column and characterised by UV-vis analysis, PAGE and fluorescence spectroscopy. The internal attachment of the conjugate was to the 3' and 5' hydroxyls of the sugar residues of the adjacent thymidine residues (**figure 1.26**).

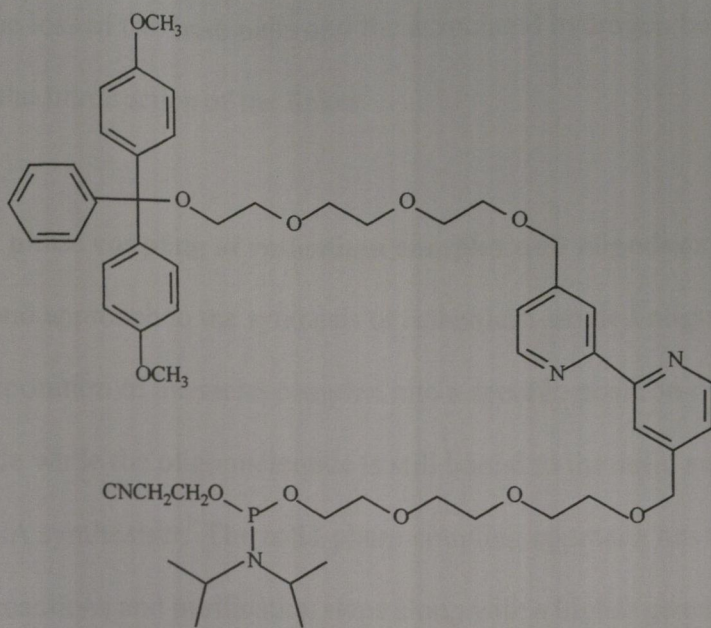


Figure 1.25 Phosphoramidite derivative of bipyridine-based linker

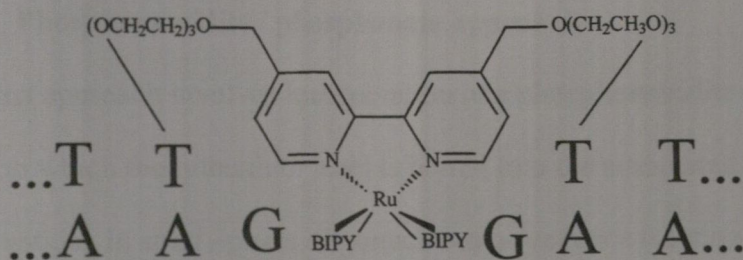


Figure 1.26 DNA duplex containing internal ruthenium complex

Melting temperature studies showed that the duplex formed between the ruthenium-labeled oligonucleotide and its complementary strand was moderately more stable than that formed between an oligonucleotide tethered by simple ethylene glycol linkers and its complementary strand. It was found that the T_m values for the conjugated ruthenium-containing duplexes were up to 17 °C less than the fully native non-ruthenium containing duplex. This decrease in thermal stability has been

attributed to the loss of two base pairs and the associated hydrogen bonding that accompanied the introduction of the linker.

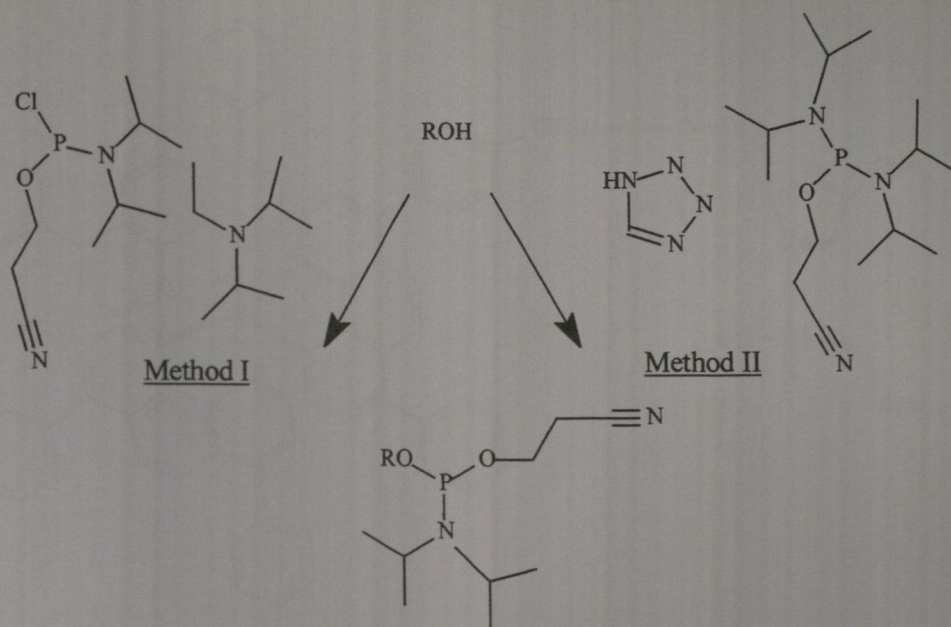
1.13.2 Solid phase coupling of ruthenium complex and oligodeoxynucleotide

A second approach to the synthesis of ruthenium-labeled oligonucleotides involves incorporation of the metal complex into a specific position on the oligonucleotide while the oligonucleotide is still bound to the solid support in the automated DNA synthesiser. The solid-phase coupling approach has the advantages of fewer side reactions and purification steps along with a higher general overall yield of final conjugate. Solid-phase coupling can be affected in two ways.

Approach 1: Phosphoramidite / phosphonate approach

The first approach involves incorporation of a phosphoramidite or phosphonate to which the ruthenium label is bound into the automated synthesis of the oligonucleotide. In solid-phase oligonucleotide synthesis (section 1.5) nucleoside phosphoramidites are coupled to a deprotected 5'-OH group on the growing oligonucleotide chain and this reaction is achieved with excellent yields. Due to the efficiency of this reaction, it has been used as an approach for incorporation of ruthenium complexes into an oligonucleotide during the course of its automated synthesis. The ruthenium complex of choice must be able to withstand reaction with the reagents of the automated synthesis cycle and must also have an unprotected hydroxyl group and be suited to phosphorous (III) chemistry. The ruthenium phosphoramidite is generally prepared in one of two ways; reaction with

(β -cyanoethyl)-diisopropylaminochlorophosphoramidite / diisopropylethylamine (DIPEA) (Method I) or reaction with (β -cyanoethoxy)-bis-diisopropylaminophosphine / tetrazole (Method II) (**scheme 1.6**).



Scheme 1.6 Phosphoramidite formation from starting hydroxyl group

Bannwarth *et al.*^{135,136} first reported the use of the phosphoramidite approach in the synthesis of ruthenium-oligonucleotide conjugates. The ruthenium complex $[\text{Ru}(\text{dip})_2\text{dip}']^{2+}$ was synthesised (where $\text{dip}' = 4,7$ -diphenylphenanthroline with one phenyl ring functionalised with a hydroxyl group attached to an alkyl linker ($-(\text{CH}_2)_5\text{OH}$). The hydroxyl group was converted in situ to the corresponding phosphoramidite. The phosphoramidite was coupled to the 5'-end of the oligonucleotide during automated DNA synthesis, followed by deprotection with

concentrated ammonia and reverse-phase HPLC purification and isolation. The final conjugate consisted of the ruthenium complex bound to the 5'-end of the oligonucleotide through a stable phosphodiester linkage (**figure 1.27**).

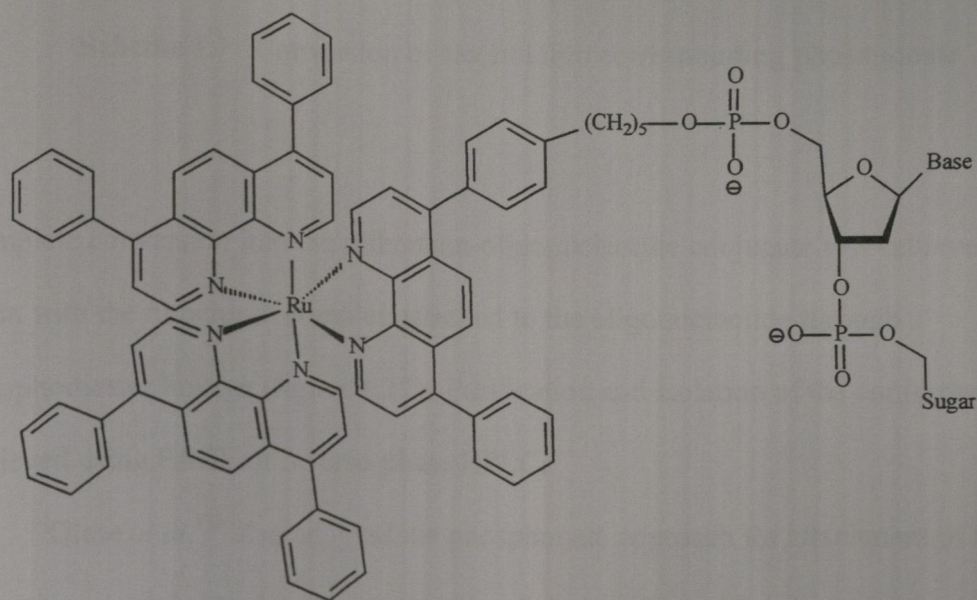
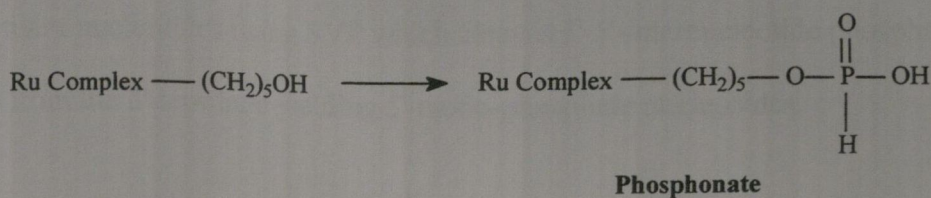


Figure 1.27 Ruthenium complex–oligonucleotide conjugate

The same group went on to report the attachment of the same ruthenium complex to the oligonucleotide using the phosphonate approach¹³⁷ due to the greater stability and ease of handling associated with phosphonates over phosphoramidites. The ruthenium complex bearing the hydroxyl functionality was converted to the corresponding phosphonate (**scheme 1.7**) and was used without further purification for the coupling reaction with the 5'-OH group of the protected oligonucleotide attached to the solid support.



Scheme 1.7 Conversion of alcohol into corresponding phosphonate

Complete conversion into the ruthenium-oligonucleotide conjugate was achieved, again with the ruthenium complex attached to the oligonucleotide through a phosphodiester linkage (**figure 1.27**). Purification and isolation of the conjugate was achieved using PAGE or reverse-phase HPLC.

Giese *et al.*¹³⁸ also adopted the phosphonate approach for attachment of a ruthenium complex to the oligonucleotide of choice. The ruthenium complex $[\text{Ru}(\text{phen})(\text{phen}')(\text{dppz})]^{2+}$ (where phen' is a phenanthroline ligand modified with the $-\text{NHCO}-(\text{CH}_2)_{11}-\text{OH}$ functionality at position C-6) was synthesised, followed by conversion into its corresponding phosphonate using tri (1*H*-imidazol-1-yl) phosphine. Activation with pivaloyl chloride was followed by reaction with 5'-OH group of the protected and solid-supported oligonucleotide. Subsequent oxidation with I_2 and deprotection with ammonia yielded the final ruthenium-oligonucleotide conjugate (**figure 1.28**). Isolation and purification was achieved using reverse-phase HPLC and PAGE techniques. Enzymatic digestion of the conjugate with snake venom phosphodiesterase (SVP, 3'-exonuclease) followed by MALDI-TOF-MS analysis of the bases confirmed the 5'-end positioning of the ruthenium complex.

Oligodeoxynucleotides can be enzymatically degraded from their 3'-terminus to their constituent nucleotides using SVP which cleaves 3'-5'-internucleotide phosphate bonds from the 3'-terminus yielding 5'-mono-phosphate nucleosides.

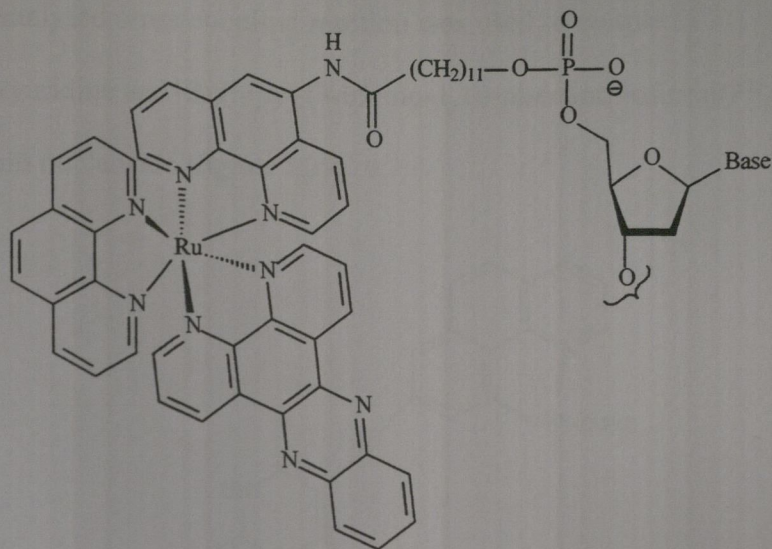


Figure 1.28 [Ru(phen)(phen')(dppz)]-ODN conjugate

Melting temperature studies of the ruthenium-labeled oligonucleotides hybridised to their complementary strand showed higher T_m values of approximately 6-8 °C compared to the native ruthenium-free duplex. The increase in stability was attributed to intercalation of the dppz ligand within the DNA duplex upon hybridisation with the complementary strand.

Site-specific modification of an oligonucleotide at the nucleobase with a ruthenium complex has been reported by Tor *et al.*¹³⁹. Initially they reported that functionalised tris-chelate complexes (bromo/ethynyl functionalities) could undergo palladium-mediated cross-coupling reactions to give the conjugated heteronuclear

complexes (Sonagashira reaction).^{140,141} This approach was then used as a starting point in the synthesis of ruthenium-containing nucleosides and their incorporation into solid-phase synthesis of ruthenium-labeled oligonucleotides. The Sonagashira palladium-catalysed cross-coupling reaction was used to couple 5-ethynyldeoxyuridine and $[\text{Ru}(\text{bipy})_2(3\text{-bromo-1,10-phenanthroline})](\text{PF}_6)_2$ to produce the ruthenium nucleoside (**figure 1.29**).

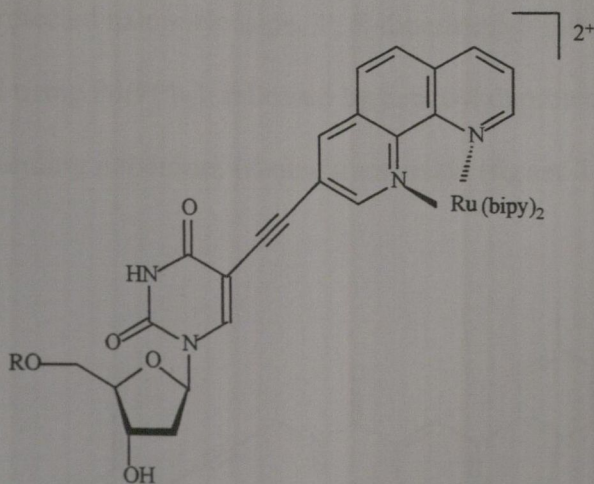


Figure 1.29 Ruthenium-derivatised nucleoside

This was subsequently converted into the corresponding ruthenium-nucleoside phosphoramidite followed by incorporation into various positions in target 20mer oligonucleotides using an automated DNA synthesiser. The completed conjugates were cleaved from the solid support using ammonium hydroxide, deprotected and purified by PAGE. The conjugate structure was confirmed by enzymatic digestion and HPLC analysis. The duplex of the 5-end modified oligonucleotides had a

comparable T_m compared with the native unlabeled duplex. The duplex formed with the centrally modified oligonucleotides showed only a slight decrease in its T_m value.

Palladium-catalysed cross coupling as a route to ruthenium-labeled nucleosides has also been used by Grinstaff *et al.*^{142,143}. An alkyne-functionalised bipyridine ligand (N-(2-propynyl)-4'-methyl-2,2'-bipyridine-4-carboxamide) was refluxed with $\text{Ru}(\text{bipy})_2\text{Cl}_2$ to give the complex $[\text{Ru}(\text{bipy})_2(\text{pmbc})](\text{PF}_6)_2$. The complex and the protected halonucleoside, 3', 5'-dibenzoyl-5-iodo-2-deoxyuridine, were cross coupled using $\text{Pd}(\text{PPh}_3)_4$ followed by benzoyl deprotection with ammonia to give the corresponding ruthenium-labeled nucleoside (**figure 1.30**).

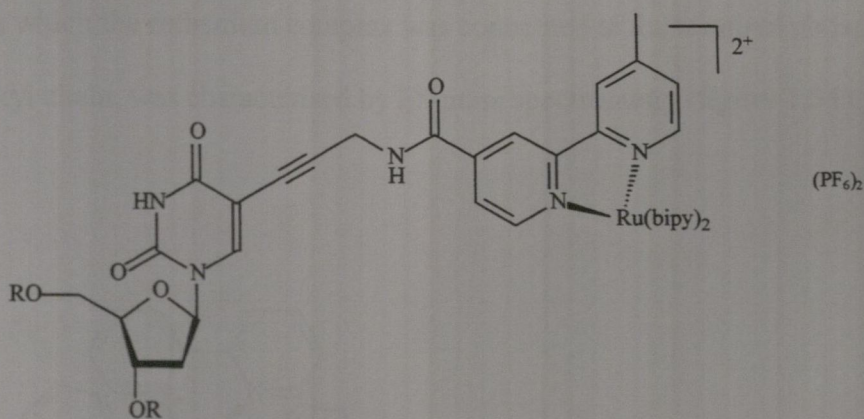


Figure 1.30 $[\text{Ru}(\text{bipy})_2(\text{pmbc})](\text{PF}_6)_2$ -derivatised nucleoside

The corresponding phosphoramidite was synthesised and this ruthenium-nucleoside phosphoramidite was incorporated into various positions in a 16mer oligonucleotide in the course of the solid-phase synthesis. Cleavage from the solid support, deprotection and reverse-phase HPLC purification followed. As seen previously for

Tor *et al.*, thermal denaturation experiments showed end-modification did not affect the T_m compared to that of the native duplex but the centrally modified oligonucleotides showed a slight reduction in overall stability.

The same group has also reported¹⁴⁴ the synthesis of oligonucleotides labeled at the 5'-end with $[\text{Ru}(\text{bipy})_3]^{2+}$. $\text{Ru}(\text{bipy})_2\text{Cl}_2$ was refluxed with 4-methyl-2,2'-bipyridine-4'-carbonyl ethanolamide to afford the tris-bipyridine ruthenium complex isolated as the PF_6^- salt. The complex was converted to its corresponding ruthenium-phosphoramidite that was then added to the 5'-end of an oligonucleotide during automated synthesis at the last step of the reaction sequence. The conjugate was cleaved from the column, deprotected and purified by reverse-phase HPLC. The final conjugate, in which the ruthenium complex was connected to the terminal phosphate by a short alkyl chain, was characterised by ES mass spectrometry (**figure 1.31**).

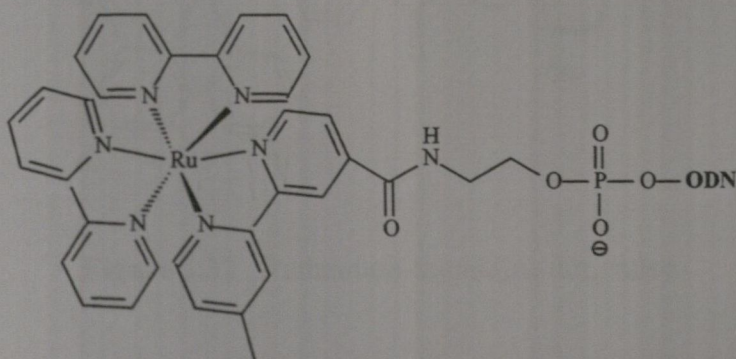


Figure 1.31 Ruthenium complex linked to the terminal phosphate *via* a short ethylene spacer.

The melting temperature of the duplex was decreased from 60 °C to 42 °C for the modified duplex indicating a destabilizing effect caused by the positioning of the complex. This destabilising effect was not observed when the complex was attached to a terminal or internal nucleobase residue.

More recently, Grinstaff *et al.*¹⁴⁵ reported the solid-phase synthesis of oligonucleotides labeled at the 5'-aminothymidine with $[\text{Ru}(\text{bipy})_2(4\text{-m-4'-cam-bpy})^{2+}]$, (where 4-m-4'-cam-bpy = 4-methyl-2,2'-bipyridine-4'-carboxamide). The mono-carboxylic acid-derivatised $\text{Ru}(\text{diimine})_3^{2+}$ complex, $\text{Ru}(\text{bpy})_2(4\text{-methyl-2,2'-bipyridine-4'-carboxylic acid})$, was coupled to 5'-amino-5'-deoxythymidine (**figure 1.32**) followed by conversion to its corresponding phosphoramidite.

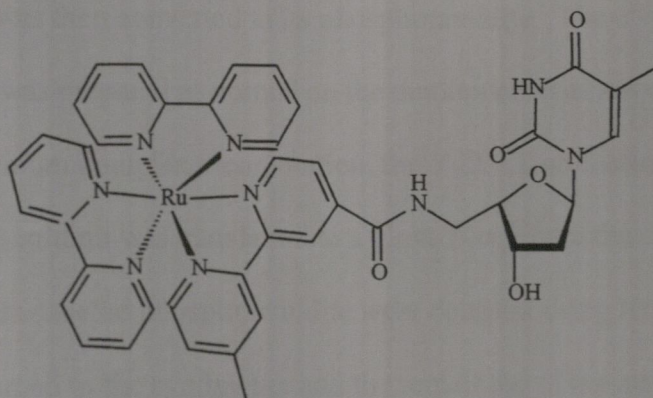


Figure 1.32 Ruthenium-thymidine derivative

The phosphoramidite was introduced at the last coupling step in the automated oligonucleotide synthesis, reacting with the 5'-terminal alcohol of the oligonucleotide. After cleavage from the column and deprotection, the conjugate was purified by

reverse-phase HPLC. A small decrease in the T_m value for the modified duplex was observed relative to the unmodified duplex. It was concluded that labeling at the 5'-terminal of an oligonucleotide did not significantly affect the overall duplex stability.

Lewis *et al.*¹⁴⁶ have reported the synthesis of the first ruthenium-linked oligonucleotides with complementary sequences capable of forming hairpin structures. This involved initial synthesis of a difunctional ruthenium (II) complex in which one functional group could be activated as the other was protected. The reaction started with conversion of 2,2'-bipyridine-4,4'-dicarboxylic acid to the corresponding bis-(N-(3-hydroxypropyl))areneedicarboxamide. One hydroxyl group was protected with DMT and the monoprotected ligand (DMT-dabp) was reacted with $\text{Ru}(\text{bipy})_2\text{Cl}_2$ to give the complex $[\text{Ru}(\text{bipy})_2(\text{DMT-dabp})](\text{PF}_6)_2$. The second hydroxyl group was then converted to its phosphoramidite. The 3'-segment of the oligonucleotide was prepared as normal on the automated synthesiser and at the position of ruthenium complex incorporation, the 5'-DMT protecting group was removed and the column was transferred to a glove box where the oligonucleotide and the ruthenium-labeled phosphoramidite were coupled using tetrazole. The column was returned to the synthesiser and the remainder of the automated synthesis was completed to form the desired hairpin. Cleavage from the support, followed by deprotection and HPLC purification afforded the final conjugate (**figure 1.33**) (95 % yield). Melting temperature studies were consistent with a hairpin conformation.

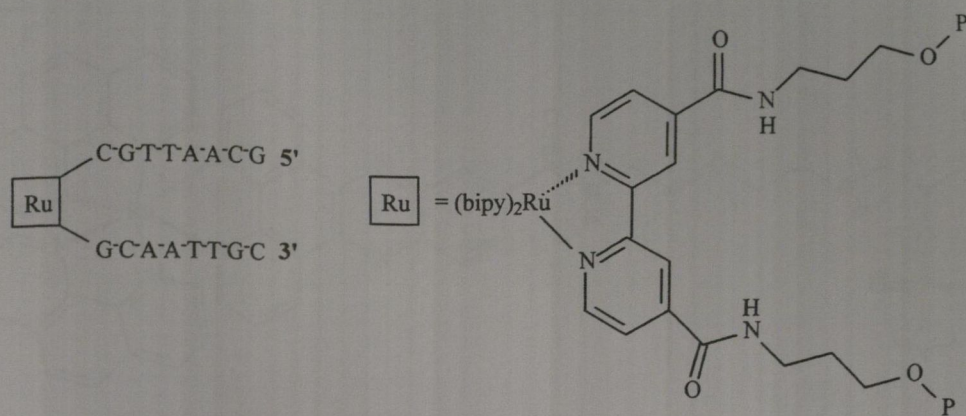


Figure 1.33 Ruthenium-bridged DNA hairpin

Chattopadhyaya *et al.*¹⁴⁷ have synthesised $[\text{Ru}(\text{phen})_2\text{dppz}]^{2+}$ -oligonucleotide conjugates (tethered at 5'-, 3'- and central positions) in which the dppz ligand is attached to the oligonucleotide *via* a glycerol-tri(ethylene glycol) fused linker. The $[\text{Ru}(\text{phen})_2\text{dppz}]^{2+}$ -derivatised complex was converted to the corresponding phosphoramidite ready for 5'- or central-oligonucleotide incorporation using standard automated synthesis. In order for the ruthenium label to be incorporated at the 3'-end of the oligonucleotide sequence, the original complex was also treated with succinic anhydride and DMAP in DCM to give the corresponding succinate block that was followed by immobilization onto the CDG-support. All three types of conjugate were synthesised on a DNA synthesiser, removed from the support, deprotected, purified by reverse-phase HPLC and characterised by MALDI-TOF-MS (**figure 1.34**).

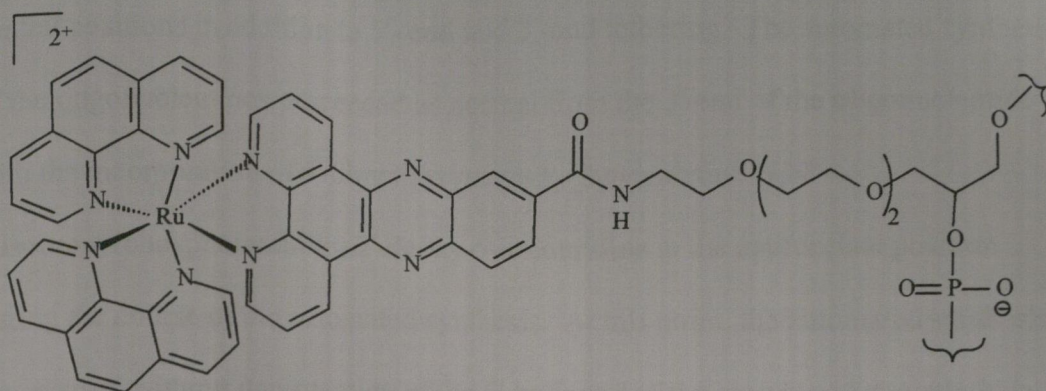


Figure 1.34 [Ru(phen)₂dppz]-oligonucleotide

Melting-temperature studies showed that the duplexes formed between the 5'-, 3'- and centrally modified ruthenium-oligonucleotide conjugates and their complementary DNA sequences were considerably more stable than the native unmodified duplex.

Approach 2 : On-column derivatisation

On column-derivatisation involves incorporation of a functional group on the oligonucleotide during its solid-phase synthesis followed by coupling with a ruthenium complex while the oligonucleotide is still bound to the solid support.

Grinstaff *et al.*^{148,149} reported the synthesis of a series of ruthenium-oligonucleotide conjugates using the on-column derivatisation approach that combined palladium cross coupling and automated solid-phase DNA synthesis approaches previously used by the group. The ruthenium complex [Ru(bpy)₂(4-m-4'-pa-bpy)](PF₆)₂ (where 4-m-4'-pa-bpy = 4-methyl-2,2'-bipyridine-4'-carbonylpropargylamine), was incorporated into the oligonucleotides at various

central positions in addition to 5'- end and 3'-end tethering. The automated synthesis of the oligonucleotides proceeded as normal from the 3'-end of the oligonucleotide with the incorporation of 5'-dimethoxytrityl-3'-(β -cyanoethyl-N,N'-diisopropylphosphoramidite)-2'-deoxy-5-iodouridine at the appropriate position during the course of the automated synthesis. At this point, the automated synthesis was paused without deprotection of the 5'-hydroxyl of the growing oligonucleotide and leaving the oligonucleotide attached to the solid support. The column was removed from the synthesiser and palladium cross coupled with the alkyne-derivatised $[\text{Ru}(\text{bpy})_3]^{2+}$ complex in an anhydrous environment. Upon completion of the cross coupling reaction, the column was replaced onto the synthesiser and the remainder of the oligonucleotide was synthesised as normal followed by cleavage from the column and base deprotection. The conjugate was purified by reverse-phase HPLC and characterised by ES mass spectrometry. No significant change in T_m values was observed for either the end- or centrally modified conjugate duplexes relative to the native unmodified duplex. Circular dichroism (CD) spectra of modified and unmodified duplexes indicated the formation of stable B-DNA duplexes.

Barton *et al.*¹⁵⁰ have also used the on-column derivatisation approach to attach the ruthenium complex $[\text{Ru}(\text{phen})(\text{bipy}')(\text{dppz})]^{2+}$ (where $\text{bipy}' = 4-(4'\text{-methyl-2,2'}$ -bipyridyl)valerate) to the 5'-terminal ribose of the oligonucleotide *via* an alkylamino linker. Initially the alkylamino linker was coupled to the 5'-terminal ribose of a CPG-supported oligonucleotide. The carboxylic acid functionality of the modified bipy ligand on the ruthenium complex was activated to the corresponding N-succinimido

ester and this was added, along with DIPEA, to the amino-functionalised oligonucleotide on the solid support. After 12 hours, the conjugates were washed with ethanol and DCM, cleaved from the resin and purified by reverse-phase HPLC. Conjugate characterisation was achieved by mass spectrometry, enzymatic digestion and base analysis. Denaturation experiments showed the modified duplex to be slightly more stable than its unmodified analogue.

1.14 Limitations of previous work

The work discussed in this thesis is built on foundation work carried out by Dr. Clare O' Keeffe,¹⁵¹ whose work describes a model system incorporating a target 24mer ODN, the sequence of which represents the breakpoint junction of the leukaemia specific translocation in CML, and a ruthenium complex conjugated to a 9mer ODN with a sequence complementary to one section of the target ODN strand. The overall aim of the system was site-specific cleavage of the target 24mer strand at a guanine residue 15 bases from the 5'-end of the target strand (G15) (**figure 1.35**).

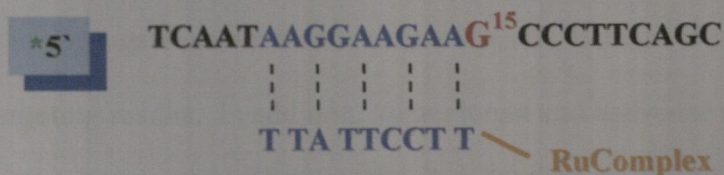


Figure 1.35 Diagrammatic representation of the model system with the 24mer target and complementary ruthenium-9mer.

Conjugation of the ruthenium complex to the 9mer was attempted in a number of ways using methods analogous to those of Barton,¹³¹ Bannwarth¹²⁹ and Schubert¹⁶³. The approach of Barton¹³¹ (using DCC and HOBT) showed no evidence of conjugate formation. The approaches of Schubert¹⁶³ (using EDC and NHS) and Bannwarth¹²⁹ (using TSU), did result in the formation of the desired conjugate, but problems such as competing reactions and difficulties with purification and isolation of the desired conjugate resulted in low overall yields. Conjugate analysis showed that a large amount of unconjugated ODN (84%) was present in the final sample retrieved. Photocleavage experiments with this conjugate mixture showed cleavage at the target G15 residue was achieved, but only in addition to cleavage at other guanine residues. Results indicated that along with the large excess of free 9mer present in the conjugate sample, the length of the antisense ODN may have been too short to form a stable duplex with the target 24mer strand, thus inhibiting optimal interaction between the target base and the ruthenium complex. It is now widely accepted that a longer antisense ODN is required for optimal duplex stability. Based on these findings, modification of the model system was necessary in order to achieve site-specific cleavage in a more efficient manner exclusively at the target base. Improvement in conjugate isolation and purification was required in order to achieve better phototargeting results. In addition, longer target and antisense strands were utilised to increase the overall stability of the system, thus allowing optimal interaction between the photosensitiser and target base.

1.15 Aims of work

The principle objective of the work described in this thesis is the augmentation of an antisense effect in a model Chronic Myeloid Leukaemia (CML) system through photochemical targeting using ruthenium-oligodeoxynucleotide (ODN) conjugates as the antisense vectors. The target 34mer oligodeoxynucleotide in the system has a sequence specific to the *bcr-abl* fusion section of the CML mRNA. The main aim is inhibition of the *bcr-abl* mRNA expression thus causing subsequent inhibition of the corresponding oncoprotein production.

Two approaches were adopted to target the 34mer oligodeoxynucleotide in a sequence specific manner. Each involved the initial synthesis of a ruthenium complex, $[\text{Ru}(\text{phen})_2\text{phen}'](\text{PF}_6)_2$ or $[\text{Ru}(\text{TAP})_2\text{phen}'](\text{PF}_6)_2$ (where phen = 1,10-phenanthroline, TAP = 1,4,5,8-tetraazaphenanthrene and phen' = 5-(4-carboxybutanamido-1,10-phenanthroline) and its subsequent attachment to a 17mer oligodeoxynucleotide with a sequence complementary to a section of the target 34mer.

The first approach using the $[\text{Ru}(\text{phen})_2\text{phen}']$ -ODN conjugate (conjugate 1) is based on site-specific photooxidative damage of the target 34mer ODN. The model system (**figure 1.36 (A)**) consists of the target 34mer hybridised to the ruthenium-17mer conjugate. The system is irradiated with visible light causing excitation of the ruthenium complex and subsequent site-specific photooxidative damage in the target strand. The expected site of damage is G21 *i.e.* the guanine residue 21 bases from the 5'-end of the target 34mer.

The second approach using the $[\text{Ru}(\text{TAP})_2\text{phen}']\text{-ODN}$ conjugate (conjugate 2) is based on site-specific photoadduct formation with the target 34mer ODN. The model system (**figure 1.36 (B)**) consists of the target 34mer hybridised to the ruthenium-17mer conjugate. Again the system is irradiated with visible light causing excitation of the ruthenium complex and subsequent adduct formation with the target strand. The photoadduct is expected to form between the ruthenium complex and G21 on the target 34mer strand.

Both systems are also investigated under various conditions (*e.g.* varying the type of target strand, varying the position of the target guanine and including various reagents) to optimise the photochemical targeting approaches and understand the mechanisms involved.

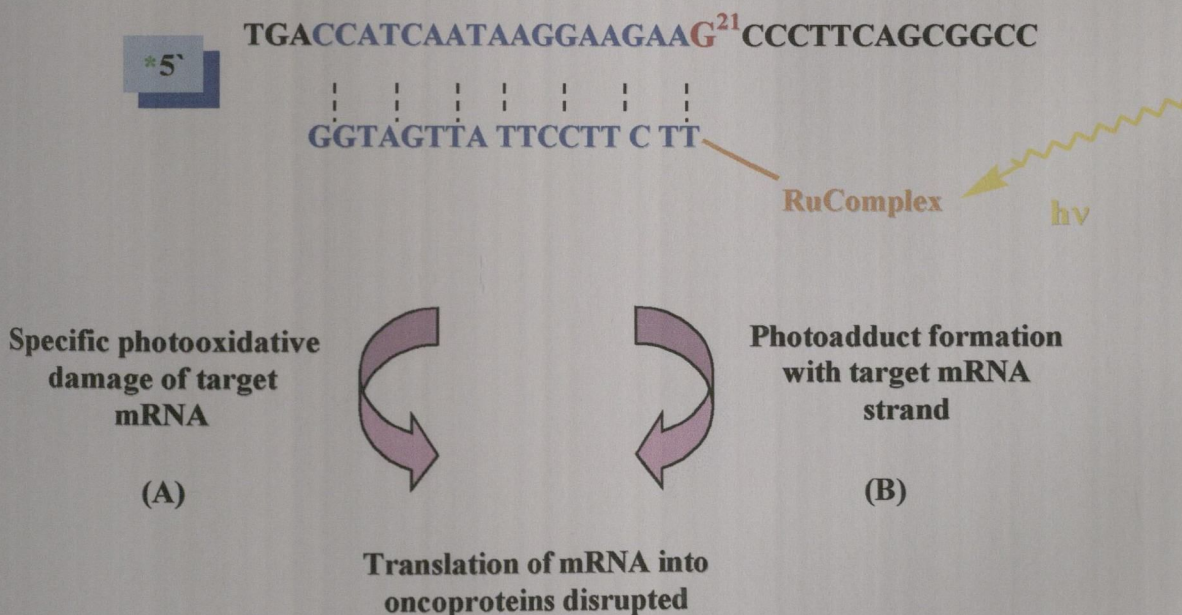


Figure 1.36 Diagrammatic representation of the model system with the 34mer target and complementary ruthenium-17mer. Photooxidative (A) and photoadduct forming (B) targeting approaches are shown

CHAPTER 2

SYNTHESIS OF RUTHENIUM- OLIGODEOXYNUCLEOTIDE CONJUGATES

2.1 Introduction

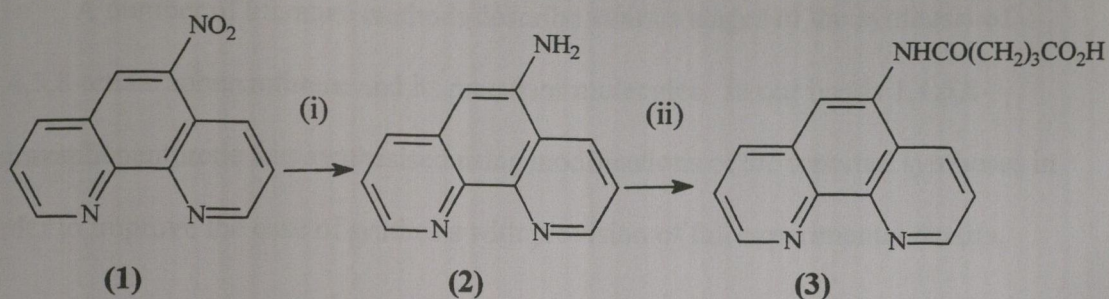
In order to achieve the required photochemical targeting of the target 34mer oligodeoxynucleotide strand representing a section of the *bcr-abl* messenger RNA in Chronic Myeloid Leukaemia, two different ruthenium-oligodeoxynucleotide conjugates were synthesised. On its own, the introduction of an antisense oligodeoxynucleotide complementary to a section of the target strand will down-regulate oncoprotein production through steric blocking and RNaseH-induced cleavage of the mRNA. By attaching a ruthenium complex to the antisense oligodeoxynucleotide, the photochemical properties of the complex can be utilized to enhance the antisense effect. The two targeting approaches of choice (photooxidative – induced cleavage of the target strand and photoadduct formation with the target strand) required the initial synthesis of two ruthenium complexes bearing suitable ligands for the approach of choice. The nature of the attached ligands affects the photoreactivity of a complex, therefore the choice of ligands will determine how oxidising each complex is after excitation.

The first conjugate, [Ru(phen)₂phen']-ODN, bearing the weak π -accepting 1,10-phenanthroline ligands, was designed to induce site-specific photooxidative cleavage of the target 34mer. The second conjugate, [Ru(TAP)₂phen']-ODN, bearing the more π -deficient 1,4,5,8-tetraazaphenanthrene ligands, was designed to undergo photoadduct formation with the target strand.

This chapter describes the synthesis of both ruthenium complexes, their conjugation to a 17mer complementary to a section of the target 34mer and the subsequent purification, isolation and analysis of both conjugates.

2.2 Synthesis of 5-(4-carboxybutanimido)-1,10-phenanthroline

The 5-(4-carboxybutanimido)-1,10-phenanthroline ligand, phen', (**3**) was synthesised as shown in reaction scheme 2.1.



(i) SnCl_2 , ultrasonication, ethanol, room temp.

(ii) Glutaric anhydride, pyridine, 100°C .

Scheme 2.1 Synthesis of 5-(4-carboxybutanimido)-1,10-phenanthroline

Reduction of commercially available 5-nitro-1,10-phenanthroline (**1**) to 5-amino-1,10-phenanthroline (**2**) was best achieved using tin (II) chloride and ultrasonication at room temperature, based on a method reported for the reduction of nitrobenzodiazepine derivatives.¹⁵² Reduction of (**1**) was also successful using a graphite / hydrazine monohydrate procedure¹⁵³ with better yields being obtained using activated charcoal¹⁵⁴ in place of the graphite. Reduction of (**1**) by palladium catalysed hydrogenation has also been described,¹¹⁹ although in our hands yields were lower than those obtained with either of the above two methods. 5-(4-Carboxybutanimido)-1,10-phenanthroline (**3**) was prepared from 5-amino-1,10-phenanthroline (**2**) using glutaric anhydride as described by Barton *et al.*¹⁵⁵. Yields

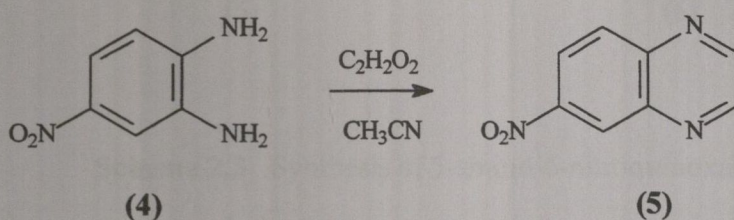
for the reaction were modest (~40 %), possibly due to cyclisation of (3) to the corresponding glutarimide.¹⁵⁵

2.3 Synthesis of 1,4,5,8-tetraazaphenanthrene (TAP)

A number of literature methods describe various stages of the synthesis of 1,4,5,8-tetraazaphenanthrene and its precursor molecules. In our hands 1,4,5,8-tetraazaphenanthrene was synthesised using modifications of the reported syntheses in order to improve the ease of synthesis with provision of full experimental details.

2.3.1 Synthesis of 6-nitroquinoxaline

The first stage involved the synthesis of 6-nitroquinoxaline (5) by reaction of 4-nitro-1,2-phenylenediamine (4) and glyoxal in acetonitrile based on a procedure reported by Foley *et al*¹⁵⁶ (scheme 2.2).



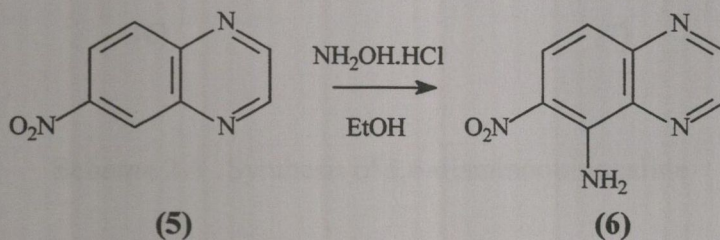
Scheme 2.2 Synthesis of 6-nitroquinoxaline

IR analysis of the product showed the absence of the characteristic bands associated with N-H asymmetrical and symmetrical stretching vibrations and N-H bending

vibrations. The 6-nitroquinoxaline product was characterised by ^1H NMR, ^{13}C NMR and melting point analysis.

2.3.2 Synthesis of 5-amino-6-nitroquinoxaline

6-Nitroquinoxaline (**5**) was then reacted with hydroxylamine hydrochloride in ethanol based on a method reported by Nasielski-Hinkens *et al.*¹⁵⁷ (scheme 2.3). The resulting 5-amino-6-nitroquinoxaline product (**6**) was purified by elution chromatography on a silica column using 100% chloroform and eluted as the first fraction. ^1H NMR, ^{13}C NMR and melting point analysis confirmed the presence of (**6**) with no further purification needed.

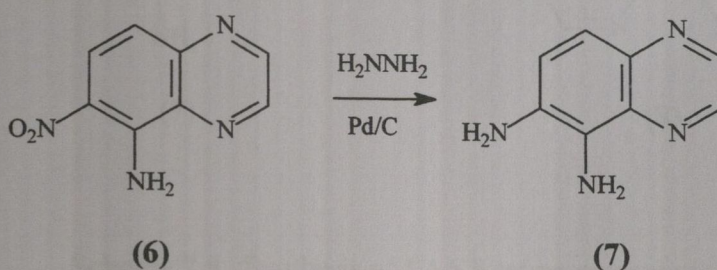


Scheme 2.3 Synthesis of 5-amino-6-nitroquinoxaline

The second fraction was eluted with a mixture of chloroform and methanol and ^1H NMR and melting point analysis showed the presence of the 2-amino-6-nitroquinoxaline isomer.¹⁵⁸

2.3.3 Synthesis of 5,6-diaminoquinoxaline

Reduction of 5-amino-6-nitroquinoxaline (6) using Pd/C and hydrazine monohydrate afforded the 5,6-diaminoquinoxaline (7) product in slightly better yield than previously reported (scheme 2.4). In our hands recrystallisation from toluene and not benzene as previously reported by Nasielski-Hinkens *et al.*,¹⁵⁷ successfully purified the final 5,6-diaminoquinoxaline product as confirmed by ¹H NMR, ¹³C NMR and melting point analysis.

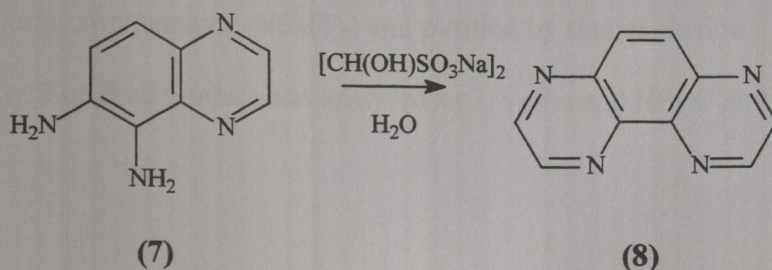


Scheme 2.4 Synthesis of 5,6-diaminoquinoxaline

2.3.4 Synthesis of 1,4,5,8-tetraazaphenanthrene

Minimal literature details exist for conversion of 5,6-diaminoquinoxaline to the desired 1,4,5,8-tetraazaphenanthrene ligand and subsequent purification steps. Brennan *et al.*¹⁵⁹ reported a method for the *in situ* production of 1,4,5,8-tetraazaphenanthrene from 5,6-dinitroquinoxaline using tin (II) chloride dihydrate and glyoxal sodium bisulfite followed by recrystallisation of the final product from

benzene / petroleum ether. In our hands, 5,6-diaminoquinoxaline (7) was reacted with the bisulfite adduct of glyoxal (scheme 2.5). After rendering the reaction mixture basic with potassium hydroxide, the final 1,4,5,8-tetraazaphenanthrene product (8) was extracted with chloroform as confirmed by ^1H NMR and melting point analysis. No recrystallisation step proved necessary in obtaining the final TAP ligand.



Scheme 2.5 Synthesis of 1,4,5,8-tetraazaphenanthrene

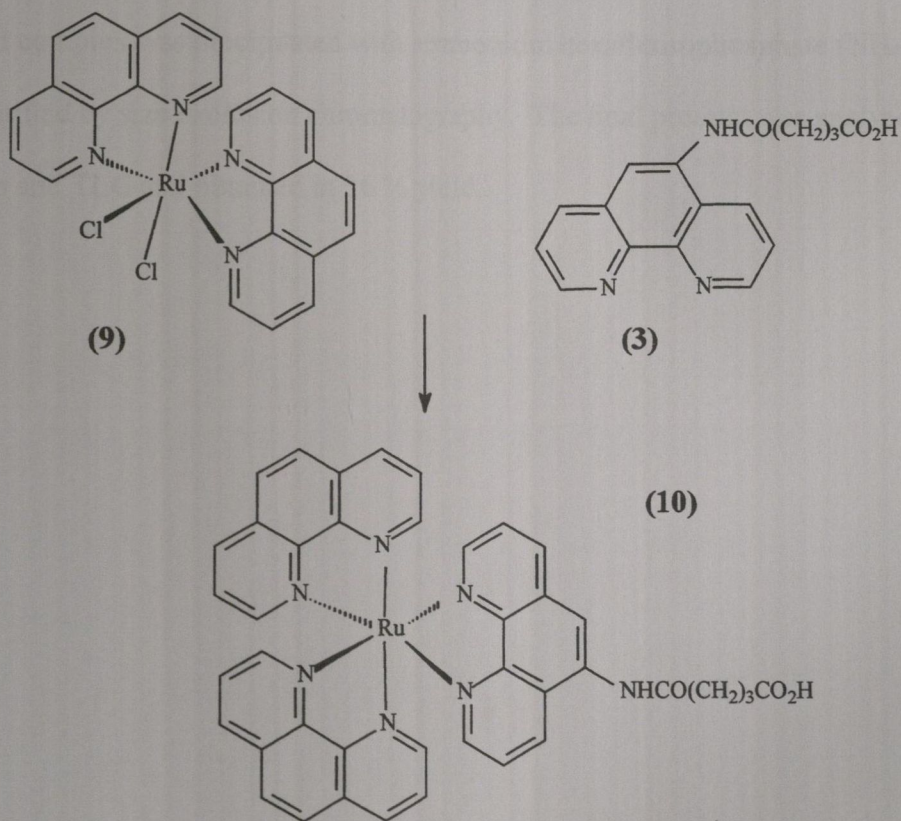
2.4 Synthesis of ruthenium bis(1,10-phenanthroline)-5-(4-carboxybutanamido)-1,10-phenanthroline dihexafluorophosphate.

The required ruthenium complex, ruthenium bis(1,10-phenanthroline) 5-(4-carboxybutanamido)-1,10-phenanthroline (10) was obtained as its dihexafluorophosphate salt by reaction of 5-(4-carboxybutanamido)-1,10-phenanthroline (3) and ruthenium bis(1,10-phenanthroline) dichloride (9).

$[\text{Ru}(\text{phen})_2\text{Cl}_2]$ can be obtained by refluxing RuCl_3 , 1,10-phenanthroline and LiCl in DMF as reported by Sullivan *et al.*¹⁶⁰ for synthesis of the analogous compound

[Ru(bipy)₂Cl₂]. Alternatively [Ru(phen)₂Cl₂] can be synthesised by refluxing RuCl₃ and 1,10-phenanthroline in DMF followed by precipitation of the desired product with LiCl as described by Whitten *et al.*¹⁶¹.

[Ru(phen)₂phen[′]](PF₆)₂ (**10**) was synthesised by refluxing phen[′] (**3**) and [Ru(phen)₂Cl₂] (**9**) in an ethanol / water mixture based on a procedure described by Meyer *et al.*¹⁶² for the synthesis of [Ru(2,2′-bipyridine)₂(5-amino-1,10-phenanthroline)](PF₆)₂ (**scheme 2.6**). The desired complex was precipitated with ammonium hexafluorophosphate (NH₄PF₆) and purified by size exclusion chromatography. The final product was analysed by UV-Vis and HPLC and obtained in 78 % yield.

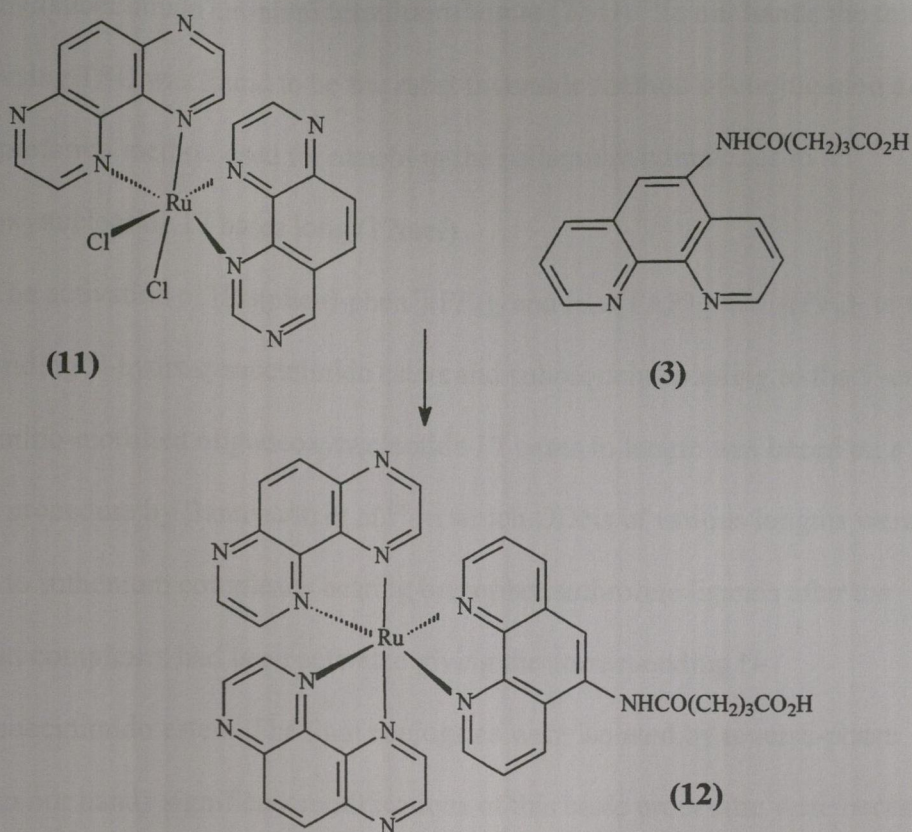


Scheme 2.6 Synthesis of [Ru(phen)₂phen[′]](PF₆)₂

2.5 Synthesis of ruthenium bis(1,4,5,8-tetraazaphenanthrene)-5-(4-carboxybutanamido)-1,10-phenanthroline dihexafluorophosphate.

The required ruthenium complex, ruthenium bis(1,4,5,8-tetraazaphenanthrene) 5-(4-carboxybutanamido)-1,10-phenanthroline (**12**) was obtained as its dihexafluorophosphate salt by reaction of 5-(4-carboxybutanamido)-1,10-phenanthroline (**3**) and ruthenium bis(1,4,5,8-tetraazaphenanthrene) dichloride (**11**). $[\text{Ru}(\text{TAP})_2\text{Cl}_2]$ can be obtained by procedures reported by Sullivan *et al.*¹⁶⁰ and Whitten *et al.*¹⁶¹ as described in section 2.4.

$[\text{Ru}(\text{TAP})_2\text{phen}^+](\text{PF}_6)_2$ (**12**) was synthesised by refluxing phen⁺ (**3**) and $[\text{Ru}(\text{TAP})_2\text{Cl}_2]$ (**11**) in an analogous manner described for $[\text{Ru}(\text{phen})_2\text{phen}^+](\text{PF}_6)_2$ in section 2.4 based on the procedure reported by Meyer *et al.*¹⁶² (scheme 2.7). The desired complex was precipitated with ammonium hexafluorophosphate (NH_4PF_6) and purified by size exclusion chromatography. The final product was analysed by UV-vis and TLC and obtained in 36 % yield.



Scheme 2.7 Synthesis of $[\text{Ru}(\text{TAP})_2\text{phen}'](\text{PF}_6)_2$

2.6 Activation of $[\text{Ru}(\text{phen})_2\text{phen}'](\text{PF}_6)_2$ and $[\text{Ru}(\text{TAP})_2\text{phen}'](\text{PF}_6)_2$ and subsequent coupling of both complexes to 17mer oligodeoxynucleotide

Several different procedures have been reported for the formation of ruthenium complex-oligodeoxynucleotide conjugates (Ru-ODNs). Schubert *et al.*¹⁶³ reported a method using N-dimethylaminopropyl-N-ethylcarbodiimide (EDC) and N-hydroxysuccinimide (NHS). Barton *et al.*¹³¹ used dicyclohexylcarbodiimide (DCC) and 1-hydroxybenzotriazole (HOBT) and Bannwarth *et al.*¹²⁹ used N,N,N',N'-

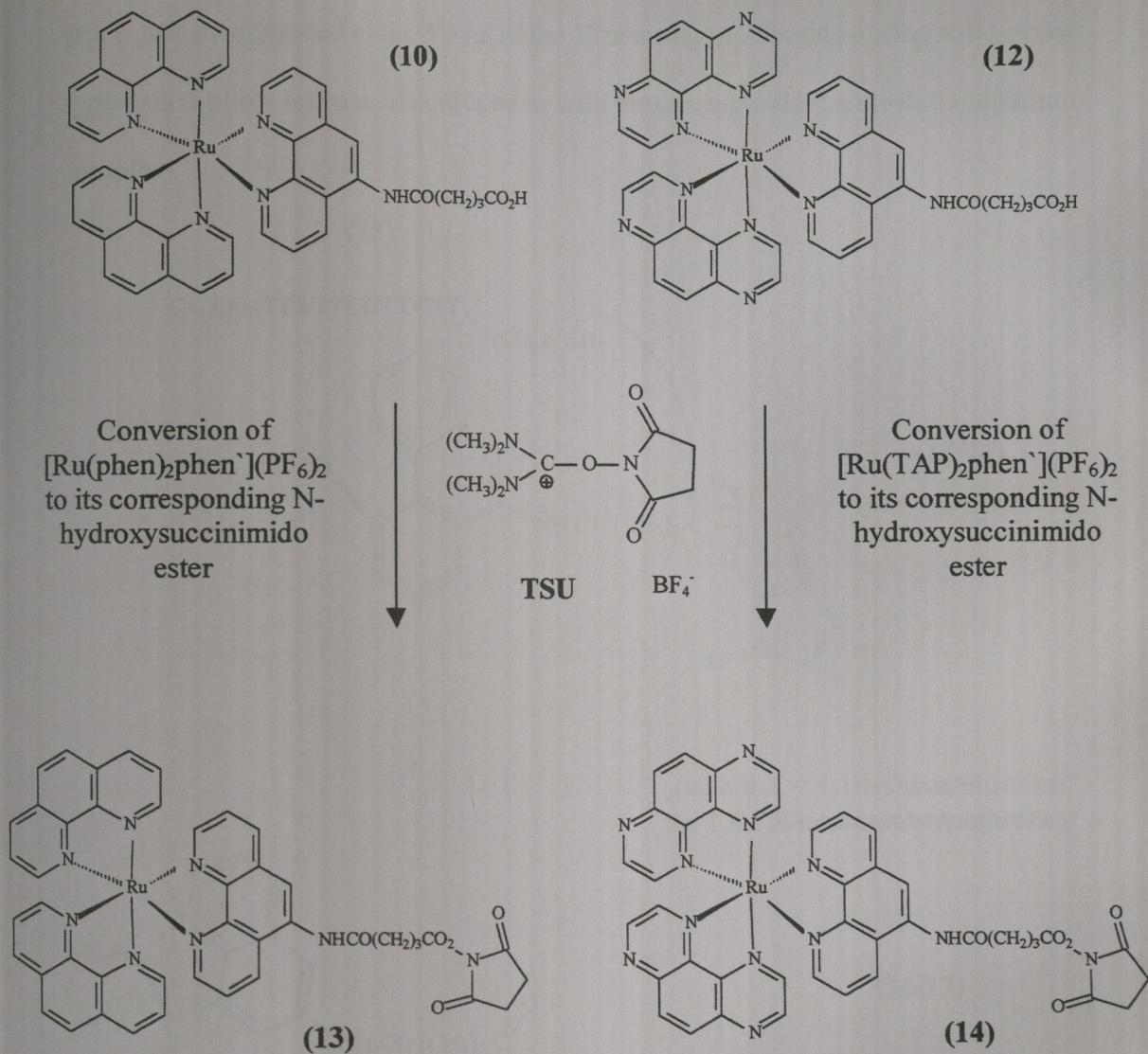
tetramethyl(succinimido)uronium tetrafluoroborate (TSU). In our hands the third method using TSU was found to be the most favorable method of conjugation and was the preferred method used for attaching the ruthenium complexes to an oligodeoxynucleotide 17 bases long (17mer).

The activation of $[\text{Ru}(\text{phen})_2\text{phen}'](\text{PF}_6)_2$ and $[\text{Ru}(\text{TAP})_2\text{phen}'](\text{PF}_6)_2$ to their corresponding N-hydroxysuccinimido esters and subsequent coupling to the 5'-end of a hexylamino-modified oligodeoxynucleotide 17 bases in length was based on a reported procedure by Bannwarth *et al.*¹²⁹ in which ODNs of various lengths were attached to ruthenium complexes bearing bathophenanthroline ligands after the ruthenium complexes had been activated giving the corresponding N-hydroxysuccinimido esters. The final conjugates were isolated by reverse-phase HPLC. In our hands significant modifications of this basic procedure were necessary due to the differences between the $[\text{Ru}(\text{phen})_2\text{phen}'](\text{PF}_6)_2$ and $[\text{Ru}(\text{TAP})_2\text{phen}'](\text{PF}_6)_2$ complexes and those used by Bannwarth *et al.*

Bannwarth *et al.* converted their ruthenium complex with one bathophenanthroline ligand functionalised with a carboxylic acid to the corresponding N-hydroxysuccinimido ester by treatment with N,N,N',N'-tetramethyl (succinimido)uronium tetrafluoroborate (TSU) in the presence of the Hünig base, diisopropylethylamine (DIPEA). The DMF was subsequently removed and the product was washed with ether and dried.

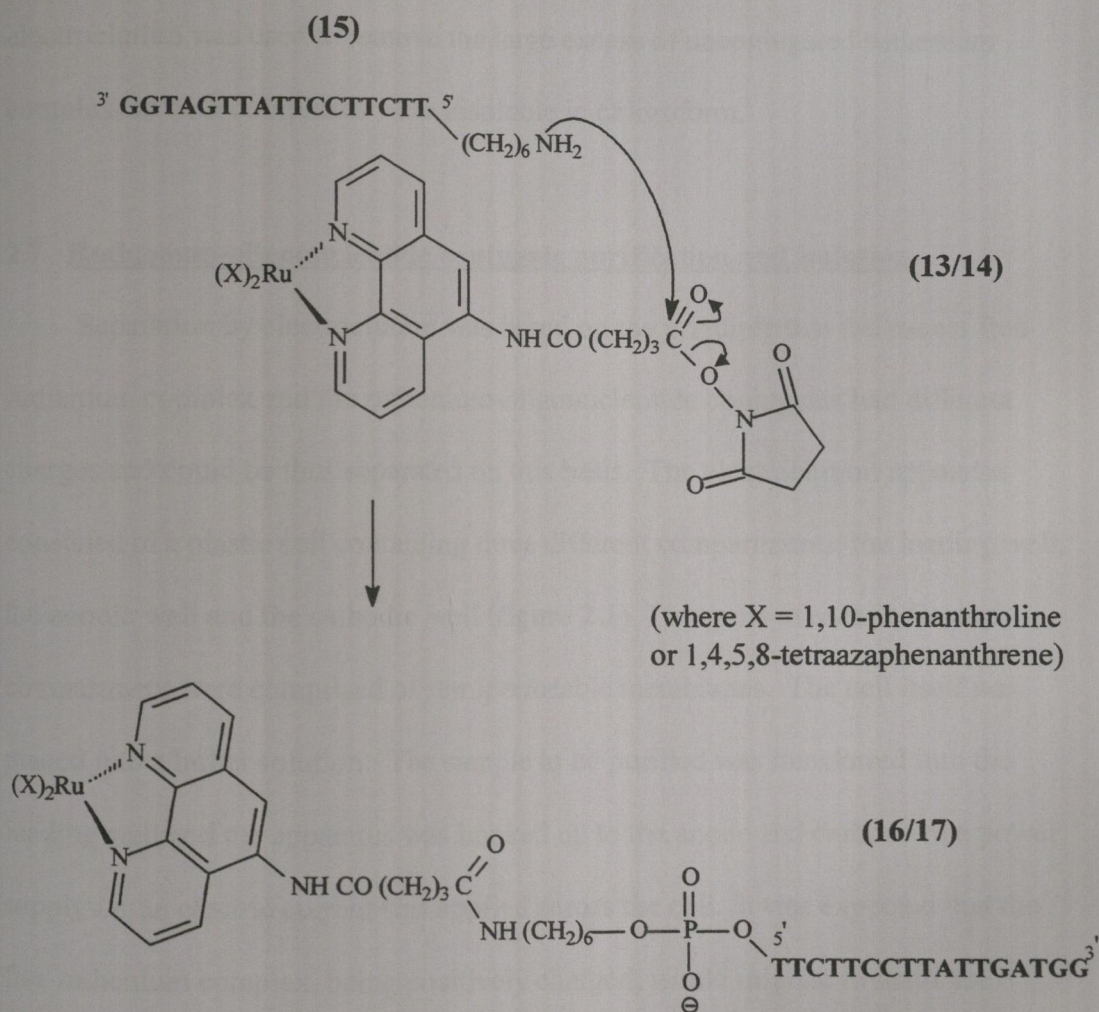
In our hands the ruthenium complex of choice (either $[\text{Ru}(\text{phen})_2\text{phen}'](\text{PF}_6)_2$ or $[\text{Ru}(\text{TAP})_2\text{phen}'](\text{PF}_6)_2$ and DMF were added to a mixture of TSU and DIPEA followed by reaction at room temperature. The resulting mixture was analysed by

TLC and HPLC indicating that quantitative conversion of each ruthenium complex into its corresponding N-hydroxysuccinimido ester (**13**) and (**14**) was achieved (scheme 2.8).



Scheme 2.8 Conversion of $[\text{Ru}(\text{phen})_2\text{phen}'](\text{PF}_6)_2$ and $[\text{Ru}(\text{TAP})_2\text{phen}'](\text{PF}_6)_2$ to the corresponding N-hydroxysuccinimido esters.

The coupling reaction between the activated N-hydroxysuccinimido esters of both complexes (13/14) and a presynthesised 17mer oligonucleotide (15) was effected to give the corresponding ruthenium-oligonucleotide conjugate (16/17) (scheme 2.9). The 17mer oligonucleotide was synthesised using standard phosphoramidite chemistry using an automated DNA synthesiser. A hexylamino group was incorporated at the 5'-end of the 17mer oligonucleotide during solid-phase synthesis to allow for ease of conjugation with the corresponding activated ruthenium complex.



Scheme 2.9 Synthesis of ruthenium-oligonucleotide conjugates

In coupling oligonucleotides of various lengths to ruthenium complexes, Bannwarth *et al.*¹²⁹ used a DMF / dioxane / water solvent mixture to ensure all the conjugation components were completely dissolved. Chloroform was then used to remove the excess free ruthenium complex from the reaction mixture and the final conjugated product was isolated using reverse-phase HPLC. In our hands the mixture of activated complex for both ruthenium complexes was used without further purification and added in a large excess, along with diisopropylamine, to the 17mer oligonucleotide already dissolved in sterile water. After overnight reaction, electroelution was used to remove the large excess of unconjugated ruthenium complex, as both complexes were insoluble in chloroform.

2.7 Ruthenium-oligonucleotide conjugate purification and isolation

Separation by electroelution was based on the principle that the excess free ruthenium complex and the ruthenium-oligonucleotide conjugates had different charges and could be thus separated on this basis. The electroelution apparatus consisted of a plastic cell containing three different compartments; the loading well, the anodic well and the cathodic well (**figure 2.1**). The walls of each individual compartment were comprised of semipermeable membranes. The cell itself was placed into a buffer solution. The sample to be purified was transferred into the loading well and the apparatus was hooked up to the anode and cathode of a power supply *i.e.* an electric current was applied across the cell. It was expected that the free ruthenium complex, being positively charged, would migrate towards the cathode and be retained in the cathodic well. Any ruthenium-oligonucleotide

conjugated species and any unreacted 17mer oligonucleotide, being negatively charged, would be expected to migrate towards the anode and be retained in the anodic well. The semi-permeable membranes of the loading well allow free migration of cations and anions upon application of a current, but the membranes separating the anodic and cathodic wells from the rest of the cell are less permeable, thus ensuring complete containment of any ruthenium-oligonucleotide conjugated product in the anodic well without any further migration into the surrounding buffer solution.

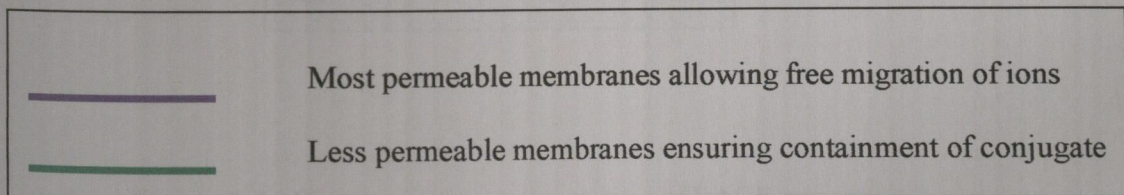
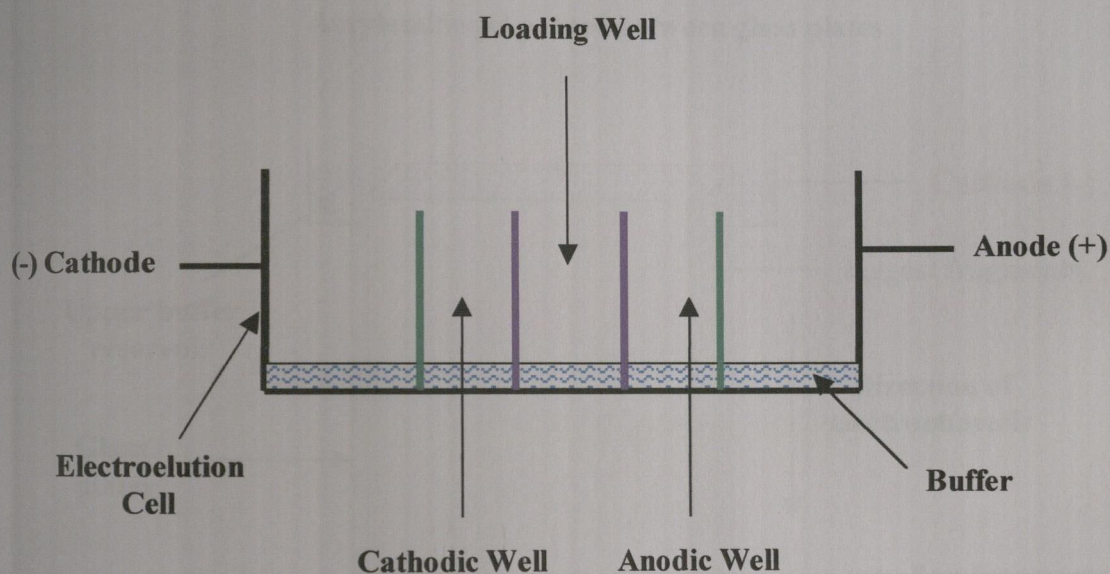


Figure 2.1 Diagrammatic representation of electroelution apparatus

The overnight conjugation reaction mixture for both complexes was added to the loading well of the electroelution apparatus and an electric potential was applied. After a period of time an orange / brown solution collected in the anodic well. The contents of the anodic well were collected and as, in principle, this material would contain any unconjugated 17mer oligonucleotide in addition to any ruthenium-oligonucleotide conjugate that was present, further purification was needed. Polyacrylamide gel electrophoresis (PAGE) purification was used to separate the two species.

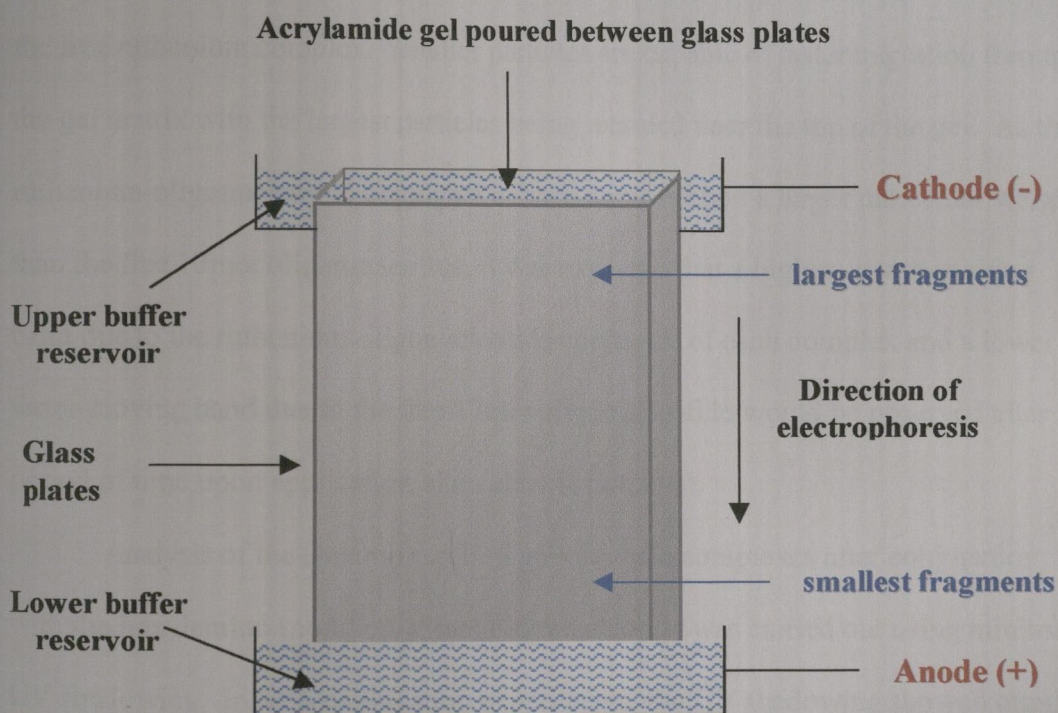


Figure 2.2 Diagrammatic representation of PAGE apparatus

The unconjugated 17mer oligonucleotide and the ruthenium-oligonucleotide conjugate for both complexes were separated on the basis of their differing molecular weights using a 12 % acrylamide gel. The gel was poured between two glass plates and placed in contact with upper and lower buffer reservoirs (**figure 2.2**). Both species to be separated have an overall negative charge and would be expected to migrate through the gel matrix towards the anode at the bottom upon application of an electric potential. Any unconjugated ruthenium complex present in the sample to be electrophoresed would be expected to remain in the loading well at the top of the gel or to migrate slightly upwards towards the cathode due to the positive charge of the free ruthenium complex. Smaller particles are capable of faster migration through the gel matrix with the largest particles being retarded near the top of the gel. As the ruthenium-oligonucleotide conjugate of each complex had a larger molecular weight than the free 17mer oligonucleotide, it was expected that a higher slower-moving band due to the ruthenium-oligonucleotide conjugate of each complex and a lower faster-moving band due to the free 17mer oligonucleotide would be observed after a period of time upon application of an electric potential.

Analysis of the electrophoresed gels for both complexes after conjugation with the hexylamino-modified 17mer oligonucleotide was carried out using minimal UV shadowing. In both conjugation experiments, the UV shadowing showed orange bands of reduced mobility with respect to the lower free 17mer oligonucleotide band that were attributed to the ruthenium-oligonucleotide conjugate of both complexes (**figure 2.3**).

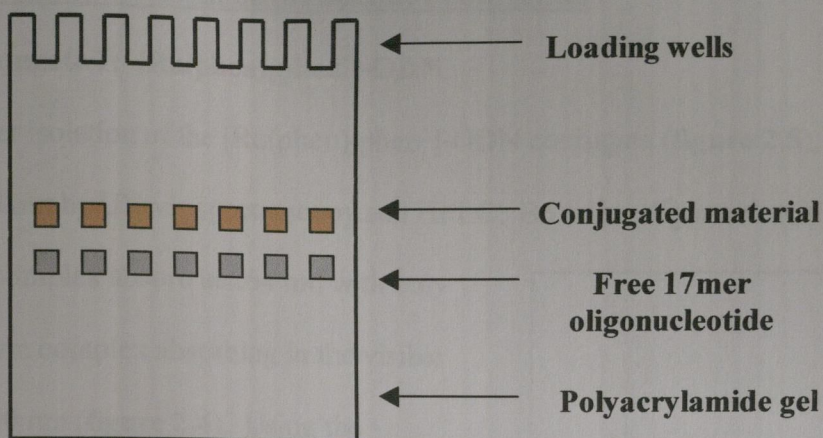


Figure 2.3 Diagrammatic representation of conjugation experiment gel after UV shadowing

The bands attributed to the conjugated material were excised from the gel and the final conjugated species was isolated from the gel matrix by further electroelution. The excised bands were crushed and transferred to the loading well of the electroelution apparatus and an electric potential was applied. The ruthenium-oligonucleotide conjugate migrated as expected into the anodic well leaving the polyacrylamide gel matrix behind in the loading well. Due to the relatively bulky structure of polyacrylamide, it was unable to pass through the semipermeable membranes of the loading well designed to allow free migration of cations and anions and thus provided a convenient method of isolating the ruthenium-oligonucleotide conjugates from the gel matrix.

2.8 Analysis of ruthenium-oligonucleotide conjugates

2.8.1 Conjugate 1: [Ru(phen)₂phen']-ODN

After isolation of the [Ru(phen)₂phen']-ODN conjugate (**figure 2.5**), analysis was carried out by UV-vis spectroscopy and HPLC. Both the oligonucleotide and the ruthenium complex absorb at 264 nm with only the ruthenium complex absorbing in the visible region at 450 nm (**figure 2.4**). Using the extinction coefficient values for the free 17mer, the free ruthenium complex and the linked species, the efficiency of the coupling reaction was calculated. The coupling reaction was carried out twice giving yields of 7 % and 10 % respectively. HPLC analysis of the conjugate showed one peak with a retention time of 13.01 min.

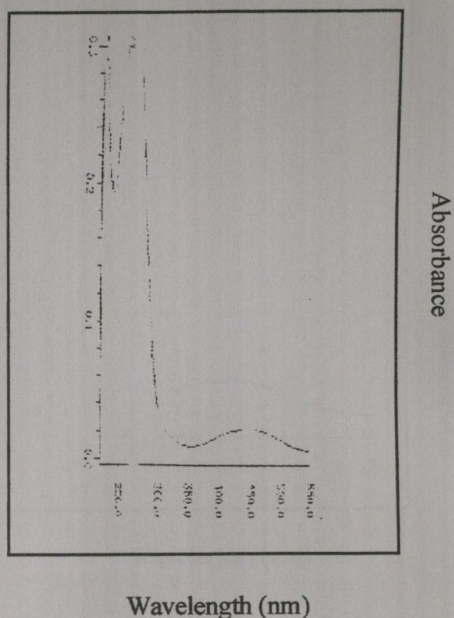


Figure 2.4 UV-vis spectrum of conjugate 1

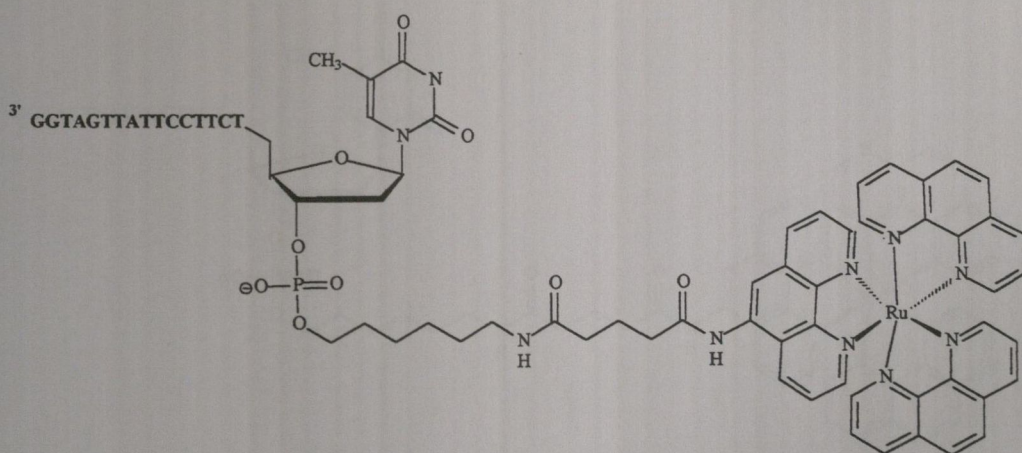


Figure 2.5 Structure of [Ru(phen)₂phen']-oligonucleotide conjugate 1

2.8.2 Conjugate 2: [Ru(TAP)₂phen']-ODN

The second [Ru(TAP)₂phen']-ODN conjugate (**figure 2.7**) was also analysed by UV-vis spectroscopy and HPLC analysis after isolation. Again both the oligonucleotide and the ruthenium complex show absorption in the UV region at 267 nm with the ruthenium complex absorbing in the visible region with λ_{max} at 415 nm and 470 nm (**figure 2.6**). As in section 2.8.1, the extinction coefficients of the species involved were used to calculate the efficiency of the reaction. The yield for the coupling reaction of the second conjugate was calculated to be 15 %. HPLC analysis of the conjugate showed one peak with a retention time of 8.99 min.

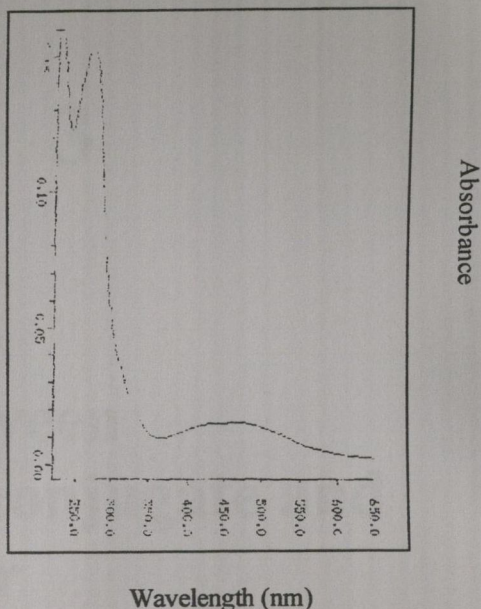


Figure 2.6 UV-vis spectrum of conjugate 2

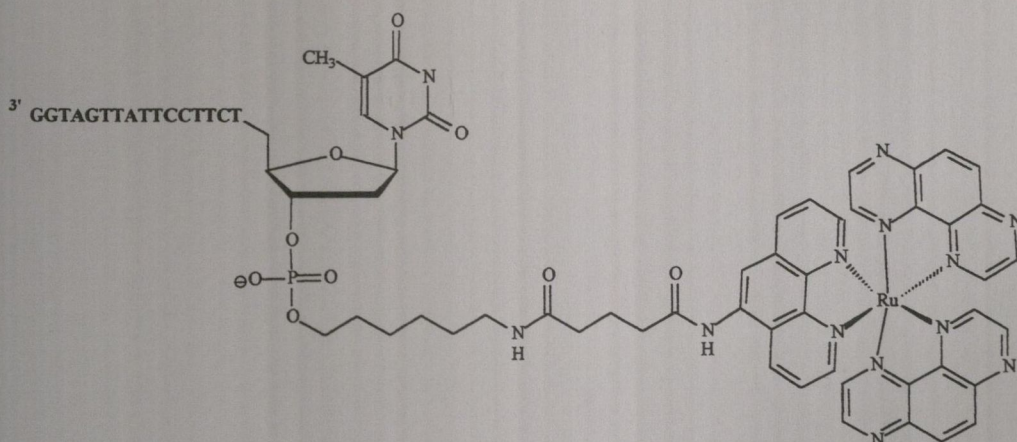


Figure 2.7 Structure of [Ru(TAP)₂phen']-oligonucleotide conjugate 2

CHAPTER 3

Interaction between [Ru(phen)₂phen']-ODN conjugate and target 34mer

3.1 Introduction

The target 34mer oligodeoxynucleotide (ODN) chosen for this work represents the fusion section of the *bcr / abl* messenger RNA (mRNA) which is specific only to cells affected by Chronic Myeloid Leukaemia (CML). The work discussed in this chapter describes the photochemical targeting of the 34mer target using the ruthenium-oligodeoxynucleotide conjugate, $[\text{Ru}(\text{phen})_2\text{phen}']\text{-ODN}$ (where phen = 1,10-phenanthroline and phen' = 5-(4-carboxybutanamido-1,10-phenanthroline) with a view to site-specific cleavage of the target strand. With regard to *in vivo* application of the work, cleavage of a mRNA strand will disrupt the normal translational step of gene expression, in which the mRNA information is used to build the corresponding cancer-causing proteins (oncoproteins), and thus down-regulating the normal gene expression of the starting oncogene.

The results of photocleavage experiments of the target 34mer ODN using the free ruthenium complex $[\text{Ru}(\text{phen})_2\text{phen}']^{2+}$ and the standard $[\text{Ru}(\text{phen})_3]^{2+}$ complex are described. The photocleavage of the 34mer target strand using the ruthenium-ODN conjugate is investigated by addition of various reagents to study the mechanism by which the ruthenium complex induces strand damage. The range of oxidative damage is also studied with variant target strands in place of the parent 34mer target ODN in order to investigate the effect of gradually moving the target guanine base further away from the ruthenium complex. The system is also studied with a random sequence in place of the 34mer ODN target to ensure sequence specificity of the ruthenium-conjugate for the 34mer target and not for induction of photocleavage in random non-leukaemic related ODN sequences.

3.2 Description of model system

The ultimate aim of this section of work was the site-specific photooxidative induced cleavage in the parent 34mer target oligodeoxynucleotide (ODN) representing the leukaemic mRNA using the previously synthesised [Ru(phen)₂phen']-ODN conjugate. This involved the design and optimisation of a model *in vitro* Chronic Myeloid Leukaemia (CML) system representing the *in vivo* situation where the ruthenium-ODN conjugate could be used as an antisense vector in addition to the utilisation of the photochemical properties of the ruthenium complex itself to specifically target a particular base in the target 34mer sequence. The resulting photocleavage of the target sequence would, *in vivo*, cause disruption of normal gene expression, therefore the mRNA would be unable to produce the corresponding oncoproteins and in theory, the symptoms of CML would not be manifested in the patient.

The model system used for this work consisted of a target 34mer ODN with a sequence specific to the *bcr / abl* fusion section of CML mRNA and of the ruthenium-ODN conjugate, [Ru(phen)₂phen']-ODN (**figure 3.1**). *In vivo*, the target strand is RNA, but for the purpose of the model system a single-stranded DNA oligodeoxynucleotide of equivalent sequence was used. The ODN conjugated to the ruthenium complex was 17 bases in length and was complementary to one section of the target 34mer ODN. This was to ensure that upon hybridisation of the two complementary regions, the ruthenium complex would be orientated in such a position as to allow maximum induction of site-specific damage at the target base. The design of the ruthenium-ODN conjugate also ensured that the 17mer would bind

only to the leukaemic mRNA and not to any other random DNA sequence. This was very important in relation to the clinical application of the work, as the conjugate must only bind to and cleave the leukaemic mRNA and not any other nucleic acid sequence.

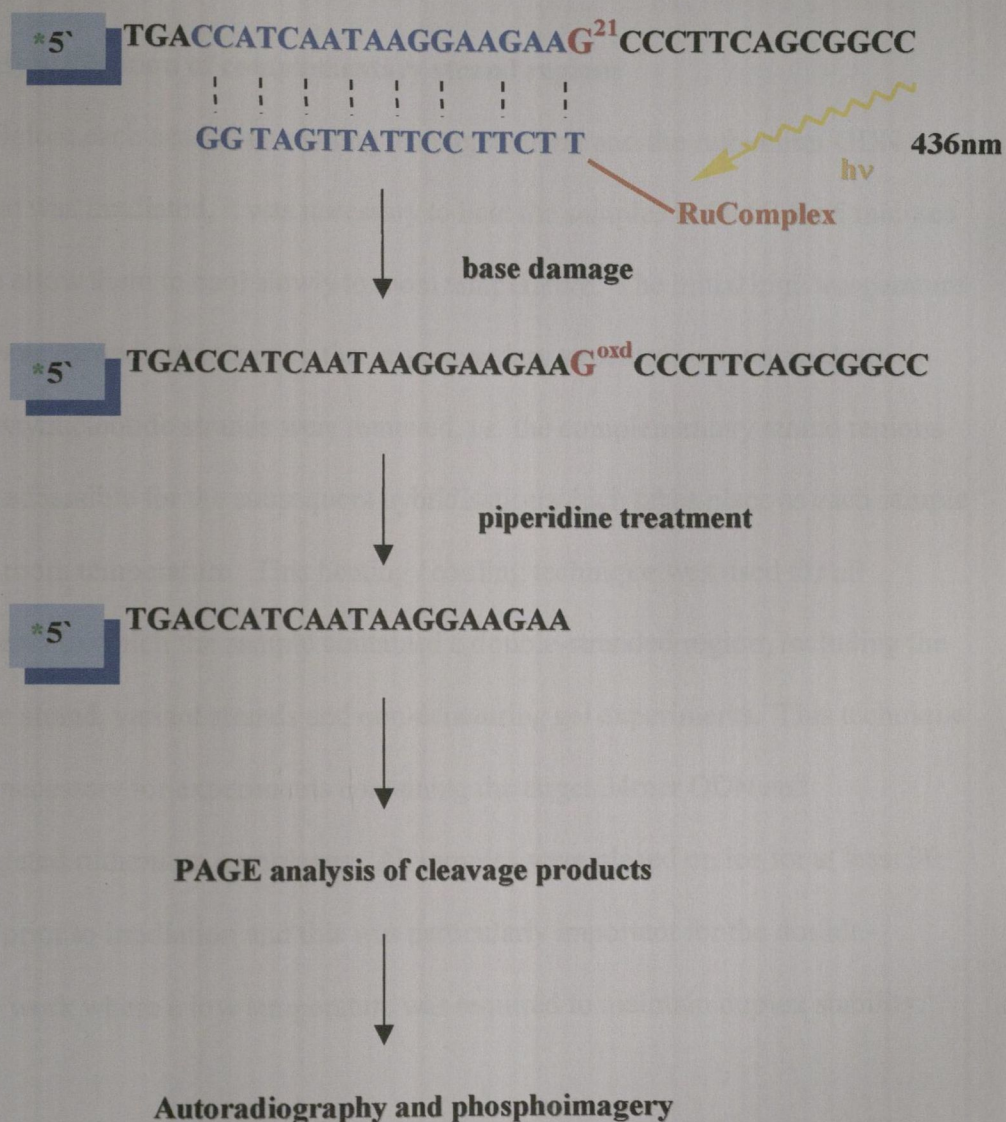


Figure 3.1 Model system of target 34mer and [Ru(phen)₂phen⁺]-ODN conjugate

The target base in the 34mer ODN target strand was a guanine residue situated 21 bases from the 5'-end, referred to as G21. For all the work described in the following chapters, bases are described in relation to their position from the 5'-end of the particular ODN sequence *e.g.* G32 would refer to a guanine residue 32 bases from the 5'-end and T25 would refer to a thymine residue 25 bases from the 5'-end.

3.2.1 Hybridisation of complementary strand regions

Before each sample containing the target strand and the ruthenium-ODN conjugate was irradiated, it was necessary to heat the samples to 80 °C for 5 minutes and then allow them to cool slowly to room temperature. The initial high temperature heating was carried out to ensure that any secondary structures present in the oligodeoxynucleotide strands were removed, *i.e.* the complementary strand regions are fully accessible for the subsequent hybridisation which takes place as each sample cools to room temperature. This heating / cooling technique was used for all experiments in which the sample contained a double-stranded region, including the nonsense strand, variant strands and non-denaturing gel experiments. This technique was not necessary for experiments containing the target 34mer ODN and unconjugated ruthenium complexes. All samples were placed on ice for at least 30 minutes prior to irradiation and this was particularly important for the double-stranded work where a low temperature was required to maintain duplex stability.

3.2.2 Ionic strength conditions

The buffer salt concentration was also a consideration in the optimisation of the system. A high salt concentration is known to encourage secondary structure formation *e.g.* hybridisation, hairpinning etc., and previous work carried out by this research group had shown that a greater yield of photocleavage was obtained at high salt concentration (10 mM potassium phosphate buffer / 100 mM NaCl) compared to results at low salt concentration (10 mM potassium phosphate buffer).¹⁵¹ Working in a high salt environment also had the advantage of being closer to the actual physiological salt concentration of approximately 150 mM, thus making the work more applicable to biological systems.

3.2.3 Irradiation conditions

All samples containing either the free ruthenium complex or the ruthenium-ODN conjugate were irradiated at 436 nm for varying periods of time. The irradiations were carried out with a Pyrex™ glass filter in place to remove wavelengths less than 330 nm, thus making it possible to selectively excite the ruthenium complex in the presence of the nucleotides that absorb strongly at approximately 260 nm. Some experiments were also carried out with a sodium nitrite filter in place in addition to the Pyrex™ glass filter. Sodium nitrite removes wavelengths less than 400 nm. In all irradiation experiments, the beam was initially passed through a water filter to remove any excess heat generated during the course of the experiments.

3.2.4 Piperidine treatment

Cleavage of DNA as a result of nucleobase modification usually requires a second chemical step to effect the strand scission. All nucleobases are acid-labile to some degree. In general, therefore, alkaline conditions are used because nucleobases are relatively stable to alkaline conditions unless modification of the nucleobase has occurred. Piperidine treatment (1M piperidine added to sample followed by heating at 90°C for 30 minutes) will cleave DNA strands at points of nucleobase modification. Generally nucleobase oxidation will remove electron density from the heterocycle making the modified nucleobase a better leaving group in order to form an abasic site. The cleavage occurs as a phosphate elimination yielding the 3' fragment of the original strand. A second phosphate elimination yields the 5' fragment of the original strand terminating in a 3' phosphate (figure 3.2).

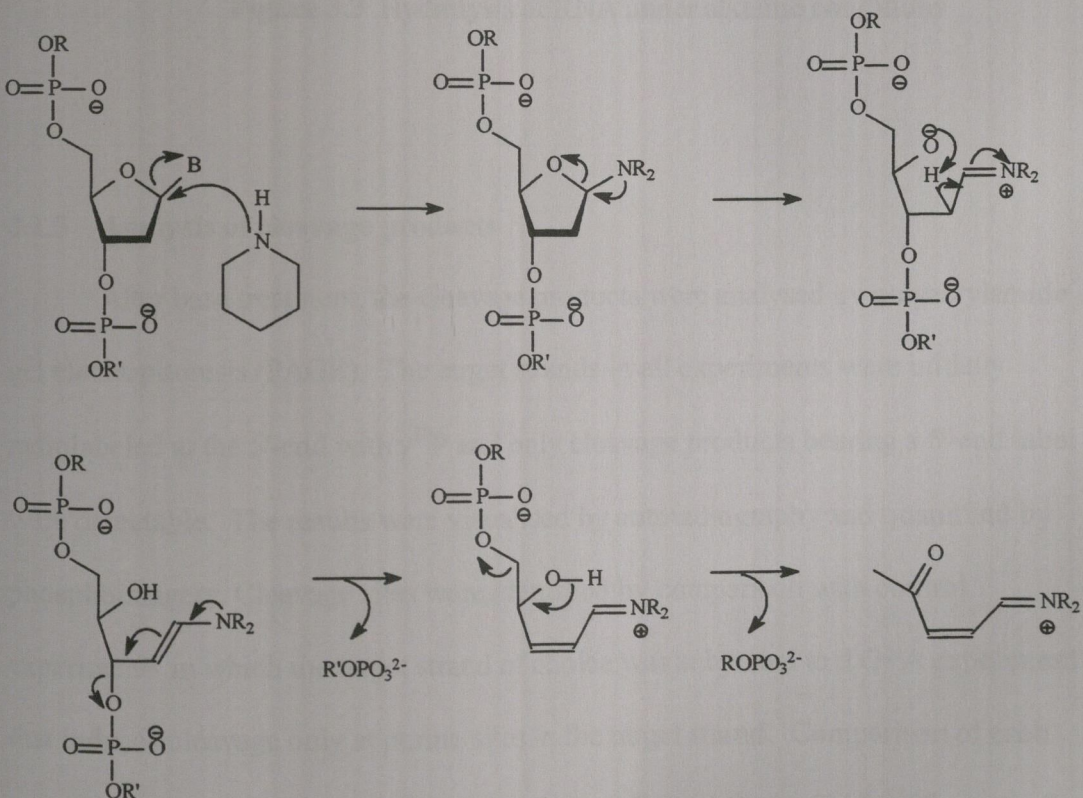


Figure 3.2 Mechanism of piperidine treatment at modified nucleobase

Unlike DNA, all the phosphodiester linkages in RNA are subject to alkaline hydrolysis due to the presence of the 2'-hydroxyl group (**figure 3.3**), therefore in order to reveal sites of nucleobase modification in RNA strands, milder reaction conditions are employed, usually using aniline.

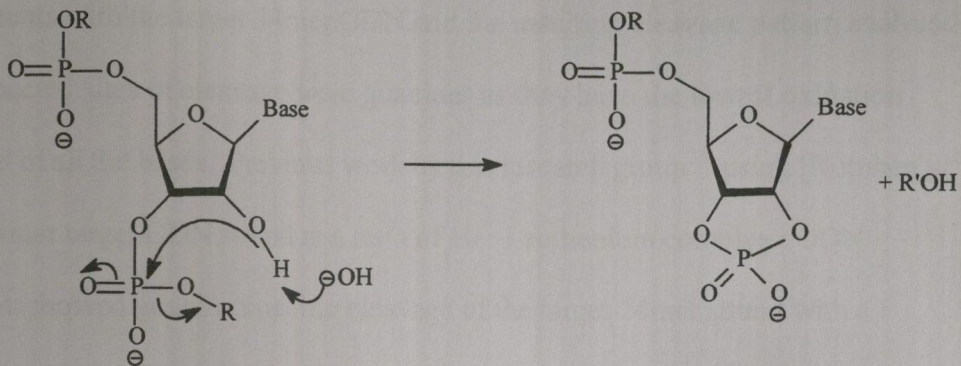


Figure 3.3 Hydrolysis of RNA under alkaline conditions

3.2.5 Analysis of cleavage products

After base treatment, the cleavage products were analysed by polyacrylamide gel electrophoresis (PAGE). The target strands in all experiments were initially radiolabeled at the 5'-end with $\gamma^{32}\text{P}$ and only cleavage products bearing a 5'-end label were detectable. The results were visualised by autoradiography and quantified by phosphoimager. Cleavage sites were identified by comparison with control experiments in which the target strand of choice was subjected to a G+A experiment that induces cleavage only at purine sites in the target strand. Comparison of each experiment with an equivalent G+A experiment allowed for rapid identification of

cleavage sites. Details of PAGE, 5'-end labeling, G+A experiments, autoradiography and phosphoimagery are discussed in chapter 5.

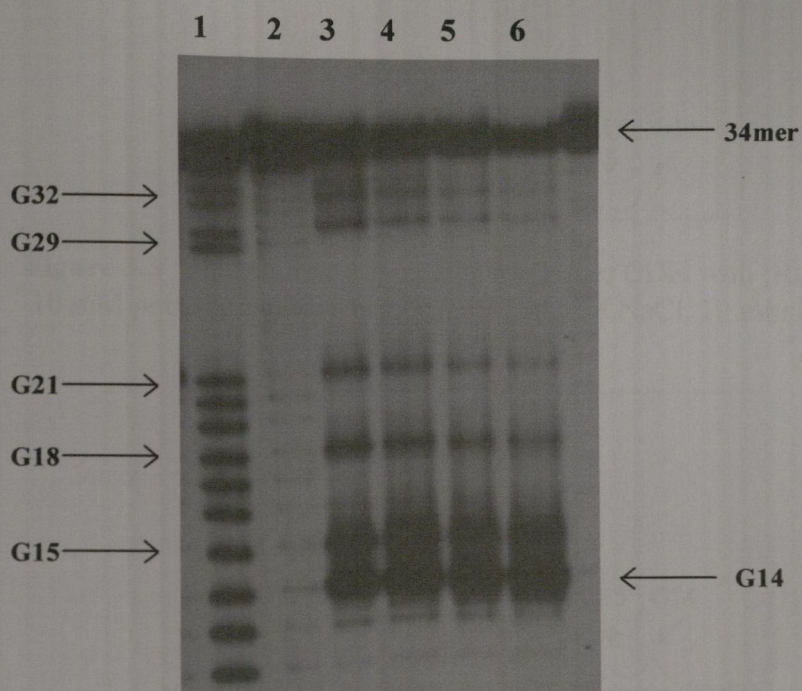
3.3 Photocleavage studies using free ruthenium complexes

Both free $[\text{Ru}(\text{phen})_3]^{2+}$ and $[\text{Ru}(\text{phen})_2\text{phen}']^{2+}$ were studied in irradiation experiments with the target 34mer ODN and the resulting cleavage pattern analysed. The expected sites of cleavage were guanines as they have the lowest oxidation potential of all the bases. Previous work by this research group¹⁵¹ using $[\text{Ru}(\text{phen})_3]^{2+}$ and a 24mer target ODN strand at a ratio of 10 : 1 ruthenium complex : ODN fragment, showed guanine specific cleavage of the target 24mer strand with a preference for the 5'-guanine of GG doublets. Higher cleavage yields were also obtained when the experiments were carried out in a high salt buffer compared to yields obtained in a low salt buffer.

3.3.1 Photocleavage of target 34mer ODN by $[\text{Ru}(\text{phen})_3]^{2+}$

Irradiation experiments with $[\text{Ru}(\text{phen})_3]^{2+}$ and the target 34mer ODN were initially carried out using a 10 : 1 ratio of ruthenium complex : ODN fragment under both high and low salt conditions using a variety of irradiation times. Irradiation at 436 nm was followed by piperidine treatment unless stated otherwise. As found for the 24mer target, results showed guanine-specific cleavage of the target 34mer ODN with a preference for the 5'-guanine of the ⁵ G14G15 ³ doublet. The work was

repeated with the ratio of ruthenium complex : ODN reduced from 10 : 1 to 1 : 1, and a similar cleavage pattern was obtained (**figure 3.4**)



Irradiations carried out in 10 mM phosphate buffer / 100 mM NaCl; all samples contain 1 : 1 ratio ruthenium : ODN. **Lane 1** G+A; **Lane 2** 0 min; **Lane 3** 2.5 min; **Lane 4** 5 min; **Lane 5** 10 min; **Lane 6** 20 min.

Figure 3.4 34mer ODN cleavage by $[\text{Ru}(\text{phen})_3]^{2+}$

Experiments comparing the effect of high and low salt buffer conditions (**figure 3.5** and **3.6**) showed that a slightly higher yield of guanine specific cleavage was observed under high salt conditions, with the maximum of cleavage observed, as

expected, at G14 of the G14G15 doublet (**table 3.1**).

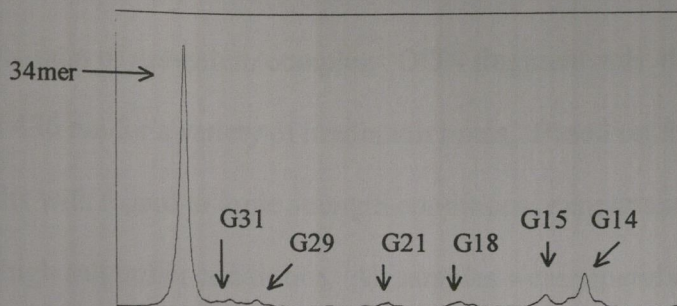


Figure 3.5 Phosphoimager results for 34mer ODN with $[\text{Ru}(\text{phen})_3]^{2+}$, 10 mM potassium phosphate buffer / 100 mM NaCl, 10 min irradiation.

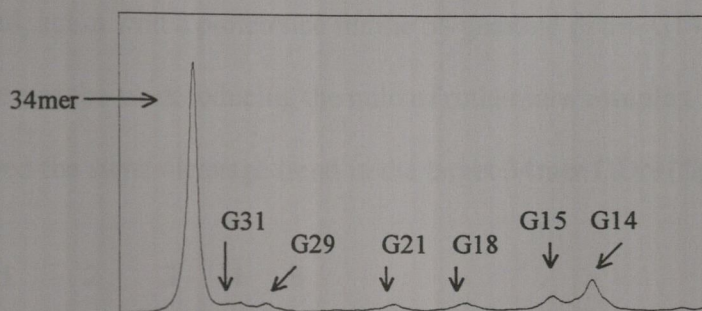


Figure 3.6 Phosphoimager results for 34mer ODN with $[\text{Ru}(\text{phen})_3]^{2+}$, 10 mM potassium phosphate buffer, 10 min irradiation.

Position cleaved	% cleavage under high salt conditions	% cleavage under low salt conditions
G31	3.3	2.7
G29	2.4	2.2
G21	2.0	2.3
G18	2.3	3.5
G15	4.8	4.5
G14	11	7.6

Table 3.1 Comparison of 34mer cleavage with $[\text{Ru}(\text{phen})_3]^{2+}$ under high and low salt conditions

3.3.2 Photocleavage of target 34mer ODN by $[\text{Ru}(\text{phen})_2\text{phen}']^{2+}$

The ability of the unconjugated ruthenium complex $[\text{Ru}(\text{phen})_2\text{phen}']^{2+}$ to induce photocleavage in the target 34mer ODN was also studied. Initial studies were carried out at a 10:1 ratio of ruthenium complex : ODN fragment with the samples being irradiated at 436 nm for a variety of irradiation times. Based on the previous $[\text{Ru}(\text{phen})_3]^{2+}$ results with regard to ionic strength conditions, experiments were carried out under high salt buffer conditions. All samples were piperidine treated after irradiation to reveal sites of oxidative damage. As expected for this type of ruthenium complex, irradiation at 436 nm induced guanine-specific cleavage in the target 34mer strand, again with a preference for the 5'- guanine of the G14G15 doublet. Repetition of the work reducing the ratio of ruthenium complex : ODN from 10 : 1 to 1:1 showed the same cleavage trend in the target 34mer ODN (**figure 3.7**).

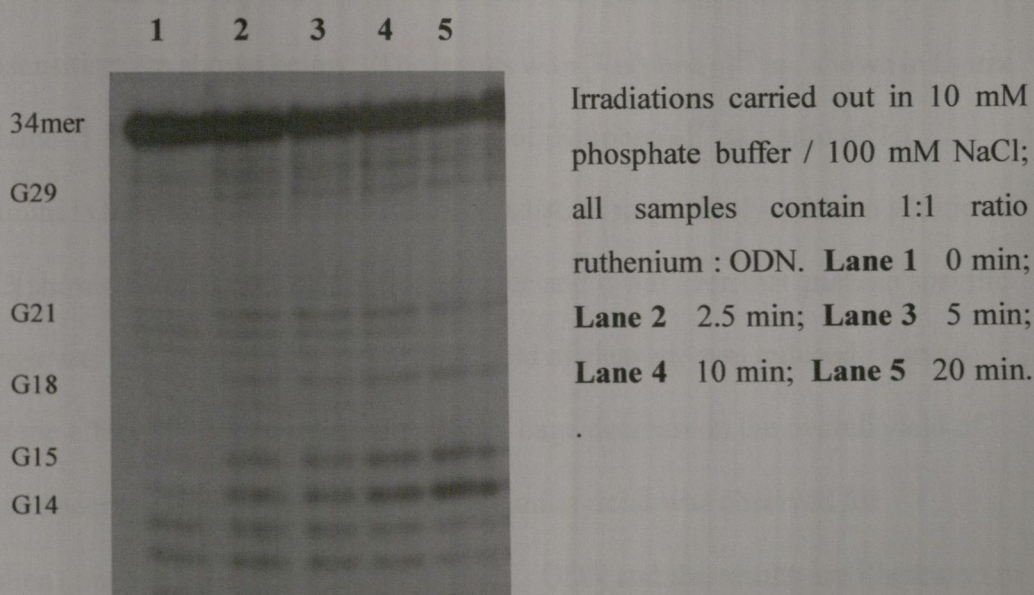


Figure 3.7 34mer ODN cleavage by $[\text{Ru}(\text{phen})_2\text{phen}']^{2+}$

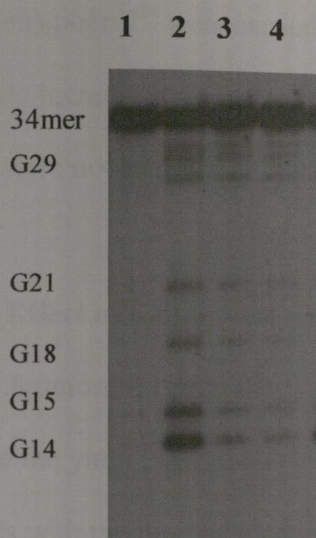
3.4 Effect of various additions on the photocleavage of target 34mer ODN by $[\text{Ru}(\text{phen})_3]^{2+}$ and $[\text{Ru}(\text{phen})_2\text{phen}']^{2+}$

3.4.1 Effect of sodium azide (NaN_3) and argon

As discussed in section 1.9, ruthenium complexes can induce base damage by two main mechanisms referred to as type 1 and type 2 damage. As a type 2 pathway involves the generation of singlet oxygen ($^1\text{O}_2$) from ground state oxygen, pathways involving $^1\text{O}_2$ should show a reduction in base damage upon inclusion of a singlet oxygen quencher, such as sodium azide (NaN_3). Alternatively, carrying out experiments under an atmosphere of argon will also decrease the amount of $^1\text{O}_2$ damage due to the decrease in the amount of molecular oxygen initially available from which $^1\text{O}_2$ can be generated.

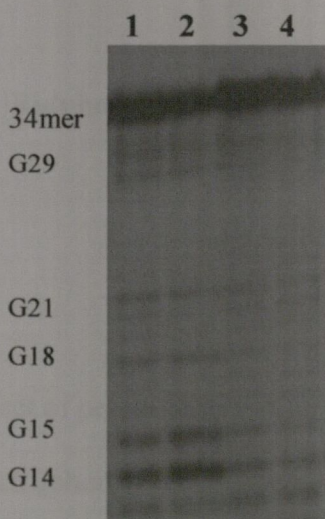
The results of experiments that included NaN_3 and argon in addition to free photosensitiser are shown below. The results with $[\text{Ru}(\text{phen})_3]^{2+}$ are shown in **figure 3.8**. Lanes 1 and 2 show the cleavage results of $[\text{Ru}(\text{phen})_3]^{2+}$ at a ratio of 1:1 ruthenium : ODN after 0 mins and 10mins irradiation respectively, with no additions. Lane 3 shows the effect of the addition of azide and it was seen that guanine specific cleavage was still achieved but the overall yield of cleavage was reduced. Lane 4 shows the effect of argon purging and again a large decrease in the overall yield of guanine specific cleavage was observed. A similar trend was observed for $[\text{Ru}(\text{phen})_2\text{phen}']^{2+}$ at a ratio of 1:1 ruthenium : ODN and the results are illustrated in **figure 3.9**. Lanes 1 and 2 show the guanine specific cleavage of the target 34mer ODN after 10 mins and 20 mins respectively. No cleavage was seen without

irradiation. Lanes 3 and 4 show the effect of azide and argon on the cleavage yield after 10 mins irradiation. A large overall decrease in the guanine specific cleavage was observed in both cases.



All samples contain 1:1 ratio $[\text{Ru}(\text{phen})_3]^{2+}$: ODN. Irradiations carried out in 10 mM phosphate buffer / 100 mM NaCl; **Lane 1** 0 min; **Lane 2** 10 min; **Lane 3** 10 min, NaN_3 **Lane 4** 10 min, argon.

Figure 3.8 Effect of azide and argon on 34mer ODN cleavage with $[\text{Ru}(\text{phen})_3]^{2+}$



All samples contain 1:1 ratio $[\text{Ru}(\text{phen})_2\text{phen}']^{2+}$: ODN. Irradiations carried out in 10 mM phosphate buffer / 100 mM NaCl; **Lane 1** 10 min; **Lane 2** 20 min; **Lane 3** 10 min, NaN_3 **Lane 4** 10 min, argon.

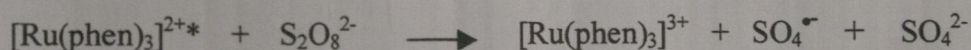
Figure 3.9 Effect of azide and argon on 34mer ODN cleavage with $[\text{Ru}(\text{phen})_2\text{phen}']^{2+}$

3.4.2 Effect of D₂O

As the lifetime of singlet oxygen is increased in D₂O, an increase in the overall cleavage yield would be expected from a cleavage mechanism dependent on singlet oxygen generation. The experiments with both [Ru(phen)₃]²⁺ and [Ru(phen)₂phen']²⁺ were carried out in a D₂O buffer solution. Results showed a moderate increase in the amount of guanine specific cleavage obtained, but these results were not as consistent and clear as the results obtained with azide and argon.

3.4.3 Effect of ammonium persulfate

Ammonium persulfate ((NH₄)₂S₂O₈) is an electron transfer agent known to increase the yield of cleavage induced by ruthenium complexes. The persulfate anion interacts with the excited state of the ruthenium complex generating the Ru(III) complex in addition to the radical anion SO₄^{•-}, which is also a highly reactive species. Ru(III) is a stronger oxidant than Ru(II), thus a higher yield of cleavage is expected (equation 3.1).



Equation 3.1 Mechanism of action of ammonium persulfate

The effect of persulfate addition was investigated in both [Ru(phen)₃]²⁺ and [Ru(phen)₂phen']²⁺ experiments. With both complexes, an increase in the overall yield of guanine specific cleavage was observed. **Figure 3.10** shows the

phosphoimagery results for the 34mer ODN target with $[\text{Ru}(\text{phen})_2\text{phen}']^{2+}$ with the inclusion of persulfate and an irradiation time of 10mins. As expected, a greater overall yield of guanine specific cleavage was achieved compared to an analogous sample containing no persulfate. **Figure 3.11** displays the difference in percentage cleavage at guanine sites for target 34mer ODN damage by $[\text{Ru}(\text{phen})_2\text{phen}']^{2+}$ with and without persulfate inclusion at comparable irradiation times.

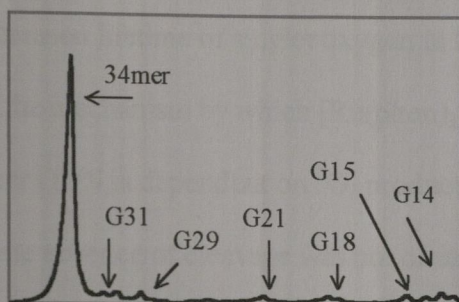


Figure 3.10 Phosphoimagery results for 34mer ODN with $[\text{Ru}(\text{phen})_2\text{phen}']^{2+}$, 10 mM potassium phosphate buffer / 100 mM NaCl, 10 min irradiation, $\text{S}_2\text{O}_8^{2-}$

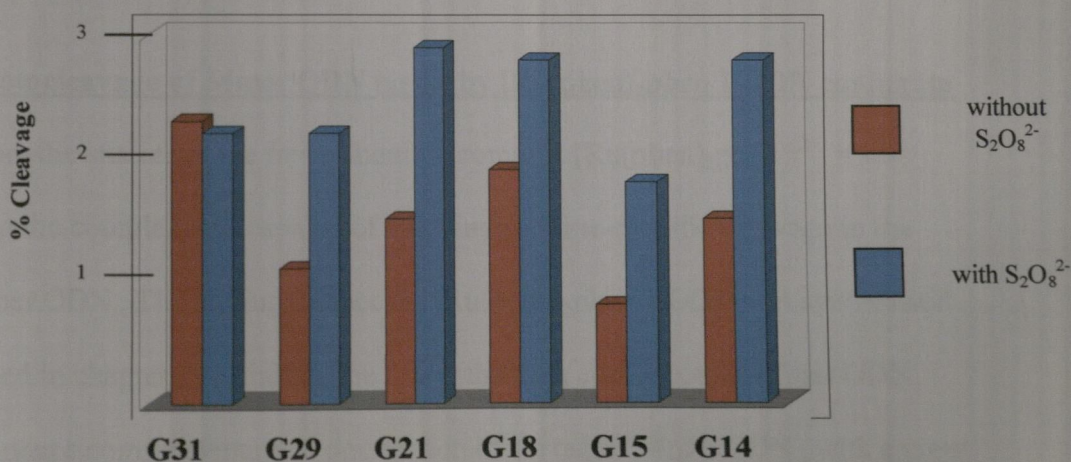


Figure 3.11 Comparison of 34mer ODN cleavage by $[\text{Ru}(\text{phen})_2\text{phen}']^{2+}$ in presence and absence of persulfate

3.5 Mechanism of base damage with free ruthenium complexes

The inclusion of a singlet oxygen quencher, sodium azide, showed a partial reduction in the overall yield of guanine specific cleavage in the target 34mer ODN by both free ruthenium complexes. A more substantial reduction was seen in the overall cleavage by both complexes in experiments purged with argon initially and maintained under an atmosphere of argon for the course of the irradiations, thus inhibiting the initial generation of singlet oxygen. In addition to these results, the results from the D₂O experiments showed a slight increase in the overall cleavage, possibly due to the increased lifetime of singlet oxygen in the D₂O environment. It can be concluded that the mechanism by which [Ru(phen)₃]²⁺ and [Ru(phen)₂phen']²⁺ cleaves the target 34mer ODN is dependent on ¹O₂ production *i.e.* a type II mechanism. A complete absence of cleavage was not observed for either the azide or argon experiments and although this results seems to suggest some cleavage by a type I mechanism, the result may have been due to traces of oxygen remaining in the experimental samples.

3.6 Photocleavage of 34mer ODN target by [Ru(phen)₂phen']-ODN conjugate

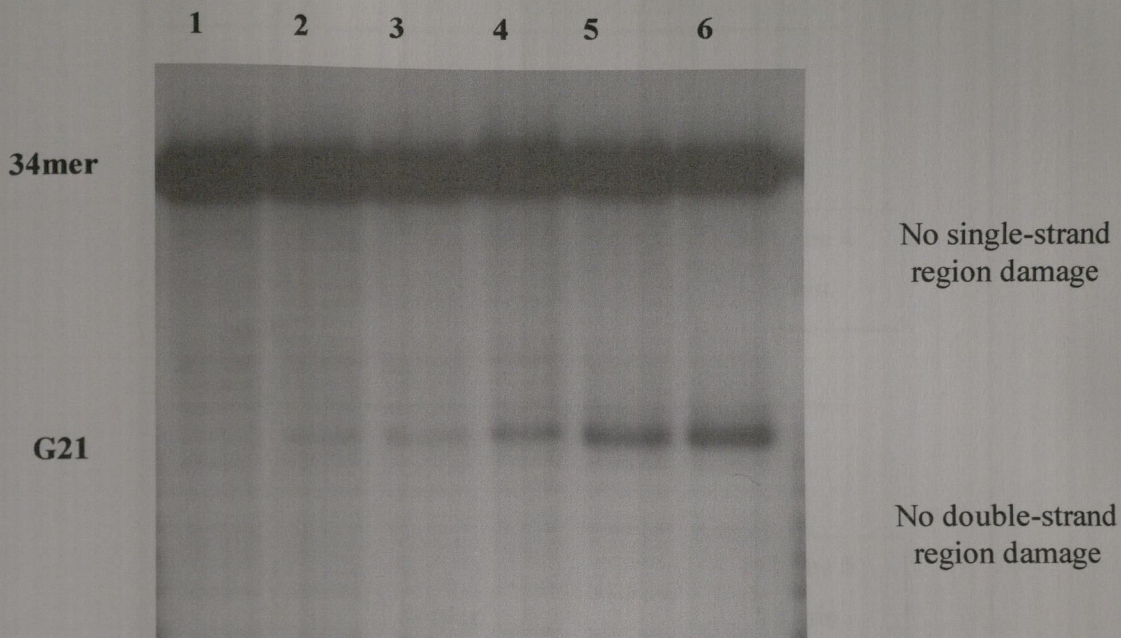
From the studies of the free ruthenium complex [Ru(phen)₂phen']²⁺, it was shown that the complex was capable of inducing guanine-specific cleavage in the target 34mer ODN. The conjugate species, [Ru(phen)₂phen']-ODN was synthesised as described in chapter 2 by linking the free ruthenium complex to a 17mer ODN with a sequence complementary to one section of the target 34mer ODN, with a view to site-specific cleavage of the target 34mer ODN at G21.

Initial work with the ruthenium-ODN conjugate was carried out in high salt conditions (10 mM potassium phosphate buffer / 100 mM NaCl) using a ratio of 10:1 ruthenium conjugate : target 34mer ODN. High salt conditions were favoured as they promote duplex formation, thus ensuring stable hybridisation between the 17mer ODN of the ruthenium conjugate and its complementary region in the target 34mer ODN. This was important in ensuring correct orientation of the ruthenium complex in the model system in order to induce optimal site-specific cleavage at the G21 target. Irradiations were carried out at various times between 0 mins and 40 mins and all samples were piperidine treated unless otherwise stated.

Results showed that optimal site-specific cleavage of the target 34mer ODN was obtained after 20 mins irradiation. Further experiments were conducted using reduced ratios of ruthenium conjugate : 34mer ODN target. Ratios of 5:1, 2:1 and 1:1 were investigated and it was found that the 1:1 ratio experiment gave results comparable to those of the 10:1 ratio experiments. Therefore all subsequent work with the $[\text{Ru}(\text{phen})_2\text{phen}']$ -ODN conjugate was carried out at the reduced ratio of 1:1.

Lanes 1-6 in **figure 3.12** show the G21 specific cleavage induced by the $[\text{Ru}(\text{phen})_2\text{phen}']$ -ODN conjugate with irradiation times of 0 min up to 20 mins using a 1:1 ratio of ruthenium conjugate : target 34mer ODN fragment. An increase in G21 cleavage was observed upon increased irradiation times, with a maximum amount of cleavage obtained after 20 mins (Lane 6). No cleavage was observed in the double-stranded region of the 34mer ODN *i.e.* no G18, G15 or G14 cleavage. Additionally, no cleavage was observed in the single-stranded region of the 34mer ODN other than at the G21 target *i.e.* no cleavage was observed at the 3'-end guanines at G32, G31 or

G29. The phosphoimagery results of selected lanes are shown in **figure 3.13** with the percentage cleavage of G21 at each irradiation time shown in **table 3.2**.



Irradiations carried out in 10 mM phosphate buffer / 100 mM NaCl; all samples contain 1:1 ratio ruthenium conjugate : 34mer ODN. **Lane 1** 0 min; **Lane 2** 1 min; **Lane 3** 2.5 min; **Lane 4** 5 min; **Lane 5** 10 min; **Lane 6** 20 min.

Figure 3.12 34mer ODN cleavage by [Ru(phen)₂phen⁺]-ODN conjugate

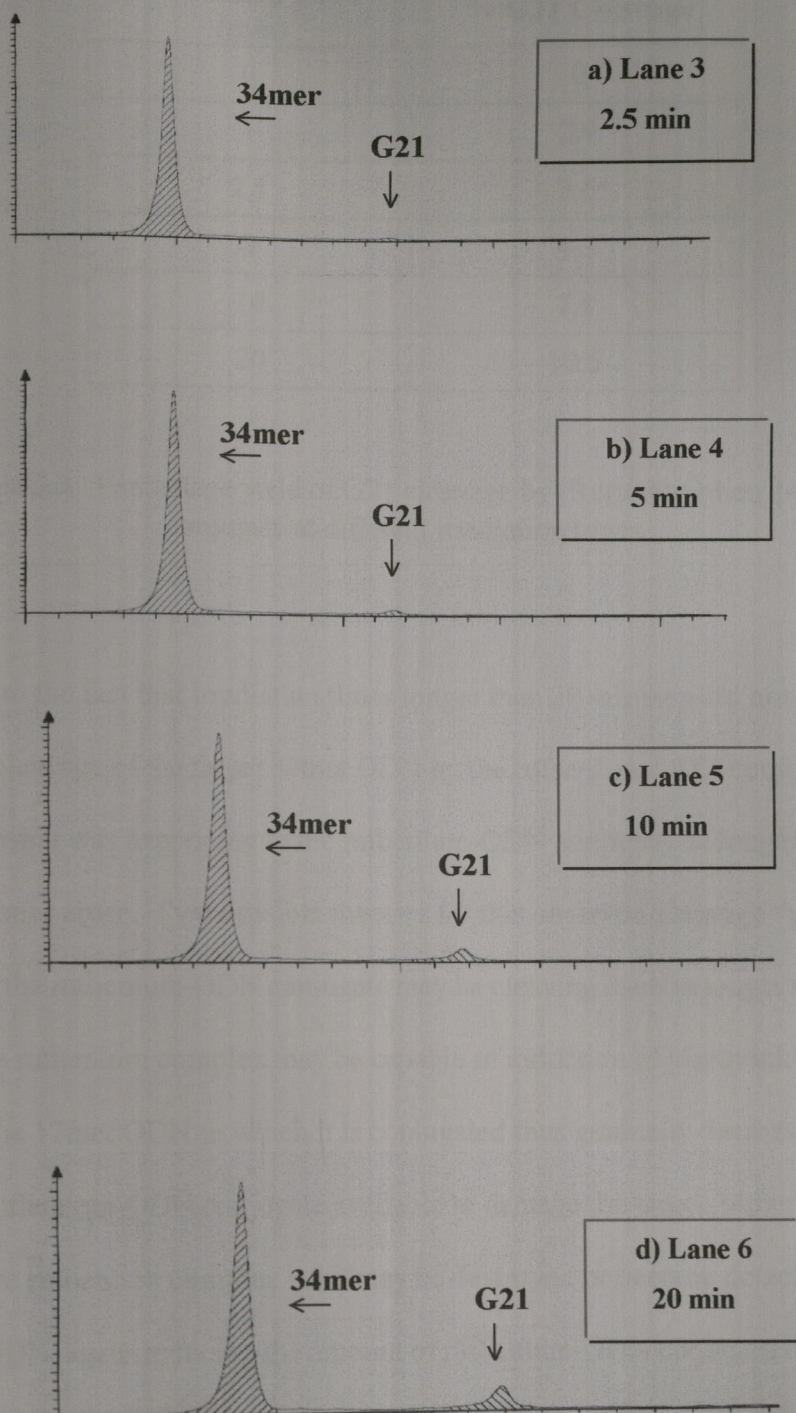


Figure 3.13 Phosphoimagery results of 34mer ODN cleavage by $[\text{Ru}(\text{phen})_2\text{phen}']\text{-ODN}$ after irradiation times of a) 2.5 min b) 5 min c) 10 min and d) 20 min

Irradiation Time (min)	% G21 Cleavage
0	0
1	2.9
2.5	3.6
5	4.3
10	7.4
20	10.6

Table 3.2 Percentage yield of G21 cleavage by [Ru(phen)₂phen`]-ODN conjugate at different irradiation times

Due to the fact that irradiation times longer than 20 minutes did not result in any further cleavage of the target 34mer ODN by the ruthenium-ODN conjugate, the question of what was happening to the ruthenium-ODN conjugate at longer irradiation times arose. Two possible theories for this observed cleavage “plateau” include that the ruthenium-ODN conjugate may be cleaving itself at longer irradiation times *i.e.* the ruthenium complex may be capable of induction of photooxidative damage in the 17mer ODN to which it is conjugated thus gradually decreasing the amount of ruthenium-ODN conjugate available to damage the target 34mer ODN. Secondly, the ruthenium complex itself may be destroyed or become detached from the 17mer ODN, again reducing the amount of ruthenium-ODN conjugated species available to induce site-specific damage in the target strand. This problem of the “leveling off” of the cleavage efficiency of the ruthenium complex is addressed in section 3.12.

3.7 Effect of the presence of sodium nitrite filter

The effect of the presence of a sodium nitrite (NaNO_2) filter on the overall ability of the ruthenium-ODN conjugate to induce site-specific cleavage in the target 34mer ODN was also investigated. Sodium nitrite removes wavelengths less than 400 nm and the beam from the lamp was passed through a solution of sodium nitrite (1 M) before being directed onto the experimental sample of interest. The Pyrex™ glass filter, which removes wavelengths less than 330 nm, was also included in the experimental setup.

The experiments were carried out under identical conditions to those described in section 3.6, except for the presence of the sodium nitrite filter *i.e.* using a 1:1 ratio of ruthenium conjugate : 34mer target ODN in high salt buffer conditions and followed by piperidine treatment.

Analysis of the results showed that site-specific cleavage of the target 34mer ODN at G21 was achieved, but that the overall yield was lower than experiments conducted in the absence of the sodium nitrite filter. G21 site-specific cleavage was induced by the $[\text{Ru}(\text{phen})_2\text{phen}']$ -ODN conjugate in experiments conducted with irradiation times of 1 min up to 20 mins. Again an increase in G21 cleavage was seen with increasing irradiation times up to a maximum amount of cleavage after 20 mins. In a similar manner to the non-filtered experiment results, no cleavage was seen in the single-stranded or double-stranded regions of the 34mer ODN target, apart from the observed cleavage at G21.

The results of the filtered and non-filtered experiments are compared in **figure 3.14**. In the non-filtered experiment, the maximum yield of G21 cleavage induced by

the ruthenium-ODN conjugate was 10.6 % after 20 mins. A maximum of 3.6 % was obtained in an identical experiment under filtered conditions. The phosphoimager results after 20 mins irradiation are shown for the non-filtered and filtered experiments in **figures 3.15 and 3.16** respectively.

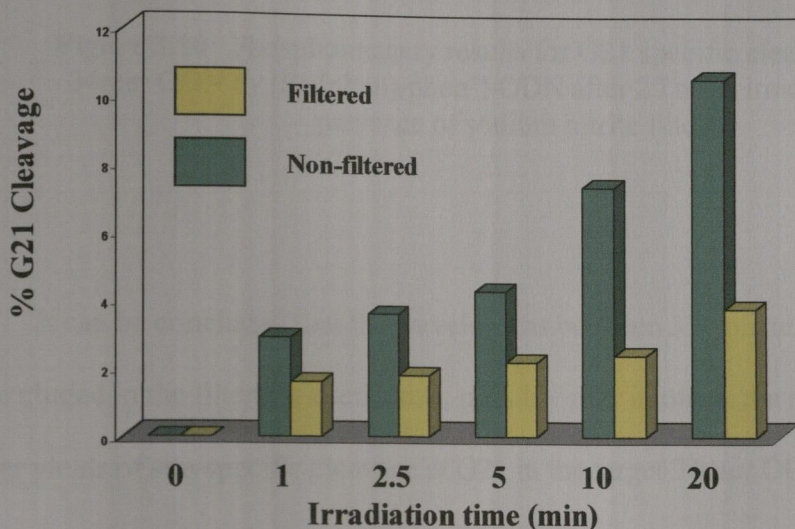


Figure 3.14 Comparison of G21 cleavage in target 34mer ODN by $[\text{Ru}(\text{phen})_2\text{phen}']\text{-ODN}$ in presence and absence of sodium nitrite filter

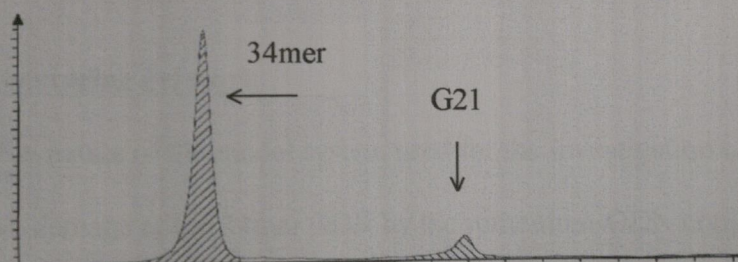


Figure 3.15 Phosphoimager results for G21 specific cleavage of target 34mer ODN by $[\text{Ru}(\text{phen})_2\text{phen}']\text{-ODN}$ after 20 mins irradiation in the absence of sodium nitrite filter

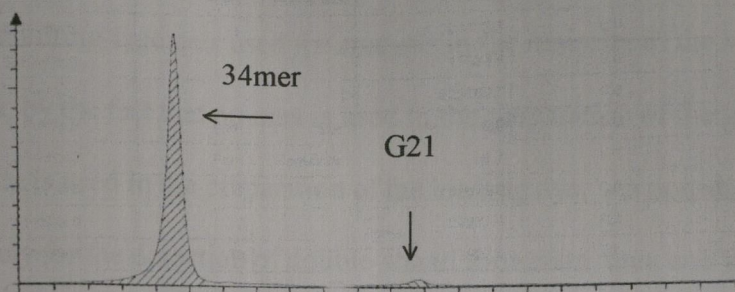


Figure 3.16 Phosphoimager results for G21 specific cleavage of target 34mer ODN by $[\text{Ru}(\text{phen})_2\text{phen}']\text{-ODN}$ after 20 mins irradiation in the presence of sodium nitrite filter

It can be concluded that the wavelengths between 330 nm and 400 nm, which are excluded in the filtered experiments, possibly play a role in the achievement of higher yields of site-specific cleavage at G21 in the target 34mer ODN.

Alternatively, passing the beam through the sodium nitrite filter could possibly remove some power from the beam thus resulting in the experimental samples being irradiated with a weaker beam and explaining the overall weaker yield of G21 damage.

3.8 Non-denaturing gel work

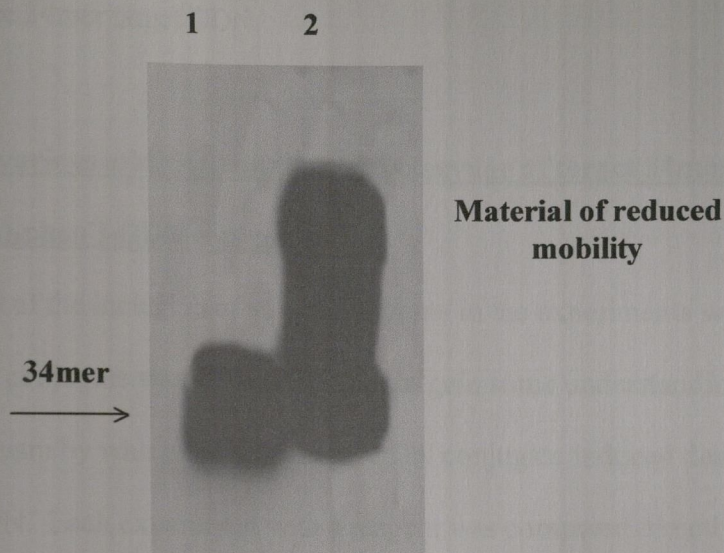
Due to the nature of the model system used for the investigation of the photooxidative damage of the 34mer ODN by the ruthenium-ODN conjugate, it was necessary to confirm that hybridisation was occurring between the complementary sections of the target 34mer ODN and the 17mer of the ruthenium-ODN conjugate before the irradiation of the samples. Various samples were analysed using non-

denaturing gels to verify duplex formation. Non-denaturing gels differ from the more common denaturing-type gels used for analysis in the majority of the work described in this thesis, by the fact that no urea is used in the preparation of the gel matrix and no formamide is used in the preparation of the loading dye. As non-denaturing gels are used solely for the detection of double-strand formation, urea and formamide are excluded as both favour the denaturation of oligodeoxynucleotide strands, thus suppressing base pairing in complementary sections. The gel itself was electrophorised at a low voltage compared to denaturing gels as the heat generated by electrophoresis can cause DNA denaturation. In addition, samples subject to non-denaturing gel analysis were not irradiated or piperidine treated, as the pattern of photooxidative damage in the target 34mer ODN was not being analysed in this case.

Only the target ODN strand was radiolabeled (section 5.9.1) *i.e.* had a radioactive label attached at its 5'-end, therefore only the target strand and anything bound to the target strand could be visualised by autoradiography. Subsequently, if the ruthenium-ODN conjugate were bound to the target 34mer ODN, a band of reduced mobility with respect to the free 34mer target band would be observed due to the fact that a duplex structure would move at a slower rate through the gel matrix compared to the free 34mer ODN target on its own.

Analysis of the non-denaturing gels, showed bands of reduced mobility for samples containing both 34mer ODN target and $[\text{Ru}(\text{phen})_2\text{phen}']$ -ODN conjugate with respect to the free 34mer target. This indicated that successful hybridisation had been achieved between the complementary sections of the duplex section after being

subjected to the heating and slow-cooling technique discussed in section 3.2.1. The results of this experiment are shown in **figure 3.17**.



All samples contain 1:1 ratio ruthenium conjugate : 34mer ODN in 10 mM potassium phosphate buffer / 100 mM NaCl. **Lane 1** 34mer target ODN; **Lane 2** 34mer target ODN and $[\text{Ru}(\text{phen})_2\text{phen}']\text{-ODN}$ conjugate.

Figure 3.17 Comparison of 34mer target / $[\text{Ru}(\text{phen})_2\text{phen}']\text{-ODN}$ duplex with free 34mer target on non-denaturing gel

Samples containing 34mer ODN target and complementary 17mer ODN were also compared to the 34mer target / ruthenium-ODN conjugate samples, with both showing bands of similar reduced mobility and indicating that the presence of the ruthenium complex at the 3'-end of the complementary 17mer ODN did not reduce

the stability of the duplex formed compared to the unconjugated system. Finally, as expected, samples containing 34mer ODN target and the free ruthenium complexes $[\text{Ru}(\text{phen})_3]^{2+}$ and $[\text{Ru}(\text{phen})_2\text{phen}']^{2+}$ showed no bands of reduced mobility with respect to the free 34mer target ODN.

3.9 Effect of various additions on the photocleavage of target 34mer ODN by $[\text{Ru}(\text{phen})_2\text{phen}']$ -ODN conjugate

The effect of the inclusion of various reagents in the experiments with the ruthenium-ODN conjugate was studied in order to gain some understanding of the cleavage mechanism by which the ruthenium-ODN conjugate induced damage in the target 34mer ODN. Each experiment with a reagent was compared directly to a control experiment containing no additions and the results were quantified by phosphoimagery.

3.9.1 Effect of sodium azide (NaN_3) and argon

As previously mentioned in section 3.4.1, azide can act as a singlet oxygen quencher, thus its inclusion will decrease the amount of damage induced by a type II singlet oxygen dependent pathway. Argon purging during the course of an experiment also reduces singlet oxygen generation and type II photooxidative damage. The phosphoimaging results of experiments containing azide and carried out under an atmosphere of argon are compared to the normal experiment in **figure 3.18**. All experiments were carried out in high salt conditions with a ratio of 1:1 ruthenium-ODN conjugate : target 34mer ODN with an irradiation time of 20 minutes

followed by piperidine treatment of the samples. All experiments were carried out in the absence of a sodium nitrite filter unless otherwise stated. **Figure 3.18(a)** shows the normal experiment with no additions included. Guanine-specific cleavage at the G21 target was achieved in a yield of 11.1%. **Figure 3.18(b)** shows the effect of argon purging during the course of the experiment. A reduction in the G21 cleavage to 8.4% was observed. With the inclusion of azide, no significant difference was observed between the yield of G21 cleavage obtained in the presence and absence of azide. This was in contrast to the effect of azide inclusion seen in experiments with the free complex $[\text{Ru}(\text{phen})_2\text{phen}']^{2+}$.

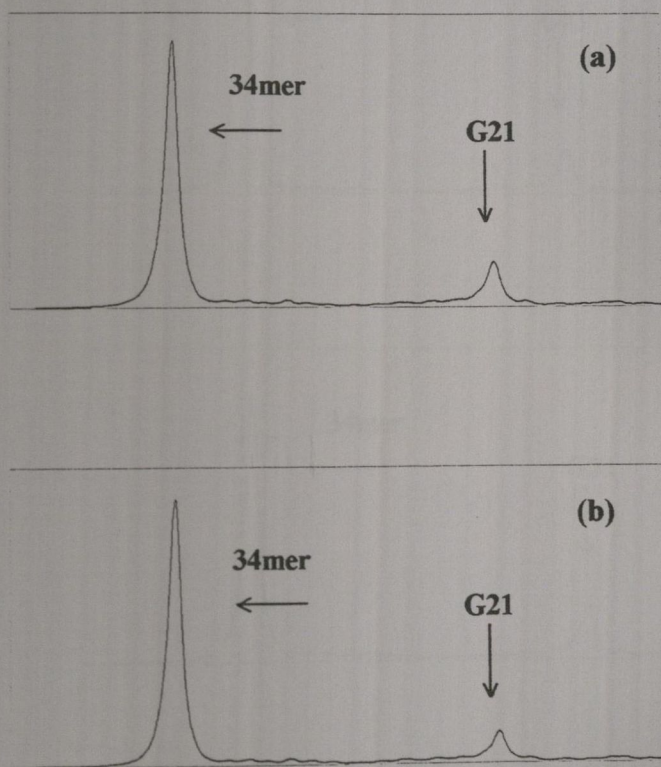


Figure 3.18 Comparison of G21 cleavage in target 34mer ODN by $[\text{Ru}(\text{phen})_2\text{phen}']$ -ODN conjugate a) with no additions and b) under argon atmosphere

3.9.2 Effect of D₂O

Cleavage pathways dependent on singlet oxygen production should show an enhancement in overall cleavage in D₂O buffer due to the increase in the lifetime of singlet oxygen. **Figure 3.19** shows the comparison between the normal experiment with no additions and of that carried out in D₂O. The normal experiment **(a)** shows 11.1 % cleavage at G21, whereas the experiment carried out in D₂O **(b)** shows an increase of G21 cleavage with an overall yield of 12.3 %.

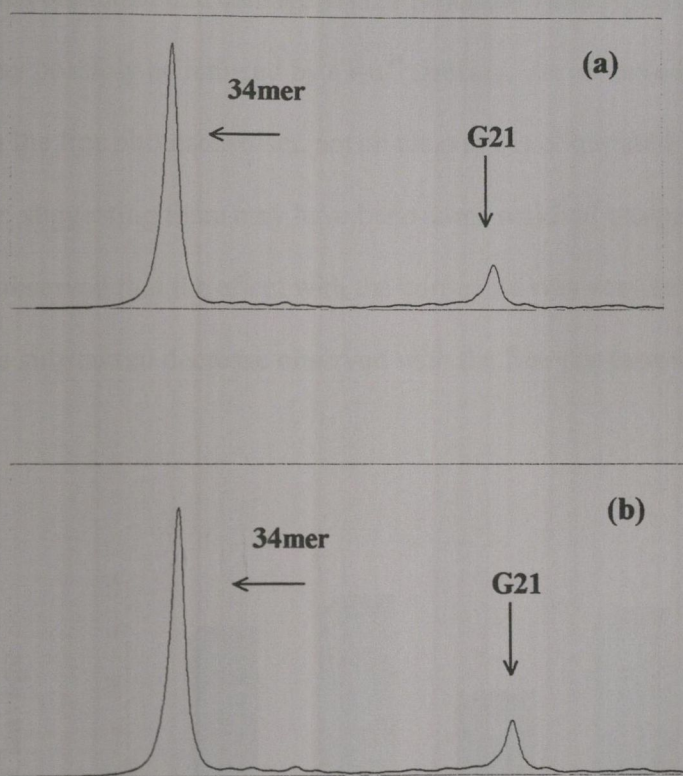


Figure 3.19 Comparison of G21 cleavage in target 34mer ODN by [Ru(phen)₂phen']-ODN conjugate a) with no additions and b) in D₂O

3.9.3 The role of singlet oxygen in guanine oxidation

The results of the experiments carried out in H₂O, D₂O, azide and argon are summarized in **figure 3.20**. A decrease in G21 cleavage was seen in an atmosphere of argon, thus inhibiting the initial generation of singlet oxygen from molecular oxygen and an increase in G21 damage was also observed when the lifetime of singlet oxygen was increased. (These experiments were repeated in the presence of a sodium nitrite filter, and although the general trend of results was the same, the overall G21 cleavage yields were significantly lower). From the effects of these additions it can be concluded that damage at G21 proceeds *via* a type II cleavage mechanism or may possibly be induced by a Ru³⁺ species. As observed for experiments with the free photosensitiser, not all cleavage is eliminated upon removal of singlet oxygen, suggesting there may have been some residual oxygen in the samples. It was observed that the effect with the conjugate was very small compared to the much more substantial decrease observed with the free photosensitiser.

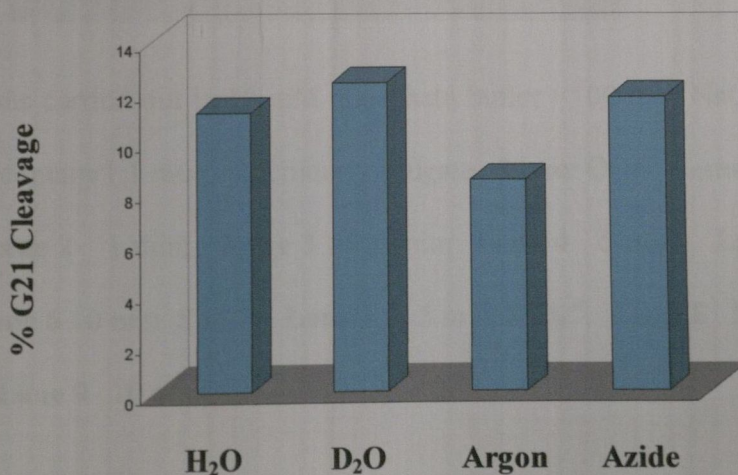
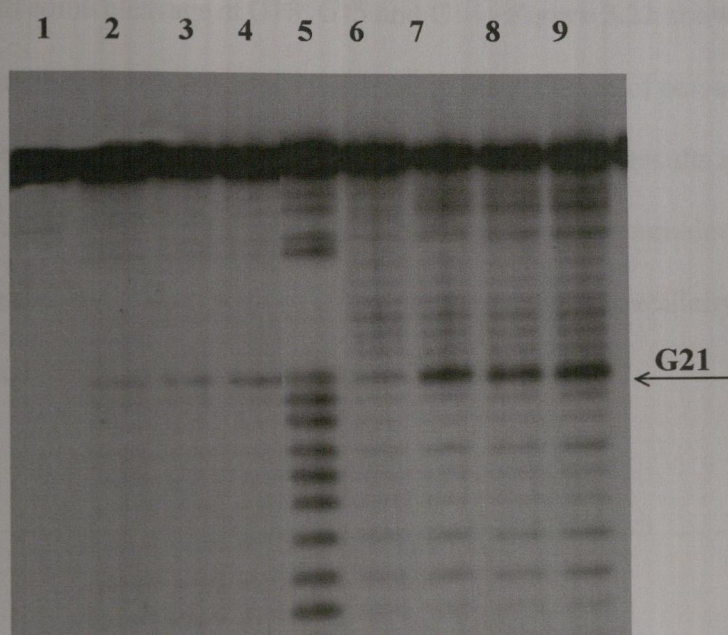


Figure 3.20 Comparison of % G21 cleavage in target 34mer ODN under normal conditions and with inclusion of additions

3.9.4 Effect of ammonium persulfate

As mentioned in section 3.4.3, the electron transfer agent ammonium persulfate ($(\text{NH}_4)_2\text{S}_2\text{O}_8$) can increase the yield of cleavage induced by a ruthenium complex by generation of Ru(III). The ruthenium-ODN conjugate / target 34mer ODN experiment was carried out in the presence and absence of persulfate and the results are shown in **figure 3.21**.



Irradiations carried out in 10 mM phosphate buffer / 100 mM NaCl; all samples contain 1:1 ratio ruthenium conjugate : 34mer ODN. **Lane 1** 0 min; **Lane 2** 1 min; **Lane 3** 2.5 min; **Lane 4** 5 min; **Lane 5** G+A **Lane 6** 0 min, $\text{S}_2\text{O}_8^{2-}$; **Lane 7** 2.5 min, $\text{S}_2\text{O}_8^{2-}$; **Lane 8** 5 min, $\text{S}_2\text{O}_8^{2-}$; **Lane 9** 10 min, $\text{S}_2\text{O}_8^{2-}$.

Figure 3.21 Comparison of 34mer target cleavage by $[\text{Ru}(\text{phen})_2\text{phen}']$ -ODN conjugate in presence and absence of persulfate

Lanes 1-4 show the experiment in the absence of persulfate over a range of irradiation times up to 10 mins. Lanes 6-9 show the same experiments in the presence of persulfate. Although lanes 7,8 and 9 show an increase in the amount of G21 cleavage obtained in the presence of persulfate relative to the non-persulfate experiments, the selectivity for only G21 decreases with increasing irradiation times. This was evident in lane 9 where increased cleavage at G21 was observed compared to the G21 cleavage seen in lane 4, but cleavage was also seen at the 3'-end guanines (G32, G31, G29) along with some cleavage at G18, G15 and G14. **Figure 3.22** shows the phosphoimaging results after 10 mins irradiation in the presence of persulfate. **Figure 3.23** shows the comparison between the phosphoimaging results after 10 mins irradiation in the presence and absence of persulfate. It can be concluded that while persulfate increases the overall yield of G21 cleavage, the G21 specificity decreases with base damage being introduced at other guanine sites.

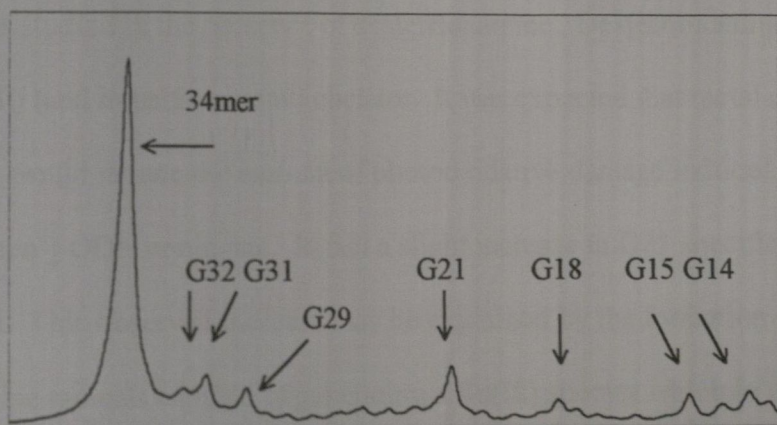


Figure 3.22 Phosphoimaging results for cleavage of target 34mer ODN by $[\text{Ru}(\text{phen})_2\text{phen}']$ -ODN after 10 mins irradiation in the presence of persulfate

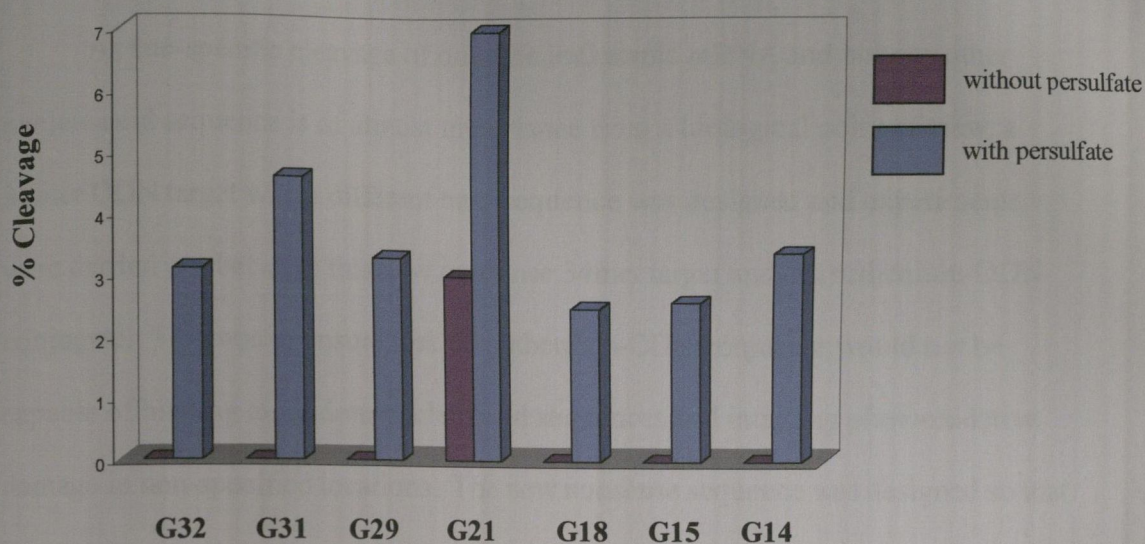


Figure 3.23 Comparison of % cleavage in target 34mer ODN by [Ru(phen)₂phen']-ODN in presence and absence of persulfate

3.9.5 Effect of desferrioxamine

The yield of cleavage at G21 in the target 34mer ODN by the ruthenium-ODN conjugate was studied in the presence of desferrioxamine. Desferrioxamine is an efficient Fe(III) (and transition metal) chelator. It was expected that metal chelation in the system would reduce the amount of photooxidative damage induced by the [Ru(phen)₂phen']-ODN conjugate. In fact a slight increase in G21 specific damage was observed. This observed increase may be explained by the formation of desferrioxamine radicals capable of generating a Ru(III) species which in turn would lead to an increase in photooxidative damage.

3.10 Nonsense strand work

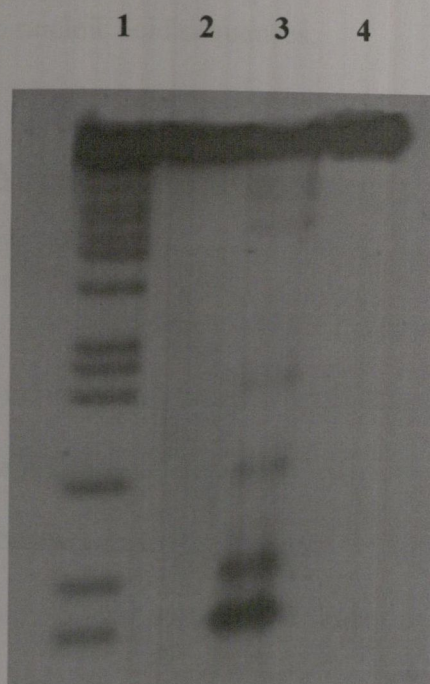
As site-specific cleavage of only the leukaemic mRNA and not any other nucleic acid sequence is of utmost importance from a biological point of view, a 34mer ODN target with a different base sequence was designed and experiments were carried out between this new nonsense 34mer target and the ruthenium-ODN conjugate. This was to ensure that the ruthenium-ODN conjugate would not be capable of binding to random nucleic acid sequences and inducing photooxidative damage in non-specified locations. The new nonsense sequence was designed so that the guanines were in the same positions as the original 34mer ODN with the remaining bases mixed up whilst keeping the overall base composition constant *i.e.* the nonsense strand had the same percentage of each base as the original 34mer target strand (**figure 3.24**).

Original 34mer 5' TGACCATCAATAAGGAAGAAG²¹CCCTTCAGCGGCC 3'
Nonsense 34mer 5' TGATACAACCACTGGCCGCTG²¹AACTACAGAGGCA 3'

Figure 3.24 Sequences of original 34mer target and nonsense strands

The results of experiments with the nonsense strand are shown in **figure 3.25**. Lane 1 is the G+A experiment of the nonsense strand. Lane 2 shows the result of irradiating the nonsense strand for 20 mins in the presence of the ruthenium-ODN conjugate under high salt conditions with a 1:1 ratio of ruthenium-ODN conjugate : nonsense strand. No cleavage was seen at any guanine site indicating that the ruthenium-ODN

conjugate was not capable of binding to the nonsense strand and inducing damage. Lane 3 shows the result of irradiating the nonsense strand in the presence of free $[\text{Ru}(\text{phen})_2\text{phen}']^{2+}$ using the same experimental conditions as lane 2. As expected, guanine-specific cleavage of the nonsense strand was achieved with a preference for the 5'-guanine of the $3' \text{G15G14 } 5'$ doublet. Lane 4 is a control lane with no photosensitiser present.



All samples containing 1:1 ratio nonsense strand: photosensitiser. Irradiations carried out in 10 mM phosphate buffer / 100 mM NaCl for 20 mins. **Lane 1** G+A; **Lane 2** ruthenium-ODN; **Lane 3** $[\text{Ru}(\text{phen})_2\text{phen}']^{2+}$; **Lane 4** nonsense strand only.

Figure 3.25 Results of nonsense strand experiments in presence of ruthenium-ODN conjugate and free $[\text{Ru}(\text{phen})_2\text{phen}']^{2+}$

To confirm that the ruthenium-ODN conjugate was not binding to the nonsense strand, the results of the experiment were analysed on a non-denaturing gel. No band of reduced mobility with respect to the nonsense strand ODN band was observed, showing that hybridisation between the nonsense strand and the 17mer ODN of the ruthenium-ODN conjugate did not occur.

The combined results of the denaturing and non-denaturing gel work in relation to the nonsense strand showed that the ruthenium-ODN conjugate is specific only for the leukaemic mRNA sequence and is not capable of inducing damage in random nucleic acid sequences.

3.11 Variant strand work

In order to fully investigate the range of oxidative damage in the model system, it was decided to replace the target 34mer ODN with a range of variant target strands in which the guanine target at position 21 was moved in increments away from the photosensitiser. Six variant strands were designed; the first with no G21 target and the remaining five with the G21 target moved 1, 2, 3, 4 and 6 bases towards the 3'-end of the target sequence. The variant strands were designated as variants 1-6 respectively. The sequence of the region complementary to the 17mer ODN of the ruthenium-ODN conjugate remained unchanged, thus allowing normal duplex formation between the new variant strands and the ruthenium-ODN conjugate (**figure 3.26**).

Variant 1 (no G21) 5' TGACCATCAATAAGGAAGAATCCCTTCAGCGGCC 3'

Variant 2 5' TGACCATCAATAAGGAAGAACG²²CCTTCAGCGGCC 3'

Variant 3 5' TGACCATCAATAAGGAAGAACCG²³CTTCAGCGGCC 3'

Variant 4 5' TGACCATCAATAAGGAAGAA²⁴CCCG²⁴TTCAGCGGCC 3'

Variant 5 5' TGACCATCAATAAGGAAGAAC²⁵CCCTG²⁵TCAGCGGCC 3'

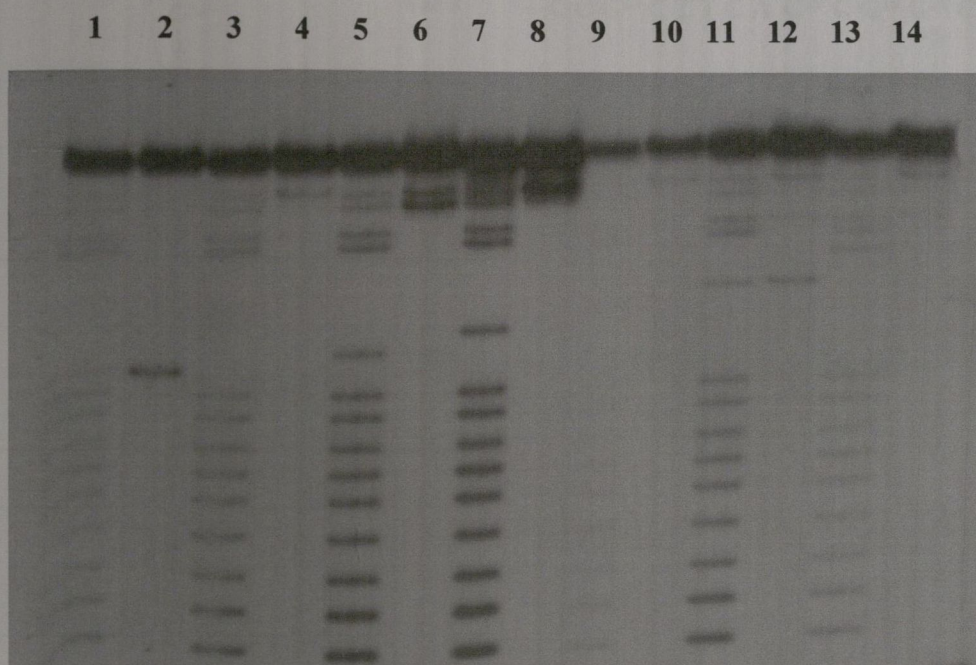
Variant 6 5' TGACCATCAATAAGGAAGAAC²⁷CCCTCG²⁷AGCGGCC 3'

Figure 3.26 Sequences of variant strands 1-6 with region complementary to 17mer ODN of ruthenium-ODN conjugate shown in red.

It had been expected that photooxidative damage at the target guanine would eventually cease as it was moved out towards the 3'-end of the variant strands. In fact, unexpectedly, the main damage observed was mainly at the 3'-end guanines. The results of the gel work are shown in **figure 3.27** with the G+A experiment for each variant strand shown in alternate lanes. The phosphoimaging results of experiments with the variant strands are shown in **figure 3.28** with the quantitative results of cleavage at each guanine site shown in **table 3.3**.

In **figure 3.27**, the original 34mer ODN target showed G21 cleavage consistent with previous similar experiments (lane 2). Variant 1 showed no cleavage at position 21 as expected as the guanine at this position was replaced with a thymine.

Cleavage was seen mainly at G32 with a small amount of G29 damage (lane 4). Variant 2 showed strong cleavage at G32 and G31 with no damage observed at the expected G22 site (lane 6). Variant 3 showed the most dramatic result with strong cleavage observed at G32 and no cleavage seen at the expected G23 site (lane 8). Variant 4 showed cleavage at G32 and G29 with no damage at the expected G24 site (lane 10). Variants 5 and 6 showed a small amount of damage at their target bases (G25 and G27 respectively), but most damage was observed at G32 and G29 (lanes 12 and 14). No double-strand damage was observed with any of the variants.



All irradiations carried out in 10 mM potassium phosphate buffer / 100 mM NaCl for 20 mins with 1:1 ratio of ruthenium-ODN conjugate: variant strand. **Lane 1** G+A 34mer; **Lane 2** 34mer; **Lane 3** G+A Variant 1; **Lane 4** Variant 1; **Lane 5** G+A Variant 2; **Lane 6** Variant 2; **Lane 7** G+A Variant 3; **Lane 8** Variant 3; **Lane 9** G+A Variant 4; **Lane 10** Variant 4; **Lane 11** G+A Variant 5; **Lane 12** Variant 5; **Lane 13** G+A Variant 6; **Lane 14** Variant 6.

Figure 3.27 Results of experiments with variants 1-6 in the presence of [Ru(phen)₂phen']-ODN conjugate

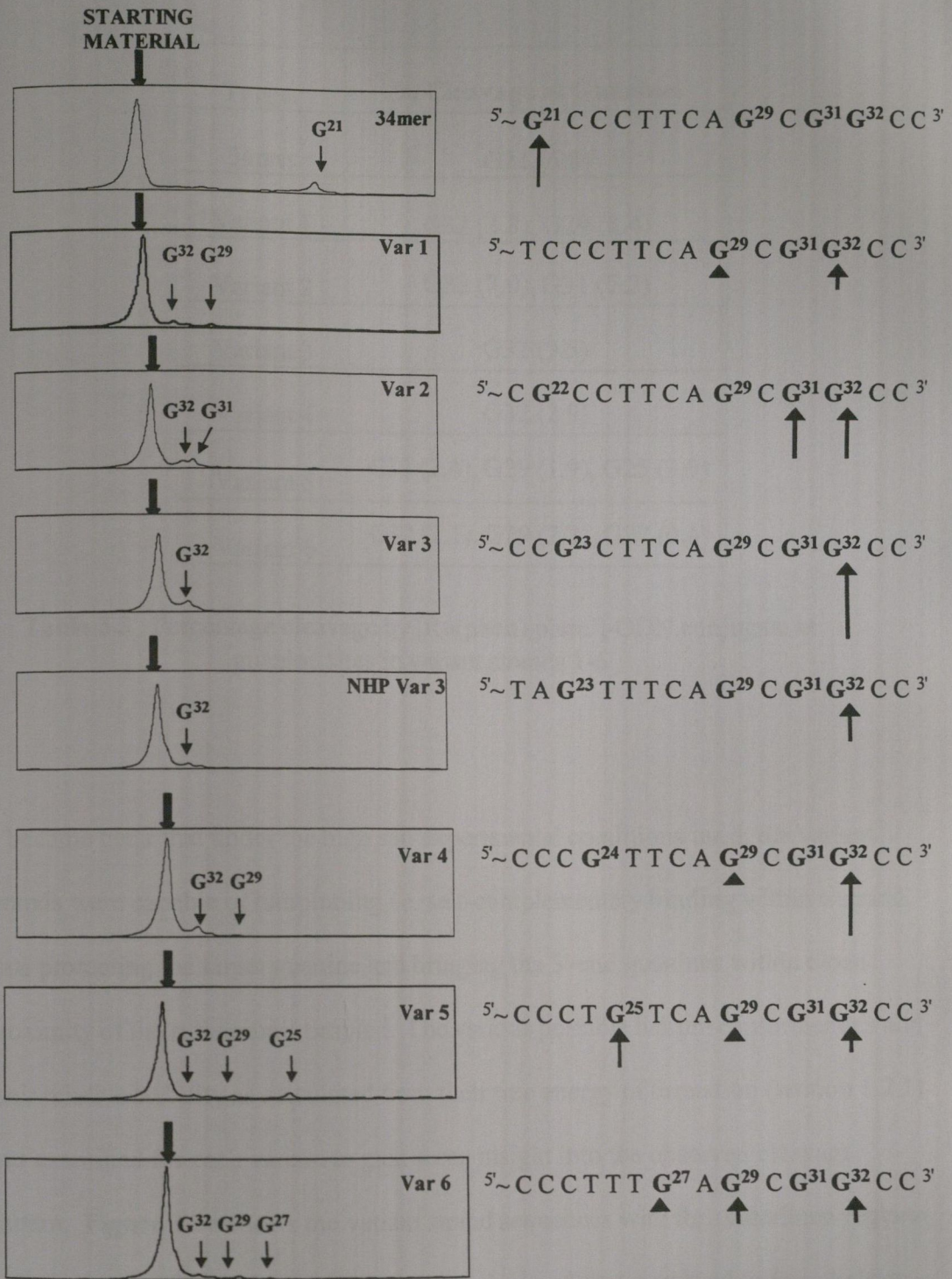


Figure 3.28 Phosphoimaging results for variants 1-6. Arrows indicate the site and extent of base damage.

Target	% Cleavage at Guanines
34mer	G21 (6.8)
Variant 1	G32 (3.8), G29 (1.4)
Variant 2	G32 (7.0), G31 (7.2)
Variant 3	G32 (9.5)
Variant 4	G32 (2.9)
Variant 5	G32 (2.4), G29 (1.9), G25 (3.9)
Variant 6	G32 (2.1), G29 (2.2), G27 (0.4)

Table 3.3 Percentage cleavage by [Ru(phen)₂phen']-ODN conjugate at guanine sites in variant strands 1-6

It became clear that under the high salt experimental conditions used, the variant strands were capable of hairpinning *i.e.* self-complementary binding within a strand, thus protecting the target guanine and bringing the 3'-end guanines within close proximity of the ruthenium complex. The various possible hairpin conformations and their relative stability as calculated from their free energy of formation (section 1.2.1) was examined for each variant to gain some insight into the observed cleavage pattern. **Figure 3.30** shows the variant strand sequences with the underlined regions indicating complementary regions within each strand that may bind to form hairpin structures. It was also noted that the site-specific cleavage observed at G21 in the original target 34mer sequence could be encouraged by the hairpin structure shown in **figure 3.29**, which has a free energy of formation of approximately -1.7 kcal/mol.

This hairpin structure seems to expose G21 to damage by the photosensitiser, whilst protecting the other guanine residues.

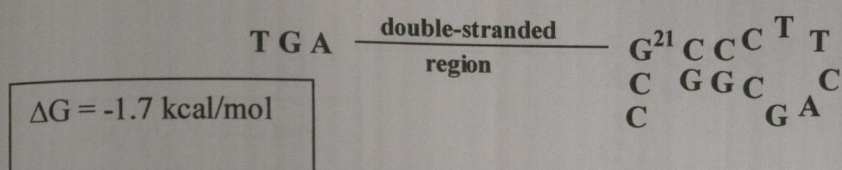


Figure 3.29 Original 34mer hairpin structure

- Variant 1 (no G21) 5' TGACCATCAATAAGGAAGAATCCCTTCAGCGGCC 3'
- Variant 2 5' TGACCATCAATAAGGAAGAACG²²CCTTCAGCGGCC 3'
- Variant 3 5' TGACCATCAATAAGGAAGAACCG²³CTTCAGCGGCC 3'
- Variant 4 5' TGACCATCAATAAGGAAGAACCCG²⁴TTCAGCGGCC 3'
- Variant 5 5' TGACCATCAATAAGGAAGAACCCTG²⁵TCAGCGGCC 3'
- Variant 6 5' TGACCATCAATAAGGAAGAACCCTTCG²⁷AGCGGCC 3'

Figure 3.30 Sequences of variant strands 1-6 with complementary regions within each strand underlined and double-stranded region shown in red

In order to form a hairpin structure, energy must be released with the amount of energy released determining how stable the hairpin will be. Of all the variant strands, the proposed hairpin in variant 3 has the lowest free energy of formation

(approximately -3.9kcal/mol). This hairpin seems to “protect” the G23 target and expose G32 to damage by the photosensitiser, thus explaining the observed cleavage pattern (**figure 3.31**).

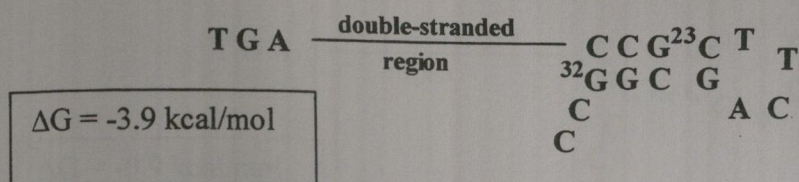


Figure 3.31 Variant 3 hairpin structure

Two different hairpin conformations are possible for variant 2 with free energy of formation values of -1.0kcal/mol and -0.5kcal/mol respectively. The cleavage pattern observed with variant 2 can be explained by the more favourable hairpin structure in which the system seems to be orientated in such a way so as to expose G32 and G31 to photooxidative damage with no damage observed at G22 (**figure 3.32**).

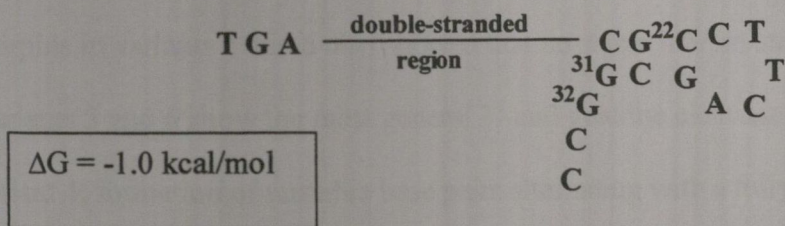


Figure 3.32 Variant 2 hairpin structure

For variant 4, the free energy of formation of the proposed hairpin structure is approximately -0.9kcal/mol . In the hairpinned conformation, the 3'-end guanines

Old Variant 3 5' TGACCATCAATAAGGAAGAA CCG²³CTTCAGCGGCC 3'

NHP Variant 3 5' TGACCATCAATAAGGAAGAA TAG²³TTTCAGCGGCC 3'

Figure 3.34 Sequences of original variant 3 and non-hairpinning variant 3.

As previously mentioned, the ruthenium-ODN conjugate induced a relatively large amount of cleavage (9.5 %) in the original variant 3 target ODN at G32. Repetition of this work substituting the new non-hairpinning variant 3 for the original variant 3 showed a large decrease in the amount of cleavage observed at G32 from 9.5 % to 2.9 %. The phosphoimaging data for this experiment is shown in **figure 3.28**. A stable hairpin conformation was unlikely to form in the non-hairpinning variant 3 target but still no cleavage was observed at the target G23 despite the fact that in this new system it should have been exposed for damage. The results indicated that the ruthenium complex was unable to induce damage in a target guanine two bases removed from the original G21 target suggesting that the ruthenium complex was only capable of inducing damage in its immediate vicinity.

The variant strand work was also carried out with the sodium nitrite filter in place during the irradiations. As with the previous experiments, the presence of the filter resulted in the same general cleavage pattern for the variant strands but with an overall decrease in cleavage yields (**table 3.4**).

Target	% Cleavage at Guanines
Variant 1	G32 (3.8) (2), G29 (1.4) (0.5)
Variant 2	G32 (7.0) (4.1), G31 (7.2)
Variant 3	G32 (9.5) (6.2)
NHP Variant 3	G32 (2.9) (1.6)
Variant 4	G32 (2.9) (1.4)
Variant 5	G32 (2.4) (0.5), G29 (1.9) (0.2), G25 (3.9) (0.7)
Variant 6	G32 (2.1) (0.5), G29 (2.2) (0.3), G27 (0.4)

Table 3.4 Comparison of cleavage yields seen in variant strands in presence and absence of sodium nitrite filter. Filtered results shown in red

3.12 3'-end labeling

As mentioned in section 3.6, the cleavage efficiency of the [Ru(phen)₂phen']-ODN conjugate seemed to level off after a certain period of time, with no increase in G21 specific cleavage being observed after approximately 20 mins irradiation. In order to investigate what was happening to the ruthenium-ODN conjugate during the course of the irradiation experiments, it was necessary to 3'-end label the conjugate with the radioisotope ³²P. The details of 3'-end labeling are discussed in section 5.9.2. In all the experiments discussed so far, the target strand was 5'-end labeled with the radioisotope ³²P, therefore only that damage induced in the target strand was detectable by autoradiography. In order to “see” the effect of irradiation on the [Ru(phen)₂phen']-ODN conjugate and to assess its relative stability during the course

of the irradiations, experiments were repeated with the 3'-end labeled conjugate in the presence of unlabeled 34mer ODN target.

Initially experiments were carried out in which the $[\text{Ru}(\text{phen})_2\text{phen}']\text{-ODN}$ conjugate was irradiated in the absence of any target strand. Phosphoimaging of the PAGE results showed that after 0 mins irradiation, 16 % of the conjugate was damaged relative to the parent conjugate band, indicating the conjugate stock sample might have degraded somewhat during storage. Irradiation of the free conjugate for 10 mins and 20 mins showed that 18.3 % and 19 % respectively of the conjugate was damaged relative to the undamaged parent conjugate. In the presence of the target 34mer ODN, the experiments were repeated for irradiation times of 0, 10 and 20 mins. After 0 mins irradiation, 15.9 % of the conjugate was damaged, again indicative of degradation of the stock sample over time, and consistent with the results observed in the absence of target 34mer ODN. After 10 mins irradiation, the overall conjugate damage increased to 17.7 % and this figure increased to 23.2 % after 20 mins irradiation. The results of the ruthenium-ODN conjugate damage in the presence and absence of target 34mer ODN are summarized in **figure 3.35**.

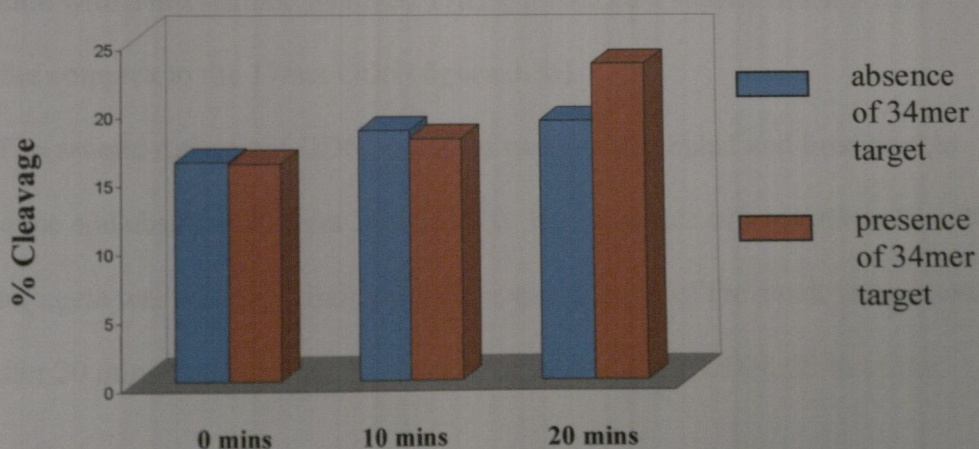


Figure 3.35 Comparison of damage induced in $[\text{Ru}(\text{phen})_2\text{phen}']\text{-ODN}$ conjugate in absence and presence of target 34mer ODN

The relatively large amount of damage induced in the ruthenium-ODN conjugate itself during the course of the irradiations may explain why the cleavage efficiency of the system levels off as the irradiation time increases. As the amount of intact ruthenium-ODN conjugate seems to decrease during the course of the experiments, it seems probable that the ruthenium complex may be capable of cleaving the 17mer ODN to which it is conjugated. Alternatively, if a gradual degradation of the stock solution of ruthenium-ODN conjugate had resulted in an increase in the amount of free ruthenium complex, base modification at guanines in the 17mer ODN may have been induced during sample handling and thus revealed after piperidine treatment.

The results of the 3'-end labeled experiment with the [Ru(phen)₂phen']-ODN conjugate were compared to that of a second ruthenium-ODN conjugate which had been previously shown to induce a much greater amount of G21 specific cleavage in the target 34mer ODN strand. This ruthenium-ODN conjugate, synthesised by C. Crean,¹⁷⁰ differed from the [Ru(phen)₂phen']-ODN conjugate in that the phen' ligand was replaced by the 4'-methyl-2,2'-bipyridine-4-carboxylic acid ligand, which after conjugation with a hexylamino modified 17mer, produced a shorter linker strand joining the complex to the 17mer ODN (**figure 3.36**).

The second ruthenium-ODN conjugate was 3'-end labeled and irradiated in the presence and absence of target 34mer ODN. In an absence of irradiation, 10.6 % of the conjugate was damaged, indicating some degradation of the stock sample over time. After 20 mins irradiation in the absence of target 34mer ODN, 25 % of the

conjugate was damaged. In the presence of the target 34mer ODN, 11.2 % of the conjugate was damaged.

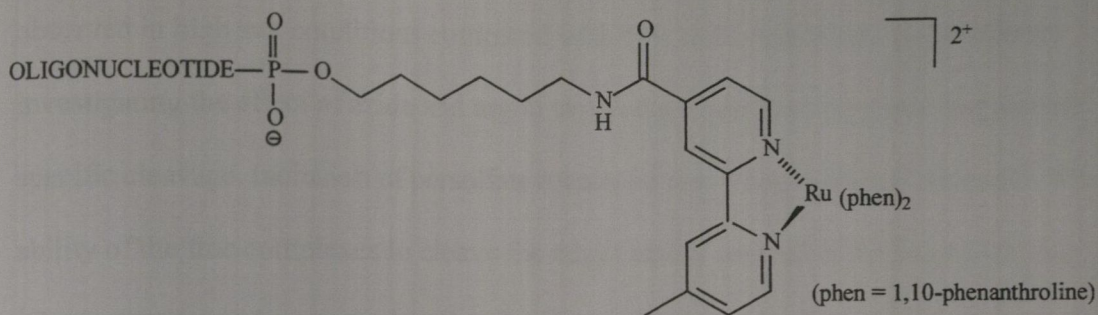


Figure 3.36 Structure of ruthenium-ODN conjugate with shorter linker chain¹⁷⁰

Relative to the [Ru(phen)₂phen']-ODN conjugate, much less of the second ruthenium-ODN conjugate was damaged after 20 mins irradiation in the presence of the unlabeled 34mer ODN target (only 11.2 % compared to 23.2 %). This result was consistent with the increased yield of cleavage observed at G21 for the second ruthenium-ODN conjugate. A possible explanation for these results may be that the shorter linker chain in the second conjugate may have been more stable to degradation during the course of the irradiations, thus resulting in a system capable of higher yields of guanine specific cleavage due to a higher overall level of ruthenium-ODN conjugate in the experimental samples.

3.13 Conclusions

Irradiation of the target 34mer ODN in the presence of the free photosensitisers showed guanine-specific cleavage with a preference for the 5'-guanine of the ^{5'}G14G15^{3'} doublet. A slightly higher overall yield of cleavage was observed in high salt conditions compared with low salt conditions. Experiments investigating the effect of azide and argon showed a significant decrease in guanine-specific cleavage. Inclusion of persulfate increased the overall yield of cleavage. The ability of the free complexes to cleave the target strand seemed to be dependent on ¹O₂ production and was concluded to involve mainly type II cleavage. Traces of oxygen in the experimental samples may explain why all cleavage was not suppressed.

Irradiation of the target 34mer ODN in the presence of the Ru-ODN conjugate revealed site-specific cleavage at the G21 target. Inclusion of azide and argon showed a small effect in reduction of cleavage compared to the free photosensitisers. This effect may be attributed to an inability to suppress ¹O₂ production in the immediate locality of the photosensitiser in the more enclosed conjugate system. Inclusion of persulfate showed an increase in G21 cleavage, but in addition to a loss of site-specificity, due possibly to generation of the sulfate radical anion. Non-denaturing gel analysis confirmed duplex formation between the target strand and the Ru-ODN conjugate. Nonsense strand work showed no tendency for the Ru-ODN conjugate to bind to random ODN sequences. Variant strand work, to investigate the range of oxidative damage, revealed 3'-end cleavage in the variant strands. This was attributed to hairpinning in the variant strands. Experiments with non-hairpinning

variant 3 showed the ruthenium complex was only capable of inducing damage in its localised vicinity. 3'-end labeling experiments showed some degradation of the conjugate in the absence of irradiation, with a slight increase in damage observed with increasing irradiation times. This conjugate damage may explain why no increase in G21 cleavage is observed with increasing irradiation times.

In conclusion, site-specific cleavage of the target 34mer ODN representing the leukaemic mRNA using the Ru-ODN conjugate was achieved in the model system. It was decided to extend this work to a conjugate system capable of forming crosslinks with the target strand. *In vivo*, forming crosslinks between the mRNA sequence and the antisense vector would again achieve the overall aim of down-regulation of leukaemic mRNA expression.

CHAPTER 4

Interaction between
[Ru(TAP)₂phen⁺]-ODN conjugate and
target 34mer

4.1 Introduction

The work in this chapter describes the photochemical targeting of the same 34mer ODN target used in chapter 3, the sequence of which represents the fusion section of the *bcr / abl* mRNA specific only to CML cells. The 34mer ODN is targeted using the ruthenium-oligodeoxynucleotide conjugate, $[\text{Ru}(\text{TAP})_2\text{phen}']\text{-ODN}$, where TAP = 1,4,5,8-tetraazaphenanthrene and phen' = 5-(4-carboxybutanamido-1,10-phenanthroline), with a view to induction of photoadduct formation between the ruthenium complex and the target strand. Photoadduct formation will result in a covalent linkage between the two species, therefore from an *in vivo* point of view, the leukaemic mRNA will become covalently bound to the ruthenium-ODN conjugate. As a result, translation of the mRNA into the corresponding CML oncoproteins will be disrupted and down-regulation of the normal gene expression of the starting oncogene achieved.

The results of photoadduct experiments with the target 34mer ODN using the free ruthenium complexes $[\text{Ru}(\text{TAP})_2\text{phen}']^{2+}$ and $[\text{Ru}(\text{TAP})_3]^{2+}$ are described. The effect of the addition of various reagents on the ability of the ruthenium-ODN conjugate to induce photoadduct formation was also investigated to study the mechanism of photoadduct formation. The variant strands studied in chapter 3 were also investigated in relation to the $[\text{Ru}(\text{TAP})_2\text{phen}']\text{-ODN}$ conjugate system in order to investigate the effect of moving the target guanine in increments away from the ruthenium complex. In addition, an investigation of the effect of exchanging the target 34mer ODN target for a random DNA sequence was carried out to ensure that

the ruthenium-ODN conjugate was unable to form photoadducts with DNA sequences unrelated to the target sequence of choice.

4.2 Description of model system

The ultimate aim of this section of work was site-specific photoadduct formation between the target 34mer ODN and the previously synthesised ruthenium-ODN conjugate, $[\text{Ru}(\text{TAP})_2\text{phen}']\text{-ODN}$. The model system designed to achieve this aim was similar to the system described in section 3.2 in the sense that the *in vitro* CML system representing the *in vivo* system was designed so that the ruthenium-ODN conjugate could be used as an antisense vector in addition to the utilisation of the photochemical properties of the ruthenium complex in order to inhibit translation of the leukaemic mRNA and down-regulate gene expression of the starting oncogene.

The model system for this work consisted of the target 34mer ODN representing the leukaemic mRNA and the ruthenium-ODN conjugate, $[\text{Ru}(\text{TAP})_2\text{phen}']\text{-ODN}$ (**figure 4.1**). The ruthenium complex was conjugated to a 17mer ODN complementary to one section of the target 34mer ODN to ensure that upon hybridisation of the two complementary regions, the ruthenium complex would be orientated in such a way as to optimise site-specific photoadduct formation between the ruthenium complex and the target base in the 34mer ODN strand. Again the target base in this second system was a guanine 21 bases from the 5'-end of the 34mer ODN target (G21).

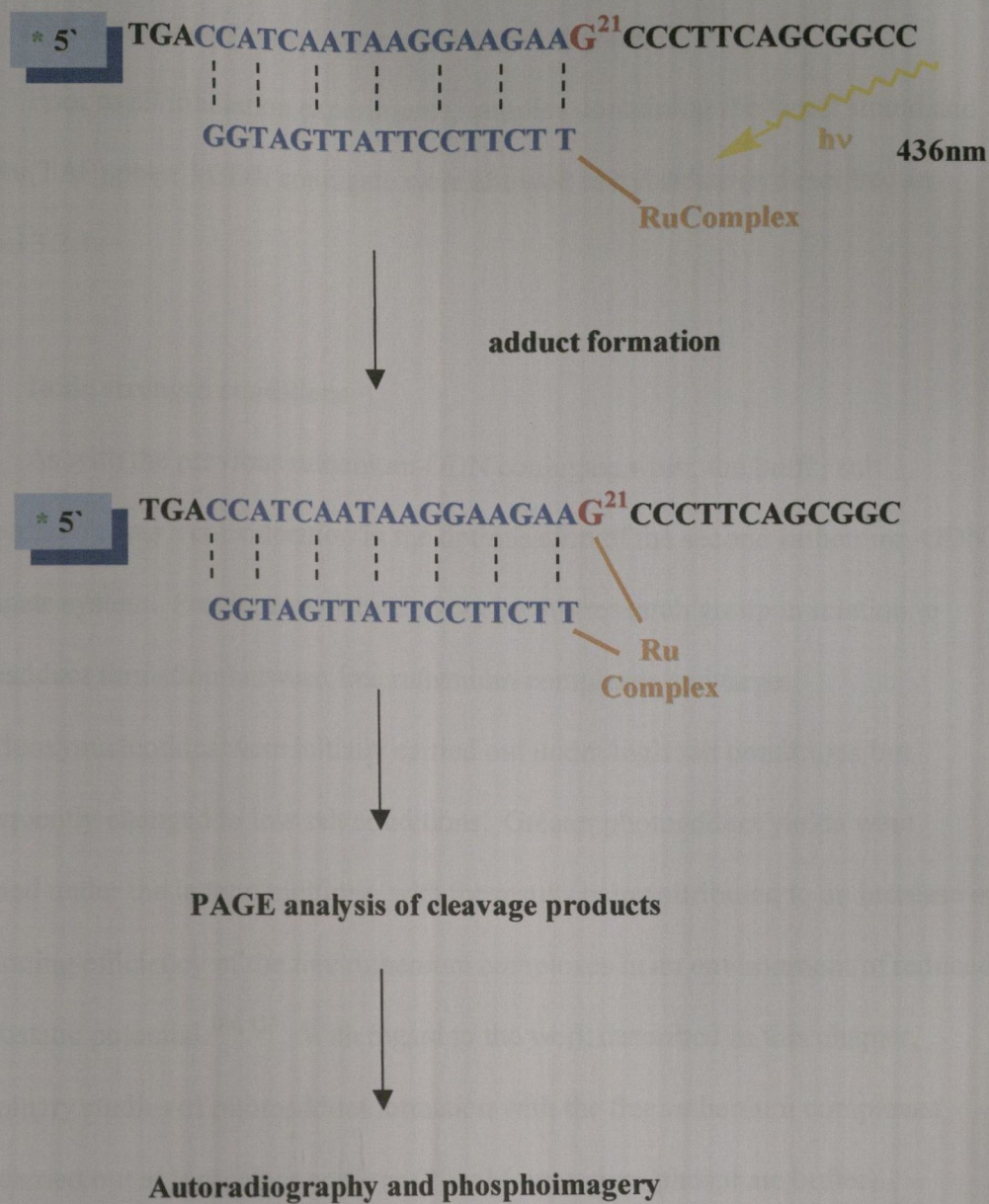


Figure 4.1 Model system of target 34mer and [Ru(TAP)₂phen⁺]-ODN conjugate

4.2.1 Hybridisation of complementary strand regions

Prior to all irradiation experiments, samples containing the target strand and the $[\text{Ru}(\text{TAP})_2\text{phen}']\text{-ODN}$ conjugate were allowed to hybridise as described in section 3.2.1.

4.2.2 Ionic strength conditions

As with the previous ruthenium-ODN conjugate work, the buffer salt concentration was a consideration in the optimisation of the second ruthenium-ODN conjugate system. Previous work carried out by this research group in relation to photoadduct formation between free ruthenium complexes and target oligodeoxynucleotides were initially carried out under high salt conditions but subsequently changed to low salt conditions. Greater photoadduct yields were obtained under the latter conditions, with the results being attributed to an increase in the binding efficiency of the free ruthenium complexes in an environment of reduced electrostatic potential.^{164, 123} With regard to the work described in this chapter, preliminary studies of photoadduct formation with the free ruthenium complexes were carried out at low salt conditions (10 mM potassium phosphate buffer). Subsequent experiments with the $[\text{Ru}(\text{TAP})_2\text{phen}']\text{-ODN}$ conjugate were carried out under both low salt and high salt (10 mM potassium phosphate buffer / 100 mM NaCl) conditions, as the ionic strength was of importance in ensuring optimal hybridisation between the target strand and 17mer ODN of the ruthenium conjugate. Comparison of results under both ionic conditions are discussed in the subsequent sections.

4.2.3 Irradiation conditions

All irradiation work was carried out as described in section 3.2.3.

4.2.4 Analysis of photoadduct formation

After the irradiation of samples, the formation of photoadducts was analysed by polyacrylamide gel electrophoresis (PAGE). Photoadduct formation involved the formation of a covalent linkage between the guanine of interest (G21) on the target strand and the [Ru(TAP)₂phen']-ODN conjugate thus forming a species of higher molecular weight than the target strand alone. As this target strand was initially radiolabeled at the 5'-end with $\gamma^{32}\text{P}$, only the target strand alone or the target strand attached to another species was detectable upon analysis. After polyacrylamide gel electrophoresis, a photoadduct is expected to appear as a band of reduced mobility with respect to the parent 34mer band. Generally samples where photoadduct production was expected were not subjected to piperidine treatment, although a small number of experiments were conducted where base treatment was included to see the effect of piperidine treatment on the photoadduct stability and to reveal any additional sites of photooxidative damage. The theory behind piperidine treatment is discussed fully in section 3.2.4. All experiments involving photoadduct formation between the ruthenium-ODN conjugate and target strand of choice were visualised by autoradiography and quantified by phosphoimager. Details of 5'-end labeling, autoradiography and phosphoimager are discussed in chapter 5.

4.3 Photoadduct formation using free ruthenium complexes

The free ruthenium complexes $[\text{Ru}(\text{TAP})_2\text{phen}']^{2+}$ and $[\text{Ru}(\text{TAP})_3]^{2+}$ (where TAP = 1,4,5,8-tetraazaphenanthrene and phen' = 5-(4-carboxybutanamido-1,10-phenanthroline) were studied in irradiation experiments with the target 34mer ODN with a view to analysis of photoadduct formation between the ruthenium complexes and the target strand. As mentioned in section 1.11.2, ruthenium complexes bearing two or more π -deficient ligands such as TAP are oxidising enough in their excited state to abstract electrons from guanines, as guanine has the lowest oxidation potential of all the bases. The resulting guanine radical cation and reduced ruthenium complex combine to give the final photoadduct product. Previous work by this research group¹⁶⁴ using $[\text{Ru}(\text{TAP})_3]^{2+}$ and a target 24mer ODN with a 10:1 ratio of ruthenium complex : ODN target in low salt buffer conditions showed evidence of photoadduct formation. Photoadducts were detected as bands of reduced mobility with respect to the parent band after PAGE and autoradiography. Higher yields of photoadduct formation were obtained under low salt conditions compared with experiments carried out under high salt conditions.

4.3.1 Photoadduct formation between target 34mer ODN and

$[\text{Ru}(\text{TAP})_2\text{phen}']^{2+}$ and target 34mer ODN and $[\text{Ru}(\text{TAP})_3]^{2+}$

Initially irradiation experiments between $[\text{Ru}(\text{TAP})_2\text{phen}']^{2+}$ and the target 34mer ODN were carried out using a 10:1 ratio of ruthenium complex : target ODN fragment under low salt conditions using a range of irradiation times up to 20 minutes. Irradiation at 436 nm was not followed by piperidine treatment unless

otherwise stated. The initial results were not as clearly defined as the photoadducts previously observed with other ruthenium complexes bearing π -deficient ligands and the 24mer ODN target. Control lanes containing the 34mer target and $[\text{Ru}(\text{TAP})_2\text{phen}]^{2+}$ in the absence of any irradiation showed a band identical to that observed for the 34mer ODN target alone in the absence of irradiation. This result indicated that neither photoadduct formation or target strand cleavage occurred in the absence of irradiation. For the remaining experiments carried out using a variety of irradiation times, no clearly defined photoadduct band was observed above the parent band attributed to the target 34mer ODN, but streaking above the parent band was evident. This streaking effect was not evident in the absence of irradiation. This material above the parent band was due to a species of reduced mobility with respect to the 34mer ODN target and was tentatively attributed to photoadduct formation between the target 34mer ODN and the free $[\text{Ru}(\text{TAP})_2\text{phen}]^{2+}$ complex.

In order to improve the photoadduct formation between the free $[\text{Ru}(\text{TAP})_2\text{phen}]^{2+}$ complex and the target 34mer ODN, the experimental conditions were varied in an effort to "fine tune" the system and achieve optimal results. The experiments with the free $[\text{Ru}(\text{TAP})_2\text{phen}]^{2+}$ complex were repeated under both high salt and low salt experimental conditions using longer irradiation times of up to 60 minutes. No significant improvement on the photoadduct resolution was achieved, again with only streaking above the target 34mer ODN band being observed. No streaking was observed above the target 34mer ODN band in the presence of the free ruthenium complex in the absence of irradiation or with the target 34mer ODN alone in the presence of irradiation.

Concentration changes were also made with a view to optimisation of photoadduct resolution. In order to ensure that a sufficient excess of ruthenium complex was present in each sample to be irradiated, the target 34mer ODN was diluted by a factor of ten prior to sample preparation. Irradiation experiments were carried out over a range of irradiation times in the presence of free $[\text{Ru}(\text{TAP})_2\text{phen}]^{2+}$ complex under low salt conditions. The free ruthenium complex was used at two different concentrations *i.e.* samples were taken from 1×10^{-4} M and 1×10^{-5} M stock solutions of the free complex. In the original undiluted experiments, samples of the free ruthenium complex taken from 1×10^{-4} M and 1×10^{-5} M stock solutions corresponded to ratios of ruthenium complex : ODN fragment of 10:1 and 1:1 respectively. Again, analysis of the results showed only streaking above the target 34mer ODN band was evident. As previously stated, this streaked material of reduced mobility was attributed to photoadduct formation and was not present in the absence of irradiation. The phosphoimager results of experiments carried out using the diluted target 34mer ODN and free ruthenium complex from stock solutions of 1×10^{-4} M and 1×10^{-5} M are shown in **figures 4.2** and **4.3** respectively.

Figure 4.2(a) shows the result of the diluted 34mer ODN target in the presence of the free $[\text{Ru}(\text{TAP})_2\text{phen}]^{2+}$ complex in the absence of irradiation. One sharp peak due to the 34mer ODN target is evident with no material of reduced mobility present. **Figure 4.2(b)** shows the result of the same experiment after 20 mins irradiation. The 34mer ODN peak is no longer as well defined, with an obvious shoulder tailing off from the parent 34mer peak. This “shoulder” corresponds to the streaking pattern evident after autoradiography.

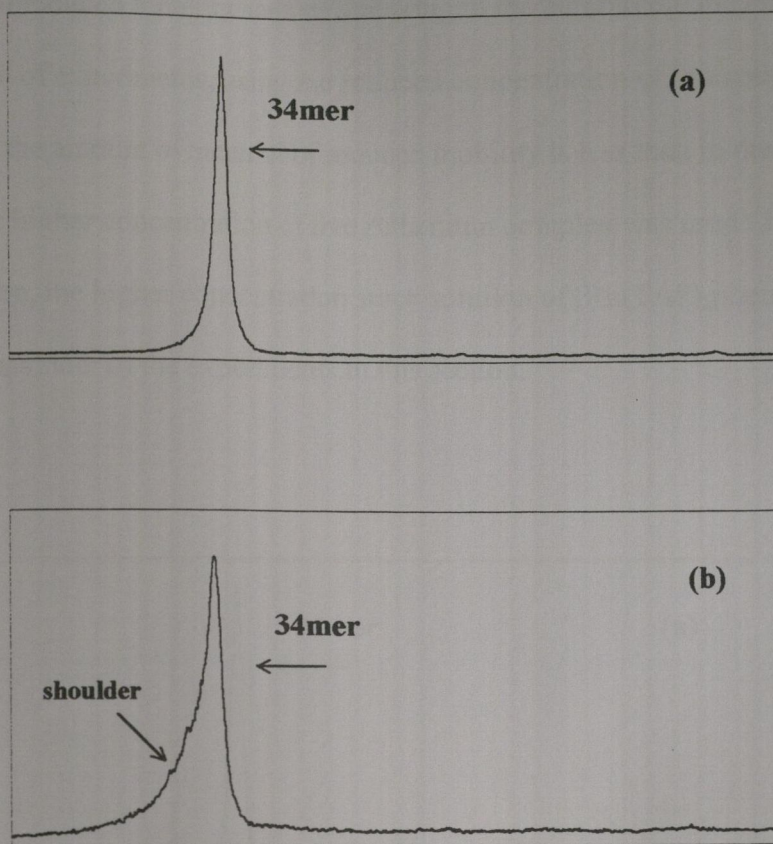


Figure 4.2 Phosphoimaging results for diluted 34mer ODN with $[\text{Ru}(\text{TAP})_2\text{phen}]^{2+}$ (1×10^{-4} M stock solution), 10 mM potassium phosphate buffer after (a) 0 min irradiation and (b) 20 mins irradiation.

Figure 4.3(a) shows the result of the 34mer ODN diluted target in the presence of free $[\text{Ru}(\text{TAP})_2\text{phen}]^{2+}$ complex from a 1×10^{-5} M stock solution in the absence of any irradiation. Again, one sharp peak due to the 34mer ODN target is evident with no material of reduced mobility present. **Figure 4.3(b)** shows the result of the same experiment after 20 mins irradiation. Like the previous set of experiments, the 34mer peak is no longer as well defined with a slight shoulder evident corresponding to

material of reduced mobility seen as streaking in the autoradiography results. In this second set of experiments, using the reduced concentration of free ruthenium complex, the amount of material of reduced mobility is less than in the experiments where the higher concentration of free ruthenium complex was used. Based on this observation, the higher concentration stock solution of $[\text{Ru}(\text{TAP})_2\text{phen}]^{2+}$ was used for the remainder of the experiments in this section.

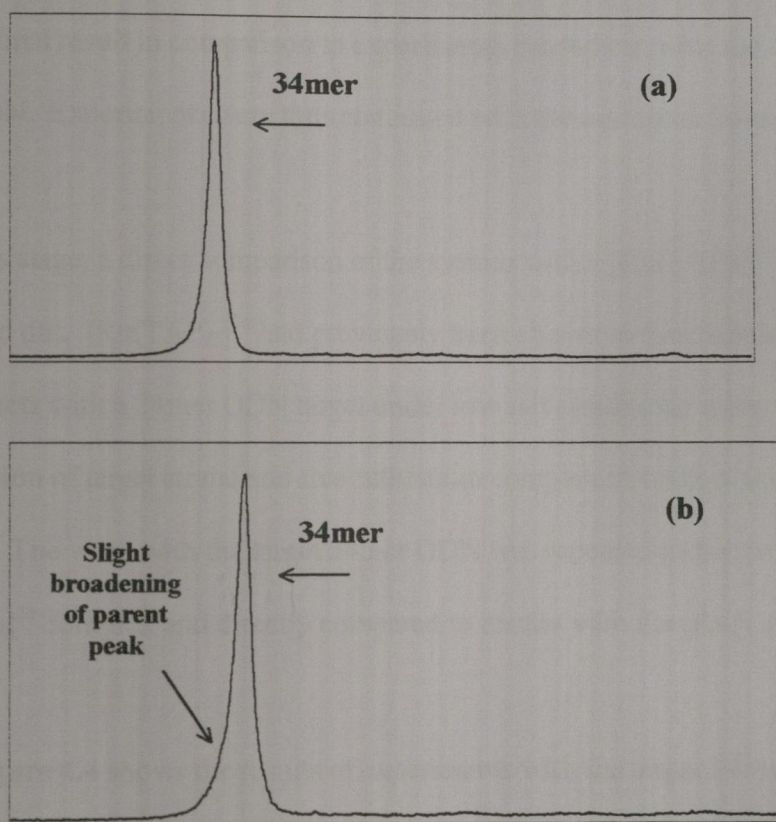


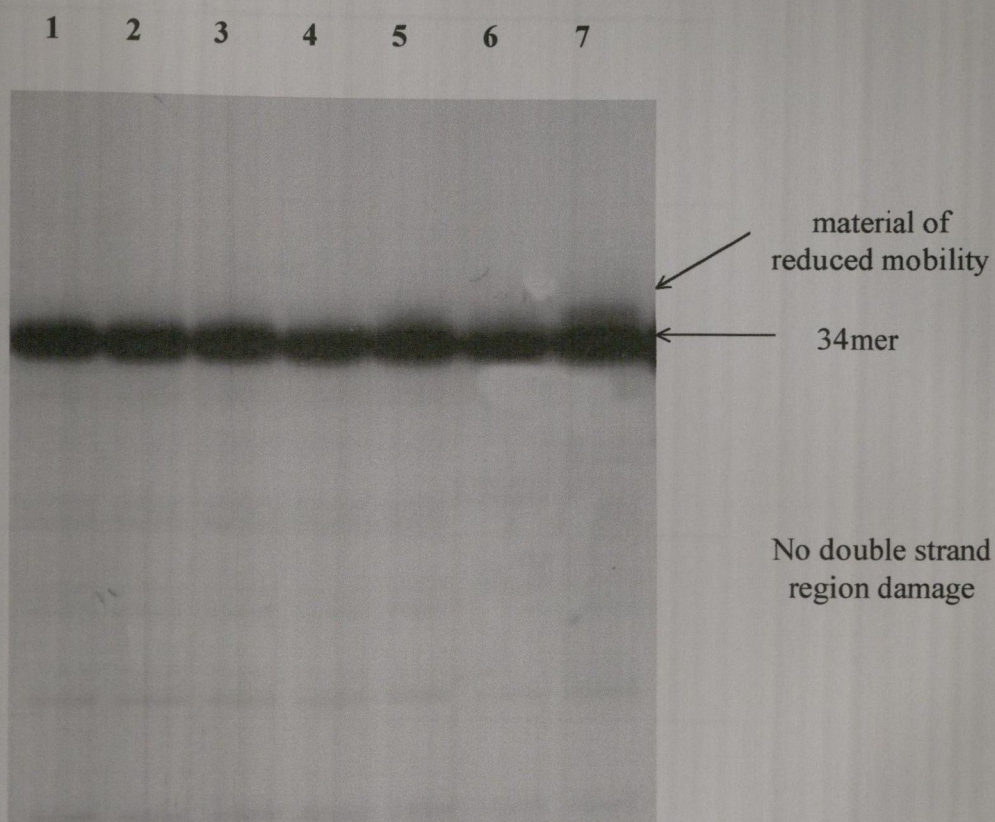
Figure 4.3 Phosphoimaging results for diluted 34mer ODN with $[\text{Ru}(\text{TAP})_2\text{phen}]^{2+}$ (1×10^{-5} M stock solution), 10 mM potassium phosphate buffer after (a) 0 min irradiation and (b) 20 mins irradiation.

Experiments were then carried out in which different concentrations of the target 34mer ODN was used. In addition to the one in ten dilution of the target 34mer ODN, samples were prepared containing target 34mer ODN at dilution factors of one in five and two in five (referring to one or two parts 34mer ODN in five parts water). The 1×10^{-4} M stock solution of the free ruthenium complex was included in each experiment. Irradiations over a range of times showed no improvement in photoadduct resolution with streaking evident above the target 34mer ODN band in each case. Reduction of the target 34mer ODN concentration did not seem to greatly affect the final result in comparison to experiments carried out with the undiluted 34mer ODN. Experiments were thus continued with the undiluted 34mer ODN stock solution.

At this stage, a direct comparison of the system with a $[\text{Ru}(\text{TAP})_3]^{2+}$ standard was carried out. $[\text{Ru}(\text{TAP})_3]^{2+}$ had previously been shown to form distinguishable photoadducts with a 24mer ODN target under low salt conditions using the same concentration of target strand and free ruthenium complex as used in this section of the work. The work with the target 34mer ODN was repeated in the presence of the $[\text{Ru}(\text{TAP})_3]^{2+}$ complex and directly compared to results with the $[\text{Ru}(\text{TAP})_2\text{phen}]^{2+}$ complex.

Figure 4.4 shows the results of experiments with the target 34mer ODN in the presence of the $[\text{Ru}(\text{TAP})_3]^{2+}$ complex with irradiation times of up to 10 mins. Lane 1 shows the result after 0 mins irradiation and as the time was increased, some material of reduced mobility was observed above the target 34mer ODN. No distinct photoadduct band was observed, but the material of reduced mobility that was not

present in the absence of illumination was indicative of photoadduct formation. The phosphoimaging results for lanes 1, 6 and 7 are shown in **figure 4.5**. The material of reduced mobility observed is seen as a broadening of the parent 34mer ODN peak.



Irradiations carried out in 10 mM phosphate buffer with a 10:1 ratio of $[\text{Ru}(\text{TAP})_3]^{2+}$: target 34mer ODN. **Lane 1** 0 min; **Lane 2** 15 sec; **Lane 3** 30 sec; **Lane 4** 1 min; **Lane 5** 2.5 min; **Lane 6** 5min; **Lane 7** 10 min.

Figure 4.4 34mer target ODN in presence of $[\text{Ru}(\text{TAP})_3]^{2+}$

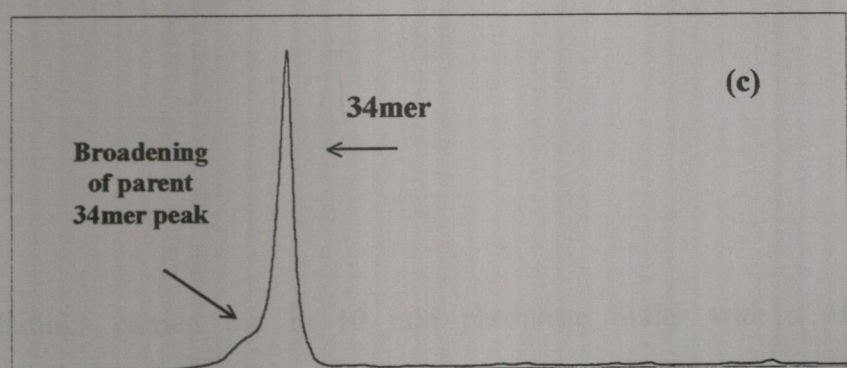
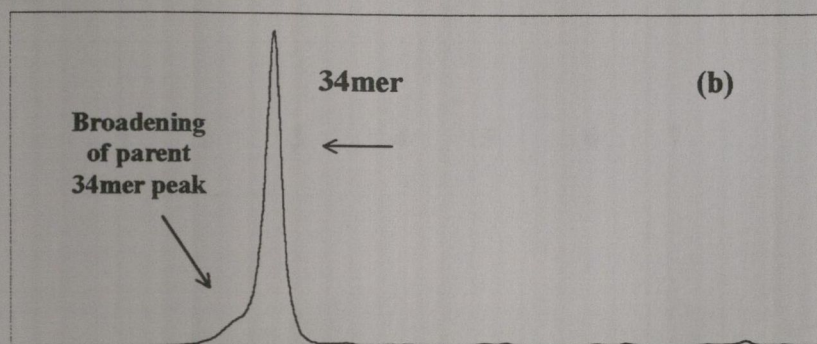
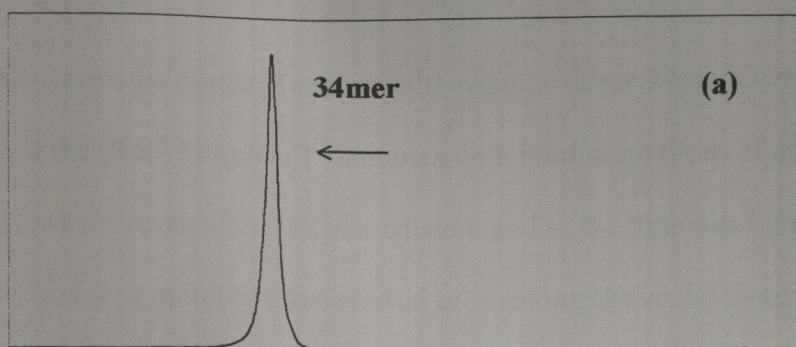
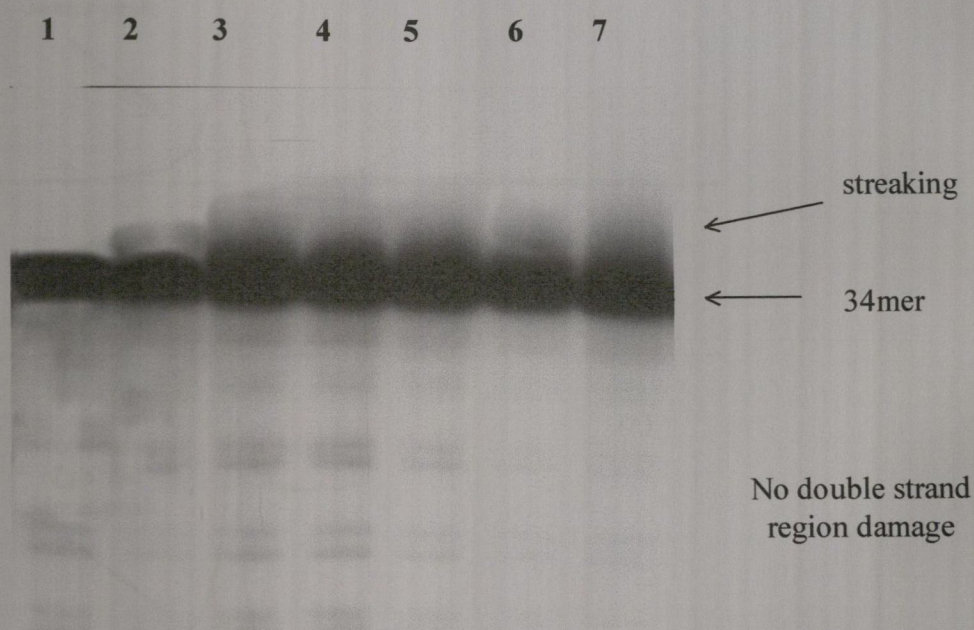


Figure 4.5 Phosphoimaging results for 34mer ODN with $[\text{Ru}(\text{TAP})_3]^{2+}$ (1×10^{-4} M stock solution), 10 mM potassium phosphate buffer after (a) 0 min irradiation, (b) 5 mins irradiation and (c) 10 mins irradiation

Figure 4.6 shows the results of experiments with the target 34mer ODN in the presence of the $[\text{Ru}(\text{TAP})_2\text{phen}]^{2+}$ complex with irradiation times of up to 10 mins. Lane 1 shows the result after 0 mins irradiation and as the time was increased, some material of reduced mobility was observed as streaking above the target 34mer ODN. The phosphoimaging results for lanes 1, 6 and 7 are shown in **figure 4.7**. The material of reduced mobility observed is seen as a broadening of the parent 34mer ODN peak.



Irradiations carried out in 10 mM phosphate buffer with a 10:1 ratio of $[\text{Ru}(\text{TAP})_2\text{phen}]^{2+}$: target 34mer ODN. **Lane 1** 0 min; **Lane 2** 15 sec; **Lane 3** 30 sec; **Lane 4** 1 min; **Lane 5** 2.5 min; **Lane 6** 5min; **Lane 7** 10 min.

Figure 4.6 34mer target ODN in presence of $[\text{Ru}(\text{TAP})_2\text{phen}]^{2+}$

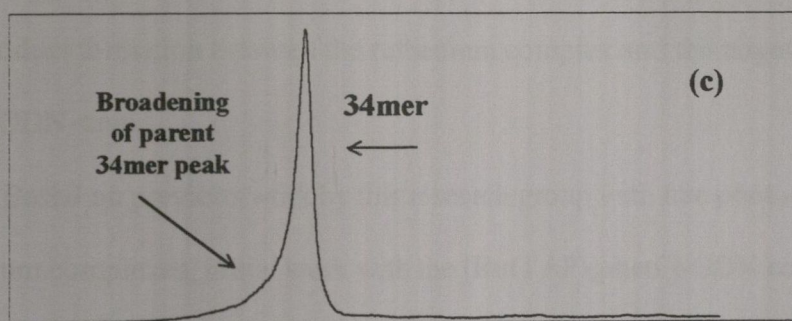
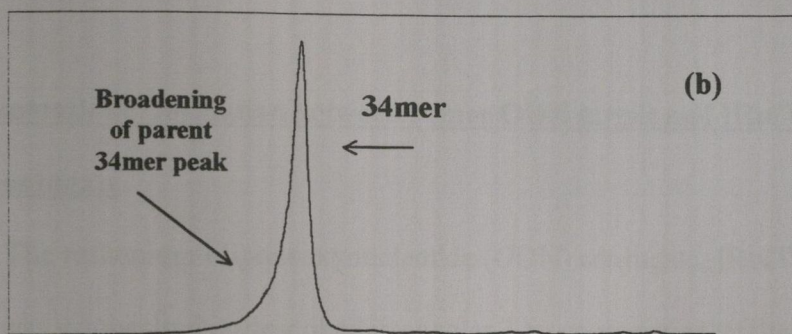
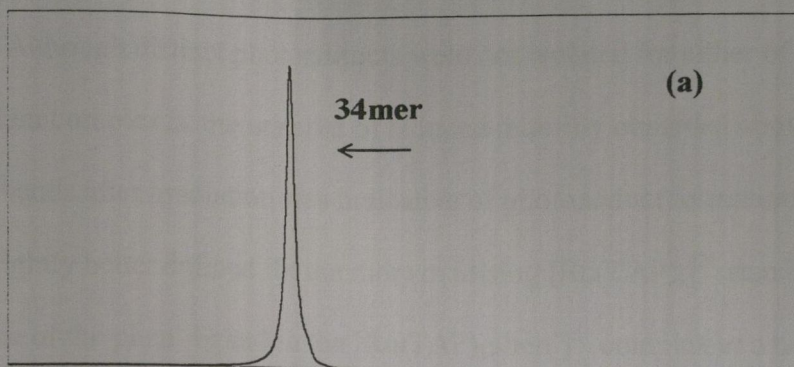


Figure 4.7 Phosphoimaging results for 34mer ODN with $[\text{Ru}(\text{TAP})_2\text{phen}]^{2+}$ (1×10^{-4} M stock solution), 10 mM potassium phosphate buffer after (a) 0 min irradiation, (b) 5 mins irradiation and (c) 10 mins irradiation

Although distinct photoadducts were not isolated for either of the free ruthenium complexes, the material of reduced mobility observed above the target 34mer bands after irradiation was indicative of photoadduct formation. The results were slightly better defined for the more oxidising $[\text{Ru}(\text{TAP})_3]^{2+}$ standard and the presence of the phen' ligand in the $[\text{Ru}(\text{TAP})_2\text{phen}']^{2+}$ complex as a negatively charged species under the experimental conditions, thus reducing interaction with the target ODN sequence, may also have contributed to the final result.

4.4 Photoadduct formation between 34mer ODN target and $[\text{Ru}(\text{TAP})_2\text{phen}']$ -ODN conjugate

The ruthenium-oligodeoxynucleotide (ODN) conjugate, $[\text{Ru}(\text{TAP})_2\text{phen}']$ -ODN, was synthesised as described in chapter 2 by conjugation of the free ruthenium complex, $[\text{Ru}(\text{TAP})_2\text{phen}']^{2+}$, to a 17mer ODN with a sequence complementary to one section of the 34mer ODN target strand. The overall aim was site-specific photoadduct formation between the ruthenium complex and the target G21 on the 34mer ODN strand.

Based on previous work by this research group with free photoadduct forming ruthenium complexes, initial work with the $[\text{Ru}(\text{TAP})_2\text{phen}']$ -ODN conjugate was carried out in low salt conditions (10 mM potassium phosphate buffer) using a 10:1 ratio of ruthenium-ODN conjugate : target 34mer ODN. An important consideration with the model system was to ensure that optimal hybridisation would occur between the 17mer ODN and the complementary region of the target 34mer ODN so as to allow optimal interaction between the ruthenium complex and the G21 target on the

34mer ODN strand. As this duplex formation is favoured under high salt conditions (10 mM potassium phosphate buffer / 100 mM NaCl), the work was also carried out under high salt conditions to investigate any significant differences caused by the differing ionic strength conditions. Samples were irradiated at various times between 0 mins and 40 mins and were not piperidine treated unless otherwise stated.

Preliminary experiments carried out under both high and low salt conditions showed that photoadduct formation with the target 34mer ODN was obtained after very short irradiation times (approximately 1 minute). No photoadduct formation was observed in an absence of irradiation. Photoadducts were identified as bands of reduced mobility with respect to the parent 34mer band as described in **figure 4.8**. After irradiation, a cross-linked species was formed between the ruthenium conjugate and the target guanine base (**figure 4.8(a)**). When the sample was analysed on a denaturing polyacrylamide gel, base pairing between the 17mer ODN and its complementary sequence on the target 34mer ODN was suppressed leaving a cross-linked species that migrated through the gel matrix at a slower rate than the target 34mer ODN on its own (**figure 4.8(b)**).

Differing ionic strengths did affect the yield of photoadduct formation with an approximately 11 % drop in photoadduct formation in high salt conditions. Therefore considering these results, all subsequent experiments were carried out under low salt conditions, as was favoured by previous research with free ruthenium complexes¹⁶⁴. Experiments were then carried out using a reduced ratio of ruthenium-ODN conjugate : target 34mer ODN of 1:1. Results with this new 1: 1 ratio gave results comparable

to those obtained in the 10:1 ratio experiments, therefore all subsequent work with the [Ru(TAP)₂phen']-ODN conjugate was carried out at the reduced 1:1 ratio.

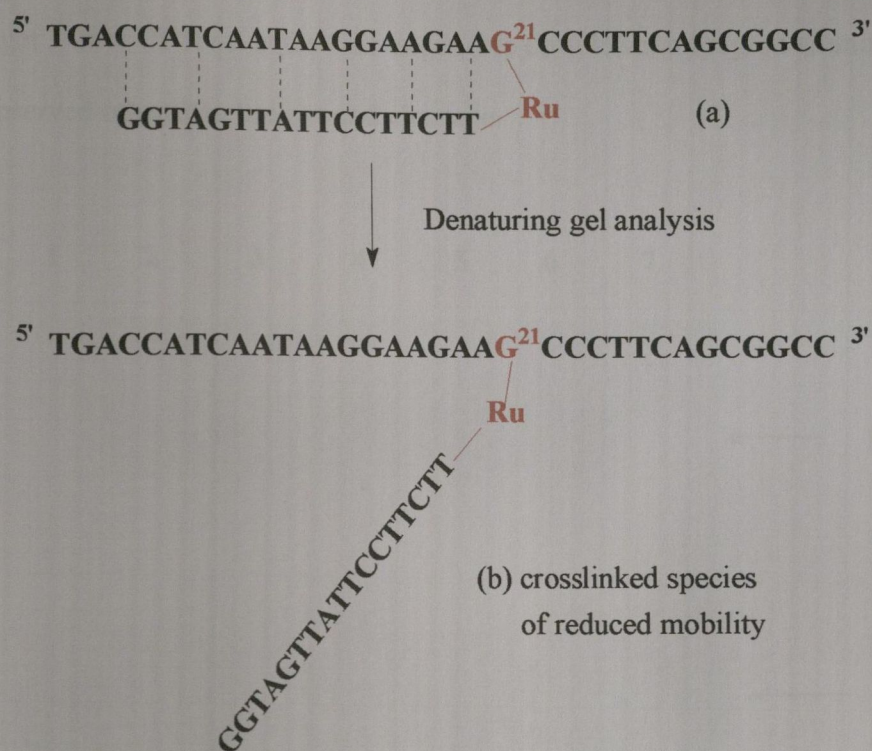
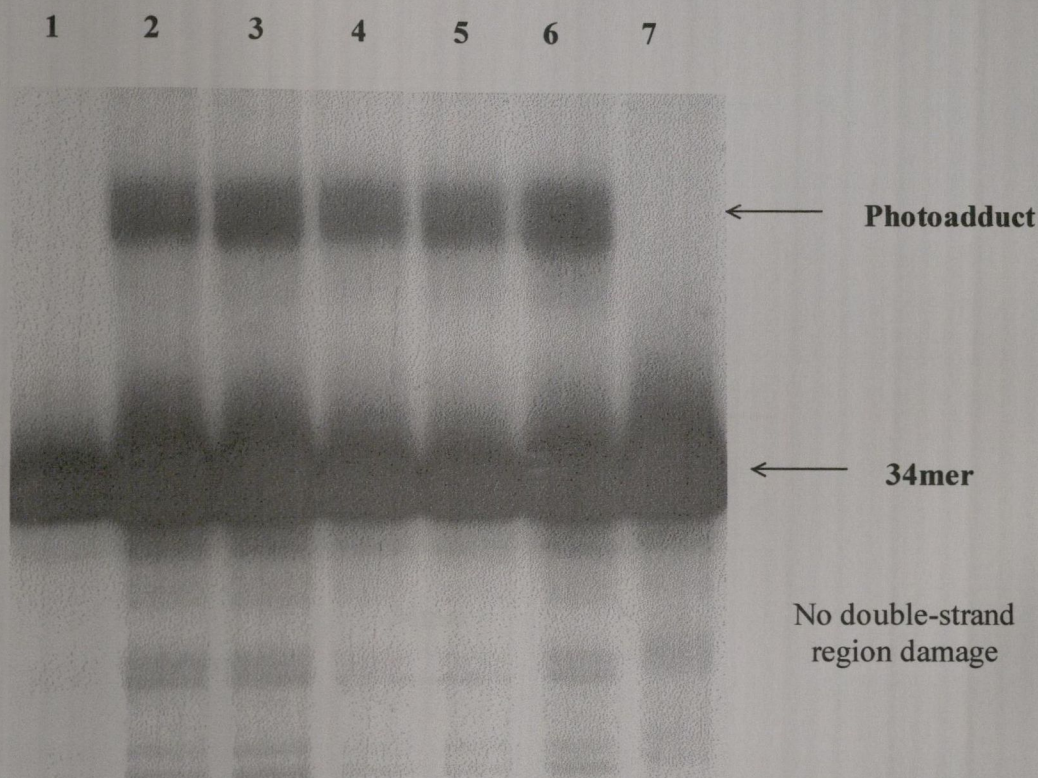


Figure 4.8 Diagrammatic representation of cross-linked ruthenium-conjugate / target 34mer ODN species before (a) and after (b) denaturing gel analysis

Lanes 1-6 in **figure 4.9** show the results of experiments in which the target 34mer ODN was irradiated in the presence of the [Ru(TAP)₂phen']-ODN conjugate with irradiation times of 0 mins up to 10 mins using a 1:1 ratio of ruthenium-ODN conjugate : target 34mer ODN. No adduct was observed in lane 1 in an absence of

irradiation. Adduct formation was observed in lanes 2-6 upon increasing irradiation times. No photoadduct was observed in lane 7 which contained only 34mer ODN target that was irradiated for 10 mins. Only one photoadduct was observed in lanes 2-6, suggesting that the ruthenium complex only forms crosslinks at one position on the target 34mer ODN *i.e.* at the G21 target. No double strand region strand damage was observed other than background cleavage.



Irradiations carried out in 10 mM phosphate buffer with a 1:1 ratio of [Ru(TAP)₂phen']-ODN : target 34mer ODN. **Lane 1** 0 min; **Lane 2** 1 min; **Lane 3** 2 min; **Lane 4** 4 min; **Lane 5** 8 min; **Lane 6** 10min; **Lane 7** 34mer only, 10min.

Figure 4.9 Photoadduct formation between 34mer ODN and [Ru(TAP)₂phen']-ODN

The phosphoimagery results of lanes 1 and 6 are shown in **figure 4.10**. As previously stated, no photoadduct formation was observed in an absence of irradiation and **figure 4.10(a)** consisted only of one peak due to the target 34mer ODN alone. **Figure 4.10(b)** shows the result after 10 mins irradiation in the presence of the $[\text{Ru}(\text{TAP})_2\text{phen}']\text{-ODN}$ conjugate. In addition to the parent 34mer ODN peak, a second peak due to photoadduct formation was also present. The overall yield of photoadduct formation in this case was 5.3 %.

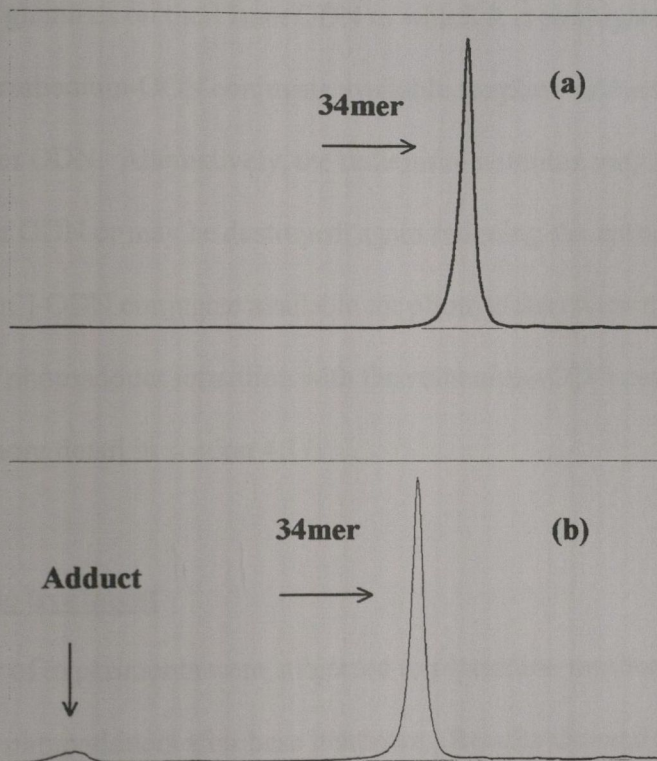


Figure 4.10 Phosphoimagery results of 34mer ODN in presence of $[\text{Ru}(\text{TAP})_2\text{phen}']\text{-ODN}$ conjugate after **a)** 0 mins irradiation and **b)** 10 mins irradiation.

In an analogous manner to the photocleavage results observed with the [Ru(phen)₂phen']-ODN conjugate, increasing irradiation times did not result in an increase of photoadduct formation, suggesting that the photoadduct formation ceases after a certain period of time. This observed "plateau" of activity by the [Ru(TAP)₂phen']-ODN conjugate may possibly be explained by one of two main theories, similar to those proposed for the [Ru(phen)₂phen']-ODN conjugate discussed in section 3.6. The [Ru(TAP)₂phen']-ODN conjugate may form photoadducts with itself *i.e.* the ruthenium complex may be capable of abstracting electrons from guanines on the 17mer ODN to which it is conjugated, thus reducing the amount of ruthenium-ODN conjugate available for photoadduct formation with the target 34mer ODN. Alternatively, the ruthenium complex may become detached from the 17mer ODN or may be destroyed, again reducing the amount of [Ru(TAP)₂phen']-ODN conjugate available for photoadduct formation. The relative inefficiency of photoadduct formation with the ruthenium-ODN conjugate is addressed in more detail in section 4.11.

4.5 Piperidine treatment

A number of experiments were subjected to piperidine treatment to assess the stability of the photoadducts after base treatment. Results showed no decrease in the overall yield of photoadduct formation. The only difference was the introduction of a small amount of guanine-specific cleavage in the target 34mer ODN strand. As the photoadduct was not affected by base treatment, it was concluded that the small

amount of cleavage observed upon piperidine treatment revealed sites of modified base damage within the target 34mer ODN after irradiation.

4.6 Effect of the presence of sodium nitrite filter

The effect of the presence of a sodium nitrite (NaNO_2) filter on the overall ability of the $[\text{Ru}(\text{TAP})_2\text{phen}']$ -ODN conjugate to form photoadducts with the G21 target in the parent 34mer ODN strand was also investigated. As discussed in section 3.7, the beam used to irradiate the experimental samples was initially passed through a sodium nitrite filter.

The experiments were repeated under identical conditions to those described in section 4.4 with the inclusion of the sodium nitrite filter in the experimental setup *i.e.* using a 1:1 ratio of ruthenium-ODN conjugate : 34mer ODN target in low salt conditions with no piperidine treatment.

Analysis of the results showed that in both filtered and non-filtered conditions, photoadduct formation with the target 34mer ODN was achieved but with a slightly lower yield of photoadduct under filtered conditions. The results of the filtered and non-filtered experiments after 10 mins irradiation are compared in **figure 4.11**.

The wavelengths between 330 nm and 400 nm which are excluded by the inclusion of a sodium nitrite filter in addition to the Pyrex™ glass filter already present, may possibly play a part in achievement of higher yields of photoadduct formation between G21 in the target 34mer ODN strand and the ruthenium complex. Alternatively, passing the beam through the sodium nitrite filter will remove power

from the beam thus causing the experimental samples to be irradiated with a weaker beam and explaining the slightly lower yield of photoadduct formation.

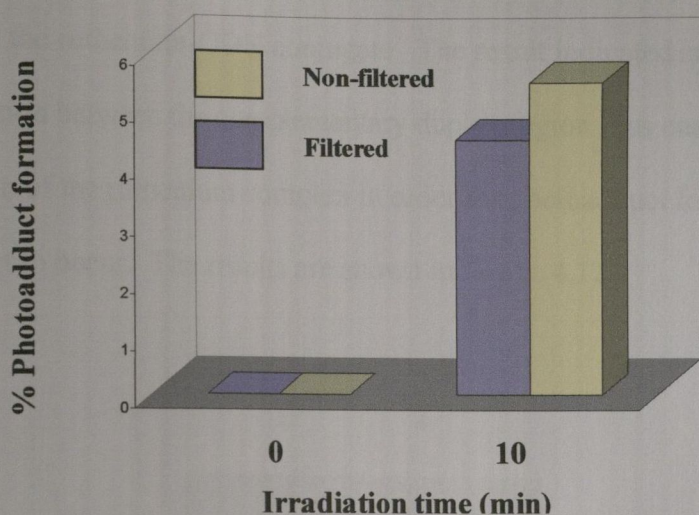
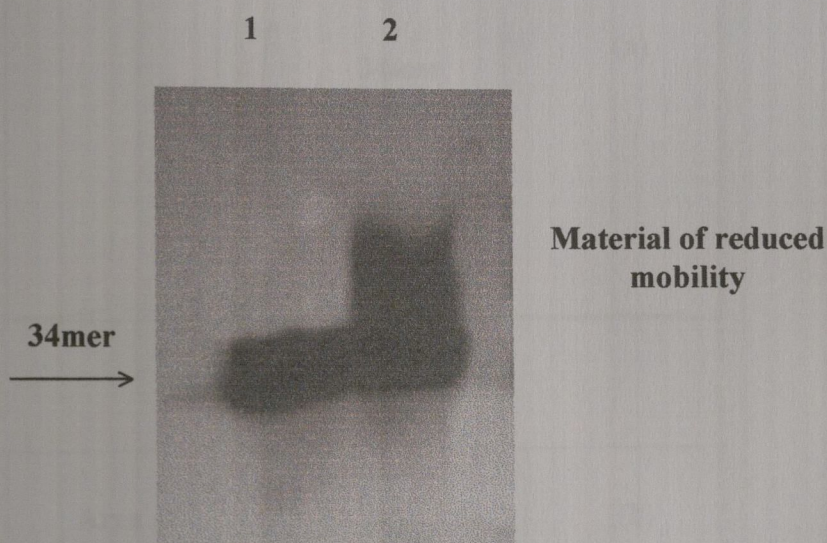


Figure 4.11 Comparison of yields of photoadduct formation between target 34mer and $[\text{Ru}(\text{TAP})_2\text{phen}']\text{-ODN}$ conjugate in presence and absence of sodium nitrite filter.

4.7 Non-denaturing gel work

Due to the nature of the model system used for the investigation of the photoadduct formation between the $[\text{Ru}(\text{TAP})_2\text{phen}']\text{-ODN}$ conjugate and the target 34mer ODN, confirmation of hybridisation between the 17mer of the ruthenium-ODN conjugate and its complementary sequence on the target 34mer ODN before sample irradiation was necessary. Different samples were analysed using non-denaturing gels to verify duplex formation. Non-denaturing gels are discussed in detail in section 3.8.

Samples containing the target 34mer ODN and the $[\text{Ru}(\text{TAP})_2\text{phen}']$ -ODN conjugate were allowed to hybridise in the normal way and were subsequently analysed on a non-denaturing gel. Bands of reduced mobility with respect to the target 34mer ODN band were observed for samples containing both the target 34mer ODN and the ruthenium-ODN conjugate. The result indicated successful hybridisation between the complementary duplex region thus ensuring correct orientation of the ruthenium complex in order for photoadduct formation with the G21 target to occur. The results are shown in **figure 4.12**.



All samples in 10 mM potassium phosphate buffer and samples with ruthenium conjugate contain 1:1 ratio of ruthenium-ODN conjugate : target 34mer ODN. **Lane 1** 34mer ODN; **Lane 2** 34mer target and $[\text{Ru}(\text{TAP})_2\text{phen}']$ -ODN conjugate.

Figure 4.12 Comparison of 34mer target / $[\text{Ru}(\text{TAP})_2\text{phen}']$ -ODN duplex with free 34mer target on non-denaturing gel.

Lane 1 shows the target 34mer ODN alone and lane 2 shows the 34mer ODN target in the presence of $[\text{Ru}(\text{TAP})_2\text{phen}']\text{-ODN}$ conjugate with the area of reduced mobility above the parent 34mer band indicative of duplex formation. **Figure 4.13** shows the phosphoimaging results for lanes 1 and 2. **Figure 4.13(a)** shows only one peak representing the target 34mer ODN alone. **Figure 4.13(b)** shows the target 34mer in the presence of the ruthenium conjugate. The peak adjacent to the parent 34mer peak indicated hybridisation between the complementary regions.

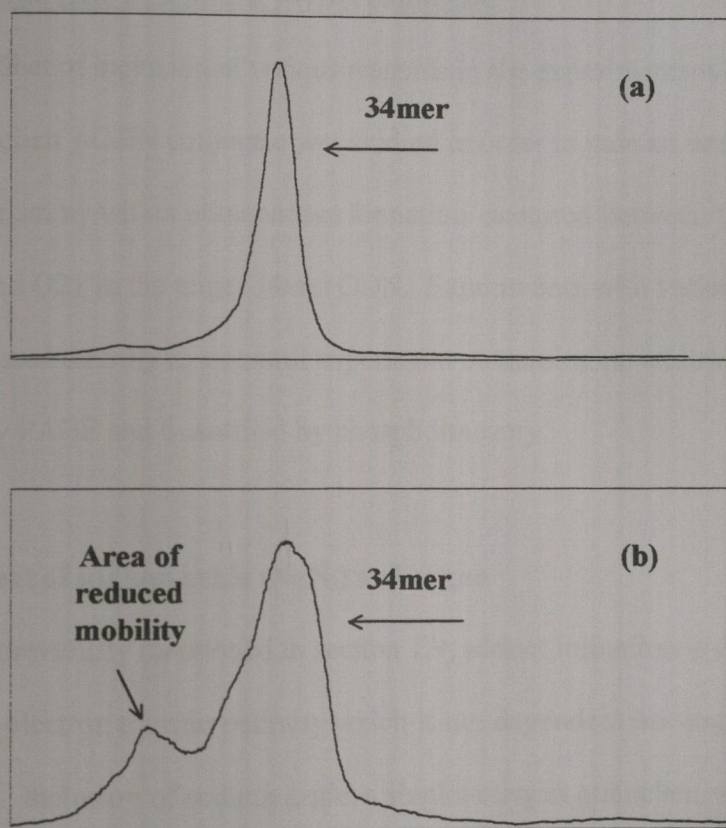


Figure 4.13 Phosphoimaging results comparing non-denaturing results of a) 34mer target ODN only and b) 34mer target ODN in presence of $[\text{Ru}(\text{TAP})_2\text{phen}']\text{-ODN}$ conjugate.

Samples containing 34mer ODN target and complementary 17mer ODN were also compared to the 34mer target / [Ru(TAP)₂phen⁺]-ODN conjugate samples. Non-denaturing gel analysis showed bands of similar reduced mobility for both samples indicating that the presence of the ruthenium complex at the 3'-end of the 17mer ODN did not reduce the stability of the duplex formed compared to the unconjugated system.

4.8 Effect of various additions on photoadduct formation between target 34mer ODN and [Ru(TAP)₂phen⁺]-ODN conjugate

The effect of inclusion of various reagents in the experiments with the [Ru(TAP)₂phen⁺]-ODN conjugate was studied in order to gain an understanding of the mechanism by which photoadduct formation occurred between the ruthenium complex and G21 in the target 34mer ODN. Experiments with various additions were compared directly to a control experiment containing no addition. Results were analysed by PAGE and quantified by phosphoimager.

4.8.1 Effect of sodium azide (NaN₃) and argon

As previously mentioned in section 1.9, adduct formation is thought to occur via a type I electron transfer pathway which is not dependent on singlet oxygen production. Inclusion of sodium azide, a singlet oxygen quencher, will decrease the amount of damage induced by a type II singlet oxygen dependent pathway. Likewise, argon purging during the course of an experiment will reduce the amount of molecular oxygen available in the experimental sample and localised environment

from which singlet oxygen can be generated, thus reducing the amount of type II damage occurring. The phosphoimagery results of experiments containing azide and carried out under an atmosphere of argon are compared to the normal experiment in **figure 4.14**. All experiments were carried out in low salt conditions with a 1:1 ratio of $[\text{Ru}(\text{TAP})_2\text{phen}']\text{-ODN}$ conjugate : target 34mer ODN with an irradiation time of 10 mins. Samples were not piperidine treated and irradiations were carried out in the absence of a sodium nitrite filter.

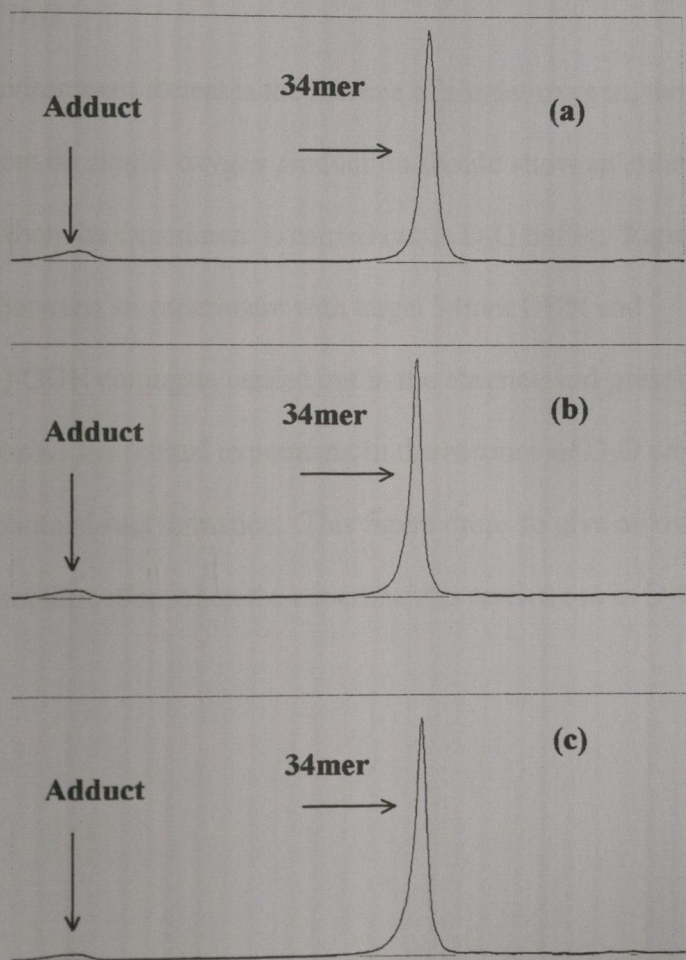


Figure 4.14 Phosphoimagery results comparing photoadduct formation with target 34mer ODN and $[\text{Ru}(\text{TAP})_2\text{phen}']\text{-ODN}$ conjugate **a)** with no additions **b)** with azide and **c)** under argon atmosphere

Figure 4.14(a) shows photoadduct formation between the target 34mer ODN and the [Ru(TAP)₂phen⁻]-ODN conjugate in the absence of any additions. A 5.5 % overall yield of photoadduct was achieved. **Figure 4.14(b)** shows the same experiment in the presence of sodium azide. A decrease in the overall yield to 4.4 % photoadduct formation was observed. **Figure 4.14(c)** shows the effect of argon purging during the course of the experiment with a further decrease in photoadduct formation to 3 %. Repetition of these experiments produced similar results.

4.8.2 Effect of D₂O

A D₂O environment increases the lifetime of singlet oxygen, therefore a pathway dependent on singlet oxygen production should show an enhancement in overall damage when the experiment is carried out in D₂O buffer. **Figure 4.15** shows the comparison between an experiment with target 34mer ODN and [Ru(TAP)₂phen⁻]-ODN conjugate carried out in the absence and presence of D₂O. **Figure 4.15(a)** shows the normal experiment in the absence of D₂O with a 5.5 % overall yield of photoadduct formation. This figure drops to give an overall yield of 4.4 % photoadduct formation when the experiment is carried out in D₂O as shown in **figure 4.15(b)**.

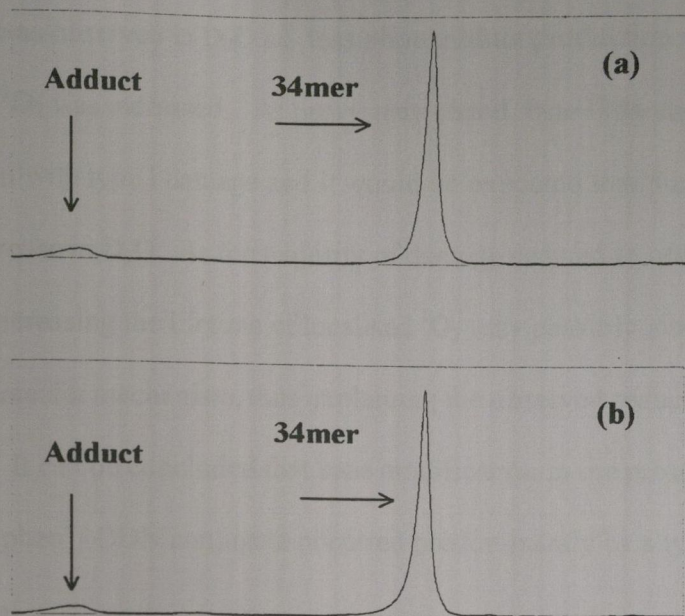


Figure 4.15 Phosphoimagery results comparing photoadduct formation with target 34mer ODN and [Ru(TAP)₂phen']-ODN conjugate **a)** with no additions and **b)** in the presence of D₂O

4.8.3 Mechanism of photoadduct formation

The results of the experiments carried out in H₂O, D₂O, azide and with argon purging are summarized in **figure 4.16**. Photoadduct formation (type I damage) involves electron transfer from guanine to the ruthenium complex generating the radical cation of the base, and experiments involving azide and argon purging would not be expected to have as significant an effect as compared with a type II pathway. A reduction in photoadduct formation was observed in both cases, with a larger decrease evident with argon. Azide may have been able to quench the excited state of the ruthenium complex. The majority of photoadduct formation was not suppressed,

indicating a type I mechanism was the major reaction. A decrease in photoadduct formation was observed in D_2O *i.e.* less photoadduct production occurred when the lifetime of 1O_2 was increased. As previously stated, type II damage may occur in conjunction with type I damage and it would be expected that the overall damage should increase in D_2O . As the majority of damage seemed to occur by a type I pathway, increasing the lifetime of localised 1O_2 may possibly interfere with the type I electron transfer mechanism, thus explaining the observed reduction in photoadduct formation. It can be concluded that base modification in the presence of the $[Ru(TAP)_2phen']$ -ODN conjugate occurred predominantly by a type I reaction mechanism.

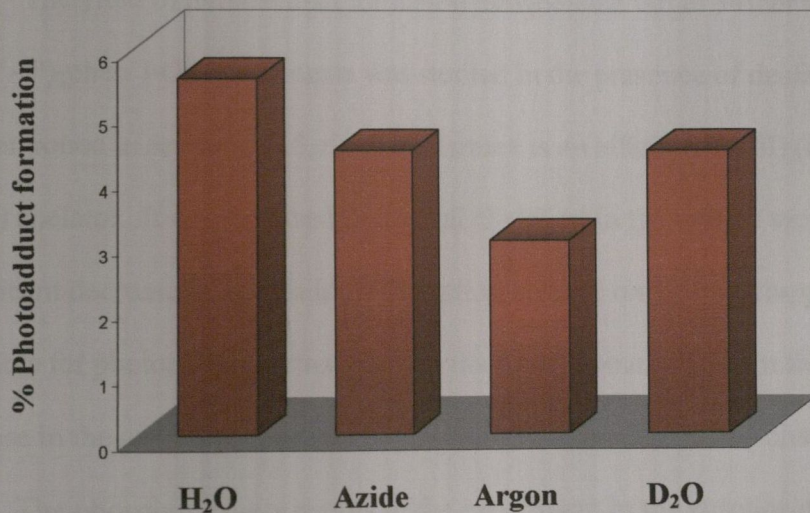


Figure 4.16 Comparison of photoadduct formation with target 34mer ODN and $[Ru(TAP)_2phen']$ -ODN conjugate with no additions and in presence of azide, argon and D_2O

4.8.4 Effect of ammonium persulfate

As mentioned in section 3.4.3, the inclusion of the electron transfer agent ammonium persulfate ($(\text{NH}_4)_2\text{S}_2\text{O}_8$) can generate a Ru(III) species from the Ru(II) complex. The Ru(III) species is a stronger oxidant than Ru(II), and in the case of photoadduct formation, should abstract an electron more readily from guanine, thus increasing the overall yield of photoadduct formation. The reactive $\text{SO}_4^{\cdot-}$ species is also generated and may also induce damage. Inclusion of ammonium persulfate in the sample of target 34mer ODN and $[\text{Ru}(\text{TAP})_2\text{phen}']\text{-ODN}$ showed an increase in photoadduct formation from 5.5 % to 6.5 % (**figure 4.17**).

4.8.5 Effect of desferrioxamine

The yield of photoadduct formation between the target 34mer ODN and the $[\text{Ru}(\text{TAP})_2\text{phen}']\text{-ODN}$ conjugate was studied in the presence of desferrioxamine. As mentioned in section 3.9.5, desferrioxamine is an efficient Fe(III) (and transition metal) chelator. It was expected that metal chelation in the system would result in a significant decrease in photoadduct formation *i.e.* less ruthenium complex would be available for photoadduct formation with the target 34mer ODN. In fact a significant increase in the overall photoadduct yield from 5.5 % to 7.9 % was observed (**figure 4.17**). The phosphoimager results of the experiment in the absence of desferrioxamine (a) and in the presence of desferrioxamine (b) are shown in **figure 4.18**. The observed increase in photoadduct formation may be explained by the formation of desferrioxamine radicals capable of generating the Ru(III) species which in turn would lead to an increase in photoadduct formation.

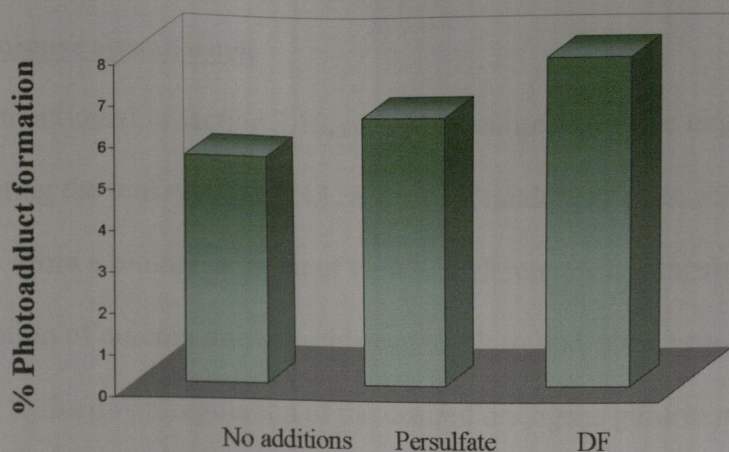


Figure 4.17 Comparison of photoadduct formation with target 34mer ODN and $[\text{Ru}(\text{TAP})_2\text{phen}']\text{-ODN}$ conjugate with no additions and in presence of persulfate and desferrioxamine (DF)

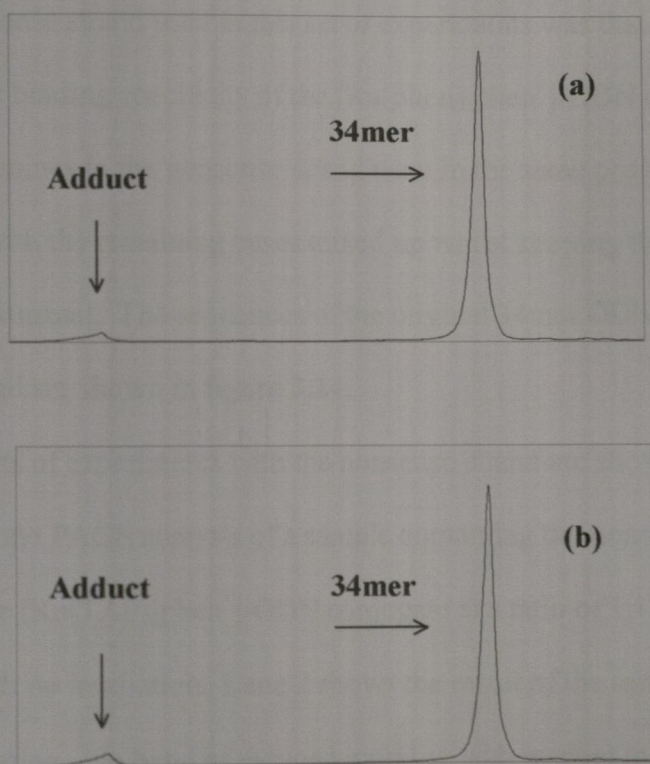


Figure 4.18 Phosphoimager results comparing photoadduct formation with target 34mer ODN and $[\text{Ru}(\text{TAP})_2\text{phen}']\text{-ODN}$ conjugate **a)** with no additions and **b)** in the presence of desferrioxamine

4.9 Nonsense strand work

As mentioned in section 3.10, only phototargeting of the target 34mer ODN representing the leukaemic mRNA, and not of random nucleic acid sequences, was desired. From a biological point of view, interference with translation or transcription of random nucleic acids can result in undesired non-specific effects in addition to the down-regulation of the desired oncogene gene expression. In relation to the $[\text{Ru}(\text{TAP})_2\text{phen}']$ -ODN conjugate work, it was necessary to ensure that the conjugate was not capable of binding to random nucleic acid sequences, thus ensuring that crosslinks would not form between the ruthenium complex of the conjugate and random guanine residues.

The nonsense strand used in this set of experiments was that designed to investigate the binding specificity of the $[\text{Ru}(\text{phen})_2\text{phen}']$ -ODN conjugate. As before, the guanines in the nonsense strand were in the same positions as the original 34mer ODN with the remaining bases mixed up whilst keeping the overall base composition constant. The sequences of the original 34mer ODN target and the nonsense strand are shown in **figure 3.24**.

The results of experiments with the nonsense strand are shown in **figure 4.19**. Lane 1 shows the PAGE analysis of a sample containing the nonsense strand in the presence of the $[\text{Ru}(\text{TAP})_2\text{phen}']$ -ODN conjugate at a ratio of 1:1 under low salt conditions with no irradiation. Lane 2 shows the result of the same experiment after 10 mins irradiation. No band of reduced mobility with respect to the parent 34mer nonsense strand was observed after irradiation, showing that the ruthenium-ODN

conjugate was not capable of binding to the nonsense strand and forming a photoadduct with the G21 target base.

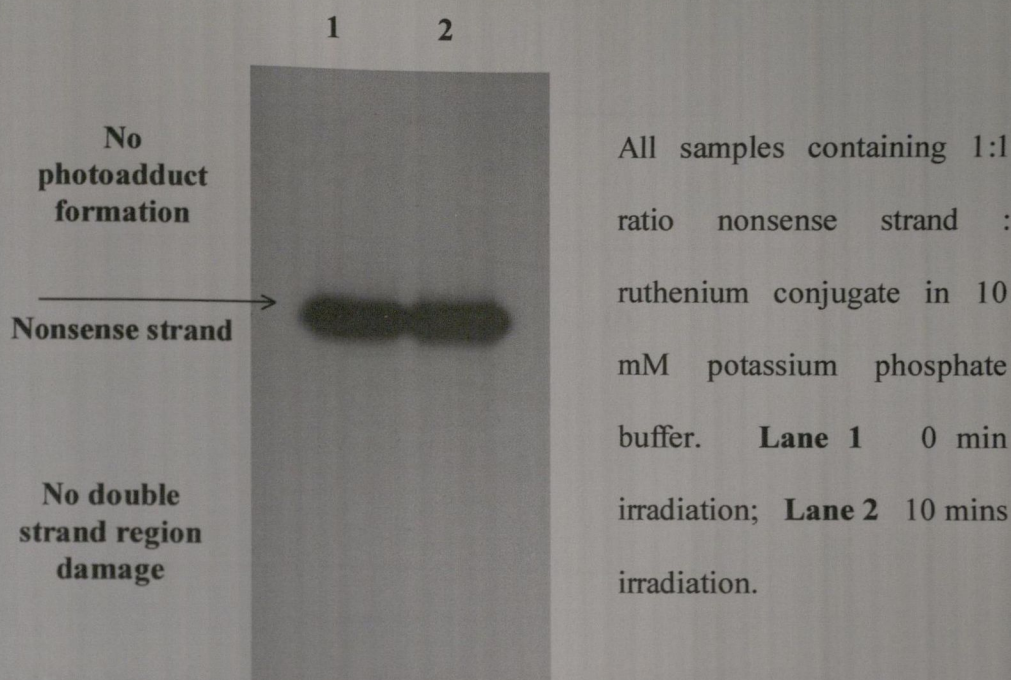


Figure 4.19 Results of nonsense strand experiments in presence of $[\text{Ru}(\text{TAP})_2\text{phen}']\text{-ODN}$ conjugate

The phosphorimager results for this experiment are shown in **figure 4.20**. Lanes 1 and 2 are shown in **figure 4.20(a)** and **figure 4.20(b)** respectively. Only one peak due to the presence of the nonsense strand was evident in each case with no peak characteristic of photoadduct formation evident in **(b)** after 10 mins irradiation.

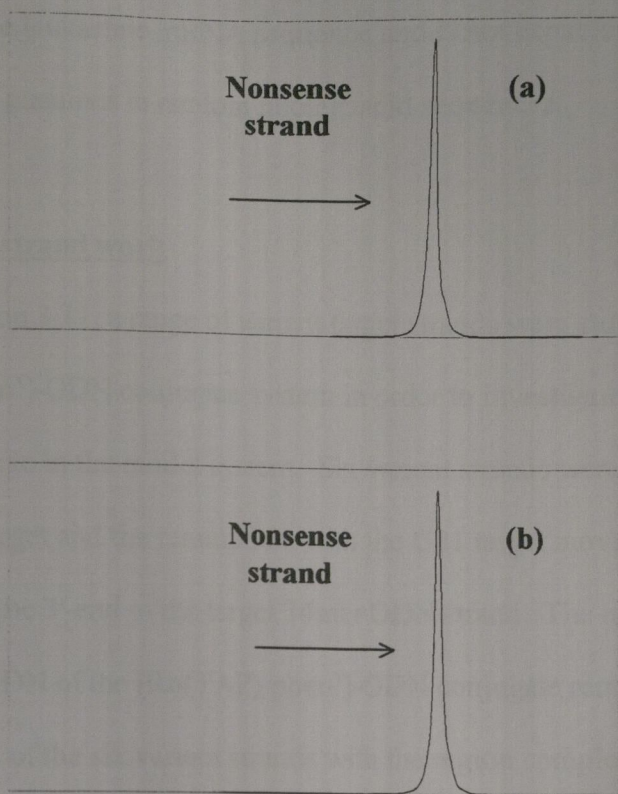


Figure 4.20 Phosphoimagery results of nonsense strand experiments in the presence of $[\text{Ru}(\text{TAP})_2\text{phen}']\text{-ODN}$ conjugate **a)** with no irradiation and **b)** after 10 mins irradiation

To confirm that the $[\text{Ru}(\text{TAP})_2\text{phen}']\text{-ODN}$ conjugate was not binding to the nonsense strand, the results of this experiment were also analysed on a non-denaturing gel. No material of reduced mobility with respect to the parent nonsense ODN was observed. The results of the denaturing and non-denaturing gel work showed that the 17mer ODN of the ruthenium-ODN conjugate was not capable of binding to the nonsense strand therefore it can be concluded that the $[\text{Ru}(\text{TAP})_2\text{phen}']\text{-ODN}$ conjugate is specific only for the target 34mer ODN

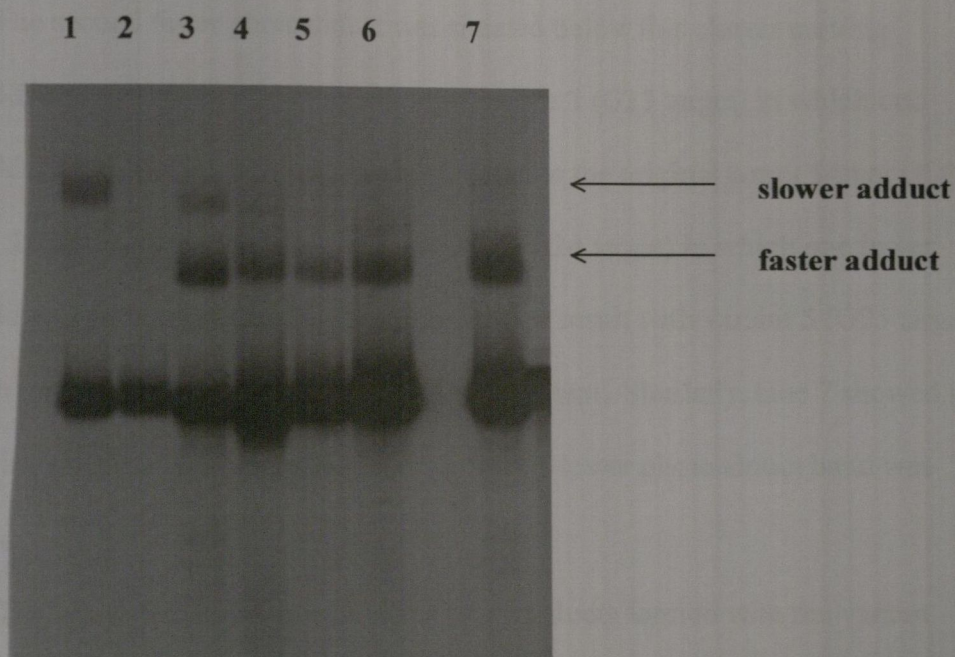
representing the leukaemic mRNA sequence and is not capable of photoadduct formation with guanines in random nucleic acid sequences.

4.10 Variant strand work

In section 3.11, a range of variant target strands were studied in relation to the $[\text{Ru}(\text{phen})_2\text{phen}']$ -ODN conjugate system in order to investigate the range of oxidative damage in the model system. Six variant strands were designed, the first with no G21 target and the remainders with the G21 target moved 1, 2, 3, 4 and 6 bases towards the 3'-end of the target 34mer ODN strand. The region complementary to the 17mer ODN of the $[\text{Ru}(\text{TAP})_2\text{phen}']$ -ODN conjugate remained unchanged. The sequences of the six variant strands with the region complementary to the 17mer ODN highlighted in red are shown in **figure 3.26**.

The same six variant strands were again studied in relation to the $[\text{Ru}(\text{TAP})_2\text{phen}']$ -ODN conjugate system to fully investigate the range of photoadduct formation as the target guanine base was moved towards the 3'-end of the target 34mer ODN. Originally it had been expected that photoadduct formation would cease as the target base was moved away in increments from its original place at position 21 in the target 34mer ODN. But subsequent analysis with the $[\text{Ru}(\text{phen})_2\text{phen}']$ -ODN system had shown that the variant strands were capable of hairpinning resulting in the majority of photooxidative damage taking place at the 3'-end guanines of the target strand. A detailed description of the possible hairpin conformations of each of the variant strands and calculations of their free energies of formation is discussed in section 3.11.

A difference between the $[\text{Ru}(\text{phen})_2\text{phen}']\text{-ODN}$ and $[\text{Ru}(\text{TAP})_2\text{phen}']\text{-ODN}$ conjugate systems was the ionic strength of the experimental samples. In the $[\text{Ru}(\text{phen})_2\text{phen}']\text{-ODN}$ conjugate system, the high salt experimental conditions seemed to strongly favour variant strand hairpinning. The $[\text{Ru}(\text{TAP})_2\text{phen}']\text{-ODN}$ conjugate experiments were carried out under low salt experimental conditions, but after PAGE analysis of the conjugate in the presence of each of the variant strands, a similar hairpinning pattern to that observed in section 3.11 seemed to explain the observed results. The results of the $[\text{Ru}(\text{TAP})_2\text{phen}']\text{-ODN}$ conjugate experiments with each of the variant strands is shown in **figure 4.21**.



All irradiations carried out in 10 mM potassium phosphate buffer for 10 mins with 1:1 ratio of $[\text{Ru}(\text{TAP})_2\text{phen}']\text{-ODN}$ conjugate : target strand. **Lane 1** original target 34mer; **Lane 2** Variant 1; **Lane 3** Variant 2; **Lane 4** Variant 3; **Lane 5** Variant 4; **Lane 6** Variant 5; **Lane 7** Variant 6.

Figure 4.21 Results of experiments with variants 1-6 in the presence of $[\text{Ru}(\text{TAP})_2\text{phen}']\text{-ODN}$

Lane 1 showed one band of reduced mobility with respect to the parent band which was attributed to the photoadduct formed between the ruthenium-ODN conjugate and the original target 34mer ODN. A control lane in which the original target 34mer ODN was irradiated in the absence of the ruthenium-ODN conjugate showed no evidence of photoadduct formation (result not shown). Lane 2 showed the result with variant 1 (no G21 target) in which no photoadduct was formed. This result was consistent with the absence of the guanine target at position 21 in the target strand. Lane 3 showed the result with variant 2 (G22 target) in which two photoadducts were evident. The slower of the two photoadducts was at approximately the same level as that observed for the ruthenium-ODN conjugate in the presence of the original 34mer ODN. The second faster photoadduct was situated below this slower moving photoadduct. Lane 4 showed the result with variant 3 (G23 target) in which one photoadduct was formed at a lower level than that in the original target 34mer ODN system. Lane 5 showed the result with variant 4 (G24 target) in which one lower photoadduct band was evident. Lane 6 showed the result with variant 5 (G25 target) in which only one lower photoadduct band was evident. Similarly, lane 7 showed the result with variant 6 (G27 target) in which only one lower photoadduct band was observed.

The phosphoimagery results of the photoadducts formed with the variant strands showed that for variants 3-6, a similar yield of photoadduct formation was achieved compared with the results obtained for the original 34mer ODN target. For variant 2, the faster photoadduct band also had a similar yield of photoadduct formation to the original 34mer ODN system. The yield of adduct formation in the

slower band observed with variant 2 was roughly one third that seen for the faster adduct band.

In order to fully understand the PAGE results observed with the variant strands, the possible hairpinning conformations were studied in conjugation with the free energy of formation values calculated in section 3.11. The complementary regions within each variant strand are shown underlined in **figure 3.30**.

In the original experiment with the target 34mer ODN strand, denaturing gel analysis of photoadduct formation (**figure 4.8**) produced a cross-linked species (**figure 4.22**) that moved at a relatively slow rate through the gel matrix. This was seen as the photoadduct band in lane 1 of **figure 4.21**.

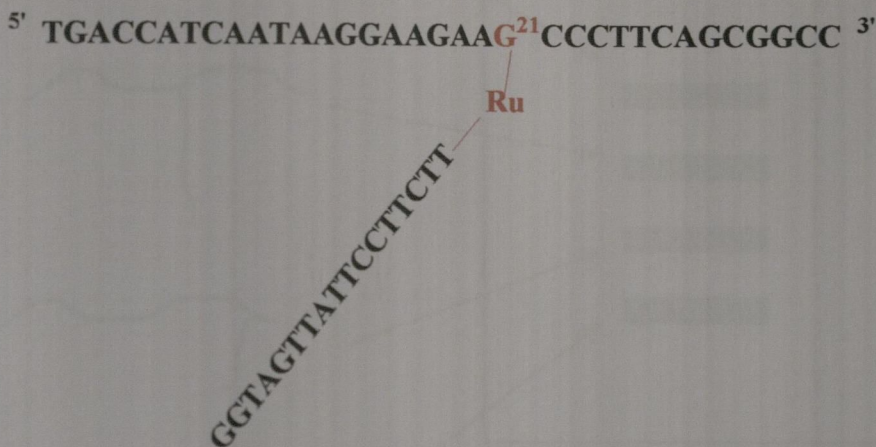


Figure 4.22 Crosslinked species formed between original 34mer ODN and [Ru(TAP)₂phen']-ODN conjugate

The polyacrylamide gel matrix can be thought of as a series of beads or pores through which nucleic acid fragments migrate, with smaller fragments migrating at a quicker rate through the gel matrix. Following this logic, an unmodified nucleic acid strand should migrate at a faster rate than a crosslinked species that would be sterically hindered. The greater the extent of crosslinking, the slower the fragment would move through the gel matrix. The relative speed of migration of three fragments crosslinked to different degrees in comparison to the unmodified strand and their positions on a denaturing gel is shown in **figure 4.23**.

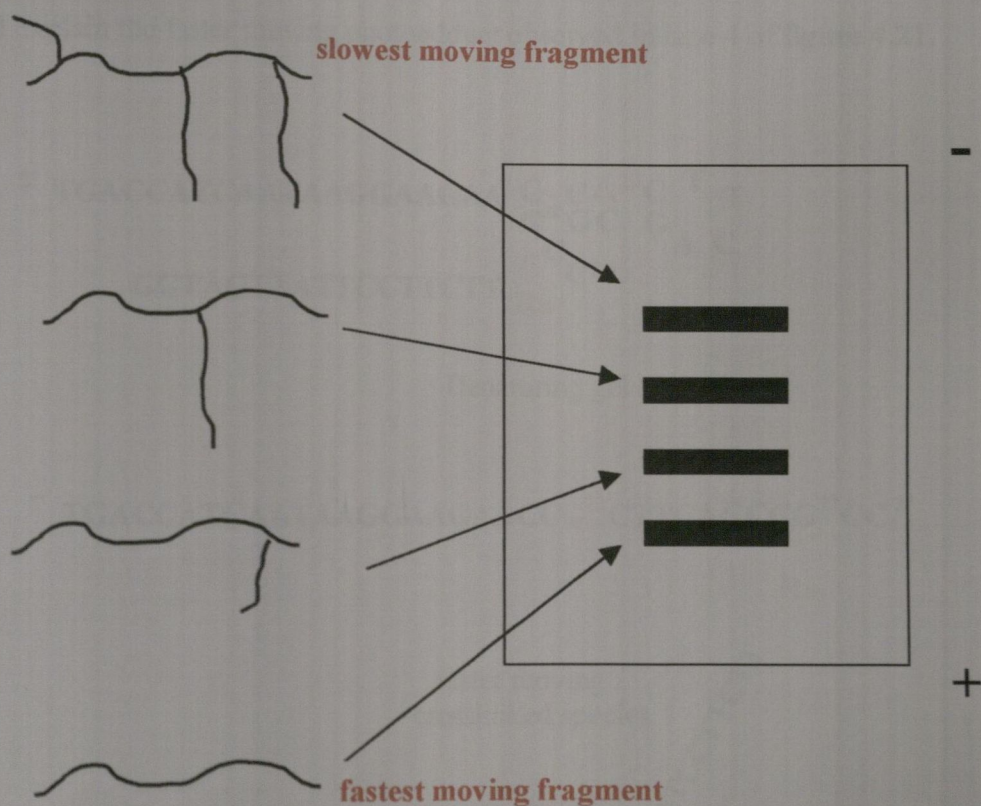


Figure 4.23 Comparison of mobility of crosslinked fragment through denaturing gel matrix

The proposed hairpin structure in variant 3 has the lowest free energy of formation of all the variant strands *i.e.* it should form the most stable hairpin structure. The hairpin structure seems to expose G32 at the 3'-end of the strand to interaction with the [Ru(TAP)₂phen⁻]-ODN conjugate. Photoadduct formation between the ruthenium complex and G32 followed by denaturing gel analysis would form the crosslinked species illustrated in **figure 4.24**. This species is less sterically hindered than the G21 crosslinked species seen with the original 34mer ODN. And would be expected to move more quickly through the gel matrix. Therefore photoadduct formation between G32 in variant 3 and the ruthenium-ODN conjugate would explain the faster moving photoadduct observed in lane 4 of **figure 4.21**.

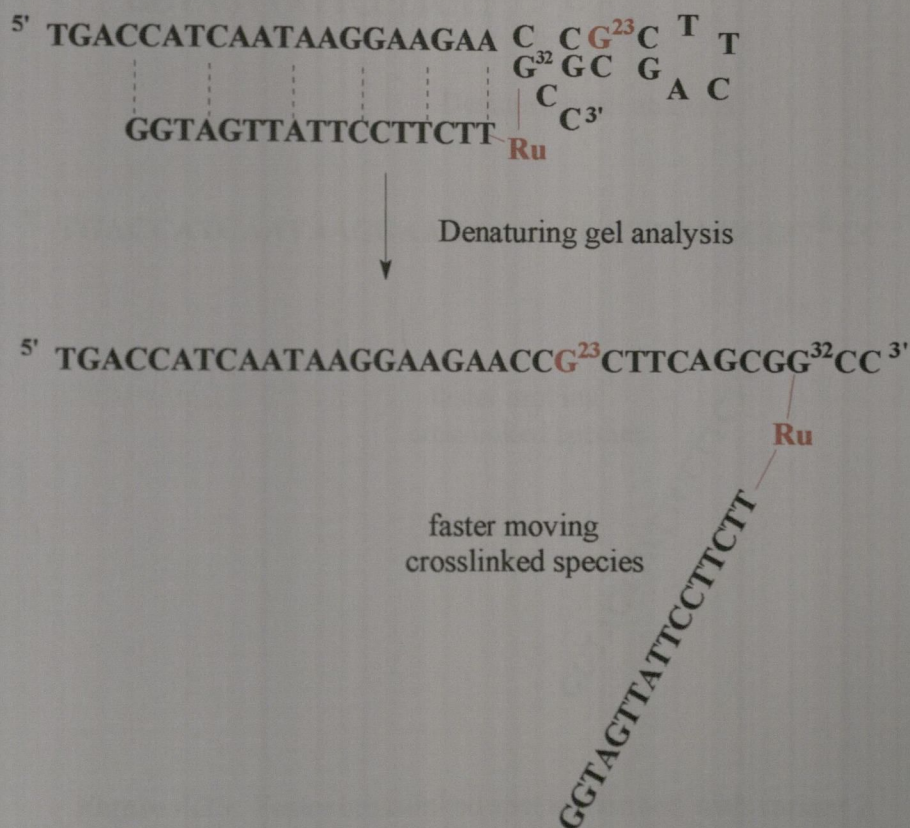


Figure 4.24 Crosslinked species formed with variant 3

Variant 2 has two possible hairpin conformations, the first of which is slightly energetically more favourable than the second. In the first and more stable conformation, G32 is exposed for photoadduct formation with the ruthenium complex. The crosslinked species formed after denaturing gel analysis is illustrated in **figure 4.25**. Again, this species is sterically less hindered than the G21 crosslinked species of the original system and would be expected to migrate through the gel matrix at a faster rate. The faster moving (lower) photoadduct in lane 3 can be attributed to photoadduct formation between G32 and the ruthenium–ODN conjugate.

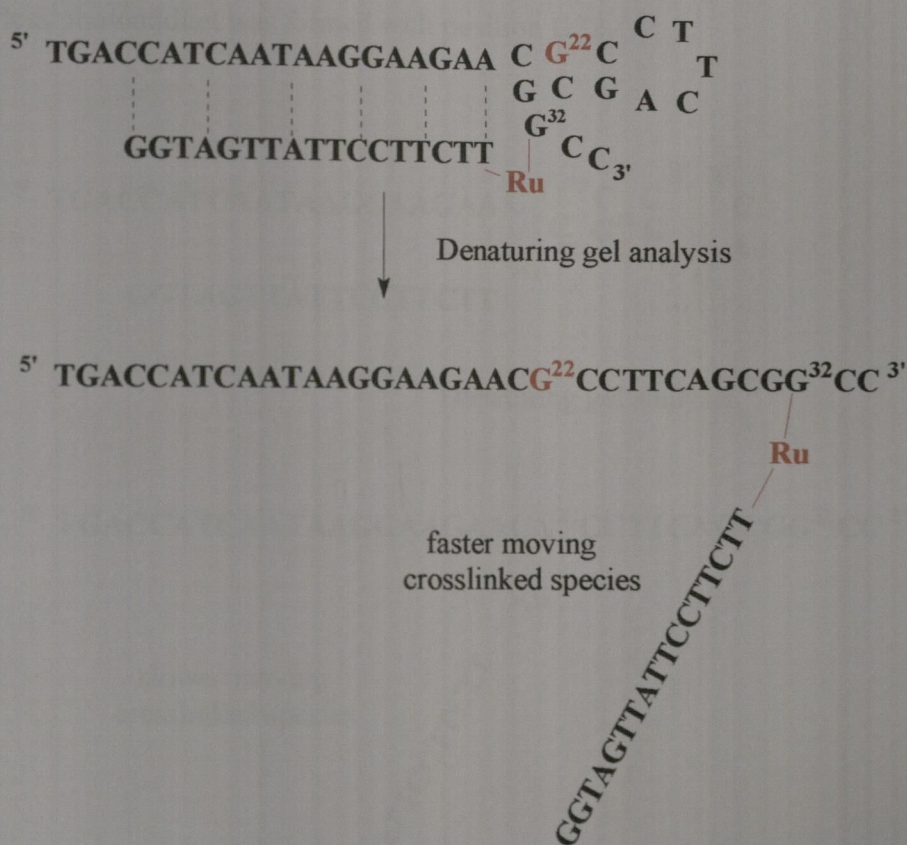


Figure 4.25 Faster crosslinked species formed with variant 2

The second slightly less stable hairpin conformation seems to expose G22 to photoadduct formation in preference to G32. Denaturing gel analysis would produce the species shown in **figure 4.26**. This more sterically hindered crosslinked species would be expected to move at a slower rate through the gel matrix, approximately equivalent to the original G21 crosslinked species. This photoadduct can be attributed to the slower moving band seen in the lane 3 variant 2 experiment. Also as formation of this slower adduct is energetically less favourable than photoadduct formation with G32, it would be expected that more G32 photoadduct would be formed. This was seen from the phosphoimagery results where approximately two-thirds less photoadduct was formed with position G22.

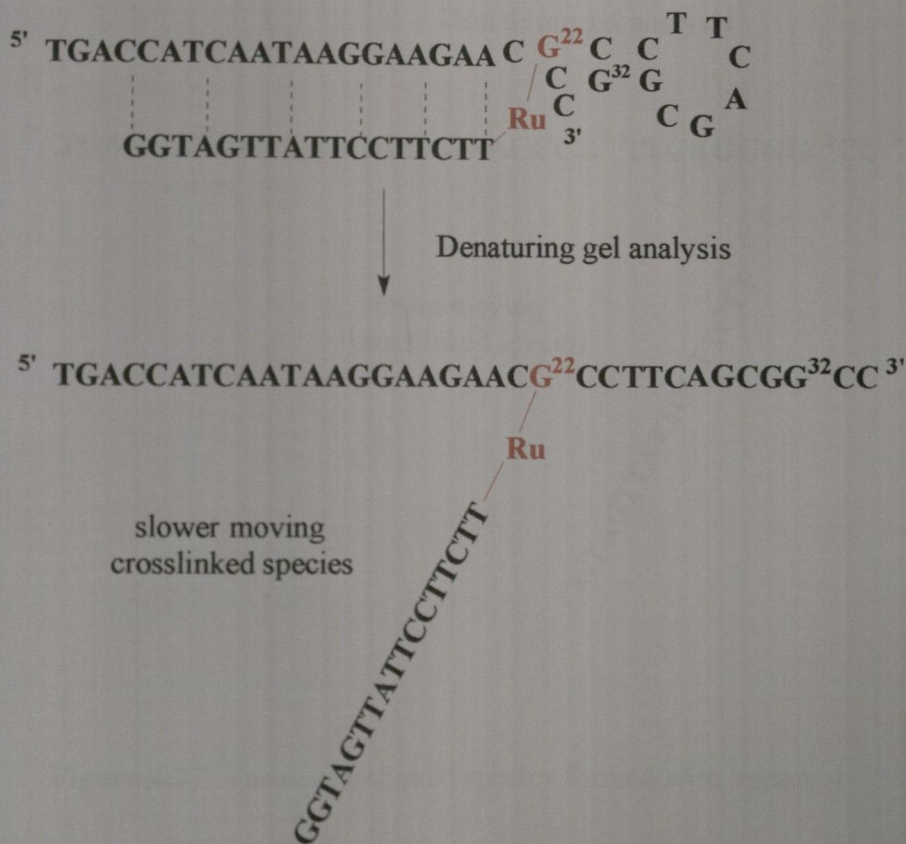


Figure 4.26 Slower crosslinked species formed with variant 2

Variant 4 forms a relatively stable hairpin structure in which G32 seems to be exposed for photoadduct formation with the ruthenium-ODN conjugate. The crosslinked species formed after denaturing gel analysis is illustrated in **figure 4.27**. As with variant 3 and the faster moving band of variant 2, this species is more likely to move quickly through the gel matrix relative to the original G21 crosslinked species. The faster moving band observed in lane 5 can be attributed to photoadduct formation between G32 in variant 4 and the ruthenium-ODN conjugate.

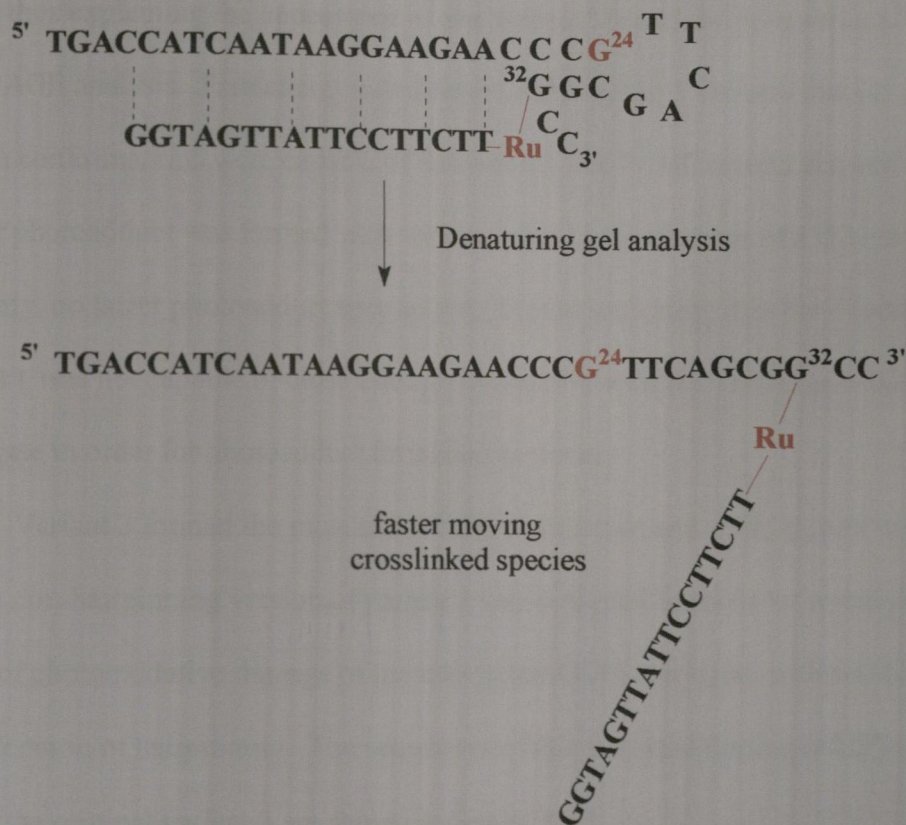


Figure 4.27 Faster crosslinked species formed with variant 4

Analysis of variants 5 and 6 showed that, based on free energy calculations, no stable hairpin conformations are formed. Analysis of the results showed that in both cases, photoadduct formation occurred producing a faster moving photoadduct species.

Based on results from the other variant strands, adduct formation between the ruthenium-ODN conjugate and variants 5 and 6 seemed to be occurring at the 3'-end of the variant strands. Unstable base pairs between complementary base doublets in the sequences (**figure 3.29**) may have brought the 3'-end of the variant strands in close enough proximity with the photosensitiser to allow photoadduct formation to occur, thus explaining the appearance of photoadduct bands for both variant 5 and 6 after PAGE analysis. Free energy calculations with variant 1 showed that no stable hairpin conformations were capable of formation. The PAGE results showed that no slower photoadduct was formed with variant 1 due to the absence of a G21 target. Similarly, no faster photoadduct species was formed indicating that the 3'-end of variant 1 was not capable of close enough interaction with the ruthenium-ODN conjugate in order for photoadduct formation to occur.

Variant 3 formed the most stable hairpin structure and as discussed in section 3.11, a non-hairpinning version of variant 3 was designed in order to investigate the range of photooxidative damage of the ruthenium-ODN conjugate without the consideration of hairpinning. The sequences of this non-hairpinning (NHP) variant 3 and of the original variant 3 are shown in **figure 3.33**.

As previously mentioned, the $[\text{Ru}(\text{TAP})_2\text{phen}']$ -ODN conjugate seemed to form a photoadduct with G32 of original variant 3. Repetition of the work

substituting the new non-hairpinning variant 3 for the original variant 3 showed no evidence of hairpin formation. The results of the work are shown in **figure 4.28**.

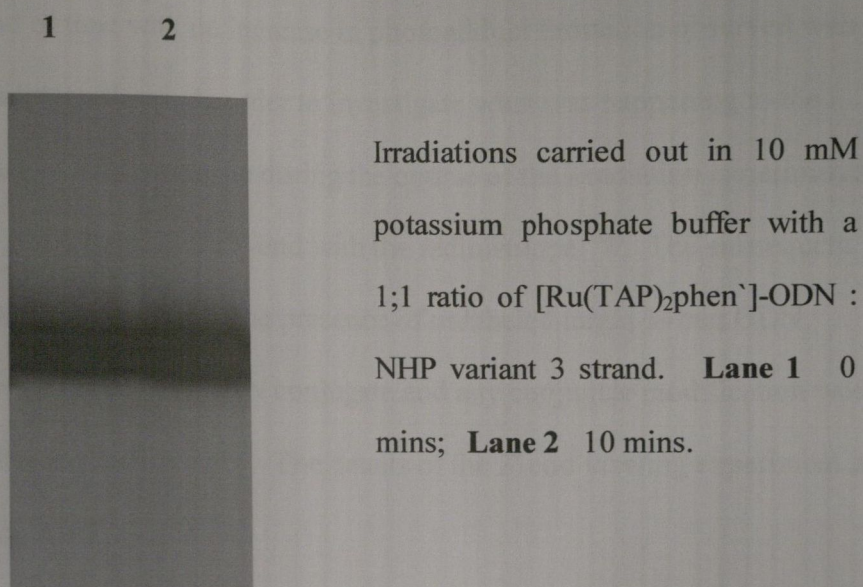


Figure 4.28 Results of experiments with non-hairpinning variant 3 in the presence of [Ru(TAP)₂phen⁺]-ODN conjugate

As a stable hairpin conformation was unlikely to form in the non-hairpinning variant 3 strand, the G23 target should be exposed for interaction with the ruthenium complex of the [Ru(TAP)₂phen⁺]-ODN conjugate. From the PAGE analysis it was seen that no photoadduct was formed indicating that the [Ru(TAP)₂phen⁺]-ODN conjugate was only capable of photoadduct formation with a target guanine in its immediate vicinity.

4.11 3'-end labeling

As discussed in section 4.4, the efficiency of photoadduct formation between the $[\text{Ru}(\text{TAP})_2\text{phen}']$ -ODN conjugate and the target strands seemed to level off after a certain period of time with no increase in photoadduct formation observed with increasing irradiation times. In order to investigate what was happening to the $[\text{Ru}(\text{TAP})_2\text{phen}']$ -ODN conjugate during the course of the irradiation experiments, the conjugate was labeled at its 3'-end with the radioisotope ^{32}P . The subsequent experiments were carried out in the presence of unlabeled target 34mer ODN, therefore only the ruthenium-ODN conjugate and any conjugate modification would be detected after autoradiography. The details of the 3'-end labeling experiment are given in section 5.9.2.

Initially experiments were carried out in which the $[\text{Ru}(\text{TAP})_2\text{phen}']$ -ODN conjugate was irradiated in the absence of any target 34mer ODN strand. Irradiation times of 0, 10 and 20 mins were used. Analysis of the results showed that all three experiments produced a parent band due to the ruthenium-ODN conjugate that showed pronounced streaking. This streaking could be attributed to material of reduced mobility above the ruthenium-ODN conjugate band. The streaking was evident even in an absence of irradiation, indicating that the ruthenium-ODN conjugate may have been able to form photoadducts with itself during the course of sample preparation. If the conjugate formed a photoadduct with the 17mer ODN, subsequent analysis on a denaturing gel would form a cross-linked species that would migrate at a slower rate than the ruthenium-ODN conjugate alone, thus producing an area of reduced mobility above the parent ruthenium-ODN conjugate band.

The experiments were repeated in the presence of the unlabeled 34mer ODN target at irradiation times of 0, 10 and 20 mins. In the absence of irradiation, an area of reduced mobility with respect to the parent conjugate band was observed. This may suggest that the ruthenium-ODN conjugate was capable of forming photoadducts with itself during the course of sample preparation, thus reducing the amount of conjugate available in the experimental sample for photoadduct formation with the target 34mer ODN. Irradiation times of 10 and 20 minutes again showed this area of reduced mobility above the parent band in conjunction to a higher band, similar to the photoadduct band observed in the 5'-end labeled experiments. This higher band was consistent with photoadduct formation between the ruthenium-ODN conjugate and G21 of the target 34mer ODN strand.

The relatively low efficiency of photoadduct formation between the $[\text{Ru}(\text{TAP})_2\text{phen}']$ -ODN conjugate and the target 34mer ODN may be explained by the fact that photoadduct formation within the conjugate itself would reduce the amount of conjugate available to form photoadducts with G21 target. If only a small percentage of the $[\text{Ru}(\text{TAP})_2\text{phen}']$ -ODN conjugate was available for photoadduct formation with the target 34mer strand, only a small overall yield of adduct formation with the G21 target would be observed.

4.12 Conclusions

Irradiation of the target 34mer ODN in the presence of the free photosensitisers showed material of reduced mobility with respect to the parent 34mer band and was attributed to photoadduct formation. More defined results were observed for the

more oxidising $[\text{Ru}(\text{TAP})_3]^{2+}$ standard compared with the $[\text{Ru}(\text{TAP})_2\text{phen}]^{2+}$ complex. In addition to its weaker oxidising ability, the presence of the phen⁻ ligand in the latter complex as a negatively charged species under the experimental conditions, may also have reduced optimal interaction with the target 34mer ODN.

Irradiation of the target in the presence of the Ru-ODN conjugate showed site-specific photoadduct formation with G21 in the target strand. This was observed as a band of reduced mobility with respect to the parent 34mer band. No photoadduct formation was observed in an absence of irradiation. It was observed that photoadduct formation reached a maximum after approximately 20 minutes irradiation, after which time it leveled off. Inclusion of azide and argon showed a small decrease in photoadduct formation. It was concluded that the mechanism occurred mainly by a type I pathway. Increased photoadduct formation was observed in the presence of persulfate.

Non-denaturing gel analysis confirmed duplex formation between the Ru-ODN conjugate and the target strand. Nonsense strand work showed the conjugate hybridised specifically with its complementary region on the target strand and not with random ODN sequences. Variant strand work, to investigate the range of photoadduct formation, revealed 3'-end photoadduct formation in the variant strands due to hairpinning conformations. Experiments with non-hairpinning variant 3 showed the conjugate was only capable of photoadduct formation with the target strand in its immediate vicinity. 3'-end labeling experiments suggested that the conjugate may have been able to form photoadducts with itself, thus reducing the amount of free conjugate available in experiments with the target strand and possibly

explaining the relatively low efficiency of photoadduct formation observed between the conjugate and the target strand.

CHAPTER 5

Materials and methods

CHAPTER 5

Materials and methods

5.1 Apparatus

5.1.1 Spectroscopic measurements

^1H NMR and ^{13}C NMR spectra were recorded using 300 MHz (Bruker) and 400 MHz (Bruker) instruments.

Absorption spectra were recorded using Unicam UV-4 and Shimadzu UV-2401 spectrometers.

Infra Red measurements were recorded using Genesis II FTIR and Perkin Elmer paragon 1000 spectrometers.

Mass spectrometry measurements were recorded using Micromass LCT electrospray TOF spectrometer, Shimadzu LC-10AD solvent delivery module, Micromass, Mass Lynx software.

5.1.2 HPLC

High performance liquid chromatography (HPLC) was carried out using Shimadzu SCL-10A (PDA detector, shimadzu class software) and Perkin Elmer series 2000LC pump (Perkin Elmer 235C diode array detector, Perkin Elmer Turbochrom 4.1 software). Nucleosil C18 RP 10 μm 250 x 4 mm column, Supelco inc., Sigma Aldrich.

5.1.3 Instruments

Uncorrected melting points were recorded on a Griffin melting point apparatus.

Bench centrifuge; MSE micro-centaur and Centrifuge 5415D.

Bench vortex; Super Mixer (Cat. No.1291, Lab-line Instruments Inc.)

Experimental solutions were made up using accurate calibrated micropipettes (Gilson, P20, P200 and P1000).

Dry block, Multi-Block Heater, Lab Line Instruments Inc. Model No. 2050-1

ODN samples and stocks were lyophilised (to remove solvent or reduce volume) using a Savant Speedvac Concentrator (Stratech Scientific London) that was attached to a vacuum pump.

Electrophoresis sequencing system obtained from Life Technologies Inc. USA.

Polyacrylamide gel electrophoresis (PAGE) was carried out using a power supply unit (Chandos E. 36, Joe Walsh Scientific, Dublin or EC 3000-90 power supply).

Combs and spacers were obtained from Gibco BRL apparatus, Life Technologies Inc., USA.

Electroelution was carried out using a Biotrap (Schleicher and Schuell) electroelution apparatus (details described in section 2.7)

5.1.4 Autoradiography

X-ray films (Curix, 100NIF, 35 x 43 cm, Agfa Ltd. and Hyperfilm™ MP, 35 x 43 cm, Amersham pharmacia biotech) were developed using a Fuji RG2 X-ray film processor.

5.1.5 Phosphoimagery

Phosphoimagery was carried out using a Fujifilm FLA-3000 phosphoimager.

5.1.6 Light source

Samples were irradiated using a 500W mercury lamp or 100W fibreoptic lamp.

Isoing Pyrex™ glass filter was used to remove wavelengths less than 330 nm. Sodium nitrite filter was used to remove wavelengths less than 400 nm.

5.2 Reagents

All reagents used in the synthesis of the ruthenium complexes were obtained from Sigma Aldrich and used without further purification unless otherwise stated.

The reagents used to prepare the buffers, salt solutions and polyacrylamide gels were purchased from Sigma, Aldrich or Merck and used without further purification.

γ -³²P ATP (5000 Ci / mmol) and α -³²P ATP (5000 Ci / mmol) were purchased from Amersham International plc.

Polynucleotide kinase (PNK) enzyme and buffer were purchased from Bio Labs, New England.

Terminal deoxynucleotidyl transferase (TdT) enzyme and buffer were purchased from Promega.

5.3 Solutions and buffers¹⁶⁵

5.3.1 Solvents

Reagent grade solvents obtained from Riedel-de Haen were used for the synthesis of the ruthenium complexes. The solvents used in the coupling reactions were extra pure and purchased from Aldrich in their anhydrous form. Spectroscopic grade

solvents purchased from Riedel-de Haen were used for HPLC and mass spectroscopy. Water used for HPLC was filtered using the milli-pore filtration system prior to use.

5.3.2 Water

Singly distilled water autoclaved prior to use was used for all the oligodeoxynucleotide work.

5.3.3 Buffers

Potassium phosphate buffer (100 mM)

Potassium phosphate buffer (100 mM) was prepared by addition of K_2HPO_4 (1 M, 61.5 ml) and KH_2PO_4 (1 M, 38.5 ml) with pH adjustment to 7.0. Autoclaved water was used to make both solutions.

NaCl solution (500 mM)

Sodium chloride salt solution (500 mM) was prepared by dissolving NaCl (14.61g) in autoclaved water (500 ml).

High salt buffer

8 μ l buffer sample (12.5 mM potassium phosphate buffer / 125 mM NaCl)

Potassium phosphate buffer (125 μ l, 100 mM), NaCl (250 μ l, 500 mM) and water (625 μ l).

7 μ l buffer sample (14.29 mM potassium phosphate buffer / 142.9 mM NaCl)

Potassium phosphate buffer (142.9 μ l, 100 mM), NaCl (285.8 μ l, 500 mM) and water (571.3 μ l).

Low salt buffer

8 μ l buffer sample (12.5 mM potassium phosphate buffer)

Potassium phosphate buffer (125 μ l) and water (1 ml).

7 μ l buffer sample (14.29 mM potassium phosphate buffer)

Potassium phosphate buffer (142.9 μ l) and water (1 ml).

TBE buffer (Tris-borate / EDTA)

A 10 X stock of TBE buffer was prepared by addition of Trizma base

(tris[hydroxymethyl]aminomethane, 99 %, 54 g), boric acid (27.5 g), EDTA (0.372 g) and autoclaved water (500 ml). Common working dilutions were 1 X and 5 X.

5.4 Synthesis of ligands

5.4.1 5-Amino-1,10-phenanthroline (2)¹⁵³

Method A

5-Nitro-1,10-phenanthroline (1) (200 mg, 0.89 mmol), hydrazine monohydrate (200 mg, 3.99 mmol), activated charcoal¹⁵⁴ (267 mg) and absolute ethanol (700 mg) were refluxed for 2 hours under an atmosphere of nitrogen. The resulting black solution was filtered on celite and the yellow/orange filtrate was collected. The residue on the filter was washed several times with absolute ethanol. The combined filtrate was evaporated under reduced pressure to give 5-amino-1,10-phenanthroline (2) as a

yellow powder (110 mg, 63 %), mp 259 °C, (lit¹⁶⁶ 259 °C-260 °C); TLC analysis (Al₂O₃ plates, 99:1 CH₂Cl₂: MeOH) showed an R_f value of 0.3 for (2); ν_{\max} (Nujol)/cm⁻¹ 3400 cm⁻¹ (NH); ESI MS: calcd 195, found [M + H⁺] 196.

Use of graphite instead of activated charcoal in the above method, as described by Han *et al.*¹⁵³, also afforded the desired 5-amino-1,10-phenanthroline (2), but in lower yield (45 %).

Method B¹⁵²

A mixture of 5-nitro-1,10-phenanthroline (1) (100 mg, 0.44 mmol) and powdered tin(II) chloride dihydrate (400 mg, 1.77 mmol) in absolute ethanol (6 ml) was ultrasonicated at room temperature for 2 hours. The reaction mixture changed from an orange colour to a dark orange/red colour during the period of ultrasonication. The reaction mixture was added to distilled water (50 ml), rendered alkaline with aqueous ammonia, and extracted with dichloromethane (2 x 25 ml). The yellowish organic layer was dried with sodium sulfate and filtered. The filtrate was evaporated under reduced pressure to give 5-amino-1,10-phenanthroline (2) (60 mg, 69 %) as a yellow powder identical on TLC and IR with the product obtained in method A above.

5.4.2 5-(4-Carboxybutanamido)-1,10-phenanthroline (3)¹⁵⁵

5-Amino-1,10-phenanthroline (2) (517 mg, 2.65 mmol) was dissolved in distilled anhydrous pyridine (25 ml). The reaction vessel was flushed with nitrogen before addition of the pyridine. The reaction mixture was stirred and heated to 70 °C and

glutaric anhydride (612 mg, 4.34 mmol) was added. The reaction mixture was then heated to 100 °C. After 1 hour, further glutaric anhydride (306 mg, 2.17 mmol) was added and heating was continued at 100 °C. After 2 hours, a third portion of glutaric anhydride (612 mg, 4.34 mmol) was added and heating was continued for one more hour (3 hours in total). The reaction mixture was allowed to cool and then concentrated under vacuum to approximately 5 ml. Acetonitrile (135 ml) was added, the solution was stirred at room temperature for 2 hours, and the resulting precipitate collected by suction filtration and purified by elution chromatography on a silica column with a 1:1 MeOH: H₂O solution containing a few drops of ethanol. 5-(4-Carboxybutanamido)-1,10-phenanthroline (**3**) (300 mg, 37 %), mp 200 °C, was collected as an off-white powder and showed on TLC as a single spot (R_f value of 0.6; silica plates, 1:1:2 H₂O: DMF: NH₄Cl (2 M)); δ_{H} (400 MHz; DMSO-*d*₆) 1.87 (2H, q, *J* 7.03, 6.03, CH₂CH₂CH₂), 2.14 (2H, t, *J* 6.5, CH₂COO), 2.55 (2H, t, *J* 7.03, CH₂CON), 4.3 (1H, br s, OH), 7.71 (1H, dd, *J* 8.03, 4.01, C(8)H), 7.78 (1H, dd, *J* 8.53, 4.01, C(3)H), 8.37 (1H, s, C(6)H), 8.41 (1H, d, *J* 8.03, C(7)H), 8.91 (1H, d, *J* 8.53, C(4)H), 8.99 (1H, d, *J* 3.01, C(9)H), 9.1 (1H, d, *J* 4.02, C(2)H), 11.67 (1H, br s, NH).

5.4.3 6-Nitroquinoxaline (**5**)¹⁵⁶

4-Nitro-1,2-phenylenediamine (**4**) (1g, 6.53 mmoles) and glyoxal (40 %, 2.1 ml, 17.24 mmoles) were added to acetonitrile (21 ml) and stirred at 50 °C for 12 hours. The reaction was allowed to cool to room temperature. Water (8.3 ml) was added to the reaction mixture precipitating a brown solid (1.02 g, 89 %), mp 177 °C (lit¹⁶⁷ 175

°C- 177 °C). TLC analysis (silica plates, 70:30 ethyl acetate: hexane) showed an R_f value of 0.53 for (5); δ_{H} (400 MHz; DMSO-*d*₆) 8.37 (1H, d, *J* 2.52, C(8)H), 8.59 (1H, dd, *J* 2.52, C(7)H), 8.93 (1H, d, *J* 2.52, C(5)H), 9.17 (2H, s, C(2)H, C(3)H). δ_{C} (100 MHz; *d*₆-DMSO) 123.25 (s, C(5)), 125.54 (s, C(7)), 131.28 (s, C(8)), 140.97 (s, C(4a)), 144.62 (s, C(8a)), 147.57 (s, C(3)), 148.04 (s, C(2)), 148.76 (s, C(6)).

5.4.4 5-Amino-6-nitroquinoxaline (6)¹⁵⁷

6-Nitroquinoxaline (5) (0.5 g, 2.86 mmol) and powdered hydroxylamine hydrochloride (1.19 g, 17.16 mmol) in ethanol (29 ml) was stirred on ice and cooled to 0 °C. A solution of potassium hydroxide (2.34 g) in ethanol (11.4 ml) was added dropwise over 1 hour resulting in a dark brown reaction mixture. The solution was stirred at room temperature (90 mins), poured onto ice (145 g) and refrigerated (24 hrs). The precipitated yellow/ brown solid was dissolved in acetone, adsorbed onto silica and purified by elution chromatography on a silica column using 100 % chloroform. 5-amino-6-nitroquinoxaline (6) was collected as a yellow solid (181 mg, 33.5 %), mp 235-237 °C (lit¹⁶⁸ 235 °C). TLC analysis (silica plates, 100 % CHCl₃) gave an R_f value of 0.6 for (6); δ_{H} (400 MHz; DMSO-*d*₆) 7.19 (1H, d, *J* 10, C(8)H), 8.30 (1H, d, *J* 10, C(7)H), 8.49 (br s, NH₂), 8.94 (1H, d, *J* 2, C(3)H), 9.10 (1H, d, *J* 2, C(2)H).

5.4.5 5,6-Diaminoquinoxaline (7)¹⁵⁷

To a stirred solution of 5-amino-6-nitroquinoxaline (6) (50 mg, 0.26 mmol) and Pd/C (10 %, 16 mg) in ethanol (6 ml), hydrazine monohydrate (98 %, 230 μ l) was added and the reaction was heated to 60 °C. The reaction was followed by TLC (silica plates, 100 % CHCl₃) until all of (6) had disappeared. The reaction mixture was filtered through celite to remove the catalyst and the red/orange filtrate was evaporated under vacuum. The resulting solid was recrystallised from toluene producing red needles (40 mg, 96 %), mp 142-143 °C (lit¹⁵⁷ 144-145 °C); δ_{H} (400 MHz; DMSO-*d*₆) 8.59 (1H, d, *J* 2, C(2)H), 8.51 (1H, d, *J* 2, C(3)H), 7.27 (1H, d, *J* 9.0, C(7)H), 7.2 (1H, d, *J* 9, C(8)H), 5.24 (br s, NH₂), 5.13 (br s, NH₂).

5.4.6 1,4,5,8-Tetraazaphenanthrene (8)¹⁵⁹

5,6-Diaminoquinoxaline (7) (9.4 mg, 0.06 mmol) and glyoxal (bisulfite adduct, 17 mg, 0.06 mmol) were dissolved in distilled water (800 μ l) and heated under reflux for 2 hours. The solution was then made basic with a potassium hydroxide/ water solution and the product was extracted with chloroform and evaporated down producing an off-white solid (7 mg, 30 %), mp 240-242 °C (lit¹⁵⁹ 242 °C); δ_{H} (400 MHz; DMSO-*d*₆) 9.22 (2H, d, *J* 2, C(6)H, C(3)H), 9.19 (2H, d, *J* 2, C(7)H, C(2)H), 8.35 (2H, s, C(9)H, C(10)H).

5.5 Synthesis of ruthenium complexes

5.5.1 Ruthenium bis(1,10-phenanthroline)-5-(4-carboxybutanamido)-1,10-phenanthroline dihexafluorophosphate (**10**)¹⁶²

A 10 % molar excess of 5-(4-carboxybutanamido)-1,10-phenanthroline (**3**) (100 mg, 0.32 mmol) dissolved in hot absolute ethanol (30 ml) was added to a hot solution of Ru(phen)₂Cl₂.H₂O (156 mg, 0.29 mmol) in water (20 ml). The solution was stirred and deaerated with argon for 20 minutes and then refluxed for 3 hours under argon.

A 5-fold molar excess of NH₄(PF₆)₂ (264 mg, 1.62 mmol) dissolved in a little distilled water was added to produce an orange/ brown precipitate. The solution was allowed to cool somewhat and the most of the ethanol was then removed by rotary evaporation. The remaining mixture was filtered and the resulting solid dried under vacuum to give crude ruthenium bis(1,10-phenanthroline) 5-(4-carboxybutanamido)-1,10-phenanthroline dihexafluorophosphate (**10**) (244 mg, 78 %) which was purified using size exclusion chromatography on a Sephadex LH20 column (45cm x 2.5cm) eluting with methanol. TLC analysis (silica plates, 1:1:2 H₂O: DMF: NH₄Cl (2 M)) gave an R_f value of 0.27 for (**10**); λ_{\max} (CH₃CN)/nm 262 and 450 nm; HPLC analysis (70:30 H₂O: CH₃CN, 1.5ml/min, semiprep reverse phase C18 column) showed a single peak with a retention time of 2.04 mins.

5.5.2 Ruthenium bis(1, 4, 5, 8-tetraazaphenanthrene)-5-(4-carboxybutanamido)-1,10-phenanthroline dihexafluorophosphate (**12**)¹⁶²

A 10% molar excess of 5-(4-carboxybutanamido)-1,10-phenanthroline (**3**) (10 mg, 0.032 mmol) dissolved in hot absolute ethanol (3 ml) with a few drops of distilled water was added to a hot solution of Ru(TAP)₂Cl₂ (15 mg, 0.028 mmol) in water (2 ml). The solution was stirred and deaerated with argon for 20 minutes and then refluxed for 3 hours under argon. A 5-fold molar excess of NH₄PF₆ (26.4 mg, 0.162 mmol) dissolved in a little distilled water was added to produce a brown/ orange precipitate. The solution was allowed to cool somewhat and then the total reaction volume was reduced by about half and the ruthenium bis(1, 4, 5, 8-tetraazaphenanthrene) 5-(4-carboxybutanamido)-1,10-phenanthroline dihexafluorophosphate (**12**) was collected (11.4 mg, 36 %) and purified using size exclusion chromatography on a Sephadex LH20 column (45 cm x 2.5 cm) eluting with methanol. TLC analysis (silica plates, 1:1:2 H₂O: DMF: NH₄Cl (2 M)) gave an R_f value of 0.38 for (**12**); λ_{max} (CH₃CN)/nm 267, 415 and 470 nm.

5.6 Ruthenium complex activation

5.6.1 Activation of [Ru(phen)₂phen'] (PF₆)₂ (**10**) to give the corresponding N-hydroxysuccinimido ester (**13**)¹⁶⁹

Anhydrous DMF (600 μl) and [Ru(phen)₂phen'] (PF₆)₂ (**10**) (35 mg, 0.03 mmol) were added to a 2 ml Eppendorf™. The mixture was vortexed for 1 minute and then centrifuged. N, N, N', N'-tetramethyl(succinimido)uronium tetrafluoroborate (TSU) (15 mg, 0.05 mmol) and diisopropylethylamine (DIPEA) (11 μl, 0.06 mmol) were

added to a second Eppendorf™ and this mixture was also vortexed for 1 minute and centrifuged. The contents of the first Eppendorf™ were added to the second Eppendorf™ and the entire mixture was vortexed for 1 minute, centrifuged and finally placed on a shaker in the dark at room temperature for 2 hours. TLC analysis (silica plates, 1:1:2 DMF: H₂O: NH₄Cl (2 M)) gave an R_f value of 0.36 for **(13)**; λ_{max} (CH₃CN)/ nm 262 and 450 nm; HPLC analysis (70:30 H₂O: CH₃CN, 1.5 ml/min, analytical reverse phase C18 column) gave one peak with a retention time of 4.80 min.

5.6.2 Activation of [Ru(TAP)₂phen']₂(PF₆)₂ (13**) to give the corresponding N-hydroxysuccinimido ester (**14**)¹⁶⁹**

The activation was carried out as in section 5.6.1 using the following reactant quantities; [Ru(TAP)₂phen']₂(PF₆)₂ (11.4 mg, 0.011 mol), anhydrous DMF (250 μ l), TSU (5 mg, 0.02 mmol) and DIPEA (7 μ l). TLC analysis (silica plates, 1:1:2 DMF: H₂O: NH₄Cl (2 M)) gave an R_f value of 0.53 for **(14)**; λ_{max} (CH₃CN)/ nm 267, 415 and 470 nm.

5.7 Coupling reactions

Coupling of the N-hydroxysuccinimido ester (13**) and (**14**) to the 17mer (**15**).**

The coupling reactions were carried out in the lab of Prof. R. J. H. Davies in the School of Biology and Biochemistry, Queen's University, Belfast. The ODN **(15)** (15 odu, 9.98×10^{-8} mol) was dissolved in water (30 μ l). This was achieved by vortexing and heating (65 °C, 1 minute) until everything was fully dissolved. The

solution was centrifuged. The activated ruthenium complex (100 μl , 5×10^{-6} mol) and diisopropylethylamine (DIPEA) (6.8 μl , 0.04 mmol) were added to the ODN solution and the entire mixture was vortexed, centrifuged and shaken overnight in the dark at room temperature. Water (120 μl) was added to the reaction mixture followed by electroelution (130 V, 45 mins). The orange solution collected from the anodic well was extracted with 1ml of 1-butanol for every 100 μl of solution present. (The 1-butanol was added, the solution was vortexed and centrifuged and the supernatant removed). The orange pellet that remained was lyophilised. The loading solution (22 μl , 90 % formamide loading solution, 10 % TBE buffer) was added to the lyophilised sample and the reaction products were loaded onto a polyacrylamide gel (12 %) for PAGE analysis. Electrophoresis (260 V, 1.5 hours) followed by UV shadowing showed orange bands of reduced mobility with respect to the free 17mer band. These orange bands were excised from the gel and electroeluted to remove any conjugated species (**16** / **17**) from the gel itself. The orange solution from the anodic well was extracted with 1- butanol and dried down; $\lambda_{\text{max}}(\text{H}_2\text{O})/\text{nm}$ 264 and 450 nm (**16**); $\lambda_{\text{max}}(\text{H}_2\text{O})/\text{nm}$ 267, 415 and 470 nm (**17**). HPLC analysis of conjugate 1 (**16**) (85:15 – 95:5 H_2O ; CH_3CN , 1.5ml/min, C18 analytical reverse phase column) gave one peak with a retention time of 13.01 min. HPLC analysis of conjugate 2 (**17**) (95: 5 – 70:30 H_2O ; CH_3CN , 1.5ml/min, C18 analytical reverse phase column) gave one peak with a retention time of 8.99 min. The coupling reaction between (**13**) and (**15**) was carried out twice giving percentage yields of 7 % and 10 % respectively for conjugate 1 (**16**). The coupling reaction between (**14**) and (**15**) gave conjugate 2 (**17**) in 15 % yield.

5.8 Oligodeoxynucleotide synthesis

The oligodeoxynucleotide strands were synthesised by Clarke Stevenson, Queen's University, Belfast. The 34mer and 17mer oligodeoxynucleotides were synthesised using standard phosphoramidite chemistry on an Applied Biosystems 391 DNA synthesiser and the variant strands were synthesised on a Beckman Oligo 1000M DNA synthesiser. A primary aminoethyl group was incorporated onto the 5'-end of the 17mer using 5'-AminoModifier phosphoramidite (Glen Research). All the ODNs were cleaved and deprotected in concentrated ammonia (28 %). The 17mer was initially purified by Reverse Phase Cartridge technique prior to ruthenium complex conjugation. All other ODNs were purified by denaturing (7 M urea) PAGE, detected with minimal UV shadowing and eluted by electroelution (Schleicher and Schuell BioTrap system) followed by 1-butanol concentration and ethanol precipitation.

5.9 Radiolabeling experiments

5.9.1 5'-end labeling ¹⁵¹

The oligodeoxynucleotides were synthesised without a phosphate group at their 5' termini and therefore could be labeled by the transfer of the $\gamma^{32}\text{P}$ from $\gamma^{32}\text{P}[\text{ATP}]$ using the enzyme bacteriophage T4 polynucleotide kinase (PNK).

The ODN (5 μl of 5 pm stock), radioactive isotope ($\gamma^{32}\text{P}[\text{ATP}]$, 2 μl , specific activity 5000ci / mmol), PNK buffer (10 X, 2 μl) and autoclaved water (9 μl) were placed in a sterile Eppendorf™ and vortexed. The PNK enzyme (20 units, 2 μl) was added and the tube was tapped to mix the contents as vortexing denatures the enzyme. The Eppendorf™ was incubated at 37 °C for 40 mins and then at 68 °C for 20 mins. The

radiolabeled ODNs were then precipitated with ethanol to separate them from unincorporated $\gamma^{32}\text{P}[\text{ATP}]$. Ammonium acetate (3 M, 100 μl) and cold ethanol (98 %, 400 μl) were added to the reaction mixture which was then vortexed and stored at $-20\text{ }^{\circ}\text{C}$ for 20 mins, followed by centrifugation for 20 mins and removal of the supernatant. Ethanol (80 %, 1 ml) was added to the pellet. Again, the sample was stored at $-20\text{ }^{\circ}\text{C}$ for 20 mins, centrifuged for 20 mins followed by removal of the supernatant. The pellet was lyophilised (approximately 2 hrs) and then suspended in the appropriate amount of autoclaved water to give the correct ODN concentration for the irradiation work.

5.9.2 3'-end labeling¹⁶⁵

The oligodeoxynucleotides were synthesised without a phosphate group at their 3' termini and therefore could be labeled by the transfer of the $\alpha^{32}\text{P}$ from $\alpha^{32}\text{P}[\text{ATP}]$ using the enzyme terminal deoxynucleotidyl transferase (TdT).

The ODN (5 μl of 5 pm stock), radioactive isotope ($\alpha^{32}\text{P}[\text{ATP}]$, 2 μl , specific activity 5000ci / mmol), PNK buffer (5 X, 4 μl) and autoclaved water (7 μl) were placed in a sterile Eppendorf™ and vortexed. The PNK enzyme (20 units, 2 μl) was added and the tube was tapped to mix the contents as vortexing denatures the enzyme. The Eppendorf™ was incubated at $37\text{ }^{\circ}\text{C}$ for 75 mins and then at $68\text{ }^{\circ}\text{C}$ for 20 mins. The radiolabeled ODNs were then precipitated with ethanol to separate them from unincorporated $\alpha^{32}\text{P}[\text{ATP}]$. Ammonium acetate (3 M, 100 μl) and cold ethanol (98 %, 400 μl) were added to the reaction mixture which was then vortexed and stored at $-20\text{ }^{\circ}\text{C}$ for 20 mins, followed by centrifugation for 20 mins and removal of the

supernatant. Ethanol (80 %, 1 ml) was added to the pellet. Again, the sample was stored at -20°C for 20 mins, centrifuged for 20 mins followed by removal of the supernatant. The pellet was lyophilised (approximately 2 hrs) and the suspended in the appropriate amount of autoclaved water to give the correct ODN concentration for the irradiation work.

5.10 Sample preparation

5.10.1 5'-end labeled work

Each sample was made up in a sterile Eppendorf™, with the addition of the appropriate buffer, to give a final volume of 10 μl . The samples contained the following;

1. Radiolabeled target 34mer strand (or variant strand)
(1 μl of 1×10^{-5} M stock solution).
2. Photosensitiser (Ruthenium-ODN conjugates or free ruthenium complexes)
(1 μl of 1×10^{-5} M stock solution).
3. High salt buffer (10 mM potassium phosphate buffer / 100 mM NaCl) or low salt buffer (10 mM potassium phosphate buffer) (8 μl).

4. Variations

4.1 Sodium azide (NaN_3)

1 μl of 1×10^{-1} M stock solution was added to the radiolabeled target (1 μl) and photosensitiser (1 μl) along with 7 μl of the appropriate buffer.

4.2 Ammonium persulfate ($(\text{NH}_4)_2\text{S}_2\text{O}_8$)

1 μl of 1×10^{-2} M stock solution was added to the radiolabeled target (1 μl) and photosensitiser (1 μl) along with 7 μl of the appropriate buffer.

4.3 D_2O

For experiments in which the effect of D_2O was investigated, the experimental buffer was prepared using D_2O in place of H_2O prior to sample preparation. Each experimental sample was prepared as normal using the D_2O buffer.

4.4 Argon

For experiments in which the effect of argon was investigated, the experimental sample was purged with argon before and during the course of the irradiations.

4.5 Desferrioxamine

1 μl of 100 μM stock solution was added to the radiolabeled target (1 μl) and photosensitiser (1 μl) along with 7 μl of the appropriate buffer.

5.10.2 3'-end labeled work

Each sample was made up in a sterile Eppendorf™, with the addition of the appropriate buffer, to give a final volume of 10 µl. The samples contained the following;

1. Radiolabeled ruthenium-ODN conjugate
(1 µl of 1×10^{-5} M stock solution).
2. Target 34mer ODN strand
(1 µl of 1×10^{-5} M stock solution).
3. High salt buffer (10 mM potassium phosphate buffer / 100 mM NaCl) or low salt buffer (10 mM potassium phosphate buffer) (8 µl).

5.11 Experimental setup

To each Eppendorf™, the appropriate combination from section 5.10 was added. All samples were then vortexed and centrifuged. Samples containing double-strand experiments were heated at 80 °C for 5mins and then allowed to cool slowly to room temperature (typically 2-3hours). All samples were placed on ice for one hour prior to irradiation. Irradiations were carried out on ice, using an isoing Pyrex™ glass filter or sodium nitrite (1M) filter. All samples were lyophilised after irradiation.

5.12 Piperidine treatment

Following irradiation, base modifications in the target strand were cleaved by piperidine treatment. Piperidine (1 M, 15 μ l) was added to the appropriate samples, which were then vortexed and centrifuged. Samples were then heated at 90 $^{\circ}$ C for 35 mins, centrifuged and lyophilised for approximately 1 hour.

5.13 G + A experiment

The G + A experiment was included as a control experiment in all gels. The reaction cleaves oligodeoxynucleotides at guanines and adenines only, thus allowing the sites of cleavage in other samples to be identified. Radiolabeled ODN (2 μ l), formic acid (98 %, 3 μ l) and potassium phosphate buffer (10 mM, 5 μ l) were added to a sterile EppendorfTM, vortexed vigorously, centrifuged and heated at 37 $^{\circ}$ C for 20 mins. The samples were then lyophilised. Piperidine (1 M, 10 μ l) was added to the samples, which were then heated at 90 $^{\circ}$ C for 35 mins, centrifuged and lyophilised.

At this stage, autoclaved water (20 μ l) was added to all the samples (normal and G + A), which were subsequently vortexed, centrifuged and lyophilised for approximately 2 hours

5.14 Polyacrylamide gel electrophoresis (PAGE)

5.14.1 Denaturing gel

Denaturing gels are polymerized in the presence of urea, which suppresses base pairing in nucleic acids. A 20 % acrylamide gel was used to separate

oligodeoxynucleotides less than 100 bases long¹⁶⁵ and was prepared by mixing urea (31.5 g), 30 % acrylamide stock (37.5 ml), 10 X TBE buffer (7.5 ml) and autoclaved water (7.5 ml). The 30 % acrylamide stock solution consisted of acrylamide (190 g), N, N-methylenebisacrylamide (10 g) and autoclaved water (500 ml). Ammonium persulfate (10 %, 450 μ l) and N, N, N', N'-tetramethylethylenediamine (TEMED, 35 μ l) were added just before the gel was poured. The glass plates, spacers and comb were washed with warm soapy water and ethanol. The sides of the plates to be in contact with the gel were silated with a few drops of dimethyldichlorosilane. The two plates were taped together with the spacers in place. The gel was poured using a 50 ml plastic syringe, with the plates at an angle of approximately 20°. The comb was inserted and the gel was allowed to set for approximately 2 hours. Following removal of the comb, the gel was placed on the rig, and using 1 X TBE buffer, was pre-electrophoresed for 1 hour at 50-60 W. The loading dye was prepared (80 % formamide in water, 0.25 % bromophenol blue and 0.25 % xylene cyanol) and 6 μ l was added to each sample, including the G + A sample. Samples were vortexed, centrifuged and loaded onto the gel. The gel was electrophoresed for approximately 2 hours at 50-60 W.

5.14.2 Non-denaturing gel

Non-denaturing gels were used solely for the detection of duplex formation. They did not contain urea or formamide, which would suppress base pairing, therefore samples to be analysed in this manner were not irradiated or piperidine treated. The samples were placed in sterile Eppendorfs™ with the volumes of radiolabeled target,

photosensitiser and buffer being the same as for the denaturing work. The double-stranded samples were heated to 80 °C for 5 mins and allowed to cool slowly to room temperature (2-3 hours). Autoclaved water (20 µl) was added to each sample and then all samples were lyophilised for approximately 2 hours. The 20 % acrylamide non-denaturing gel was prepared by mixing 30 % acrylamide stock solution (66.6 ml), 5 X TBE (20 ml) and autoclaved water (12.7 ml). Ammonium persulfate (10 %, 700 µl) and N, N, N', N'-tetramethylethylenediamine (TEMED, 35 µl) were added just before the gel was poured. The gel apparatus was prepared and the gel was poured as described for the denaturing gel. After removal of the comb, the gel was pre-electrophoresed for 1 hour at 15-17 W (important to use low voltage as heat can denature DNA). A glycerol-based loading-dye was prepared (30 % glycerol in water, 0.25 % bromophenol blue and 0.25 % xylene cyanol) and 6 µl was added to each sample that was then loaded onto the gel. This gel was run for approximately 8 hours at 15-17 W.

5.15 Authoradiography

After the period of electrophoresis, the denaturing and non-denaturing gels were removed from the glass plates, covered in Clingfilm™ and placed in a cassette with an intensifying shield (which amplifies the level of radioactivity). An x-ray film was added to the cassette in a darkroom and the cassette was placed at -70 °C to activate the intensifying screen. The films were exposed for an appropriate period of time depending on the age of the radiolabeled material. The films were then developed in a dark room using an automatic developer (Fugi RG2 X-ray film processor).

5.16 Phosphoimagery

Polyacrylamide gels containing radiolabeled material analysed by autoradiography were subsequently quantified by phosphoimagery. In phosphoimagery, radioisotopic samples are exposed to storage phosphor screens. The screens are subsequently “read” using a rapid pulsed laser scanner, and the data is then digitized for display and analysis. Phosphoimagers have a greater sensitivity to radioisotopes compared with x-ray films with only 1 / 20 of the exposure time required for data analysis.

Conclusions and future work

Conclusions and future work

The work discussed in this thesis has shown it was possible to successfully synthesise and purify ruthenium-oligodeoxynucleotide (ODN) conjugates with different attached ligands. The ruthenium-ODN conjugates were shown subsequently to be successful as photochemical targeting agents in a model Chronic Myeloid Leukaemia (CML) system.

In the first system studied, the $[\text{Ru}(\text{phen})_2\text{phen}']$ -ODN conjugate was shown to induce site-specific base damage at the G21 target in the target 34mer ODN strand leading to cleavage of the target strand. The use of additives in this model system to investigate the role of singlet oxygen showed a small decrease in cleavage relative to the large decrease observed in experiments with the free photosensitisers. The more enclosed conjugate system may have contributed to an inability to suppress $^1\text{O}_2$ production in the immediate vicinity of the photosensitiser. It was concluded that the observed cleavage was result of type II cleavage. A complete absence of cleavage was not observed by the use of additives and may have been due to traces of oxygen remaining in the experimental samples. In the second system studied, the $[\text{Ru}(\text{TAP})_2\text{phen}']$ -ODN conjugate was shown to form photoadducts with the target guanine residue in the target strand. Inclusion of various additives in the experiments indicated that photoadduct formation occurred mainly by a type I reaction pathway.

Variant strand work indicated that in both systems, the site-specific phototargeting was localised i.e. the ruthenium complexes only seemed capable of inducing short-range damage. 3'-end labeling of the conjugates indicated damage of

the conjugates during the course of the experiments, thus explaining the relatively poor efficiency of the systems.

Future work in this area of research would involve optimisation of the model system and application to an *in vivo* system. Site-specific photochemical targeting has been demonstrated, but an increase in the overall yields of photocleavage and photoadduct formation would be necessary in order to achieve an optimal therapeutic effect. Exploration of other ruthenium-ODN conjugates with different attached ligands and linker chain lengths may possibly reveal a more efficient system. In relation to improving photoadduct formation, synthesis of the complex with a 4'-methyl-2,2'-bipyridine-4-carboxylic acid ligand (phen'') in place of the phen' ligand, resulting in a shorter linker chain between the complex and the 17mer ODN, may increase the efficiency of the system. The [Ru(phen)₂phen'']-ODN conjugate synthesised by C. Crean,¹⁷⁰ has been shown to significantly improve the yield of site-specific cleavage in the target strand compared to the [Ru(phen)₂phen']-ODN conjugate.

The introduction of the ruthenium-ODN conjugates into CML cell lines to assess their therapeutic application remains the overall aim of work of this nature, but due to the problems previously discussed in relation to degradation of antisense vectors by internal cellular components, the possibility of conjugation of the ruthenium complexes to modified oligodeoxynucleotides would need to be explored. This work would need to be carried out in close conjugation with a biological research group in order to obtain a conjugate capable of interrupting the leukaemic mRNA expression whilst also capable of withstanding an *in vivo* environment.

REFERENCES

-
- ¹ C. R. Dekker, A. M. Michelson and A. R. Todd, *J. Chem. Soc.*, 1953, 947.
- ² S. Zamenhof, G. Brawermann and E. Chargaff, *Biochem. Biophys. Acta.*, 1953, **9**, 402.
- ³ J. D. Watson and F. H. C. Crick, *Nature*, 1953, **171**, 737.
- ⁴ B. Lewin, *Genes V*, Ed. Oxford University Press Inc., New York, 1994.
- ⁵ M. D. Matteucci and M. H. Caruthers, *Tetrahedron Lett.*, 1980, **21**, 719.
- ⁶ S. L. Beaucage and M. H. Caruthers, *Tetrahedron Lett.*, 1981, **22**, 1859.
- ⁷ M. D. Matteucci and M. H. Caruthers, *J. Am. Chem. Soc.*, 1981, **103**, 3185.
- ⁸ K. Miyoshi and K. Itakura, *Tetrahedron Lett.*, 1979, **38**, 3635.
- ⁹ K. K. Ogilvie, N. Theriault and K. L. Sandana, *J. Am. Chem. Soc.*, 1977, **99**, 7741.
- ¹⁰ N. Usman, K. K. Ogilvie, M.-Y. Jiang and R. J. Cedergren, *J. Am. Chem. Soc.*, 1987, **109**, 7845.
- ¹¹ F. H. Crick, L. Burnett, S. Brenner and R. J. Watts-Tobin, *Nature*, 1961, **192**, 1232.
- ¹² F. H. Crick, *Nature*, 1970, **227**, 561.
- ¹³ C. Yanofsky, *Sci. Am.*, 1967, **216**, 80.
- ¹⁴ R. M. Burger, *Chem. Rev.*, 1998, **98**, 1153.
- ¹⁵ P. Lissoni, S. Barni, M. Mandala, A. Ardizzoia, F. Paolorossi, M. Vaghi, R. Longarini, F. Malugani and G. Tancini, *Eur. J. Cancer*, 1999, **35**, 1688.
- ¹⁶ R. J. Mersny, *J. Drug Targ.*, 1999, **7**, 1.
- ¹⁷ W. F. Anderson, *Nature*, 1998, **392**, 25.
- ¹⁸ I. M. Verma and N. Somia, *Nature*, 1997, **389**, 239.
- ¹⁹ A. M. Gewirtz, D. L. Sokol and M. Z. Ratajczak, *Blood*, 1998, **92**, 712.
- ²⁰ G. Duval-Valentin, N. T. Thoung and C. Hélène, *Proc. Natl. Acad. Sci.*, 1992, **89**, 504.
- ²¹ H. E. Moser and P. B. Dervan, *Science*, 1987, **238**, 645.

-
- ²² D. Praseuht, I. Perrouault, T. Le Doan, M. Chassignol, N. Thuong and C. Hélène, *Proc. Natl. Acad. Sci. USA*, 1988, **85**, 1349
- ²³ P. A. Beal and P. B. Dervan, *Science*, 1991, **251**, 1360.
- ²⁴ N. T. Thuong and C. Hélène, *Angew. Chem. Int. Ed. Engl.*, 1993, **32**, 666.
- ²⁵ D. Praseuth, A. L. Guieysse and C. Hélène, *Biochim. Biophys. Acta.*, 1999, **1489**, 181.
- ²⁶ I. Haq, J. Ladbury, B. Showdhry and T. Jenkins, *J. Am. Chem. Soc.*, 1996, **118**, 10693.
- ²⁷ J. L. Mergny, G. Duval-Valentin, C. H. Nguyen. L. Perrouault, B. Faucon, M. Rougère T. Montenay-Garestier, E. Bisagni and C. Hélène, *Science*, 1992, **256**, 1681.
- ²⁸ G. C. Silver, C. H. Nguyen, A. S. Boutorine, E. Bisagni, T. Garestier and C. Hélène, *Bioconj. Chem.*, 1997, **8**, 15.
- ²⁹ C. Nguyen, C. Marchand, S. Delage, J. Sun, T. Garestier, C. Hélène and E. Bisagni, *J. Am. Chem. Soc.*, 1998, **120**, 2501.
- ³⁰ F. X. Barre, C. Giovannangeli, C. Hélène and A. Harel-Bellan, *Nucleic Acids Res.*, 1999, **27**, 743.
- ³¹ A. L. Guieysse, D. Praseuth, C. Giovannangeli, U. Asseline and C. Hélène, *J. Molc. Biol.*, 2000, **296**, 373.
- ³² S. L. Young, S. H. Krawczyk, M. D. Matteucci and J. J. Toole, *Proc. Natl. Acad. Sci. USA*, 1991, **88**, 10023.
- ³³ T. J. Povsic, S. A. Strobel and P. B. Dervan, *J. Am. Chem. Soc.*, 1992, **114**, 5934.
- ³⁴ K. B. Grant and P. B. Dervan, *Biochem.*, 1996, **35**, 12313.
- ³⁵ M. J. Taylor and P. B. Dervan, *Bioconj. Chem.*, 1997, **8**, 354.
- ³⁶ J. C. François, T. Saison-Behmoaras, C. Barbier, M. Chassignol, N. T. Thuong and C. Hélène, *Proc. Natl. Acad. Sci. USA*, 1989, **86**, 9702.
- ³⁷ G. C. Silver, J. S. Sun, C. H. Nguyen, A. S. Boutorine, E. Bisagni and C. Hélène, *J. Am. Chem. Soc.*, 1997, **119**, 263.

-
- ³⁸ O. Baudoïn, C. Marchand, M. P. Teulade-Fichou, J. P. Vigneron, J. S. Sun, T. Garestier, C. Hélène and J. M. Lehn, *Chem. Eur. J.*, 1998, **4**, 1504.
- ³⁹ R. Zain, C. Marchand, J. S. Sun, C. H. Nguyen, E. Bisagni, T. Garestier and C. Hélène, *Chem. Biol.*, 1999, **6**, 771.
- ⁴⁰ C. Marchand, C. H. Nguyen, B. Ward, J. S. Sun, E. Bisagni, T. Garestier and C. Hélène, *Chem. Eur. J.*, 2000, **6**, 1559.
- ⁴¹ S. Choi, M. Kim, S. K. Kim, P. Lincoln, E. Tuite and B. Nordèn, *Biochem.*, 1997, **36**, 214.
- ⁴² P. Hausen and H. Stein, *Eur. J. Biochem.*, 1970, **14**, 278.
- ⁴³ S. T. Crooke, *Biochim. Biophys. Acta.*, 1999, **31**, 1489.
- ⁴⁴ R. V. Giles, D. G. Spiller and D. M. Tidd, *Anti-Cancer Drug Des.*, 1993, **8**, 33.
- ⁴⁵ M. L. Stephenson and P. C. Zamecnik, *Proc. Natl. Acad. Sci. USA*, 1978, **75**, 258.
- ⁴⁶ M. L. Stephenson and P. C. Zamecnik, *Proc. Natl. Acad. Sci. USA*, 1978, **75**, 280.
- ⁴⁷ B. N. Trawick, A. T. Daniher and J. K. Bashkin, *Chem. Rev.*, 1998, **98**, 939.
- ⁴⁸ S. T. Crooke, *Antisense Nuc. Acid Drug Dev.*, 1998, **8**, 7.
- ⁴⁹ U. Galderisi, A. Cascino and A. Giodano, *J. Cell Physiol.*, 1999, **181**, 251.
- ⁵⁰ S. Specter and G. Lancz, *Clinical Virology Manual*, 1992, (2nd Ed. Elsevier).
- ⁵¹ C. Hélène and J. Toulme, *Biochem. Biophys. Acta.*, 1990, **99**, 1049.
- ⁵² E. Zamaratski, D. Ossipov, P. I. Pradeepkumar, N. Amirkhanov and J. Chattopadhyaya, *Tetrahedron*, 2001, **57**, 593.
- ⁵³ C. R. Noe and L. Kaufhold, *New Trends in Synthetic Medicinal Chemistry*, Ed.(F. Gualtieri, Wiley-VCH, 2000) **Chpt. 9**.
- ⁵⁴ P. H. Seeberger and M. H. Caruthers, *Applied Antisense Oligonucleotide Technology*, Eds. (C. A. Stein and A. M. Krieg, Wiley-Liss, 1998) **Chpt. 3**
- ⁵⁵ J. F. Milligan, *J. Med. Chem.*, 1993, **36**, 1923.
- ⁵⁶ E. Uhlmann and A. Peyman, *Chem. Rev.*, 1990, **90**, 543.
- ⁵⁷ S. L. Beaucage, *Tetrahedron*, 1993, **36**, 1923.

-
- ⁵⁸ C. A. Stein, *Trends Biotech.*, 1996, **14**, 147.
- ⁵⁹ C. A. Stein and Y. C. Cheng, *Science*, 1993, **261**, 1004.
- ⁶⁰ T. L. Tonkinson and C. A. Stein, *Nucleic Acids Res.*, 1994, **22**, 4268.
- ⁶¹ C. A. Stein, R. Pal, A. L. Devico, G. Hoke, S. Mumbauer, O. Kinstler, M. G. Samgadhara and R. L. Letsinger, *Biochem.*, 1991, **30**, 2439.
- ⁶² A. M. Krieg, J. Tonkinson, S. Matson, Q. Y. Zhao, M. Saxon, L. M. Zhang, U. Bhanja. L. Yakubov and C. A. Stein, *Proc. Natl. Acad. Sci. USA*, 1993, **90**, 1048.
- ⁶³ D. M. Tidd, P. Hawley, H. M. Warenus and I. Gibson, *Anti Cancer Drug Des.*, 1988, **3**, 117.
- ⁶⁴ S. Agrawal and E. R. Kandimalla, *Molc. Med. Today*, 2000, **6**, 72.
- ⁶⁵ M. Manoharan, *Biochim. Biophys. Acta.*, 1999, **1489**, 117.
- ⁶⁶ H. M. Kantarjian, A. Deisseroth, R. Kurzrock, Z. Estrov and M. Talpaz, *Blood*, 1993, **82**, 691.
- ⁶⁷ K. S. Zuckerman, *Current Opinion in Haematology*, 1993, 189.
- ⁶⁸ O. Yehuda, D. Abeliovich, S. Ben Yehuda, I. Sverdlin, R. Cohen, G. Varadi, R. Orr, Y. J. Ashkenazi, J. Heyd, G. Lugassy and D. Ben Yehuda, *Cancer Gen. and Cytogen.*, 1999, **114**, 100.
- ⁶⁹ Anon, *The Lancet*, 1992, **340**, 1262.
- ⁷⁰ J. W. Voncken, C. Morris, P. Pattengale, G. Dennert, C. Kikly, J. Groffen and N. Heisterkamp, *Blood*, 1992, **79**, 1029.
- ⁷¹ A. McGahon, R. Bissonnette, M. Schmitt, K. M. Cotter, D. R. Green and T. G. Cotter, *Blood*, 1994, **83**, 1179.
- ⁷² C. M. Verfaillie, R. S. McIvor and R. C. H. Zhao, *Molc. Med. Today*, 1999, **5**, 359.
- ⁷³ C. Szczylik, T. Skorski, N. C. Nicolaides, L. Manzella, L. Malaguarnera, D. Venturelli, A. M. Gewirtz and B. Calabretta, *Science*, 1991, **253**, 562.
- ⁷⁴ S. G. O'Brien and T. F. C. M. Smetsers, *Applied Antisense Oligonucleotide Technology*, Eds. (C. A. Stein and A. M. Krieg, Wiley-Liss, 1998) **Chpt. 11**.
- ⁷⁵ A. DiBacco and T. G. Cotter, *Brit. J. Cancer*, 1998, **78**, 84.

-
- ⁷⁶ M. T. Rizzo, E. Regazzi, D. Garau, L. Akard, M. Dugan, H. S. Boswell, V. Rizzoli and C. Carlo-Stella, *Cancer Res.*, 1999, **59**, 5047.
- ⁷⁷ R. E. Clarke, *Leukemia*, 2000, **14**, 347.
- ⁷⁸ S. Dhut, T. Chaplin and B. D. Young, *Leukemia*, 1990, **4**, 745.
- ⁷⁹ P. de Fabritiis, S. Amadori, M. C. Petti, M. Mancini, E. Montefusco, A. Picardi, T. Gieser, K. Campbell, B. Calabretta and F. Mandelli, *Leukemia*, 1995, **9**, 662.
- ⁸⁰ B. Armitage, *Chem. Rev.*, 1998, **98**, 1171.
- ⁸¹ J. Cadet and R. Teoule, *Photochem. Photobiol.*, 1978, **28**, 661.
- ⁸² J.-P. Lecomte, A. Kirsch-De Mesmaeker, M. M. Feeney and J. M. Kelly, *Inorg. Chem.*, 1995, **34**, 6481.
- ⁸³ L. Jacquet, R. J. H. Davies, A. Kirsch-De Mesmaeker and J. M. Kelly, *J. Am. Chem. Soc.*, 1997, **119**, 11763.
- ⁸⁴ S. Steenken and S. V. Jovanovic, *J. Am. Chem. Soc.*, 1997, **119**, 617.
- ⁸⁵ L. P. Candeias and S. Steenken, *J. Am. Chem. Soc.*, 1989, **111**, 1094.
- ⁸⁶ Y. Jenkins and J. K. Barton, *J. Am. Chem. Soc.*, 1992, **114**, 8736.
- ⁸⁷ D. H. Johnston, C.-C. Cheng, K. J. Campbell and H. H. Thorp, *Inorg. Chem.*, 1994, **33**, 6388.
- ⁸⁸ C. J. Burrows and J. G. Muller, *Chem. Rev.*, 1998, **98**, 1109.
- ⁸⁹ J. Cadet, M. Berger, C. Decarroz, J. E. Wagner, J. E. Van Lier, Y. M. Ginot and P. Vigny, *Biochimie*, 1986, **68**, 613.
- ⁹⁰ J.-L. Ravanat and J. Cadet, *Chem. Res. Toxicol.*, 1995, **8**, 379.
- ⁹¹ T. P. A. Devasagayam, S. Steenken, M. S. W. Obendorf, W. A. Schulz and H. Sies, *Biochem.*, 1991, **30**, 6283.
- ⁹² C. Sheu and C. S. Foote, *J. Am. Chem. Soc.*, 1995, **117**, 6439.
- ⁹³ C. Sheu and C. S. Foote, *J. Am. Chem. Soc.*, 1993, **115**, 10446.
- ⁹⁴ C. Sheu and C. S. Foote, *J. Am. Chem. Soc.*, 1995, **117**, 474.
- ⁹⁵ S. Boiteux, E. Gajewski, J. Laval and M. Dizdaroglu, *Biochem.*, 1992, **31**, 106.
- ⁹⁶ S. Steenken, *Chem. Rev.*, 1989, **89**, 503.

-
- ⁹⁷ P. M. Cullis, M. E. Malone and L. A. Merson-Davies, *J. Am. Chem. Soc.*, 1996, **118**, 2775.
- ⁹⁸ H. Kasai, Z. Yamaizumi, M. Berger and J. Cadet, *J. Am. Chem. Soc.*, 1992, **114**, 9692.
- ⁹⁹ G. W. Buchko, J. Cadet, B. Morin and M. Weinfeld, *Nucleic Acid. Res.*, 1995, **23**, 3954.
- ¹⁰⁰ S. Raoul, M. Berger, G. W. Buchko, P. C. Joshi, B. Morin, M. Weinfeld and J. Cadet, *J. Chem. Soc., Perkin Trans. 2*, 1996, **3**, 371.
- ¹⁰¹ D. Angelov, A. Spassky, M. Berger and J. Cadet, *J. Am. Chem. Soc.*, 1997, **119**, 11373.
- ¹⁰² O. I. Kovalsky, G. I. Panutin and E. I. Budowsky, *Photochem. Photobiol.*, 1990, **52**, 509.
- ¹⁰³ H. Sugiyama and I. Saito, *J. Am. Chem., Soc.*, 1996, **118**, 7063.
- ¹⁰⁴ I. Saito, M. Takayama, H. Sugiyama, K. Nakatani, A. Tsuchida and M. Yamamoto, *J. Am. Chem. Soc.*, 1995, **117**, 6406.
- ¹⁰⁵ I. Saito, T. Nakamura and K. Nakatani, *J. Am. Chem. Soc.*, 2000, **122**, 3001.
- ¹⁰⁶ M. F. Sistare, S. J. Codden, G. Heimlich and H. Holden Thorp, *J. Am. Chem. Soc.*, 2000, **122**, 4742.
- ¹⁰⁷ Y. Kan and G. B. Schuster, *J. Am. Chem. Soc.*, 1999, **121**, 10857.
- ¹⁰⁸ *Metal Ions in Biological Systems*, A. Sigel and H. Siegel (Eds), 1996 (Dekker, New York)
- ¹⁰⁹ B. Norden, P. Lincoln, B. Akerman and E. Tuite, *Met. Ions Biol. Syst.*, 1996, **33**, 177.
- ¹¹⁰ J. M. Kelly, A. B. Tossi, D. J. McConnell, C. OhUigin, C. Hélène and T. Le Doan, *Free Radicals, Metal Ions and Biopolymers*, P. C. Beaumont, D. J. Deebie and C. Rice-Evans (Eds), 1989 (Richelieu Press, London).
- ¹¹¹ A. B. Tossi and J. M. Kelly, *Photochem. Photobiol.*, 1989, **49**, 545.
- ¹¹² K. Kalyanasundaram, *Coord. Chem. Rev.*, 1982, **46**, 159.
- ¹¹³ A. Kirsch-De Mesmaeker, C. Moucheron and N. Boutonnet, *J. Phys. Org. Chem.*, 1998, **11**, 566.

-
- ¹¹⁴ A. M. Pyle, J. P. Rehmman, R. Meshoyrer, C. V. Kumar, N. J. Turro and J. K. Barton, *J. Am. Chem. Soc.*, 1989, **111**, 3051.
- ¹¹⁵ M. Casu, G. Saba, A. Lai, M. Luhmer, A. Kirsch-De Mesmaeker, C. Moucheron and J. Reisse, *Biophys. Chem.*, 1996, **59**, 133.
- ¹¹⁶ A. Kirsch-De Mesmaeker, R. Nasielski-Hinkins, D. Maetens, D. Pauwels and J. Nasielski, *Inorg. Chem.*, 1984, **23**, 377.
- ¹¹⁷ C. Hiort, P. Lincoln and Bengt Nordén, *J. Am. Chem. Soc.*, 1993, **115**, 3448.
- ¹¹⁸ C. Moucheron, A. Kirsch-De Mesmaeker and S. Choua, *Inorg. Chem.*, 1997, **36**, 584.
- ¹¹⁹ J-P. Lecomte, A. Kirsch-De Mesmaeker, M. Demeunynck and J. Lhomme, *J. Chem. Soc. Faraday Trans.*, 1993, **89**, 3261.
- ¹²⁰ C. Sentage, J. C. Chambron, J. P. Sauvage and N. Paillous, *J. Photochem. B. Biol.*, 1994, **26**, 165.
- ¹²¹ M. B. Fleischer, K. C. Waterman, N. J. Turro and J. K. Barton, *Inorg. Chem.*, 1986, **25**, 3549.
- ¹²² J-P. Lecomte, A. Kirsch-De Mesmaeker, J. M. Kelly, A. B. Tossi and H. Gröner, *Photochem. Photobiol.*, 1992, **55**, 681.
- ¹²³ J-P. Lecomte, A. Kirsch-De Mesmaeker, M. M. Feeney and J. M. Kelly, *Inorg. Chem.*, 1995, **34**, 6481.
- ¹²⁴ L. Jacquet, J. M. Kelly and A. Kirsch De-Mesmaeker, *J. Chem. Soc. Chem. Commun.*, 1995, **9**, 913.
- ¹²⁵ C. Moucheron and A. Kirsch De-Mesmaeker, *J. Phys. Org. Chem.*, 1998, **11**, 577.
- ¹²⁶ P. Vicendo, S. Mouysset and N. Paillous, *Photochem. Photobiol.*, 1997, **65**, 647.
- ¹²⁷ E. Gicquel, N. Paillous and P. Vicendo, *Photochem. Photobiol.*, 2000, **72**, 583.
- ¹²⁸ R. E. Holmlin, P. J. Dandliker and J. K. Barton, *Angew. Chem. Int. Ed. Engl.*, 1997, **36**, 2714.
- ¹²⁹ W. Bannwarth, D. Schmidt, R. L. Stallard, C. Hornung, R. Knorr and F. Müller, *Helv. Chim. Acta.*, 1988, **71**, 2085.

-
- ¹³⁰ J. Telser, K. A. Cruickshank, K. S. Schanze and T. L. Netzel, *J. Am. Chem. Soc.*, 1989, **111**, 7221.
- ¹³¹ Y. Jenkins and J. K. Barton, *J. Am. Chem. Soc.*, 1992, **114**, 8736.
- ¹³² T. J. Meade and J. F. Kayyem, *Angew. Chem. Int. Ed. Engl.*, 1995, **34**, 352.
- ¹³³ I. Ortmans, S. Content, N. Boutonnet, A. Kirsch-De Mesmaeker, W. Bannwarth, J.-F. Constant, E. Defrancq and J. Lhomme, *Chem. Eur. J.*, 1999, **5**, 2712.
- ¹³⁴ K. Wiederholt and L. W. McLaughlin, *Nucleic Acid Res.*, 1999, **27**, 2487.
- ¹³⁵ W. Bannwarth and D. Schmidt, *Tetrahedron Lett.*, 1989, **12**, 1513.
- ¹³⁶ W. Bannwarth, W. Pfeleiderer and F. Müller, *Helv. Chim. Acta.*, 1991, **74**, 1991.
- ¹³⁷ W. Bannwarth and F. Müller, *Helv. Chim. Acta.*, 1991, **74**, 2000.
- ¹³⁸ E. Meggers, D. Kusch and B. Giese, *Helv. Chim. Acta.*, 1997, **80**, 640.
- ¹³⁹ D. J. Hurley and Y. Tor, *J. Am. Chem. Soc.*, 1998, **120**, 2194.
- ¹⁴⁰ D. Tzalis and Y. Tor, *J. Am. Chem. Soc.*, 1997, **119**, 852.
- ¹⁴¹ P. J. Connors Jr., D. Tzalis, A. L. Dunnick and Y. Tor, *Inorg. Chem.*, 1998, **37**, 1121.
- ¹⁴² S. I. Khan, A. E. Beilstein, G. D. Smith, M. Sykora and M. W. Grinstaff, *Inorg. Chem.*, 1999, **38**, 2411.
- ¹⁴³ S. I. Khan, A. E. Beilstein and M. W. Grinstaff, *Inorg. Chem.*, 1999, **38**, 418.
- ¹⁴⁴ S. I. Khan, A. E. Beilstein, M. Sykora, G. D. Smith, X. Hu and M. W. Grinstaff, *Inorg. Chem.*, 1999, **38**, 3922.
- ¹⁴⁵ X. Hu, G. D. Smith, M. Sykora, S. J. Lee and M. W. Grinstaff, *Inorg. Chem.*, 2000, **39**, 2500.
- ¹⁴⁶ F. D. Lewis, S. A. Helvoight and R. L. Letsinger, *Chem. Commun.*, 1999, 327.
- ¹⁴⁷ D. Ossipov, P. I. Pradeepkumar, M. Holmer and J. Chattopadhyaya, *J. Am. Chem. Soc.*, 2001, **123**, 3551.
- ¹⁴⁸ S. I. Khan and M. W. Grinstaff, *J. Am. Chem. Soc.*, 1999, **121**, 4704.

-
- ¹⁴⁹ S. I. Khan, A. E. Beilstein, M. T. Tierney, M. Sykora and M. W. Grinstaff, *Inorg. Chem.*, 1999, **38**, 5999.
- ¹⁵⁰ H. Wagenknecht, E. D. A. Stemp and J. K. Barton, *J. Am. Chem. Soc.*, 2000, **122**, 1.
- ¹⁵¹ C. O' Keeffe, *Ph. D. thesis*, 1998, University of Dublin.
- ¹⁵² J. Feely, P. V. Kavanagh, S. M. McNamara and J.E.O'Brien., *Ir. J. Med. Sc.*, 1999, **168**, 8.
- ¹⁵³ B. H. Han, D. H. Shin and S. Y. Cho, *Tetrahedron Lett.*, 1985, **26**, 6233.
- ¹⁵⁴ Darco G-60, 100 mesh powder (Aldrich).
- ¹⁵⁵ N. Y. Sardesai, S. C. Lin, K. Zimmermann and J. K. Barton, *Bioconj. Chem.*, 1995, **6**, 302.
- ¹⁵⁶ D. F. Gloster, L. Cincotta and J. W. Foley, *J. Heterocycl. Chem.*, 1999, **36**, 25.
- ¹⁵⁷ R. Nasielski-Hinkens and M. Benedek-Vamos, *J. Chem. Soc., Perkin Trans. I*, 1975, **13**, 1229 (Supp. 21349).
- ¹⁵⁸ M. Woźniak, A. Barański, K. Nowak and H. Poradowska, *Liebigs. Ann. Chem.*, 1992, 899.
- ¹⁵⁹ F. H. Case and J. A. Brennan, *J. Am. Chem. Soc.*, 1959, **81**, 6297.
- ¹⁶⁰ B. P. Sullivan, D. J. Salmon and T. J. Meyer, *Inorg. Chem.*, 1978, **17**, 3334.
- ¹⁶¹ G. Sprintschnik, H. W. Sprintschnik, P. P. Kirsch and D. G. Whitten, *J. Am. Chem. Soc.*, 1977, **15**, 4947.
- ¹⁶² C. D. Ellis, L. D. Margerum, R. W. Murray and T. J. Meyer, *Inorg. Chem.*, 1983, **22**, 1283.
- ¹⁶³ F. Schubert, A. Knaf, U. Moller and D. Cech, *Nucleosides Nucleotides*, 1995, **14**, 1443.
- ¹⁶⁴ M. Feeney, *Ph.D. thesis*, 1997, University of Dublin
- ¹⁶⁵ T. Maniatis, E. F. Fritch and J. Sambrook, *Molecular Cloning, a laboratory manual*, (2nd Ed. Cold Spring Harbour Lab, 1989)
- ¹⁶⁶ E. Kofit and F. H. Case, *J. Org. Chem.*, 1962, **27**, 865.
- ¹⁶⁷ S. J. Yan and W. H. Burton, *J. Heterocycl. Chem.*, 1978, **15**, 297.

¹⁶⁸ F. I. Abdel-Hay and M. Anwar, *Egypt. J. Chem.*, 1982, **25**, 335.

¹⁶⁹ W. Bannwarth, D. Schmidt, R. L. Stallard, C. Hornung, R. Knorr and F. Müller, *Helv. Chim. Acta.*, 1998, **71**, 2085.

¹⁷⁰ C. Crean, *Ph. D. thesis*, 2001, University of Dublin.